UNIVERSITÀ DEGLI STUDI DI BRESCIA

PH.D. PROGRAM IN
INDUSTRIAL AND MECHANICAL ENGINEERING

Scientific Disciplinary Sectors
ING-IND/10 Thermal engineering and industrial energy systems
ICAR/08 Structural mechanics

XXX CYCLE

A mechano-biological model of the coupling between cellular contractility and VEGFR2/VEGF interactions.

Advisors:
Prof. Gian Paolo Beretta and Prof. Alberto Salvadori

Ph.D. Candidate:
Valentina Damioli

Contents

Sommario

Il presente lavoro riguarda l'utilizzo di modelli matematici per la simulazione di processi biologici ed é frutto di una collaborazione tra i Dipartimenti di Ingeneria Meccanica e Civile e il Dipartimento di Medicina Molecolare e Translazionale. Per questo motivo, il presente lavoro ha carattere fortemente multidisciplinare, e le discipline coinvolte sono la biologia, termodinamica e cinetica chimica, la meccanica dei solidi classica e non-lineare. La collaborazione tra ricercatori che provengono da diversi settori sta diventando sempre pi utilizzata per far fronte all'esigenza di capire i dettagli di complessi fenomeni biologici, come quello dell'angiogenesi. Angiogenesi é la formazione di nuovi vasi sanguigni a partire da qualli pre-esistenti. Questo processo inizia quando una cellula endoteliale viene stimolata da proteine extracellulari, chiamate fattori di crescita o ligandi, che hanno la funzione di interagire fisicamente con proteine transmembrana, note come recettori. Essi sono presenti sulla membrana cellulare delle cellule endoteliali, che formano il vaso sanguigno. Questo legame produce una modifica conformazionale del recettore stesso, la sua dimerizzazione e fosforilazione, scaturando il primo segnale intracellulare verso il nucleo. Infine, una cascata di segnali, generata da questa prima interazione, comporterà una trascrizione genetica che à responsabile della duplicazione e proliferazione di nuove cellule endoteliali per formare nuovi vasi sanguigni. In vivo, i fattori di crescita possono essere, per esempio, rilasciati dalle cellule tumorali che hanno bisogno di nutrimenti e ossigeno per continuare a crescere e a proliferare nei tessuti e organi circostanti. I ligandi sono localizzati e immmobilizzati nella matrice extracellulare; mentre i recettori sono liberi di diffondere nel doppio strato lipidico, che compone la membrana cellulare ed hanno la funzione di percepire i segnali extracellulari e di trasmettere il messaggio all'interno della cellula. I biologi che collaborano con noi, hanno condotto esperimenti di reclutamento e rilocalizzazione dei recettori sulla mebrana da parte dei fattori di crescita che sono stati immobilizzati su un substrato. L'esperimento, semplicemente, consiste nell'appogiare una singola cellula endoteliale su un substrato sul quale, in precedenza, sono stati immobilizzati dei ligandi. La cellula inizialmente si accascia e si deforna, cambiando la sua geometria, e contemporaneamente si osserva la diffusione dei recettori verso la zona di contatto tra la cellula e il substrato dove sono presenti i ligandi. In quel momento avviene il legame tra recettore e ligando. Dal punto di vista biologico, molte informazioni su queste interazioni sono già note, ma le conoscenze in merito alla rilocalizzazione dei recettori sono ancora insufficienti. Per questo motivo, lo scopo della nostra ricerca é stato quello di descrivere questo processo scrivendo un modello matematico, semplificando questo problema utilizzando equazioni alla derivate parziali scritte in forma forte e in forma debole e poi discretizzando con il metodo degli elementi finiti e metodi di analisi numerica. Le equazioni sono poi state implementate mediante un codice in un programma agli elementi finiti e sono state ottenute delle simulazioni che sono in buon accordo con i dati sperimentali. Nel modello preliminare si é tenuto conto solo del processo chemo-diffusivo del problema, scegliendo una geometria e la deformazione della cellula molto semplificati. Infine, il modello matematico tiene conto della deformabilità della cellula in grandi deformazioni.

Chapter 1

Introduction

1.1 Motivations and research objectives

Motivations. Angiogenesis plays a major role in revascularization. Deprivation of these blood vessel networks, resulting in diseased states related to reduced vascular perfusion which could be treated by pro-angiogenic strategies. Recovery of the vascular network after injury is a key factor in the preventing wound expansion and ulcer formation. During cell and tissue transplantation, wound healing in diabetic conditions as well in aging patients suffering from slower heal recovery can take advantages of pro-angiogenic research. Other diseases such as limb, cardiac, coronary artery ischemias arise from reduced vascular perfusion. Thus, therapeutic angiogenesis is considered as the most strategy for revascularizing ischemic tissue and holds prime importance for tissue engineering and regenerative medicine in recent years. The clinical applications in the field of tissue engineering are still limited because the lack of good strategies that are able to provide adequate amount of oxigen and nutrients through blood vessels. Insufficient vascularization in the initial stage after implantation of tissue-engineered construct can lead to hypoxia and tissue death. Several strategies to overcome this issue are under research, such as the delivery of growth factors (VEGF, BMP), that stimulate the recruitment of endothelial cells. Thus, the modulation of angiogenesis process, such as the attivation of vascular endothelial growth fator receptors by ligands can ehnance these strategies. Moreover, angiogenesis plays a fundamental role in tumor growth and cancer proliferation. Tumor development is sustained by angiogenesis, necessary to provide the nutriments for cancer proliferation. Tumor angiogenesis is modulated by the interaction between specific pairs of membrane receptors expressed by endothelial cells and extracellular ligands produced by the tumor cell. The understanding of tumor angiogenesis has leaded to the development of antiangiogenic therapies but these therapies have not achieved the expected results yet.

Research objectives. The goal of theoretical and experimental biology is to study complex living systems and understand their fundamental mechanisms. Nowadays a wide amount of information about angiogenesis phenomena are still unknown. In vitro and in vivo information from experiments are difficult to analyze and disciplines as mathematics, thermodynamics and computational modeling can enable to attempt to fully understand how and why a biological process works. An open communication among different disciplines is the key. Recently, several successful ongoing collaborations, among different areas, such as biology and engineering, exist in the angiogenesis field and analyze what aspects of their approaches led them to achieve novel and impactful biological insight. Mathematical and computational approaches, if applied correctly, can hugely aid to solve biological complexity and increase the discovery of the general principles. Experimentalists and modelers must be work together, because a predictive capacity of a mathematical model will increase as the level of communication with experimentalists increases.
This thesis is the result of a first collaboration among the Mechanical and Industrial, Civil and Molecular and Translational Medicine Departments at the University of Brescia, consequently, this research is the outcome of the interplay among several disciplines, as biology, thermodynamics, solid mechanics and numerical methods. The main goal was to describe the VEGFR-2 recruitment and relocalization on endothelial cell membrane driven by ligands by means of mathematical equations. We started from the simplest mathe-

matical description of these phenomena, by a chemo-diffusion preliminar model. Then the model has been enriched by adding complexity: we coupled integrins and the cell mechanics in large deformations, with the ultimate aim of reproducing the real condition for receptor relocation driven by growth factors. Summarizing, we investigated

- VEGFR-2 relocalization modeling by means of

    - a preliminar thermodynamical model by means of a chemo-diffusion problem taking into account of chemical kinetics on a spherical geometry, presented in Chapter 3,
    - a chemo-diffusion model through a discretized weak form with a simplified mechanics to describe the cell-subtrate contact on a surface, proposed in Chapter 4;

- interaction among VEGFR-2/ligand complex coupled with low affinity integrins through a matematical formulation taking into account the interplay with the latter co-receptors, presented in Chapter 5;

- the VEGFR-2 relocalization by considering cell spreading, contractility and the cell-substrate contact through a mathematical formulation in order to take into account for the large deformations, described in Chapter 6.

Computational simulations have been performed in Chapters 3 and 4 by comparison with experimental evidence and co-designed tests have been carried out to confirm our results. Experimental data necessary to run the simulations, such as the receptor diffusivity and the species concentrations, are described in Chapter 2. In the following Chapter we presented fundamental biological concepts to contextualize the problem and we proposed a brief state-of-the-art of the methods used to investigate similar biological systems.

1.2 Biological background of blood vessel

1.2.1 Angiogenesis and vasculogenesis

Blood vessels originate from two different mechanisms, *vasculogenesis* and *angiogenesis* (Figure 1.1). During embryonic development, blood vessels develop from endothelial precursors called angioblasts, which give rise to the first primitive vascular plexus at specific sites, in a process previously called vasculogenesis [1, 2]. Subsequent growth and expansion of the vessels throughout the body occurs mainly by proliferation and movement of the **endothelial cells (ECs)** of these first vessels, in a process called angiogenesis [3]. During this time, vessel walls mature integrate tightly with supporting cells (such as smooth muscle cells and pericytes, namely the perivascular cells that wrap around blood capillaries) and surrounding matrix [4]. Angiogenesis is the new blood vessels formation from pre-existing ones and is a vital factor necessary for a wide range of physiologic and pathologic processes. For instance, angiogenesis is involved in tissue repair and regeneration, in the ovulation, in tumor growth, and in retinopathies for repair or regeneration of tissue and during pregnancy to build the placenta. These processes give rise to the formation of a vascular network through a tightly controled balance between pro- and anti-angiogenic signals. Understanding the mechanisms implicated in angiogenesis regulation and reach the knowledge of how to control "good" and "bad" angiogenesis can be the key to improving treatment efficacy [1]. Angiogenesis is responsible for the remodeling and sprouting of this circulatory system. Endothelial cells, which form the linings of the blood vessel, during later development, exhibit heterogeneity generating mature, functional blood vessels, due to microenvironmental signals to them [1, 4].

Vasculogenesis concerns in situ differentiation and growth of precursors, while angiogenesis involves two different mechanisms: *non-sprouting angiogenesis* or *intussusception* and *sprouting angiogenesis* (Figure 1.2). Quiescent endothelial cells, interconneted whith each other by tight cell adhesion junctions, constitute a monolayer covering the inner surface of blood vessels. Intussusception divides existing vessel lumens by formation and insertion of tissue crease and columns of interstitial tissue into the vessel lumen [2, 5]. Intussusception includes the creation of new vessels by in situ formation in the wall of large veins. Sprouting angiogenesis is a complex multistep process, which requires the interaction among different cellular types, soluble factors, cell surface receptors and **extracellular matrix (ECM)** components, with endothelial cells playing the central role in this process. The molecular regulation of these distinct mechanisms depends on
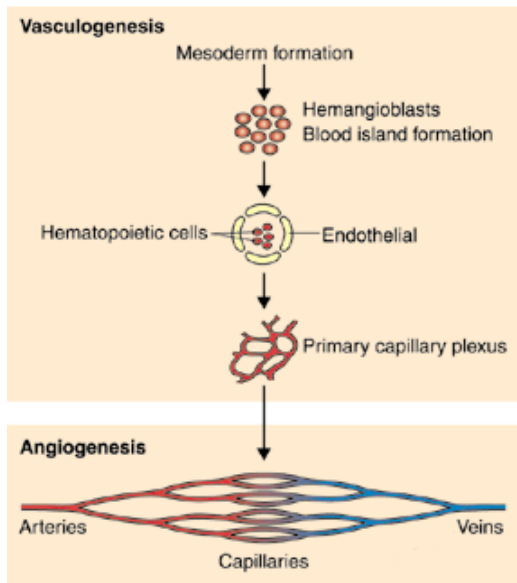
Figure 1.1: Genesis of the vascular system. During development, mesodermal cells (that are cells of mesoderm, the middle of the three primary germ layers of the embryo) differentiate into hemangioblasts leading to the formation of primitive blood islands. Then, the peripheral hemangioblasts differentiate into angioblasts, the precursors of endothelial cells. Subsequently, ECs migrate, allowing the fusion of the blood islands and their remodeling into tubular structures, giving rise to the first primitive vascular plexus. This vascular network rearranges into larger vessels, through the process of vasculogenesis of the embryo. In contrast to this phenomenon, angiogenesis is a neovascularization process by which new blood vessels form from pre-existing ones. Adapted from [6].

the most important angiogenic regulators, **vascular endothelial growth factor (VEGF)** and its receptor **VEGFR-2** (also known as **KDR**), both described later in this Chapter. The sprouting process is based on endothelial cell migration, proliferation and vessel formation. Sprouts exhibit long estensions of the endothelial cell at the tip directed towards the VEGF-producing cells [2, 5].

1.2.2 Endothelial cells

To understand how the vascular system grows, for instance toward tumor cells, it is necessary to focus on ECs. In the circulatory system, the largest blood vessels are arteries and veins, which have a thick wall of connective tissue and many layers of smooth muscle cells. The inner wall is lined by a thin single sheet of ECs, the endothelium, separated from the surrounding outer layers by a *basal lamina* [3] (see Figure 1.3). The endothelium is a dynamic organ and highly heterogeneous [1], surrounded by the extracellular
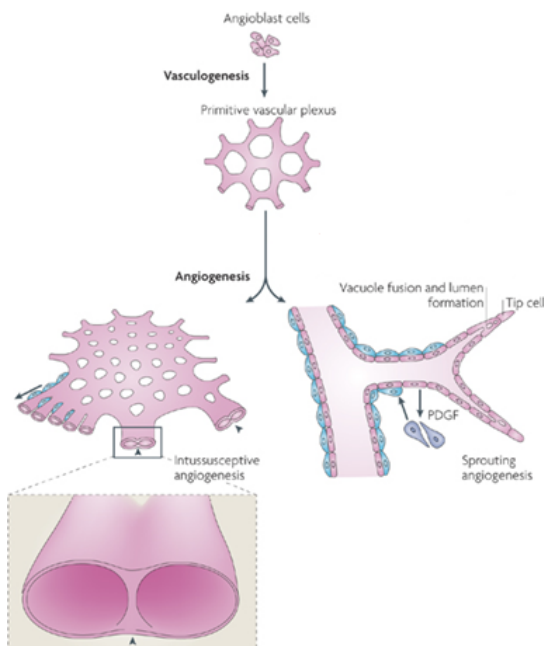
Figure 1.2: Vasculogenesis involves the differentiation of ECs from precursor angioblast cells to form a primitive vascular plexus, which can expand by angiogenesis. Two types of angiogenesis are shown: intussusceptive and sprouting angiogenesis. Intussusceptive angiogenesis involves the splitting and growing of vessels in situ. In sprouting angiogenesis, ECs proliferate behind the tip cell of a growing branch in response to cytokines, namely small proteins that are necessary for cell signalling, such as vascular endothelial growth factor (VEGF). Neighbouring mesenchymal cells migrate towards the neovessel in response to platelet-derived growth factor (PDGF). Adapted from [7].

matrix, namely the vascular basement membrane, and is constituted mainly by proteins and proteoglycans, that confers shape and stability to the vessel. Accessory cells, including pericytes and smooth muscle cells, are embedded in the basement membrane, give stability and monitor the maturation of ECs. Pericytes are required for normal microvascular structure and function because they provide structural support, protect endothelial cells from apoptosis, and actively control the stability of the vessels [1]. ECs have the ability to adapt their number and network of the blood vessels to create a suitable system, extending by cell migration into almost every region of the body [3].
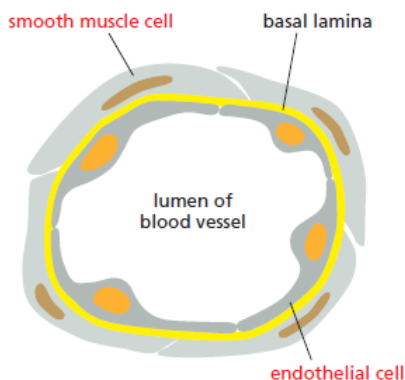
Figure 1.3: Simplified cross section of a blood vessel, showing the ECs lining the lumen, basal lamina, (an extracellular structure with supportive primary funcion for ECs) and the smooth muscle cells around them as well. Source [3].

As described above, ECs originate at specific sites, in the early embryo, from precursors, called hemangioblasts. From these sites, during vasculogenesis, early embryonic ECs migrate, proliferate, and differentiate to create the first rudimental blood vessels [3]. Subsequent growth and branching of the vessels throughout the body occurs mainly by proliferation and movement of the ECs of these first vessels, in a process, previously described, called angiogenesis [3]. Each new vessel originates as a capillary sprout from the side of an existing capillary. During angiogenesis, ECs migration involves three major mechanisms [8], namely

1. *chemotaxis*, the directional migration toward a gradient of soluble chemoattractants,

2. *haptotaxis*, the directional migration toward a gradient of immobilized ligands,

3. *mechanotaxis*, the directional migration generated by mechanical forces.

1.2.2.1 Mechanical properties of ECs: elastic modulus

Mechanical properties describe how cells perceive mechanical forces and respond to them and it is necessary quantify these characteristics. The work proposed by Caille et al. [9] provides Young's modulus values of the cytoplasm and nucleus from experiments and validated with finite element simulations. Single ECs of three different conformations, round cells, spread cells and isolated nuclei, were underwent to compression between a rigid and a flexible microplates. The compression was imposed by displacing the rigid glass carrying the cell or nucleus by steps of $2.5\,\mu\mathrm{m}$ every $10\,s$ towards the flexible glass [9]. This mechanical test allows measurement of the uniaxial force applied to the cell and the resulting deformation. Measurements were made in the shortes possible time and on round and spread cells to rule out cellular adaptation and avoid the influence of cell morphology on the nucleus mechanical properties. It is been observed that round cells deform at lower forces than spread cells and nuclei [9]. The finite element models consider the nucleus and the cytoplasm (rest of the cell) as separate homogeneous hyperelastic materials. The models simulate the compression and yield the force-deformation curve for a given set of elastic moduli. These parameters are varied to obtain a best fit between the theoretical and experimental data. The elastic modulus of the cytoplasm is found to be on the order of $500\,\mathrm{Pa}$ for spread and round cells. The elastic modulus of the endothelial nucleus is on the order of $5000\,\mathrm{Pa}$ for nuclei in the cell and on the order of $8000\,\mathrm{Pa}$ for isolated nuclei [9].

Other works are based on modern atomic force microscopy (AFM) techniques which provide the analysis of local mechanical properties and the topography of the living cells at a high spatial resolution and force sensitivity. In particular, AFM is used for mapping mechanical properties of a single cell that yields information on cellular structures including cytoskeleton structure [10]. The effort is to choose an appropriate

mechanical model for the estimation of cellular Youngs modulus using AFM. For instance, the Hertz model has been used in the majority of cases dedicated to the assessment of elastic modulus of cells. The Hertz model describes the simple case of elastic deformation of two perfectly homogeneous smooth bodies touching under load [10]. The elasticity of ECs was measured with AFM, and analyzed by applying the Hertz model [11]. The Youngs modulus value measured is on order of $10000\,\text{Pa}$ in the work presented by Sato et al. [11]. Other theoretical models used in studies of cell elastic properties based on AFM are the finite element method and the theory of elastic shells [10]. However, the Hertz method supposes unrealistic assumptions about cell indentation experiments, about the geometry of the probe tip or the material properties of the cell, including homogeneous, isotropic, linear elastic material properties, infinitesimal deformations, and infinite sample thickness and dimensions [12]. For this reason, an alternative pointwise approach to analyze the AFM indentation data has been presented [12]. In addition, it is been observed that there are significant variations of the values of elastic modulus at different cell regions, then Mathur et al. [13] showed that the elastic modulus values of ECs were $700\,\text{Pa}$ over the nucleus; $300\,\text{Pa}$ over the cell body in proximity to the nucleus, and $130\,\text{Pa}$ on cell body near the edge.

1.2.3   Physiological and pathological angiogenesis

During the embryogenesis process, a strong angiogenic activity occurs and it is responsible and necessary for tissues and organs growth. In contrast with this, in healthy adult body, vessels remain dormant (quiescent) and neovascularization happens rarely, being restricted to cycling ovary and placenta during pregnancy. ECs keep their angiogenesis abitity, since they can respond to hypoxic and inflammatory stimuli, as it happens during wound healing. Several pathologies are due to a lack of equilibrium of the angiogenic stimulus leading to either an excessive or insufficient neovascularization. Accordingly, a good regulation of angiogenesis is necessary in human physiology to keep homeostasis, namely the tendency of a system to maintain internal stability, such as the regulation of body temperature, the pH of extracellular fluid, or the concentrations of sodium, potassium and calcium ions, as well as that of glucose in the blood plasma. A lack of vessel maintenance is usually associated to pathological conditions such as stroke, neurodegenerative diseases or obesity, whereas excessive angiogenesis is reported in ocular and inflammatory disorders, diabetes, cirrhosis, multiple sclerosis, endometriosis, AIDS and autoimmune diseases [14]. Also, tumor development depends on the formation by angiogenesis of a structure of blood vessels devoded to supply the tumor with oxygen and nutrients and to remove waste products [14].

1.2.4   Pro- and anti-angiogenic therapies

Angiogenic therapy targets to promote neovasculature through several strategies by using pro-angiogenic factors. These include growth factor such as VEGF, fibroblast growth factor, platelet-derived growth factor. Growth factors delivery system is a challenging approach that can help to promote the ideal condition for tissue regeneration and they have been applied to a wide range of in vivo and in vitro models in tissue engineering, diabetic conditions, cardiovascular disorders and chronic wounds to improve angionenesis [15]. It has been proved that some peptides derived from grown factors, ECM, receptors promote angiogenesis. In addition, synthetic peptides has proved to enhance EC proliferation [15]. Thus, a wide range of pro- and anti-angiogenic processes cause angiogenesis and drug delivery systems can potentially improve to enhance or reduce angiogenesis in a more controlled manner [16]. For instance, the fact that tumours are dependent on blood supply has inspired many researchers to search for anti-angiogenic molecules and to design anti-angiogenic strategies for cancer treatment [17]. As a consequence, inhibition of angiogenesis represents a target for blocking tumor growth, possibly bypassing the multidrug resistance problem, since ECs, unlike tumor cells, are genetically stable. The identification of the mechanical laws that regulate VEGF receptor localization may open new perspectives to develop innovative anti-angiogenic strategies through the modulation of EC activation. Innovative drug delivery systems can increase the effectiveness of anti-cancer therapies. Several anti-angiogenic molecules alone or in combination with traditional treatments are in clinical trials in the past decade [18]. These analysis are based on strategies that interfere with pro-angiogenic ligands and their receptors or their intracellular signalling. These approaches offer new perspective for the successful treatment of cancer. However, there are two major problems that justify caution in clinical and laboratory studies on humans. One of the obstacles to the success of anticancer therapies is related to the inefficient

distribution of drugs to cancer cells [19] and the problem of drug resistance. Inefficient distribution is due to several reasons, as the abnormal structure and function of tumor blood vessels [19]. The combination of several therapies, such as blocking the signaling of few growth factors (Figure 1.4), have been shown to be more efficient rather than a single therapy [16]. For example, researchers have simultaneously administered antibodies against VEGFR-2 to suppress tumor growth as well as an anti-angiogenic antibody to enhance the efficacy of a conventional chemotherapy drug. This can be especially useful when a certain type of tumor is known to be resistant to one treatment but not to another [20]. Drug delivery models are being developed that couple well-studied principles of material transport and pharmacokinetics with new biomaterials [16]. Some of these therapeutic systems have been translated to the clinic with success. Despite this, additional research is needed to improve the delivery of drugs and to identify new strategies [16].

(a)   (b)
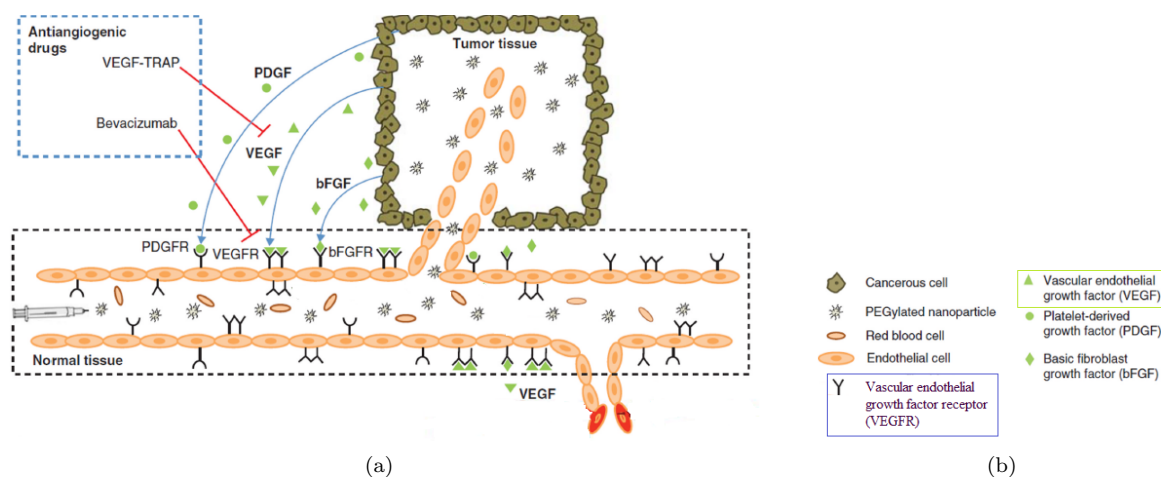
Figure 1.4: Antiangiogenic drugs, such as VEGF-TRAP and bevacizumab, block the angiogenic effect of the growth factors VEGF and VEGFR. Modified from [16].

1.2.5   Angiogenesis at the molecular level

The neovascularization is regulated by a balance between pro- and anti-angiogenic signals and requires proliferation, survival, migration and differentiation of ECs. Moreover, stromal cells as well as pericytes and smooth muscle cells need to be recruited in order to generate a mature and functional vasculature. A wide range of molecules lead such phenomena. Among others, growth factors, cell surface receptors, ECM proteins and enzymes modulate the angiogenic process, triggering to a fine regulation.

1.2.5.1   Pro-angiogenic factors

The pro-angiogenic factors are molecules known as **growth factors** that cooperate to modulate ECs behaviour. Several molecules including growth factors, inflammatory molecules and citokines have been described as positive or negative modulators of angiogenesis.

Pro-angiogenic factors can be divided in direct pro-angiogenic factors, which have direct effects on ECs and indirect factors, such as:

- **direct factors**: angiopoietins (Ang1 and Ang2 [21]), delta-like-ligand-4 (Dll4) [22], platelet-derived growth factor (PDGF) [23], Slits [24], hepatocyte growth factor (HGF) [25], some cytokines [Interleukin (IL) such as IL-8 [26], IL-1 [27], IL-6 [28]], sempahorin 4 [29, 30] and the recently discovered Gremlin [31];

- **indirect factors**: transforming growth factor-β (TGFβ), TNFα [32, 33], angiogenin and pleiotropic factors, such as fibroblast growth factor (FGF) [34].

Angiopoietins (Ang), from the family of vascular growth factors, are well-known pro-angiogenic molecules that play a central role in blood vessel plasticity modulation and contribute to vascular maintenance by binding Tie-2 tyrosine kinase receptor, expressed almost exclusively in ECs. Ang-1 induces ECs to recruit pericytes and smooth muscle cells to become annexed in the vessel wall, being involved either in maintaining vasculature quiescence or in the remodelling and maturation of newly formed vascular network. As consequence, Ang-1 enhances survival, migration and network formation of ECs in vitro, contributing to angiogenesis in vivo. Beside angiopoietins, Dll4, a kind of Notch ligands, are well-characterized players in angiogenesis. PDGF is considered a potent mitogen since it stabilizes newly formed vessels [23].

TNF-α and angiogenin stimulate non-endothelial cells to produce direct pro-angiogenic factors, contributing to in vivo angiogenesis [32, 33]. Also FGF simultaneously target the different cell types (ECs, pericytes and smooth muscle cells) that participate to the new blood vessels formation is involved in angiogenesis modulation. FGF2 is an heparin-binding protein which concurrently induces proliferation and migration of ECs and up-regulates VEGF expression in target cells.

At last, others angiogenic factors such as the viral proteins HIV-1 Tat and p17 can modulate angiogenesis [35, 36, 37]. Tat represents the main viral transactivator factor of HIV that drives the expression of several cytokines and growth factors, lowering the efficiency of the immune response and contributing to the arise of different AIDS-associated diseases [36]. Tat released by HIV-1-infected cells leads to different angiogenesis-related AIDS-associated diseases. Tat binds and activates VEGFR-2, eventually leading to ECs proliferation and chemotaxis in vitro and neovascularization in vivo [38] and interacts with heparan sulfate proteoglycans (HSPGs) [39]. HSPGs are glycoproteins, found at the cell surface and in the ECM, where they interact with a wide range of growth factors.

1.2.5.2 Anti-angiogenic factors

The action of pro-angiogenic factors is usually counter-balanced by that of anti-angiogenic ones. The most widely investigated angiogenesis inhibitors are the proteolytic cleavage products of ECM or serum components, such as endostatin, angiostatin, arresten, and tumstatin (by remembering that proteolytic cleavage is the hydrolysis of peptide bonds in a protein). Multiple cytokines can also exert anti-angiogenic properties, including interferons (IFN-α) [40] and certain interleukins (IL-10 [41], IL-12 [42] and IL-18 [43]). Several other molecules are known to negatively regulate angiogenesis. Among those, sempahorin 3 decreases angiogenesis, by modulating VEGF activity and inhibiting ECs migration [44]. Also, there are few known naturally occurring anti-angiogenic molecules, which include platelet factor 4, known as CXCL4 [45], and the ECM protein thrombospondin1(TSP-1) [46]. TSP-1 inhibits the release of VEGF from ECM, through suppression of metalloproteases (MMPs) activity [47], MMPs are the main enzimes capable of degrading ECM proteins. TSP-1 also binds directly to VEGF, and this interaction can mediate the uptake and clearance of VEGF from the ECM [48, 49].

1.2.5.3 Modulation of growth factors activity by the extracellular matrix

The extracellular matrix (ECM) is the non-cellular component present within all tissues and organs, and provides not only essential physical scaffolding for the cellular constituents but also initiates crucial biochemical and biomechanical cues that are required for tissue morphogenesis, differentiation and homeostasis. The ECM is composed of water, proteins and polysaccharides, each tissue has an ECM with a unique composition and topology that is generated during tissue development through a dynamic and reciprocal, biochemical and biophysical dialogue between the various cellular components (e.g. epithelial, fibroblast, adipocyte, endothelial elements) and the evolving cellular and protein microenvironmen. The ECM generates the biochemical and mechanical properties of each organ, such as its tensile and compressive strength and elasticity, and also mediates protection by a buffering action that maintains extracellular homeostasis and water retention. In addition, the ECM directs essential morphological organization and physiological function by binding growth factors and interacting with cell-surface receptors to elicit signal transduction and regulate gene transcription. During angiogenesis process, growth factors, by binding their specific receptors, modulate the intracellular signalling pathways that support cell proliferation, migration and morphogenesis. The microenvironment plays a central role by governing the sensitivity of cells to those factors. In blood vessels, ECs lay on the ECM and the latter confers a mechanical sustain for ECs, but also influences their survival,

differentiation, shape, polarity and mobility [50] [51]. During angiogenesis ECM remodelling by matrix metalloproteinase leads to the exposure of usually masked binding sites, resulting in higher ECs migration and invasion [52]. The ECM can control cell behaviour by binding, sequestering or accumulating growth factors and cytokines (FGFs, VEGFs). In this way the ECM act as a 'reservoir' regulating the availability and activity of signalling molecules [53, 54]. Besides, ECM-immobilized angiogenic growth factors reach high local concentrations, retain the capacity to engage their signalling receptors [55, 57] and can sustain a long-term stimulation of target cell [58]. Also, several anti-angiogenic molecules are ECM components or fragments generated by ECM remodelling, such as TSP-1 [59] and endostatin and arrestin [60] respectively. Additionally, the biophysical properties of the ECM are emerging as crucial regulators of important cellular functions including cell migration [61]. The ECM contains protein fibers connected in a hydrated gel composed of glycosaminoglycans (GAGs) and proteoglycans (including HSPGs). The main components of the ECM are laminins, collagens, fibronectin and elastins. HSPGs are abundant components and they typically consist of a core protein with a variable number of GAGs. Beside their presence in the ECM, HSPGs can be found in free forms in body fluids or expressed on the membrane of most eukaryotic cell types, including ECs, where they represent low affinity and high capacity receptors for a wide array of heparin-binding proteins (growth factors, cytokines, chemokines, enzymes and ECM components) [62, 63]. HSPGs mainly act as co-receptors. HSPGs also contribute to a productive binding of VEGFs with signalling VEGFRs [64]. Also Gremlin, a non-canonical VEGFR-2 ligand, binds HSPGs, which are crucial for a productive interaction with the receptor [65]. Integrin receptors provide cells with the possibility to interact and sense the ECM. Integrins are a large family of transmembrane heterodimeric receptors. Integrins link directly the basement membrane to cell cytoskeleton and signal transduction, contributing both to mechanical support and cell migration proliferation and survival. Several common intracellular signalling pathways, including focal adhesion kinase (FAK), Src, MAPKs, phsphoinositide-3-kinase (PI3K), Rho-GTPase are activated by integrin engagement [52, 66, 67, 68]. During angiogenesis, integrins expression and ECM composition modulate the sensitivity of EC to growth factors [69, 71]. The cross talk between **tirosine kinase receptor (TKR)** and integrins leads to improve modulation of the cellular responses [72, 73]. $\alpha_v\beta_3$ integrin supports and modulate VEGF- and FGF-driven angiogenesis [74, 75]. Beside their role in co-operating with TKRs, integrins can mediate TK-independent angiogenic activity of growth factors [76]. This may imply a direct interaction. What discussed above is only a partial list of signalling molecules and pathways involved in angiogenesis. Thus, it is clear how angiogenesis is a complex process involving several molecular pathways, interconnected each others, that need to be finely orchestrated in order to drive the well ordinated growth of new vessels from pre-existing ones.

1.2.6 Cystine-knot proteins

The ligands object of the present work belong to the cystine-knot proteins family, classified in three groups [77, 78]: growth factor cystine-knots (such as TGF-β and VEGF family), inhibitor cystine-knots and cyclic cystine-knots. In addition to these well-known components, new proteins are being added to the cystine-knot proteins family, collected in a group called C-terminal cystine-knot proteins (CTCK). Members of CTCK are the bone morphogenetic protein (BMP) antagonists, which include Gremlin.

1.2.6.1 Vascular endothelial growth factor (VEGF)

Vascular endothelial growth factor (VEGF) is the most important molecules to control the vascular development of ECs. VEGF is a protein which is able to bind or stick to other molecules. The substance that is bound by another protein is referred to as a **ligand** for that protein (from the Latin word 'ligare', meaning 'to bind'). VEGF was first described in 1983 by Dvorak and collaborators [79], as a tumour-secreted **vascular-permeabilty factor (VPF)**, and was first molecularly defined and cloned by Ferrara in 1989 [80]. In mammals, the VEGF family consists of five members, VEGF-A, VEGF-B, VEGF-C, VEGF-D, VEGF-E and placenta growth factor (PLGF) [81, 82]. VEGF-A is a protein that occurs in at least six molecular isoforms, which consist of 121, 145, 165, 183, 189, and 206 amino acids [8, 83]. Although VEGF-A$_{121}$, VEGF-A$_{183}$ and VEGF-A$_{189}$ are expressed in various tissues, VEGF-A$_{165}$ is the most abundantly expressed form, whereas VEGF-A$_{145}$ and VEGF-A$_{206}$ are relatively rare. VEGF-A is the most important and is a very specific mitogen for vascular ECs [8, 81]. VEGF-A provokes the full cascade of events required for angiogen-

esis and is overexpressed in a variety of tumors [8, 81, 83]. After the VEGFs production, these ligands are able to bind the heparin domain and diffuse through the tissue, and act on nearby ECs, stimulating them to proliferate, and to form sprouts. The tip cells of the sprouts detect the VEGF gradient and move toward its source [3].

Vascular permeability. The permeability of the vasculature is a feature of the capillary wall to prevent the movement of fluid or solutes driven by a physical force. It is the main responsible of the regulation of exchange of nutrients and water between tissues and blood [84]. Vascular permeability is vital for the health of normal tissues and plays a central role as characteristic of many disease states in which it is greatly increased. Examples are acute inflammation and pathologies associated with angiogenesis such as tumors, wounds, and chronic inflammatory diseases [85]. VEGF, as said before, is a protein synthesized and secreted by a variety of cells, serves as an EC-specific mitogen and a potent angiogenic factor. In addition, VEGF is a key regulators of permeability. Intradermal injection of VEGF increases vascular permeability of ECs, a critical event in inflammation and angiogenesis. VEGFs may increase vascular permeability by inducing platelet-activating factor (PAF) synthesis [86].

1.2.6.2 VEGF receptor (VEGFR)

The region of a protein that associates with a ligand, known as the ligand's *binding site*, usually consists of a cavity in the protein surface formed by a particular amino acids placement [3]. VEGF exerts its effects after binding to homologous TKRs.
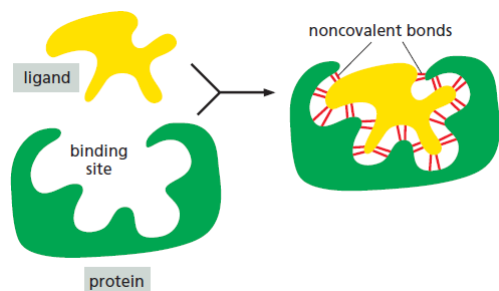
Figure 1.5: The selective binding of a protein to another molecule. Many weak bonds are needed to enable a protein to bind tightly to a second molecule, or ligand. Source [3].

Many extracellular signal proteins operate through TKRs. The binding of the signal protein to the ligand-binding domain (as shown in Figure 1.5) on the extracellular side of the receptor activates the tyrosine kinase domain on the cytosolic side. This leads to the **phosphorylation** of tyrosine side chains on the cytosolic part of the receptor, creating *phosphotyrosine docking sites* for various intracellular signaling proteins, which relay the signal. Phosphorylation is a phenomenon that implies the addition of a phosphoryl group to a molecule (Figure 1.6(a)). For most TKRs, ligand binding causes the receptor **dimerization**, that is bringing the two cytoplasmic kinase domains together and thereby promoting their activation (Figure 1.6(b)). Dimerization stimulates kinase activity by a variety of mechanisms. In many cases, dimerization simply brings the kinase domains (green area) close to each other in an orientation that allows them to phosphorylate each other on specific tyrosines in the kinase active sites, thereby promoting conformational changes that fully activate both kinase domains [3].

Three different vascular endothelial growth factor receptors types, VEGFR-1, VEGFR-2 and VEGFR-3, have been identified in ECs. Each VEGF ligand (-A, -B, -C, -D, -E and PLGF) binds in a specific manner to three TKRs, which exert different affinity for different VEGFs [4, 8, 82, 87]. **VEGFR-2**, known as **fdk-1/KDR**, is a transmembrane protein, which binds VEGF-A ligand, with high affinity [82]. This interpay is the most effective in inducing tumour angiogenesis, through a complex signaling cascade [4, 8, 82, 87]. A schematic illustration of the ligand specificity and effects of each VEGFRs is shown in Figure 1.7. VEGFR-2 is expressed on vascular and lymphatic endothelium. VEGFR-2 binds all VEGF-A isoforms, VEGF-C, -D and -E. Downstream effects of VEGFR-2 activation in the vascular endothelium include cell proliferation, migration, permeability and survival, resulting in angiogenesis [82].

(a)   (b)
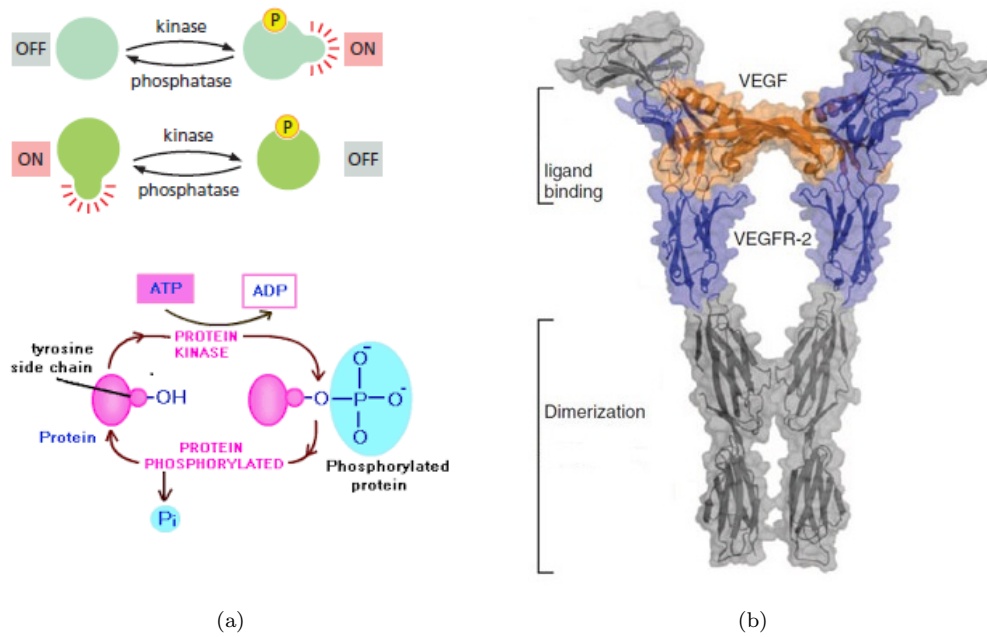
Figure 1.6: (a-(A)) The general reaction transfers a phosphate group from ATP to an amino acid side chain of the target protein by a protein kinase. Removal of the phosphate group is catalyzed by a second enzyme, a protein phosphatase. (a-(B)) The phosphorylation of a molecule by a protein kinase can either increase or decrease the protein's activity, depending on the site of phosphorylation and the structure of the protein. Source [3]. (b) A structural model of the ligand/receptor complex interaction for dimerization upon ligand-induced activation and its binding site, as determined by X-ray. Adapted from [88].

1.2.7 Bone morphogenetic proteins (BMPs)

BMPs are ECM-associated molecules that belong to the TGF-β family of cystine-knot proteins. BMPs exert pro-angiogenic function and can directly modulate angiogenesis by aiming ECs, or may indirectly support angiogenesis by inducing the expression of other pro-angiogenic molecules [89]. To date over 20 members have been identified in humans with varying functions during processes such as embryogenesis, skeletal formation, hematopoesis and neurogenesis [90]. Despite their functions have been identified, few is known about the regulation at the ECM, membrane surface, and receptor activation [90].

A BMP antagonist: Gremlin. In addition to the tissue-specific expression of BMP ligands and cell surface receptors, a crucial regulatory step of BMP signalling is their modulation by specific extracellular BMP antagonists [91]. Recently, it is been demonstrated [31, 92] the capacity of VEGFR-2 to interact with another non-canonical ligand, known as **Gremlin-1**, a BMP antagonist, that leads to VEGFR2-dependent angiogenic responses in vitro and in vivo. Gremlin-1 is a secreted protein that is known to regulate bone formation during development. Mitola et al. [92] report the novel role of Gremlin as a VEGFR-2 agonist and the function of the Gremlin protein. Gremlin induces angiogenesis by binding to VEGFR-2 and triggering intracellular signaling pathways in ECs. Gremlin is produced by human tumors and is expressed by tumor endothelium. Thus, Gremlin may play an important role in tumour vascularization [92], and for this reason is being studied.

1.2.8 Ligands specificity

The binding of ligands to individual surface receptors can be determined by standard techniques, and rate constants and equilibrium constants are measured in the same units as for interaction in solution. The

11

Figure 1.7: Schematic illustration of ligand specificity and the effect of each of the VEGFRs. Source [82].

kinetics constants of association and dissociation rate, k^+ and k^-, and their ratio $K_d = \frac{k^-}{k^+}$ are measured from Surface Plasmon Resonance (SPR), well-described in Chapter 2, and BiaEvaluation[1] where VEGFR-2 are immobilized on a microchip and VEGF and Gremlin are the analytes injected and flowed over the gold chip, as shown in Figures 1.8 and 1.9 respectively.

Determination of interaction kinetics is the most characteristic application for Biacore systems. The label-free real-time detection allows interactions to be monitored with high resolution as they happen, and the results can be interpreted in relation to a mathematical model of the interaction mechanism to evaluate kinetic parameters.

The work proposed by Maiolo et al. [94], the nanoscale mechanical phenomena interconnected with VEGFR-2 surface recognition by its canonical growth factor VEGF-A and its noncanonical ligand have been investigated. The in-plane forces developed upon surface recognition of VEGFR-2 by the two ligands have been quantified. For this end, interactions of the extracellular domain of VEGFR-2 with these ligands have been investigated by integrating SPR spectroscopy data with nanoliter CONtact Angle MOlecular REcognition (CONAMORE) assays. SPR analysis revealed substantial differences between VEGF-A/sVEGFR2 and Gremlin/sVEGFR2 interactions in terms of binding and dissociation kinetic rate constants, k^+ and k^-, where sVEGFR2 means immobilized extracellular domain of VEGFR-2. SPR experiments and analysis were performed immobilizing the sVEGFR2 with a density of approximately $(2.2 \pm 0.03) \times 10^{10}$ molecule/mm^2 to an Au-coated SiO_2 5×5 mm^2 chip. Binding of VEGF-A and Gremlin to immobilized sVEGFR2 was monitored as a function of time by tracking the SPR intensity change upon binding progression. VEGF-A was scanned for concentrations ranging from 2.5 to 400 nM and Gremlin was scanned for concentrations ranging from 5 to 200 nM. The ligand solutions were flowed on the chip for 4 min. In particular for VEGF-A ligand the sample volume is 40 μL, with a flow rate of $10\frac{\mu L}{min}$, and dissociation time of 120 s. For Gremlin

---

[1]BIAevaluation is a stand-alone software package for presentation and evaluation of sensorgram data from real-time Biomolecular interaction analysis (BIA) analyses. BIAa technology based on Surface Plasmon Resonance (SPR), is nowadays used to identify in details a wide range of biological interplays among molecules, proteins, and other biomolecules [93]. The software supports the evaluation of kinetic constants from sensorgram data using numerical integration and global fitting methods.

Figure 1.8: Parameters values for VEGF and VEGFR-2 interaction: $k^+ = 5.02 \cdot 10^5$ and $k^- = 4.64 \cdot 10^{-7}$, and its ratio $K_d = 9.25 \cdot 10^{-13}$.

Figure 1.9: Values for Gremlin and VEGFR-2 interaction: $k^+ = 1.3 \cdot 10^5$ and $k^- = 9.44 \cdot 10^{-8}$, and its ratio $K_d = 7.27 \cdot 10^{-13}$.

Table 1. Mass and Mechanical VEGF-A/sVEGFR2 and Gremlin/sVEGFR2 Binding Parameters Evaluated by SPR and CONAMORE[a]

	k_{on} (M^{-1} s^{-1})	K_{off} (s^{-1})	K_d^{σ} mass (nM)	K_d^{σ} mech (nM)
VEGF-A	$(8.5 \pm 3) \times 10^4$	$(1.5 \pm 0.3) \times 10^{-4}$	34 ± 8	2 ± 0.7
gremlin	$(8 \pm 2) \times 10^4$	$(2 \pm 0.3) \times 10^{-3}$	65 ± 20	32 ± 9

[a]k_{on} and k_{off}: Binding and dissociation kinetic rate constants, respectively. K_d^{σ} mass: Surface mass dissociation constant. K_d^{σ} mech: Surface nanomechanical dissociation constant.

Figure 1.10: Values of $k^+ = k_{on}$ and $k^- = k_{off}$ for the interplay between VEGFR-2 and Gremlin. [94]

the sample volume $40\,\mu$L, flow rate $5\frac{\mu L}{min}$, and dissociation time $240\,s$. Examples of the binding curves are reported in Figures 1.8 and 1.9. The binding and dissociation kinetic rate constants were evaluated from fitting dose sensorgrams with a 1:1 Langmuir association/dissociation equation [95]. The k^+ and k^- values, reported in Figure 1.10, represent the mean over a set of sensorgrams of the same ligand at different doses. The equilibrium constant can be infered from [94] as

$$K^{eq}\,(\text{Gremlin}) = \frac{k^+}{k^-} = \frac{(8 \pm 2) \times 10^4}{(2 \pm 0.3) \times 10^{-3}} \simeq 4 \times 10^7\,M^{-1} \tag{1.1}$$

The lateral interactions take place in the plane of the membrane, i.e., in two instead of three space dimensions [96]. For several reasons, the kinetic parameters of these interactions cannot be easily deduced from the rate constants of the same interaction in solution [96]:

1. anchoring of the proteins into the membrane reduces the translational and rotational freedom, and results in a preferred orientation of the interaction partners to each other along the normal of the surface;

2. lateral and rotational diffusion of the membrane anchored protein is much slower than in solution.

For these reasons we tried to asses the kinetic parameters from our first thermodynamical model presented in Chapter 3.

1.2.9   Co-receptors: Integrins

Integrins are transmembrane proteins, localized on the cell membrane, that are able to bind the surrounding ECM to the cytoskeleton. The binding among integrins and matrix components (as specific extracellular ligands, e.g. *fibrinogen*) triggers the propagation of intracellular signaling cascades that affect the cell mechanical behavior. When integrins cluster at sites of matrix contact, they influence the assembly of cell-matrix junctions called **focal adhesion (FA)** [3]. Among the many proteins recruited into these junctions the most important is the cytoplasmic tyrosine kinase called **focal adhesion kinase (FAK)** [3]. Integrins by means of cell-matrix junctions, as talin and vinculin, are able to attach contractile F-actin/myosin II bundles, connecting them to the ECM (Figure 1.11).
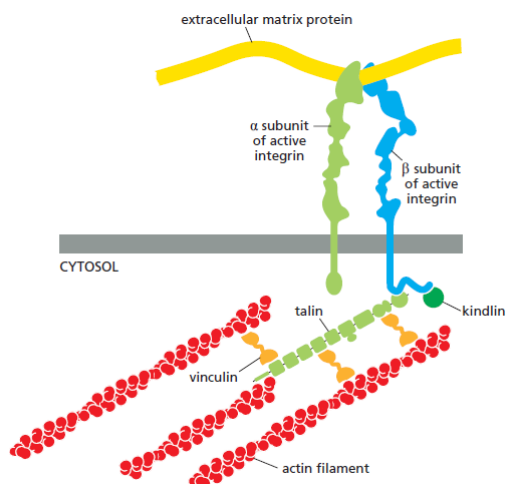
Figure 1.11: The subunit structure of an active integrin molecule, linking extracellular matrix to the actin cytoskeleton. Source [3].

Humans contain 24 types of integrins, formed from the products of 8 different β-chain genes and 18 different α-chain genes, dimerized in different combinations. Each integrin dimer has distinctive properties and functions. The binding of integrins to their matrix ligands is affected by the concentration of Ca^{2+} and Mg^{2+} in the extracellular environment [3, 72, 97]. Several integrins are not constitutively active; they can be, and often are, expressed on cell surfaces in an inactive or 'off' state, in which they do not bind ligands and do not signal [98]. Integrins are flexible, dynamic adhesive machines, and they exist in different conformations [72, 98, 99](as shown in Figure 1.12):

- **low-affinity**, inactive, and bent-clasped conformation;

- the progressive extension of the integrin unbent-clasped form;

- unbent and unclasped, **high-affinity** configuration.

Although cell adhesion to the ECM and cell migration are mediated by integrins, the identification of the mechanisms by which specific integrins influence biological processes such as angiogenesis continue to be a challenge [72]. In addition to the function of integrins for supporting cell adhesion, integrins have been widely recognized as important molecules in the signal transduction from the ECM to the intracellular signaling [72].
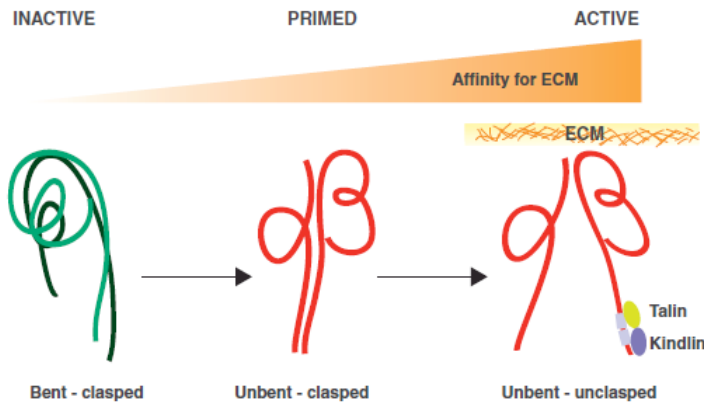
Figure 1.12: Integrins exist in several conformations and they have different affinities for ECM ligands. They can exist in low-affinity, inactive, and bent-clasped conformations. The progressive extension of the integrin extracellular domain characterizes the transition to a primed, unbent-clasped conformation, which has a medium affinity for the ECM. Active integrins display a high affinity for the ECM and are both unbent and unclasped. Source [99].

1.2.9.1 Cytoskeleton
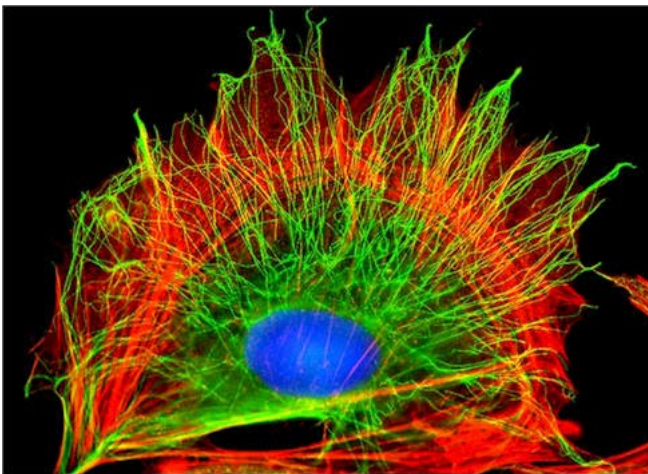
Figure 1.13: Cell in culture has been fixed and labeled to show its cytoplasmic arrays of microtubules (green) and actin filaments (red). Source [3].

Living cells have to organize themselves in space in order to operate correctly. Cells are able to interact with their surroundings and with each other and to change their shape and move around. All cells have the capacity for reorganize their internal structure as they grow, divide, and adapt to changing conditions [3]. ECs are highly spread cells and their directional migration is initiated by extracellular signals such as growth factors gradient [100]. Directional cues count in mechanical forces (for istance, cell stretching), ECM proteins (e.g. Fibronectin, Fibrinogen) and ECM/substratum stiffness. Migration cell starts by polarizing and extending protuberances (lamellipodium and filopodium) of the cell membrane, towards the signal, driven by the polymerization of actin filaments [100].

The spatial and mechanical functions of living cells depend on a considerable network of filaments called the **cytoskeleton** (Figure 1.13) [3]. The cytoskeletal network is highly dynamic and flexible. The three

major cytoskeletal network responsible for various aspects of the cell's spatial organization and mechanical properties are listed below [3]:

1. **Actin filaments** regulate the shape of the cell's surface and are necessary for whole-cell locomotion;

2. **Microtubules** determine the positions of membrane-enclosed organelles, direct intracellular transport, and form the mitotic spindle that segregates chromosomes during cell division;

3. **Intermediate filaments** provide mechanical strength.

All of these cytoskeletal structures interact with a wide range of proteins that modulate and connect them to other element of the cell or to each other as well [3]. These proteins are crucial to control cytoskeletal filaments assembly, and they contain the *motor proteins*, that transform the energy of ATP hydrolysis into mechanical force that can move the filaments themselves [3].

Actin is the major cytoskeletal component and has a fundamental role in various cellular processes such as migration and morphogenesis [3, 101]. Therefore, the regulation of the structure and dynamics of the actin cytoskeleton is essential for many processes in living cells, and abnormalities in its dynamics are associated with many deseases such as cancer [101]. It is composed by **monomeric globular subunits (G-actin)** that polymerize into helical **actin filaments (F-actin)**. F-actin are flexible structures with a diameter of 8 nm that arrange into two-dimensional and three-dimensional linear bundles networks. Although F-actin are dispersed throughout the cell, they are most distributed in the cortex, just under the plasma membrane [3]. The most important function of actin filaments is to create force for cellular processes such as cell motility [3, 101, 102, 103]. Actin filaments reach this function by two distinct mechanisms: polymerization and the actin-myosin contraction. The polymerization of actin filaments against cellular membranes provides force, for instance, to create plasma membrane protrusions during cell migration (Figure 1.14 (b)). The structure and dynamics of actin filament networks are regulated by actin-binding proteins, which control the nucleation, elongation and disassembly of F-actin as well as their arrangement in three-dimensional arrays [101]. F-actin, combined with **myosin II**, produces contractile filaments, as well as the force generated through actin polymerization. Here, the force is produced by ATP-driven movement of the myosin II motor domains along the actin filaments. Because myosin II assembles into bi-polar bundles, and the F-actin in these structures are arranged in bi-polar arrays, the motor activity of myosin II bundles results in the contraction of the actomyosin bundle [101](as shown in Figure 1.14 (b)).

The constant remodeling of the actin cytoskeleton into filopodium, lamellipodium, (Fig. 1.14b) and stress fibers is essential for cell migration [8]. Filopodium is based on membrane projections that accommodate long parallel actin filaments arranged in tight bundles [8]. Lamellipodium is composed by cytoplasmic protrusions on the leading edge of spreading cells. **Stress fibers** are bundles of contractile actin filaments linked by α-actinin and non-muscle myosin II [8].

The actin-myosin bundles contribute to cell motility. Myosin II is the kind of molecular motor, a protein that is able to convert chemical energy, in the form of ATP, to mechanical energy, producing force and cell migration [3, 102]. Stress fibers and focal adhesion (FA) are essential for cell adhesion to the substrate, for changes in cell morphology and they are well-known to produce and transmit mechanical tension [104, 105]. Stress fibres have been classified in three classes on the basis of their position: ventral stress fibres, dorsal stress fibres and transverse arcs [105]. Ventral stress fibres are the most commonly observed structures (Figure 1.15D) and lie along the base of the cell, attached to integrin-rich FA at each end. Dorsal stress fibres are connected to FA at one end only, which attaches them to the basal aspect of the cell. The rest of the structure rises towards the dorsal surface, terminating in a loose matrix of actin filaments. Transverse arcs are bundles of actin that form under the dorsal surface of migrating cells, just behind the protrusive lamellipodium [105].

1.2.9.2 Interactions among VEGFR2/ligand complex and co-receptors

VE-cadherin and PI 3-kinase. Specificity of biological responses may be explained by quantitative considerations, e.g. signal duration and strength. Signal specificity can also counter from qualitative differences in the set of proteins docking to TKR cytoplasmic tails. Moreover, biochemical signals generated from TKRs can potentially be integrated with those originating from other receptors and combined with preexisting transcription factors [87].
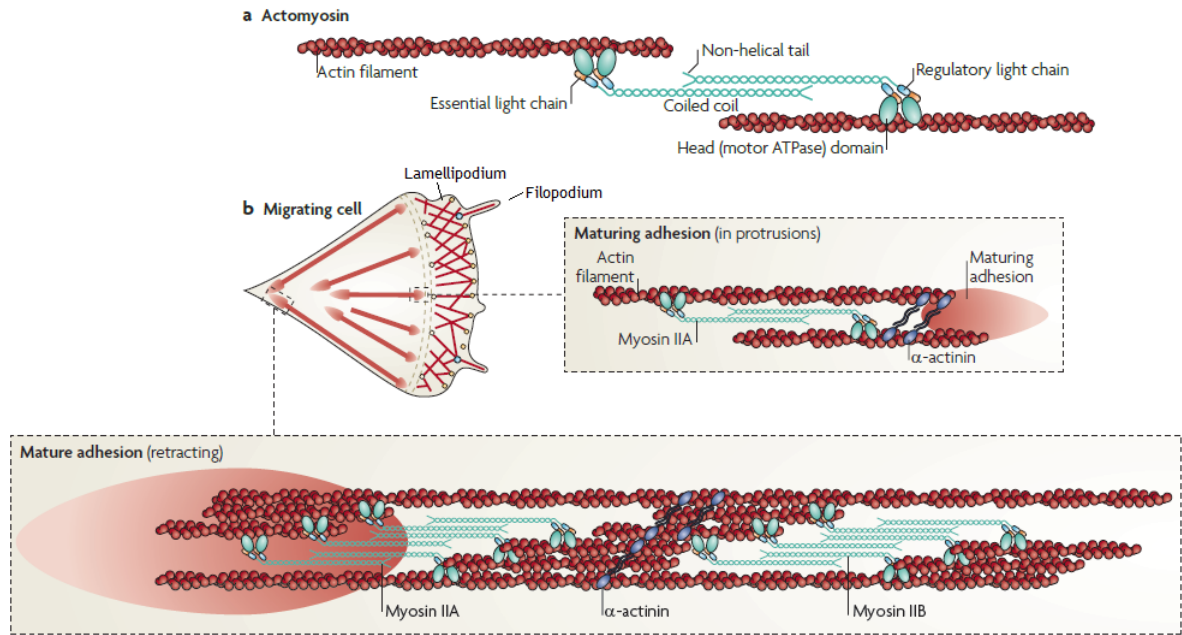
Figure 1.14: (a) Adhesions elongate along actin filaments that contain myosin II, which cross links the actin filaments and exerts tension on them. (b) Adhesion is coupled with the protrusions of the leading edge of the cell (filopodium and lamellipodium). Adhesion maturation to focal complexes and focal adhesions is accompanied by the cross-bridging of actin filaments, and actomyosin-induced contractility makes stable adhesion formation. Mature adhesions is associated with large size of F-actin bundles. Modified from [100].

One of the complexes in which VEGFR-2 participates also includes vascular endothelial cadherin (VE-cadherin), $\beta-$catenin and Phosphatidylinositol 3-kinase (PI 3-kinase). VE-cadherin is a transmembrane protein that mediates endothelial homophilic adhesion and forms clusters at intercellular junctions when cells come into contact with one another. Through its cytoplasmic tail, VE-cadherin binds $\beta-$catenin, which in turn interacts with actin [87]. (PI3K) is a major signaling mediator downstream of cell surface RTKs that plays a crucial role in the regulation of various cellular processes, such as proliferation and cytoskeletal rearrangement.

Integrin. During angiogenesis, ECs adhere to a provisional ECM, through $\alpha_v\beta_3$ integrin. Once engaged with the ECM, this integrin participates in a complex containing VEGFR-2 and PI 3-kinase. It has been demonstrated that $\alpha_v\beta_3$ integrin takes part in the full activation of VEGFR-2 provoked by VEGF-A [74] or by Gremlin [106]. It been tested that VEGFR-2 stimulation by its ligand VEGF-A$_{165}$ [74] and Gremlin [106] induces the formation of a complex with β_3 integrin, responsible for the long-term activation of the intracellular signal, triggered by canonical and noncanonical pro-angiogenic VEGFR-2 ligands. The nature of the physical interaction between KDR and β_3 subunit is been examined occuring outside the cell, demonstrated by Borges et al.[107] generating a lack of the cytoplasmic domain in the β_3 integrin. VEGFR-2/$\alpha_v\beta_3$ integrin complex could support the integration of FAK and downstream signaling pathways and would promote EC proliferation, migration and survival [87, 72]. It is possible to argue that both integrin activation and VEGFR-2 function are reciprocally linked. The sequence of the molecular events could be as follows: VEGF stimulation leads to an initial VEGFR-2 phosphorylation followed by proto-oncogene tyrosine-protein kinase (cSrc) recruitment and these events induce to the complex formation between VEGFR-2 and β_3 integrin [108]. All these phenomena promote activation of $\alpha_v\beta_3$ and result in the increase integrin ligation (attivation) and phosphorylation of β_3 integrin by cSrc. These occurances, in particular the complex formation, are responsible for prolonged and full activation of VEGFR-2 increasing its long term phosphorylation [108].

Neuropilin. In addition to interacting with VE-cadherin or $\alpha_v\beta_3$ integrin, VEGFR-2 may also complex with
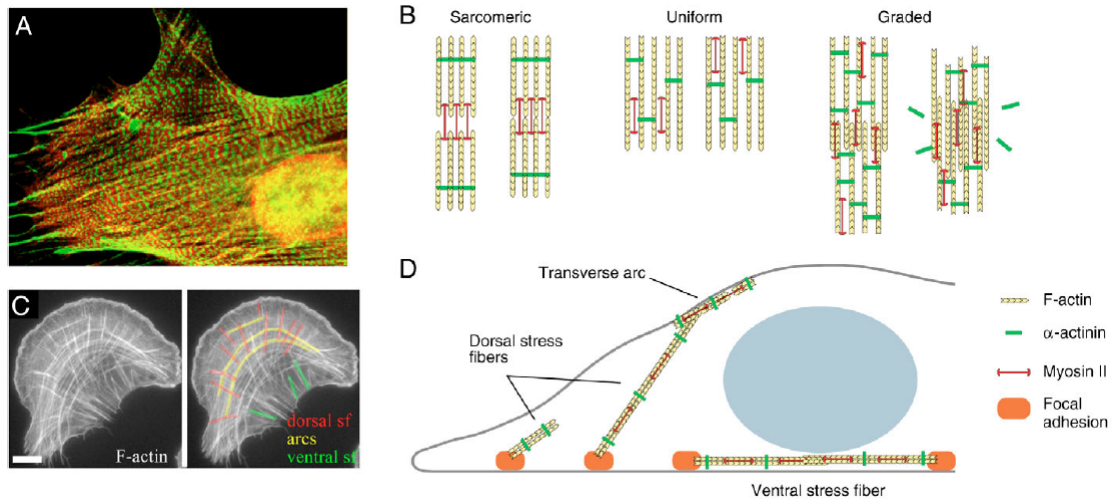
Figure 1.15: Actin stress fibre structure. (A) Non-muscle myosin (red) and α-actinin (green) (B) Stress fibers contractility model (C) The stress fibers network, indicated with red (dorsal), yellow (arcs), green (ventral) lines (D) Model of stress fibre formation. Dorsal stress fibres arise from focal contacts at the cell periphery and elongate up through the cell to join transverse arcs at the cell surface. Two dorsal stress fibres may meet a transverse arc, forming a ventral stress fibre. Source [105].
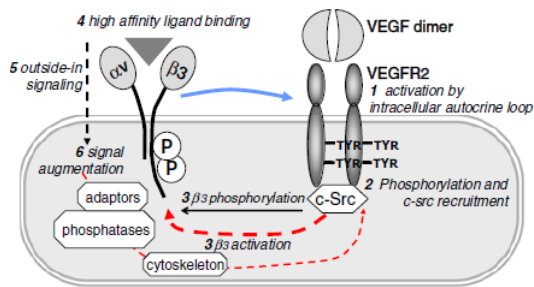
Figure 1.16: (A) The diagram shows possible sequence of molecular events involved in interaction between VEGFR-2 and $\alpha_v\beta_3$ integrin. Adapted from [108].

Neuropilin1 (Npn1), a transmembrane protein that is expressed in ECs, but has been better characterized for its involvement in axon guidance. The association between VEGFR2 and Npn1 is highly dependent on the ligand isoform: through its unique 44 amino acid stretch encoded by exon 7, VEGF-A$_{165}$, but not VEGF-A$_{121}$, triggers the formation of the VEGFR2/Npn1 complex. This isoformspecific association may be the molecular mechanism that allows greater stimulation of VEGFR2 tyrosine kinase activity by VEGF-A$_{165}$ rather than by VEGF-A$_{121}$ [87].

1.3   A state-of-the-art in mathematical models

Receptor-ligand interaction has been extensively studied in the last past thirty years from the biological and computational point of view. A theoretical framework is proposed by Bell [109] for the analysis of adhesion among cells or of cells to surfaces when the adhesion is controlled by reversible bonds between specific molecules such as enzyme and substrate. Knowing the reaction rates for reactants in solution and of their diffusion constants both in solution and on membranes, it is possible to estimate reaction rates for membrane-bound reactants. Two models are developed for predicting the rate of bond formation between cells and are compared with experiments. Bell compared his theory with measurements of the binding of cells to lectin-coated fibers or to lectin-coated cells on fibers [109]. In this work, the cell periphery is described by the fluid mosaic model and the cell membrane is a phospholipid bilayer in which various proteins are

inserted and retained by virtue of the favorable free energy of their hydrophobic amino acids in the lipid as compared to the aqueous environment [109]. The force required to separate two cells is shown to be greater than the expected electrical forces between cells, and of the same order of magnitude as the forces required to pull gangliosides and perhaps some integral membrane proteins out of the cell membrane.

Single experiments similar in design to those typically performed for Scatchard analyses of binding data conducted at physiological temperature and in the absence of inhibitors of ligand-receptor complex internalization and degradation can provide kinetic data sufficient to permit derivation of all the respective rate constants by numerical methods [110]. Mayers et al. [110] developed an analytical solution based on a kinetic model which assumes that all of these processes follow first order kinetics. The model represents interactions of surface receptors, the surface ligand-receptor complex and internalized receptor-ligand complex. The present model is applicable to systems in which there is no cell growth, nonspecific binding of the ligand can be ignored, free ligand concentration is sufficiently large to be considered constant. It has been demonstrated the applicability of this approach to the analysis of interactions of IFN-α with human epithelial tumor cells and Madin-Darby Bovine Kidney Epithelial (MDBK) cells and to the analysis of the interaction of epidermal growth factor with human fibroblasts [110].

DiMilla et al. [111] proposed a simple mathematical model which relates basic cell biochemical and biophysical properties to cell movement speed based on adhesion receptor-ligand (as integrins and fibronectin) kinetics, receptor-ligand densities, cell rheology and cytoskeletal force generation. This model incorporates cytoskeletal force generation, cell polarization, and dynamic adhesion as requirements for cell motility. A feature is the proposed existence of an asymmetry in some cell adhesion-receptor property, correlated with cell polarity. A viscoelastic-solid model for cell mechanics allowed to represent one-dimensional motion with a system of differential equations describing cell deformation and displacement along with adhesion-receptor dynamics. The cell surface is modeled as two flat rectangular sheets, representing the dorsal and ventral sides, so that to form a continuous surface. In this paper, equations under the simplifying assumption that receptor dynamics are at a quasi-steady state relative to cell locomotion are solved. The results are strictly valid for sufficiently slow cell movement, as typically observed for tissue cells such as fibroblasts. The results predict how cell speed might vary with intracellular contractile force, cell rheology, receptor/ligand kinetics, and receptor/ligand number densities.

Gilson et al. [112] have outlined a class of models of binding that have foundation in statistical thermodynamics, and are computationally friendly. A central feature of these models is the use of thorough conformational sampling over a modest number of essential degrees of freedom. This approach yields converged results in short computational times. These models are physically interpretable, because they are assembled from well-defined components that can be tested. In addition, the efficiency of these models will enable statistically significant validation studies to be carried out. It should therefore be possible to provide users with functional computational tools [112].

A simple dynamic corral model for the lateral diffusion of transmembrane proteins in the membrane by the cytoskeleton, proposed by Leitner et al. [113], can predict the average time of proteins to escape from the corral. The dynamic corral acts as a gate which when open permits an otherwise trapped protein to escape to a neighboring corral in the cytoskeletal network. It has been solved for the escape rate over a wide range of parameters of the model, and compare these results with Monte Carlo simulations. Upon introducing measured values of the model parameters for Band 3 in erythrocyte membranes, it is possible to estimate the value for one unknown parameter, the average rate at which the corral closes [113].

In the study of Gabhann et al. [114], the relative contribution of placental growth factor (PlGF)-induced VEGF displacement to the synergy is quantified using a mathematical model of ligand-receptor binding to examine the effect on ligand-receptor complex formation of VEGF and PlGF acting together. Parameters specific to the VEGF-PlGF system are used based on existing data. The model is used to simulate in silico a specific in vitro experiment in which VEGF-PlGF co-operation is observed. It is been shown that, whereas a significant change in the formation of endothelial surface growth factor-VEGFR1 complexes is predicted in the presence of PlGF, the increase in the number of VEGFR2-containing signaling complexes is less significant; these results were shown to be robust to significant variation in the kinetic parameters of the model. This is the first computational model describing transport and binding of VEGF to its receptors. It has been constructed this model to describe unsteady in vitro situations as a first step to modeling more complex, dynamic in vivo situations. In a subsequent work, Gabhann et al. [115] compared Monte Carlo simulations of the stochastic binding of the one isoform of VEFG (VEGF-$_{165}$) and VEGFR-1 and

VEGFR-2 on cells in vitro to equivalent deterministic simulations performed using the full kinetic method previously described [114]. Gabhann et al. have investigated the behavior of VEGF-VEGF receptor binding to endothelial cells using deterministic and stochastic methods, looking in particular at the area over which the cell is 'integrating' the signals from its activated receptors. For the first model type, they found that the agreement between the stochastic and deterministic results depended upon the area over which the fractional occupancy is averaged, which is equivalent to the area over which the cell is integrating the signals from its activated receptors. For the second stochastic model type, results agree with the deterministic models over all areas, ligand and receptor densities tested. The deterministic models are suitable for simulating in vitro experiments of VEGF-VEGF receptor system on endothelial cells [115].

The compartment model described by Stefanini [116] provides informative quantitative biological details such as VEGF distributions in tissue and in blood, as well as the sensitivity of VEGF distribution to specific biological parameters. This model was formulated to represent both VEGF transport throughout the entire human body and the distribution of free and bound VEGF at the molecular level in tissues, of two isoforms of the VEGF-A family.

In another study [117], it is analysed the dynamics of VEGF retention in a controlled in vitro situation of human umbilical vascular endothelial cells (HUVECs) in Matrigel. They shown that fluorescent VEGF accumulates in pericellular areas and colocalizes with VEGF binding molecules. Analysis of fluorescence recovery after photobleaching reveals that binding/unbinding to matrix molecules dominates VEGF dynamics in the pericellular region. Computational simulations using experimental measurements of kinetic parameters show that matrix retention of chemotactic signals can lead to the formation of reticular cellular networks on a realistic timescale. Taken together, these results show that VEGF binds to matrix molecules in proximity of HUVECs in Matrigel, and suggest that bound VEGF drives vascular network patterning. Gao et al. [118] shows the diffusive process of free receptors on a flat membrane wrapping around an infinitely long cylindrical and spherical ligand-coated particle. Golestaneh and Nadler presented a work [119] about the deformation and adhesion behaviors of cells in the presence of receptors and ligands by improving the existing models as Boal [120] and others authors. An isotropic continuum fluid membrane model was proposed for the cell membrane based on membrane theory. This novel constitutive model engaged the intensity of the presence of receptors on the deformation and adhesion of the cell through introduction of spontaneous area dilation. Additionally a nonlinear binding force relation was proposed based on charge-induced dipole interaction between receptors and ligands, which was enriched by a consideration of shielding phenomenon which is in agreement with intrinsic behavior of bonds. Therefore the diffusion of the receptors on the cell membrane was formulated under the influences of receptor-receptor and receptor-ligand interactions. The current study was allocated to investigate the adhesion and deformation of a cell by applying the developed model. Additionally, the influences of variety of membrane, binding and electrolytic constitutive coefficients on the cell adhesion and deformation behaviors were investigated. The results obtained shown that the ligands density on the substrate has strong effect on the adhesion and deformation of the cell. The novelty in this work is the introduction of the intrinsic membrane area dilation due to the presence of receptors [119]. A general model for the dynamic rearrangement of the cytoskeleton that incorporates cell contractility has been presented by Deshpande et al. [146]. It is shown that the model captures the general contractile features observed in experimental studies including: (i) the decrease of the forces generated by the cell with increasing substrate compliance, (ii) the influence of cell shape and boundary conditions on the development of structural anisotropy, and (iii) the high concentration of the stress fibers at the focal adhesions [146]. The model has been extended to account for additional phenomena, such as focal adhesion formation with the stresses in the connecting fibers [147]. More recently, the study presented by Ronan et al. couples a mixed mode thermodynamic and mechanical framework, in a fully 3D implementation, that predicts focal adhesion formation and growth with a material model that predicts stress fibre formation, contractility [148].

Glossary

AIDS Acquired Immunodeficiency Syndrome
Ang Angiopoietin
ADP Adenosine Diphosphate
ATP Adenosine Triphosphate
BMP/R Bone Morphogenetic Protein/BMP Receptors
Dll4 Delta-like-ligand-4
EC Endothelial Cell
ECM Extracellular Matrix
FRAP Fluorescence Recovery After Photobleaching
FA Focal Adhesion
FAK Focal Adhesion Kinase
FGF Fibroblast Growth Factor
GAG Glycosaminoglycan
HSPG Heparan Sulphate Proteoglycans
IFN-α Interferon-α
PDGF/PDGFR Platelet Derived Growth Factor /PDGF Receptor
PLGF Placenta Growth Factor
TGF-β Transforming Growth Factor-β
TKR Tyrosine Kinase Receptor
TNF-α Tumor Necrosis Factor-α
VEGF/R Vascular Endothelial Growth Factor / VEGF receptor
VPF Vascular Permeability Factor

Chapter 2

Experiments and data

2.1 Introduction

The following Chapter includes a brief description of the experiments and the analysis employed in our research, as Fluorescence Recovery After Photobleachig (FRAP), Surface Plasmon Resonance (SPR) and time-lapse analysis, to investigate phenomena that are occurring on the cell membrane. These experiments were conducted to determine the parameters necessary to run computational simulations. Some parameters values were extracted from the current literature as well. The following parameters have been investigated: the concentrations of the species involved in function on the time, receptor diffusivity coefficient, cell radius, thermodynamic parameters (equilibrium constant, Gibbs free energy). Mechanical properties (elastic modulus) of endothelial cells and kinetics constants in a bulk solution are previously described in Chapter 1. Understanding the experimental procedures, the environmental and boundary conditions of living cells, is essential to be able to characterize the system.

2.2 Biological background on cell membrane

The plasma membrane surrounds the cell boundaries and separates the cytosol and the extracellular environment. It takes many kinds of membrane proteins to enable a cell to communicate with its environment [3]. At this aim, the plasma membrane contains proteins (e.g. VEGF receptors) that act as sensors of external signals (e.g. VEGF or Gremlin), allowing the cell to change its behavior in response to environmental cues [3]. These proteins or receptors working as sensors, transferring information across the membrane reaching the nucleus and modifying its DNA. Some proteins work as links, connecting the cytoskeleton to the ECM (e.g. integrins, described below), while others serve as receptors to detect and transduce chemical signals in the cell's environment.
Biological membranes have a common structure: each is a very thin film of lipid and protein molecules, held together primarily by noncovalent interactions [3]. Cell membrane is a dynamic and fluid system because is constituted by lipid molecules, which yield the basic fluid structure of the membrane. This structure is called **lipid bilayer**, composed by a double layer of 5 nm thick, serving as a impermeable barrier to the transit of water-soluble molecules (Figure 2.1).

The most abundant membrane lipids are phospholipids. These have a polar head group containing a phosphate group and two hydrophobic hydrocarbon tails (Figure 2.2). In addition, lipid bilayer contains glycolipids and cholesterol. Glycolipids are sugar-containing lipid molecules, and instead of a phosphate-linked head group, they have sugars attached [3].
Generally, lipid molecules, in a cell membrane, are small compared to protein molecules, and there are always a large additional number of lipid molecules than protein molecules (about 50 lipid molecules for each protein molecule in cell membranes that are 50% protein by mass) [3]. Membrane proteins have several different functions because are not identical in structure and in the way they associate with the lipid bilayer [3]. The fluidity of a lipid bilayer depends on both its composition and its temperature, and it can be observed a phase
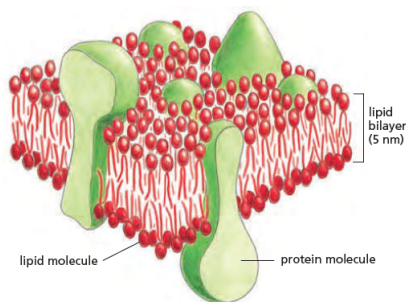
Figure 2.1: A three-dimensional schematic view of a cell membrane and the general arrangement of its lipid and protein constituents. Source [3].
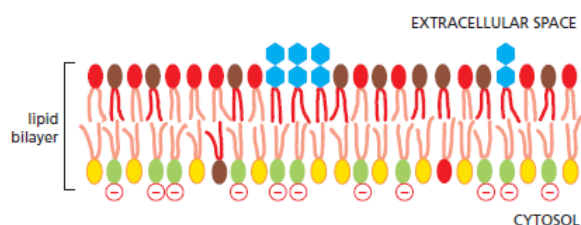
Figure 2.2: A two-dimensional view of a cell membrane. Source [3].

segregations in which specific lipids form separated domains, called **lipid rafts**. In 1972 the fluid-mosaic membrane model of membrane structure was put foward by Singer and Nicolson, built on thermodynamic fundamentals of organization of membrane lipids and proteins and their lateral mobility within the cell membrane structure [124]. Outcomes to the relationship among growth factor receptors and lipid rafts are described in [125] and it is presented a model for understanding the different observations regarding the role of membrane microdomains in the regulation of growth factor receptor functions.

Lipid rafts have been shown to affect cancer cell migration [126], but the underlying mechanisms are still not well understood. Lipid rafts can control the dynamics of actin cytoskeleton and focal adhesion in cell migration [126] and may regulate the signal transduction [127]. Experimental evidence [127] suggests that there are probably several different mechanisms through which rafts control cell signaling. For istance, lipid rafts may include incomplete signaling pathways that are triggered when a receptor is recruited into the raft [127].

Lateral diffusion. Many membrane proteins extend through the lipid bilayer, and hence are called transmembrane proteins, with part of their mass on either side. Cell-surface receptors are usually transmembrane proteins that stick to ligands in the ECM and generate different intracellular signals inside the cytosol matrix [3]. These proteins are able to move laterally within the cell membrane. The lateral motility of cell-surface receptors is sustained by their localization in microdomains and by cytoskeletal interactions [128]. Studies demonstrate [128] how cells direct different cytosolic signaling pathways although initiated by the same ligand. It is possible to alter the lateral diffusivity of cell-surface receptors by changing membrane fluidity, cooperation with cytoskeletal elements, scaffolding proteins, or membrane components allows for specific downstream signaling pathways and concludes in distinct cellular reactions [128, 129]. It is well-known that cytoskeleton can affects cell membrane receptor diffusivity. Lateral diffusion rates of membrane proteins can be measured by using the technique of fluorescence recovery after photobleaching, described later, and single molecule tracking.

Protein dynamics. A central challenge for biology research is to understand the wide networks of proteins interplay that module and control cellular processes. Proteins are necessary for most biological processes, but knowing their function is awkward because proteins inside cells are not just objects with chemically reactive surfaces. They localize to specific environments (that is, membranes, cytosol, organelle lumen or nucleoplasm), undergo diffusive movement, and often have mechanical parts and are coupled to chemical events [130, 131]. The discovery and development of Green Fluorescent Protein (GFP) from the jellyfish *Aequorea victoria*, and more recently Red Fluorescent Protein (DsRed) from the sea *anemone Discosoma striata*, have revolutionized the research ability to analyse protein localization, dynamics and interactions in living cells [130, 132]. In so doing, these fluorescent proteins allow the investigation of molecule functions within the complex environment of the cell. Any protein can be tagged with GFP, a β-barrel-shaped

23

protein that contains an amino-acid triplet (Serine-Tyrosine-Glycine) that undergoes a chemical rearrangement to form a *fluorophore*. A fluorophore (or fluorochrome, similarly to a chromophore) is a fluorescent chemical compound that can re-emit light upon light excitation. Advances in GFP reserch, for instance the optimization of the expression of GFP in different cell types and the identification of their variants with more favourable spectral properties, including increased brightness, relative resistance to the effects of pH variation on fluorescence, and photostability [130, 132], has been helpful for this research field. Paralleling to these developments, others progress in fluorescence imaging methods and microscope systems are crucial to visualize the localization of GFP fusion proteins, to quantify their concentrations and to investigate their mobility and interactions.

2.3 Experiments

2.3.1 Fluorescence Recovery After Photobleachig (FRAP) analysis

The mobility of a fluorescent protein can be evaluated using a specific type of photobleaching technique called fluorescence recovery after photobleaching (FRAP). In a typical FRAP experiment, a fluorescent molecule is irreversibly bleached within a small region of interest (ROI) using high intensity laser light. Fluorescence recovers the group of bleached molecules by replacing through unbleached molecules from outside the ROI [130, 133, 134]. GFPs are ideal for using them in FRAP analysis because they can be bleached without noticeable damage of the cell. From quantitative FRAP studies, two kinetic parameters of a protein can be obtained: the mobile fraction, M_f, which is the fraction of fluorescent proteins that can diffuse into the bleached region during the time span of the experiment, and the diffusion constant D, which is a measure of the rate of protein motion with no presence of flow or active transport. D describes the mean squared displacement that a protein traverses through a random path on time and has unit of measure area per time $[\mu m^2\,s^{-1}]$. A typical FRAP curve, which provides information on D and M_f is shown in Figure 2.3(a). The mobile fraction provides a measure of the extent to which the fluorescent protein can move within cells. It is determined by calculating the ratio of the final to the initial fluorescence intensity in the bleached region, corrected for the amount of fluorescence removed during photobleaching. When the mobile fraction is less than 100%, some fluorescent molecules might be irreversibly bound to a fixed/anchored substrate. Alternatively, non-diffusional factors, such as diffusion barriers or discontinuites within the structure where a protein localizes, might be responsible for the lower mobility [130].
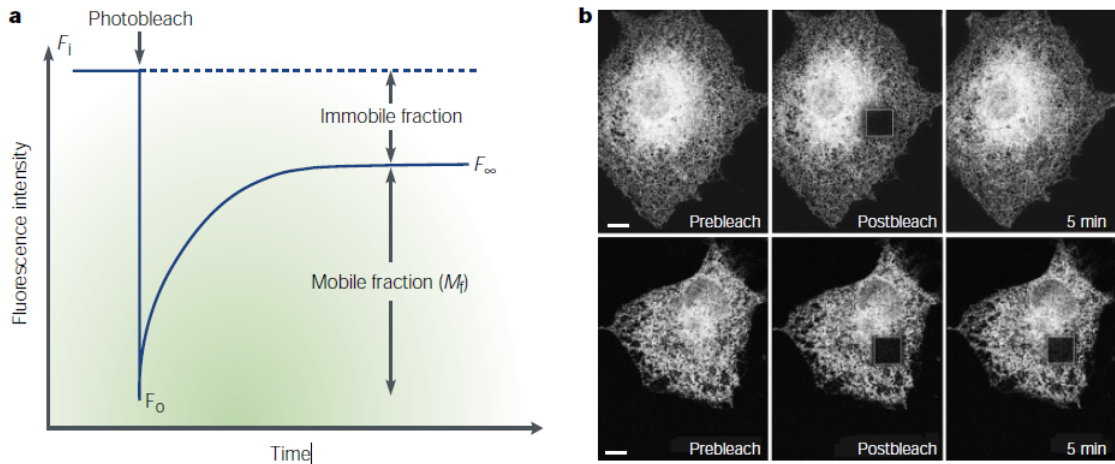
Figure 2.3: Fluorescence recovery after photobleaching. (a) Plot of fluorescence intensity in a region of interest versus time after photobleaching a fluorescent protein. (b) Example of cells expressing vesicular stomatitis virus envelope glycoprotein VSVG-GFP in the endoplasmic reticulum under control conditions (top panel) or in the presence of tunicamycin, a mixture of homologous nucleoside antibiotics (bottom panel) [130].

Diffusion theory. The diffusion constant for a particle in a free volume is described by the Stokes-Einstein formula:

$$\mathbb{D} = \frac{k\,T}{6\,\pi\,\eta\,\ell} \tag{2.1}$$

where $\mathbb{D}$ is the diffusion constant, T is the absolute temperature, η is the viscosity of the solution, k is the Boltzmann's constant and ℓ is the molecule radius. Absolute temperature is usually constant within cells, then the main factors underlying $\mathbb{D}$ are the radius of a protein and the viscosity of the environment within which it is diffusing. Membranes have a much higher viscosity than cytoplasm, because the presence of the cholesterol, then the lateral diffusion of a protein embedded in the cell membrane is slower than soluble protein diffusivity within cytoplasm [130]. Even though viscosity and cell radius are key properties, other factors have an important role in determining protein diffusion rates. These include protein-protein interactions or binding to a matrix that might slow or immobilize a protein, and collisions with other molecules, which hinder free diffusion. Such factors often prevent proteins from diffusing at their theoretical limit inside cells. For this reason, the value of $\mathbb{D}$ by FRAP analysis must be carefully interpreted [132].

2.3.2 Surface Plasmon Resonance (SPR) experiment

The use of biosensors employing surface plasmon resonance (SPR) provides excellent instrumentation for a label-free and for real-time probe of biomolecular interactions. SPR is a powerful technique for monitoring the affinity and selectivity of biomolecular interactions, for analysis of association and dissociation rate constants and modeling of biomolecular interaction kinetics, as well as for equilibrium binding analysis [135].
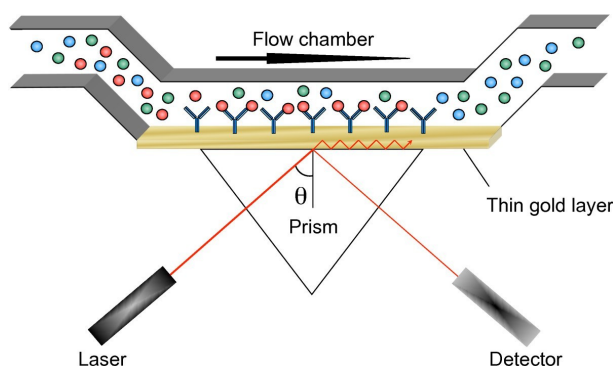
Figure 2.4: A typical SPR setup is shown for one flow cell in a SPR instrument. The gold surface of a sensor surface can be modified chemically to allow the attachment of biomolecule of interest. The analyte is then injected and flowed over the chip surface to detect its binding with the chip-immobilized protein.
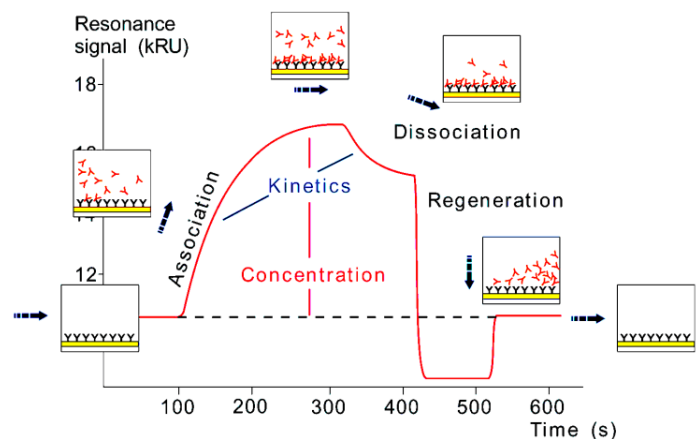
Figure 2.5: In the sensor device, the binding between the analyte and the immobilized molecule, is continusly monitored. From the plot shown in this Figure it is possible the extraction of kinetics constants.

The SPR theory is based on a physical process of light-metal film interaction, shown in Figure 2.4. A material having a high refractive (with respect to medium) index is coated with thin gold layer. This

material is treated with monochromatic light with a specific angle and some of the energy is transferred to free electron of the gold layer and forms surface plasmons. This plasmon will end up with specific refractive index. Immobilized proteins can be attached to the gold surface with a material. An analyte, molecule in the soluble phase, is sent through the channels and if association or dissociation (Figure 2.5) happens between the immobilized material and analyte the refractive index will be changed which we can measure with high precision in real time. This phenomenon can be used for the biomolecule detections.

2.3.3 Time-lapse analysis

Considerable improvement in optics hardware, electronic imaging sensors, and a wealth of fluorescent probes and labeling methods, light microscopy, over the past decades, has allowed sensitive time-lapse imaging of cells and single molecules. The time-lapse imaging studies consist of four successive steps: 1) planning of the experiment and acquisition of the image data, 2) preprocessing of the data to correct for systemic as well as random errors and to enhance relevant features, 3) analysis of the data by detecting and tracking the molecules significant to the biological questions underlying the study, and 4) analysis of the resulting trajectories to test predefined hypotheses or detect new phenomena. Time-lapse experiments involve the acquisition of not only spatial information, but also temporal information.

2.4 Results

2.4.1 Receptor diffusivity $\mathbb{D}_R$ from FRAP analysis

In order to measure the VEGFR-2 diffusivity $\mathbb{D}_R$ on the cell membrane, we performed FRAP analysis on EC culture expressing Enhanced Yellow Fluorescent Protein (EYFP)-labeled extracellular domain (ECD) of VEGFR-2 (ECD-VEGFR2-EYFP). The rate of fluorescence recovery provides quantitative information about the kinetics of diffusion of fluorescent molecule in the photo-bleached area. To measure the dynamics of VEGFR-2 on the cell membrane, fluorescence was recorded every minute for 10 minutes in an irreversibly photo-bleached membrane region of ECD-VEGFR2-EYFP EC in the absence or in the presence of 50 ng/mL of VEGF-A or Gremlin. In our experimental conditions, 77% of ECD-VEGFR2-EYFP in the plasma membrane turns out to be in a mobile form, with a lateral diffusion coefficient of $\mathbb{D}_R = 0.198 \, \mu m^2 \, s^{-1}$ in untreated ECs. Both VEGF-A or Gremlin treatments decrease the receptor mobility respectively to $0.098 \, \mu m^2 \, s^{-1}$ and $0.052 \, \mu m^2 \, s^{-1}$ (Fig. 2). All these data highlight, shown in our work [137], that non-activated receptors are mainly free to move on the cell membrane, thus suggesting that VEGFR-2 phosphorylation, its dimerization, and its interaction with membrane co-receptors or intracellular signaler reduce its motility. FRAP data support our former observations [136] that VEGFR-2 is rapidly recruited and immobilized in the membrane in close contact with ligands. These events lead to increase the receptor concentration in the basal side of the cell.

2.4.2 Ligand concentration from SPR analysis

Measures from SPR lead the ligand concentration of $620 \, \text{RU}$, where ligand is the analyte injected in the flow chamber; RU is the unit of measure which means Resonant Unit where $100 \, \text{RU} = 0.10 \frac{\text{ng}}{\text{mm}^2} = 0.10 \cdot 10^{-15} \frac{\text{g}}{\mu\text{m}^2}$. Then the ligand concentration measured by SPR is given by

$$c_L^{SPR} = 620 \, \text{RU} = 0.620 \frac{\text{ng}}{\text{mm}^2} = 0.620 \cdot 10^{-15} \frac{\text{g}}{\mu\text{m}^2} \tag{2.2}$$

The ligand weight, W_L, is measured as $22 \div 24 \, \text{kDa} = 22000 \div 24000 \, \text{Dalton}$, that in grams means $W_L = (22000 \div 24000) \cdot 1.6605 \cdot 10^{-27} \cdot 10^3 \, \text{g}$.

First of all, it is necessary to calculate the ligand molar weight M_L, measured in $[\frac{\text{g}}{\text{mol}}]$ as the product of the ligand weigth and the Avogadro's number N_A, which leads to

$$M_L = W_L \cdot N_A = (22000 \div 24000) \cdot 1.6605 \cdot 10^{-27} \cdot 10^3 \, \text{g} \cdot 6.02214129 \cdot 10^{23}, \tag{2.3}$$

and by using the average of the molecule weight, M_L becomes
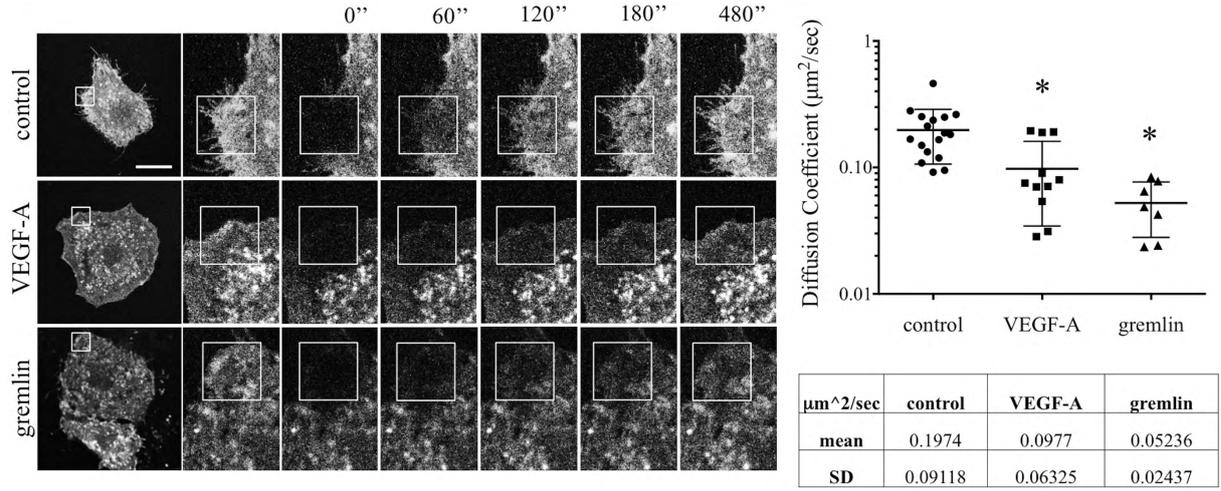
Figure 2.6: VEGF-A and Gremlin reduce VEGFR-2 motility on EC surface. (A) FRAP analysis was performed on cell plasma membrane of serum-starved ECD-VEGFR2-EYFP over-expressing ECs treated or not with VEGF-A or Gremlin. Images were acquired at one per minute for 12 minutes, 2 before and 10 after bleaching. The bleached area is indicated by a square and the recovery time is indicated over the images as seconds after photobleaching. (B) Collected images were analyzed using simFRAP ImageJ plugin to calculate diffusion coefficients. The graph shows diffusion coefficient mean s.d. of control, VEGF-A, and Gremlin treated cells [137].

$$M_L = 23000 \cdot 1.6605 \cdot 10^{-27} \cdot 10^3 \, \text{g} \cdot 6.02214129 \cdot 10^{23} = 22999.48 \frac{\text{g}}{\text{mol}} \tag{2.4}$$

Then, the initial concentration of ligands $\left[\frac{\text{mol}}{\mu\text{m}^2}\right]$ is as follows

$$c_L^{in} = \frac{c_L^{SPR}}{M_L} = \frac{0.620 \cdot 10^{-15} \frac{\text{g}}{\mu\text{m}^2}}{22999.48 \frac{\text{g}}{\text{mol}}} = 2.69 \cdot 10^{-20} \frac{\text{mol}}{\mu\text{m}^2} \tag{2.5}$$

The density of ligands, considered as a dimeric molecule which bounds two receptors, which are monomeric molecules, is given by

$$c_L^{in} = 2.69 \cdot 10^{-20} \frac{\text{mol}}{\mu\text{m}^2} \cdot N_A = 2.69 \cdot 10^{-20} \cdot 6.022 \cdot 10^{23} = 16.20 \cdot 10^3 \frac{\text{ligands}}{\mu\text{m}^2}. \tag{2.6}$$

2.4.3 Time-lapse analysis to asses the VEGFR-2 recruitment

Time-laspse experiments have been conducted to analyze VEGFR-2 recruitment. ECD-VEGFR2-EYFP co-expressing GM7373 cells[1] were cultured on glass coverslips that were flipped upside-down on Gremlin- or fibrinogen- coated microslides. The coating process, shown in Figure 2.7, is how the EC surface was covered with ligands. Time-lapse analysis of Z-stack sections was performed to follow the recruitment of VEGFR-2 at the basal side of cells during cell adhesion to the substratum. As shown in Figure 2.8, VEGFR-2 rapidly moved to the membrane portion in close contact with immobilized Gremlin (specific ligand for VEGFR-2) but not with fibrinogen (FG) (a specific ligand for $\alpha_v\beta_3$ integrin but not for VEGFR-2). VEGFR-2 recruitment driven by Gremlin was already detectable 6 to 8 minutes after EC/Gremlin interaction [136].

The time-lapse analysis provides us normalized fluorescence intensity on substratum during cellular adhesion after 120 minutes. For the case of interest, we used the values for the VEGFR-2 recruitment with immobilized Gremlin on the substrate shown on Table and Figure 2.8 A".

---

[1]Foetal bovine aortic endothelial GM7373 cells were grown in Dulbecco's modified Eagle medium containing vitamins, essential and non-essential amino acids[136].
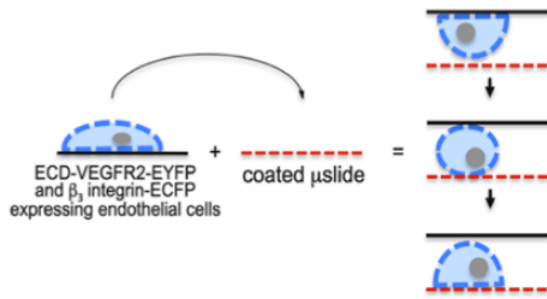
Figure 2.7: Endothelial cells cultured on glass coverslips that are flipped upside-down on Gremlin- or fibrinogen- coated microslides. [136]
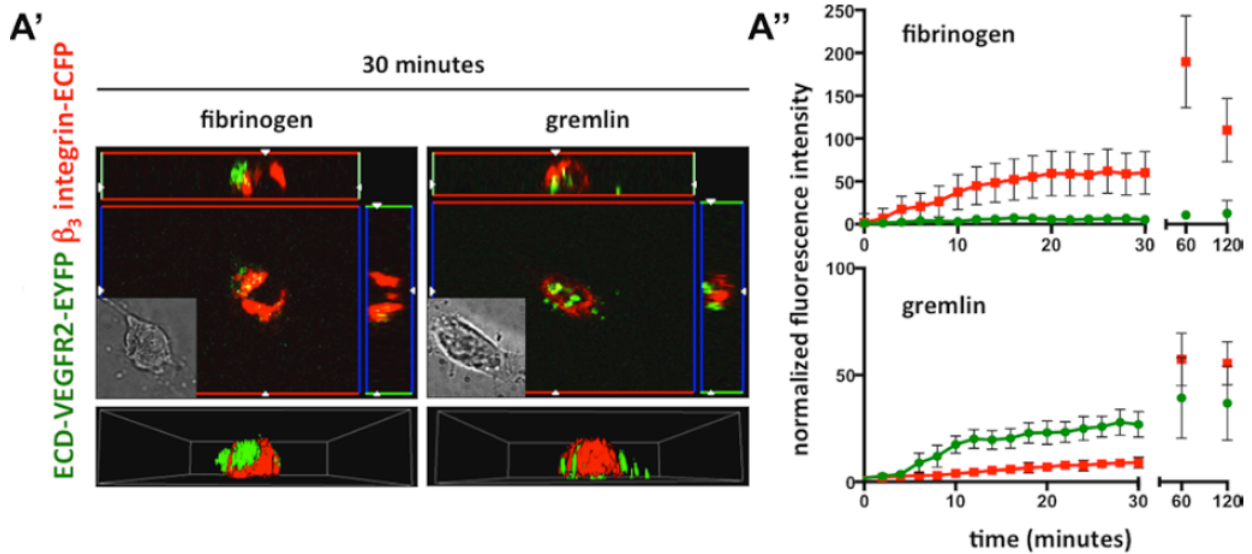
Figure 2.8: A'. Images show ECD-VEGFR2-EYFP (green) and β3-ECFP (red) distribution at the basal portion of cells in contact with the fibrinogen- or Gremlin-coated surface at 30 minutes with a 3D reconstructions. A". Quantification of normalized fluorescence of ECD-VEGFR2-EYFP (green lines) and β3-ECFP (red lines) on FG- or Gremlin-coated surfaces during cell adhesion [136].

ECD-VEGFR2-EYFP co-expressing GM7373 cells were seeded and cultured on coverslips for 24 hours in FCS-free Endothelial Cell Basal Medium. Coverslips were then flipped on immobilized Gremlin or FG coated μslides. Z-stack images in time-lapse were recorded for 120 minutes using a Zeiss Axiovert 200M epifluorescence microscope equipped with a Plan-Apochromat 63x/1.4 NA oil objective and ApoTome system. The data have been used to determine key parameters and information that will be explained in the next chapters. The fluorescence intensity is proportional to the total receptor (free plus bound) concentration on the cell membrane.

time [min]	normalized fluorescence of VEGFR-2
0	$1,8125$
2	$2,6775$
4	$3,6175$
6	$8,8875$
8	$12,0225$
10	$17,4375$
12	$20,1325$
14	$19,665$
16	$20,4075$
18	$22,86$
20	$23,0375$
22	$23,2725$
24	$24,915$
26	$25,865$
28	$27,88$
30	$26,9075$
60	$39,271833$
120	$36,814$

Furthermore, another experiment to assess whether VEGFR-2 redistributes on the EC membrane when challenged by free ligands has been performed. Adherent ECs over-expressing the ECD-VEGFR2-EYFP were exposed for 2 hours to a linear concentration gradient of free ligands, including Gremlin or VEGF-A, in a 2D chemotaxis assay. Figure 2.9A shows that ECD-VEGFR2-EYFP is equally distributed on non-treated ECs (t_0), while the gradient of ligands induces the ECD-VEGFR2-EYFP to be recruited in the lamellipodia at the leading edge of migrated ECs (t_{30}). Together, these data demonstrate that free ligands are able to induce EC polarization, leading to VEGFR-2 relocation on the surface of ECs. Although VEGFR-2 ligands are usually considered as soluble molecules, in vivo they are bound and immobilized in the ECM or on the cell membrane by heparan-sulphate proteoglycans. To characterize the influence of the immobilized VEGFR2-ligands on the VEGFR-2 rearrangement on the cell membrane, we plated ECs on ligand-coated cell plates. Similarly to immobilized Gremlin, immobilized VEGF-A induces the recruitment of VEGFR-2 to the plasma membrane at the basal aspect of ECs, thus leading to a localized and directional receptor activation (Fig. 2.9B). The concentration of VEGFR-2 at the apical side of the cell is diminished by the recruitment of VEGFR-2 at the basal portion of adherent cells, as demonstrated by the reduction of soluble ligand binding ability (Fig. 2.9C).

2.4.4 Final stationary value x_∞

VEGFR2-GM7373 cells were seeded on substrate-bound FG (Figure 2.10 a) or Gremlin (Figure 2.10 b). After 4 hours, cells were washed and incubated with free Gremlin for 90 minutes at $4°$ C. Then, cells were washed three times with phosphate buffered saline (PBS)[2] or with PBS plus 1.5 $\frac{mol}{L}$ NaCl to remove Gremlin bound to heparan sulfate proteoglycans. Finally, VEGFR2-bound Gremlin was detected by immunofluorescence analysis. The apical portion of immunostained cells was photographed using a Zeiss Axiovert 200M epifluorescence microscope equipped with a Plan-Apochromat 63X/1.4 NA oil objective and ApoTome system and apical VEGFR2-bound Gremlin was quantified in 20 cells/sample using AxioVision Extended Focus module and Image-Pro Plus software (Figure 2.10 c). Data are expressed as percentage $\pm$ s.d. of Gremlin positive area in respect to the total cell area.

---

[2]Phosphate buffered saline (PBS) is a balanced salt solution commonly used in the bio-laboratory. The essential function of a balanced salt solution is to maintain pH and osmotic balance as well as provide cells with water and essential inorganic ions. PBS is generally utilized to maintain cells for the short term in a viable condition while the cells are manipulated outside of their regular growth environment. One of the early formulas of PBS was developed by Renato Dulbecco, published in 1954 [138] which are termed DPBS for Dulbecco's phosphate buffered saline.
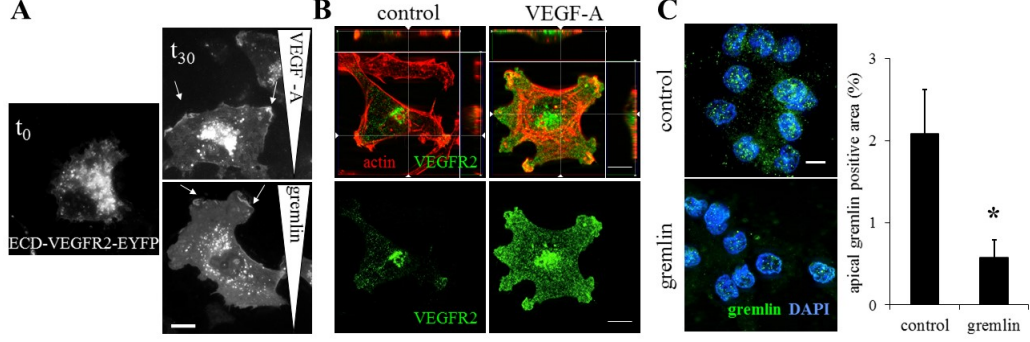
Figure 2.9: VEGF-A and Gremlin induce VEGFR2 rearrangement on EC surface. (A) ECD-VEGFR2-EYFP ECs were stimulated by a VEGF-A or Gremlin gradient for 2 hours, fixed and analysed using a Zeiss Axiovert 200M system. Arrows indicate ECD-VEGFR2-EYFP-enriched cell lamellipodia. (B) HUVECs adherent on Fibrinogen or VEGF-A-enriched substrates were stained for VEGFR-2 (green) and actin (red) and analysed using a LSM510 Meta confocal microscope. Images show the basal portion of adherent cells with the orthogonal z reconstruction of the whole cell (630; white bar: 10 m). (C) VEGFR2-EC, seeded on immobilized Gremlin or on coverglass for 4 hours, were incubated with 150 ng/mL of Gremlin for 90 minutes at 4 °C and washed with NaCl. VEGFR2-bound Gremlin, in the apical portion of the cells, was detected by immunofluorescence analysis using a Zeiss Axiovert 200 M microscope system (630x; white bar: 10 μm). Data are expressed as percentage $\pm$ s.d. of Gremlin positive area with respect to the total cell area (n = 20 cells/sample) [137].

When there is not VEGFR-2 recruitment, just the 2% of the apical side of ECs is covered by receptors, while when there is VEGFR-2 recruitment, just the 0.57% of the apical side is coated. In fact, for the case of interest, these data provide evidence for the final stationary value $x_\infty = 0.73$ furnished by the ratio of these values.

2.4.5 Receptor concentration

From the current literature, we achived the value of the receptors on the surface of the cell equal to 7000 ± 1700 binding sites/cell, from experimental evidence [31]. The binding sites are refered at the monomeric molecule but we have the ligands which are dimeric molecule; for this reason, the receptor density is multipied by the factor two.

From experimental evidence, the cell radius is taken $\ell = 20\,\mu$m, and the cell area $A = 4\,\pi\ell^2 = 5026\,\mu$m^2, by assuming a spherical geometry. The initial concentration of receptors is as follow

$$c_R^{in} = 2 \cdot \frac{7000 \pm 1700\,\text{receptor/cell}}{A \cdot N_A} = 4.3 \cdot 10^{-24}\,\frac{\text{mol}}{\mu\text{m}^2} \tag{2.7}$$

Then, the receptor density is given by

$$c_R^{in} = 2 \cdot \frac{7000 \pm 1700\,\text{receptor/cell}}{A} = (2.78 \div 3.46)\,\frac{\text{receptor}}{\mu\text{m}^2}\,. \tag{2.8}$$

2.4.6 Gibbs free energy and equilibrium constant

From the activation energy of the VEGF/VEGF-2 interactions in [139], display in Figure 2.11, the average of the Gibbs free energy ΔG is given by

$$\Delta G = -(8.9 + 8.6 + 8.5 + 8.3 + 7.5 + 7.1 + 7.5 + 6.6)/8 = -7.875\,\frac{\text{kcal}}{\text{mol}} = -32949\frac{\text{J}}{\text{mol}} \tag{2.9}$$
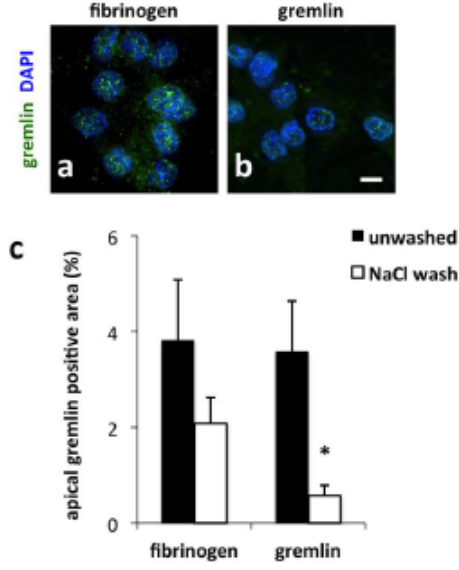
Figure 2.10: VEGFR-2 recruitment by substrate-bound Gremlin decreases its density at the apical side of ECs [137].

Table 1. Thermodynamic parameters of VEGF/VEGFR-2 interactions determined by ITC*

	N	K_d, µM	ΔG, kcal/mol	ΔH, kcal/mol	$-T\Delta S$, kcal/mol	c†
VEGF-A$_{121}$/VEGFR-2 D23	2.01	0.093	−8.9	6.6	−15.5	281
VEGF-A$_{165}$/VEGFR-2 D23	1.89	0.17	−8.6	6.5	−15.1	150
VEGF-C/VEGFR-2 D23	1.91	0.20	−8.5	12.0	−20.5	131
VEGF-E/VEGFR-2 D23	2.21	0.28	−8.3	13.2	−21.5	91
VEGF-A$_{121}$/VEGFR-2 ECD	1.97	1.12	−7.5	10.4	−17.9	57
VEGF-A$_{165}$/VEGFR-2 ECD	2.06	2.67	−7.1	12.5	−19.6	24
VEGF-C/VEGFR-2 ECD	1.9	1.21	−7.5	14.8	−22.3	53
VEGF-E/VEGFR-2 ECD	2.09	5.99	−6.6	17.7	−24.3	11
			$\Delta\Delta G$, kcal/mol	$\Delta\Delta H$, kcal/mol	$-T\Delta\Delta S$, kcal/mol	
VEGF-A$_{121}$‡			1.4	3.8	−2.4	
VEGF-A$_{165}$‡			1.5	6.0	−4.5	
VEGF-C‡			1.0	2.8	−1.8	
VEGF-E‡			1.7	4.5	−2.8	

N indicates the stoichiometry of ligand/receptor complexes.
*Error estimation: N, ± 0.01; K_d, ± 5%; ΔG, ΔH, and $-T\Delta S$, ± 0.5 kcal mol⁻¹.
†The c value is calculated as: c = N*[R2]/K_d.
‡$\Delta\Delta$ values represent the difference between the ΔG/ΔH/−TΔS values between the full-length ECD and the D23 ligand complexes.

Figure 2.11: Thermodynamic parameters of VEGF/VEGFR-2 interactions determined by isothermal titration calorimetry (ITC), namely a physical technique used to determine the thermodynamic parameters of interactions in solution [139].

This value will be used to determine the equilibrium constant, by using the equation [140]

$$K_{\text{eq}}(T) = \exp\left(-\frac{\Delta G(T)}{RT}\right) \tag{2.10}$$

with the temperature $T = 37°C = 310.15°K$ and the gas constant $R = 8.3144621 \frac{\text{J}}{\text{mol}\,°\text{K}}$.

2.5   Conclusion

Time-laspse experiments have been performed to analyze VEGFR-2 recruitment on the EC membrane. Both immobilized Gremlin and immobilized VEGF-A induce the relocalization of VEGFR-2 to the plasma membrane at the basal aspect of ECs, thus leading to a localized and directional receptor activation. The major outcome are that VEGFR-2 has a lateral mobility of about $\mathrm{D}_R = 0.198\,\mu m^2\,s^{-1}$, as measured by

means of FRAP experiments, and that free and ECM-immobilized ligands induce VEGFR-2 rearrangement on EC plasma membrane. After ligand interaction, VEGFR-2 dimerizes and transduces an intracellular signaling via its relocation on the cell membrane and the recruitment of intracellular proteins. All these data, collected in our work [137], highlight that non-activated receptors are mainly free to move on the cell membrane, thus suggesting that VEGFR-2 phosphorylation, its dimerization, and its interaction with membrane co-receptors or intracellular signaler may reduce its motility.

Chapter 3

Receptor-ligand thermodynamical model

3.1 Introduction

We propose a preliminar thermodynamic model which describe the VEGFR-2 relocation driven by growth factors justified by experimental evidence previously described. In particular, we are referring to the time lapse analysis that provide the receptor diffusion during cellular adhesion to the gremlin-immobilized substrate after two hours. We are interested in kinetics and diffusion that are confined to two dimensions, by trying to develop a tecnique to infer key parameters from experimental measurements suitably interpreted through an reaction-diffusion model. The main challenge of our research may be to understand the VEGFR-2 mobility and the features that influence its relocation to predict the receptor behavior in order to control its movement toward the abluminal part of the endothelial cell membrane. Our preliminary model of the process focuses only on the reaction and diffusion of VEGFR-2, with a very simplified geometry and a cell-substrate contact dynamics. Receptor and ligand are schematically represented as the reactants of a single chemical reaction which produces the receptor-ligand complex.

3.2 VEGFR2-ligand thermodynamical model

3.2.1 Stoichiometry and chemical kinetics

Let us introduce notation [140] for a generic reaction scheme

$$\sum_i \nu_i^{(j)} A_i = 0; \quad i = 1, \ldots, r; \quad j = 1, \ldots, s \tag{3.1}$$

where A_i are the species symbols, r the species number and j the number of chemical reactions. Rewriting the j-th reaction as

$$\sum_i \nu_i^{+j} A_i = \sum_i \nu_i^{-j} A_i \tag{3.2}$$

ν_i^{+j} are the forward stoichiometric coefficients and ν_i^{-j} the backward coefficients of the j-th reaction,

$$\nu_i^{(j)} = \nu_i^{-j} - \nu_i^{+j} \tag{3.3}$$

the net stoichiometric coefficients. Denoting concentrations by c_i from standard chemical kinetics, we may write the net rate of reaction j as

$$r_j = k_j^+(T) \prod_i (c_i)^{\nu_i^{+j}} - k_j^-(T) \prod_i (c_i)^{\nu_i^{-j}} = r_j^+ - r_j^- \tag{3.4}$$

where $k_j^+(T)$ and $k_j^-(T)$ are the forward and backward reaction rate constants at temperature T, and the net density of production (if positive) or consumption (if negative) of species i,

$$w_i = \sum_j \nu_i^{(j)} r_j \tag{3.5}$$

At equilibrium, the law of mass action is

$$K_{\text{eq}}^c(T) = \prod_i (c_i)^{\nu_i^{(j)}} \tag{3.6}$$

where $K_{\text{eq}}^c(T)$ is the equilibrium constant based on the concentrations.
By the principle of detailed balance, we have, at any temperature T

$$k_j^-(T) = \frac{k_j^+(T)}{K_{\text{eq}}^c(T)} \tag{3.7}$$

so that we may write

$$r_j = k_j^+(T) \left[\prod_i (c_i)^{\nu_i^{+j}} - \frac{1}{K_{\text{eq}}^c(T)} \prod_i (c_i)^{\nu_i^{-j}} \right] \tag{3.8}$$

The above assumes low concentrations, but can be generalized to high concentrations as follows. Denoting activities by a_i, interpreted as "effective concentrations", we rewrite the net rate of reaction j as

$$r_j = \widetilde{k}_j^+(T) \prod_i (a_i)^{\nu_i^{+j}} - \widetilde{k}_j^-(T) \prod_i (a_i)^{\nu_i^{-j}} \tag{3.9}$$

Next we write chemical potential as

$$\mu_i = \mu_i^0(T) + RT \ln a_i \tag{3.10}$$

and we insert them in the general chemical equilibrium condition for reaction j

$$\sum_i \nu_i^{(j)} \mu_i^{\text{eq}} = 0 \tag{3.11}$$

to obtain

$$\sum_i \nu_i^{(j)} \mu_i^0(T) + RT \sum_i \nu_i^{(j)} \ln a_i^{\text{eq}} = 0 \tag{3.12}$$

that is

$$\prod_i (a_i^{\text{eq}})^{\nu_i^{(j)}} = K_{\text{eq}}(T) \tag{3.13}$$

where

$$K_{\text{eq}}(T) = \exp\left(-\frac{\Delta G^o(T)}{RT}\right) \tag{3.14}$$

where $\Delta G^o(T)$ is the standard Gibbs free energy given by

$$\Delta G^o(T) = \sum_i \nu_i^{(j)} \mu_i^0 \tag{3.15}$$

Inserting a_i^{eq} in Eq. (3.9), from the condition $r_j = 0$ at the equilibrium, we obtain the detailed balance relation

$$\frac{\widetilde{k}_j^+(T)}{\widetilde{k}_j^-(T)} = K_{\text{eq}}(T) \tag{3.16}$$

One possible choice for the dependence of the activity on concentration is

$$a_i = \frac{\frac{c_i}{c_i^{\max}}}{1 - \frac{c_i}{c_i^{\max}}} \tag{3.17}$$

where $c_i^{\max}$ is some prescribed saturation value. For low concentrations $c_i \ll c_i^{\max}$ we have

$$a_i = \frac{c_i}{c_i^{\max}} \tag{3.18}$$

Comparing Eq. (3.9) with Eq. (3.4) we see that

$$\widetilde{k}_j^\pm(T) = k_j^\pm(T) \prod_i (c_i^{\max})^{\pm \nu_i^{(j)}} \tag{3.19}$$

and, at equilibrium,

$$\prod_i (c_i^{\text{eq}})^{\nu_i^{(j)}} = K_{\text{eq}}^c(T) \tag{3.20}$$

$$K_{\text{eq}}^c(T) = \prod_i (c_i^{\max})^{\nu_i^{(j)}} K_{\text{eq}}(T) \,. \tag{3.21}$$

3.2.2 Balance equations for 2D spherical geometry

In our model, we consider concentration fields $c_i(\theta, \phi, t)$ on the cell membrane surface, measured in $\left[\frac{\text{number of molecules}}{\mu m^2}\right]$ each obeying the local balance equations

$$\frac{\partial c_i}{\partial t} = \mathbb{D}_i \, \nabla_2^2 \, c_i + w_i \tag{3.22}$$

When they are known, we may compute the number of species on a portion of surface Ω, and the net rate of production (if positive) or consumption (if negative) of species i using the relations

$$n_i^\Omega(t) = \int_\Omega c_i(\theta, \phi, t) \, \mathrm{d}A \tag{3.23}$$

$$W_i^\Omega = \sum_j \nu_i^{(j)} \int_\Omega r_j(\theta, \phi, t) \, \mathrm{d}A = \int_\Omega w_i \, \mathrm{d}A \tag{3.24}$$

For simplicity, we consider spherical coordinates to map the cell assumed of constant radius ℓ. The balance equations are obtained by considering a generic control surface Ω delimited by the boundary $\partial\Omega$ and writing

$$\dot{n}_i^\Omega = -\dot{n}_i^{\Omega \to} + W_j^\Omega \tag{3.25}$$

where, assuming a fixed (time independent) control surface, we have

$$\dot{n}_i^\Omega = \frac{\mathrm{d}}{\mathrm{d}t} \int_\Omega c_i \, \mathrm{d}A = \int_\Omega \frac{\partial c_i}{\partial t} \, \mathrm{d}A \tag{3.26}$$

$$\dot{n}_i^{\Omega \to} = \int_{\partial\Omega} \vec{h}_i \cdot \underline{n} \, \mathrm{d}P = \int_\Omega \nabla_2 \cdot \vec{h}_i \, \mathrm{d}A = -\mathbb{D}_i \int_\Omega \nabla_2^2 \, c_i \, \mathrm{d}A \tag{3.27}$$

where the species' flux $\vec{h}_i$ is given by the Fick's law,
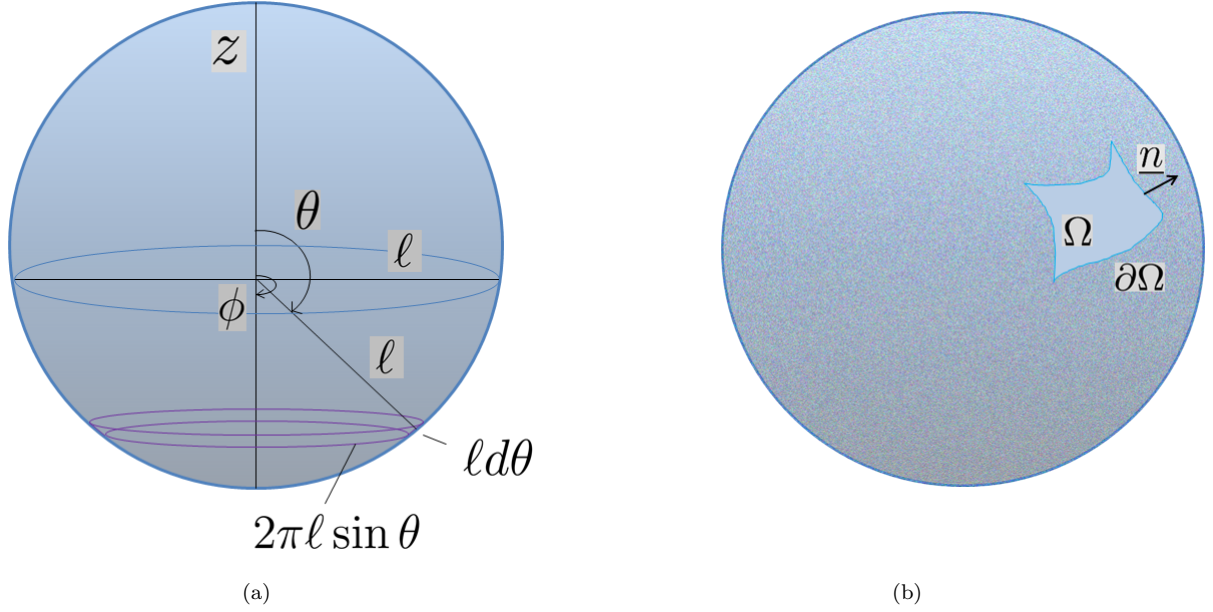
Figure 3.1: Cell geometry. Spherical coordinates: ℓ, cell radius; θ, zenith and ϕ azimuth angle. (b) Control surface Ω, boundary $\partial\Omega$, the unit vector $\underline{n}$ is orthogonal to $\partial\Omega$ and tangent to the spherical surface.

$$\vec{h}_i = -D_i \nabla_2 c_i \left[\frac{\mu m^2}{s} \frac{1}{\mu m} \frac{\text{molecule}}{\mu m^2} = \frac{\text{molecule}}{s \, \mu m} \right] \tag{3.28}$$

where the gradient operator is

$$\nabla_2 = \mathbf{i}_\theta \frac{1}{\ell} \frac{\partial}{\partial \theta} + \mathbf{i}_\phi \frac{1}{\ell \sin \theta} \frac{\partial}{\partial \phi} \tag{3.29}$$

and the Laplacian

$$\nabla_2^2 c_i = \frac{1}{\ell^2 \sin \theta} \frac{\partial}{\partial \theta} \left(\sin \theta \frac{\partial c_i}{\partial \theta} \right) + \frac{1}{\ell^2 \sin^2 \theta} \left(\frac{\partial^2 c_i}{\partial \phi^2} \right) \tag{3.30}$$

and, therefore,

$$\int_\Omega \frac{\partial c_i}{\partial t} \, \mathrm{d}A = \int_\Omega \left[D_i \nabla_2^2 c_i + w_i \right] \, \mathrm{d}A \tag{3.31}$$

which by the arbitrariness of the choice of Ω implies the local form

$$\frac{\partial c_i}{\partial t} = D_i \nabla_2^2 c_i + w_i \,. \tag{3.32}$$

3.2.3 Particular cases of interest

Consider first the simple reaction scheme between ν free receptors R and a free ligand L to form a receptor/ligand complex C = R$_\nu$L , as illustrated in Figure 3.2 for $\nu = 1$ and $\nu = 2$.
The single-reaction scheme for either case is

$$\nu \, \mathrm{R} + \mathrm{L} \rightleftharpoons \mathrm{C} \tag{3.33}$$

36

The nonzero stoichiometric coefficients are $\nu_R^+ = \nu$, $\nu_L^+ = 1$, $\nu_C^- = 1$, $\nu_R = -\nu$, $\nu_L = -1$, $\nu_C = 1$.
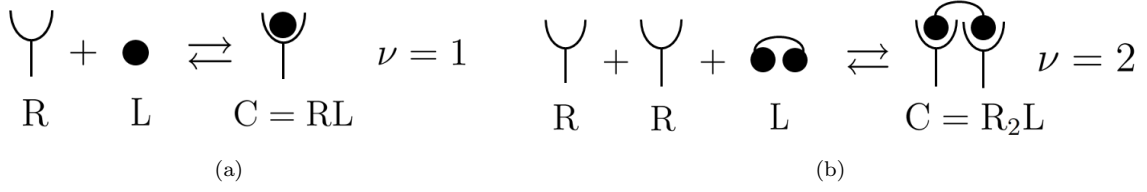
Figure 3.2: (a) Chemical reaction between a free receptor and a free ligand. (b) Chemical reaction between two free monomeric receptors and a free dimeric ligand.

Assuming low concentrations, the reaction rate is given by

$$r = k^+ c_R{}^\nu c_L - k^- c_C = k^+ \left(c_R^\nu c_L - \frac{c_C}{K_{\text{eq}}^c} \right) \tag{3.34}$$

so that

$$w_C = r, \quad w_R = -\nu r, \quad w_L = -r \tag{3.35}$$

The equilibrium constant based on concentrations becomes

$$K_{\text{eq}}^c = \frac{c_C^{\text{eq}}}{(c_R^{\text{eq}})^\nu \, c_L^{\text{eq}}} \tag{3.36}$$

Next, we need to model the fact that only portions of the membrane surface are in contact with the substrate where ligands L (and, therefore, also complexes C) are constrained. We define a "contact function" $\alpha(\theta, \phi, t)$ that is equal to zero where there is no contact and, therefore, the reaction cannot take place, and equal to unity where there is contact. For numerical reasons, we assume that α is a smooth function so that instead of a sharp step from 0 to 1 we assume a (possibly very steep but) smooth transition from 0 to 1. In our azimutal symmetry, we take

$$\alpha(\theta, \phi, t) = \text{sigm}(\theta, \pi - \theta_A(t)) \tag{3.37}$$

where sigm denotes a suitable sigmoidal function, i.e., such that $\text{sigm}(\theta, \theta_0)$ is a smooth increasing function changing rapidly from 0 to 1 around θ_0, such as $\frac{1}{1+\exp(b(\theta_0-\theta))}$ for a sufficiently large b[1].

For the angle span of attached spherical cap, we assume a simple ramp during the attachment phase assumed to last up to time τ_A, after which θ_A remains constant,

$$\theta_A(t) = \begin{cases} \theta_A^0 + \frac{t}{\tau_A}(\theta_A^\infty - \theta_A^0) & \text{for} \quad t \le \tau_A \\ \theta_A^\infty & \text{for} \quad t > \tau_A \end{cases} \tag{3.38}$$

Therefore, the local net reaction rate is given by

$$r = \left(k^+ c_R{}^\nu c_L - k^- c_C \right) \alpha = k^+ \left(c_R^\nu c_L - \frac{c_C}{K_{\text{eq}}^c} \right) \alpha \tag{3.39}$$

The balance equations (3.22) become

---

[1]For future reference, we note that the derivative $\frac{be^{-bx}}{(1+e^{-bx})^2}$ of the sigmoidal function $\frac{1}{1+e^{-bx}}$ is an approximation of the delta function.
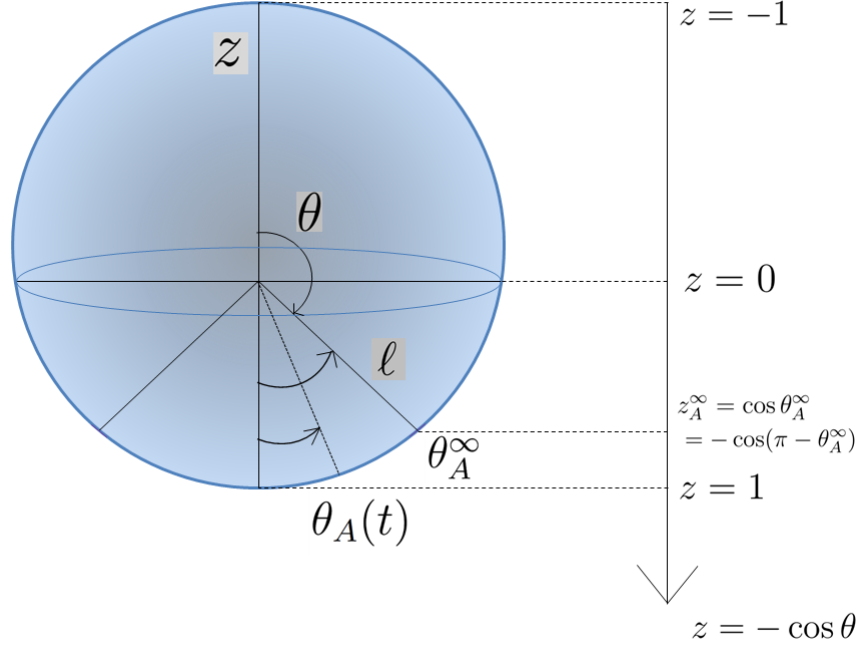
Figure 3.3: The angle span of attached spherical θ_A.

$$\begin{cases} \frac{\partial c_R}{\partial t} = \mathbb{D}_R \nabla_2^2 c_R - \nu\, r \\ \frac{\partial c_L}{\partial t} = \mathbb{D}_L \nabla_2^2 c_L - r \\ \frac{\partial c_C}{\partial t} = \mathbb{D}_C \nabla_2^2 c_C + r \end{cases} \tag{3.40}$$

where

c_R is the concentration or density of receptors on the ECM $\left[\frac{\text{number} \quad \text{of} \quad \text{molecules}}{\mu m^2}\right]$

c_L is the concentration of ligands

c_C is the concentration of the receptor-ligand complexes

$\mathbb{D}_R$ is the diffusivity of receptors $\left[\frac{\mu m^2}{s}\right]$

$\mathbb{D}_L, \mathbb{D}_C$ are the diffusivities of the ligands and complexes, that we assume negligibly small since the ligands have no mobility on the substrate.

We assume as initial conditions:

$$c_R(\theta, 0) = c_R^0, \quad c_L(\theta, 0) = c_L^0, \quad c_C(\theta, 0) = 0$$

Balance equations, using the explicit form of the 2D Laplacian and assuming azimuthal symmetry ($\partial/\partial\phi = 0$), can be rewritten as

$$\begin{cases} \frac{\partial c_R}{\partial t} = \frac{\mathbb{D}_R}{\ell^2 \sin\theta} \frac{\partial}{\partial\theta}\left(\sin\theta \frac{\partial c_R}{\partial\theta}\right) - \nu\, r \\ \frac{\partial c_L}{\partial t} = -r \\ \frac{\partial c_C}{\partial t} = +r \end{cases} \tag{3.41}$$

Additionally, it is convenient to rewrite the balance equations in dimensionless form. One possible way to choose dimensionless variables is as follows. For time we choose the standard Fourier number

38

$$\widetilde{t} = \frac{\mathbb{D}_R\, t}{\ell^2} \quad \Rightarrow \quad t = \frac{\ell^2\, \widetilde{t}}{\mathbb{D}_R} \tag{3.42}$$

where ℓ is the cell radius, t the time and $\mathbb{D}_R$ the receptors diffusivity.

So, the dimensionless time at the end of the attachment phase, is given by

$$\widetilde{\tau_A} = \frac{\mathbb{D}_R\, \tau_A}{\ell^2} \tag{3.43}$$

For the equilibrium constant we set

$$\widetilde{K} = K_{\text{eq}}^c\, B^\nu \tag{3.44}$$

where B is a reference concentration that we choose later. For concentrations we set

$$R = \frac{c_R}{B}, \quad L = \frac{c_L}{B}, \quad C = \frac{c_C}{B} \tag{3.45}$$

so that

$$r = k^+ B^{\nu+1} \left(R^\nu L - \frac{C}{\widetilde{K}} \right) \tag{3.46}$$

Substituting in the balance equation

$$\frac{\partial c_C}{\partial t} = +r \tag{3.47}$$

we obtain

$$\frac{\partial C}{\partial \widetilde{t}} = \frac{k^+ B^\nu\, \ell^2}{\mathbb{D}_R} \left(R^\nu L - \frac{C}{\widetilde{K}} \right) \alpha \tag{3.48}$$

We now choose B so that the multiplicative term $\frac{k^+ B^\nu\, \ell^2}{\mathbb{D}_R}$ of eq. (3.48) becomes 1, i.e., we set

$$B^\nu = \frac{\mathbb{D}_R}{k^+ \ell^2} \tag{3.49}$$

As a result, we obtain the important governing dimensionless parameter of the problem $\widetilde{K}$

$$\widetilde{K} = \frac{K_{\text{eq}}^c\, \mathbb{D}_R}{k^+ \ell^2} \tag{3.50}$$

In terms of the dimensionless net reaction rate

$$\widetilde{r} = \left(R^\nu L - \frac{C}{\widetilde{K}} \right) \alpha = \frac{r\, \alpha}{k^+ B^{\nu+1}} \tag{3.51}$$

the balance equations can finally be written as

$$\begin{cases} \frac{\partial R}{\partial \widetilde{t}} = \frac{1}{\sin\theta} \frac{\partial}{\partial\theta}\left(\sin\theta \frac{\partial R}{\partial\theta} \right) - \nu\, \widetilde{r} \\ \frac{\partial L}{\partial \widetilde{t}} = -\widetilde{r} \\ \frac{\partial C}{\partial \widetilde{t}} = +\widetilde{r} \end{cases} \tag{3.52}$$

with uniform initial conditions that are made possible by our use of the contact function α

$$R_0(\theta, 0) = \frac{c_R^0}{B} = c_R^0\, \frac{k^+ \ell^2}{\mathbb{D}_R} \tag{3.53}$$

$$L_0(\theta, 0) = \frac{c_L^0}{B} = c_L^0\, \frac{k^+ \ell^2}{\mathbb{D}_R} \tag{3.54}$$

$$C_0(\theta, 0) = \frac{c_C^0}{B} = 0 \tag{3.55}$$

We can for convenience change variable θ to

$$z = -\cos\theta \tag{3.56}$$

so that the range $(0, \pi)$ for θ corresponds to $(-1, 1)$ for z,

$$\mathrm{d}z = \sin\theta\,\mathrm{d}\theta \tag{3.57}$$

$$\frac{1}{\sin\theta}\frac{\partial}{\partial\theta}\left(\sin\theta\frac{\partial R}{\partial\theta}\right) = \frac{\partial}{\partial z}\left((1-z^2)\frac{\partial R}{\partial z}\right) \tag{3.58}$$

and integrals over portions of spherical surface rewrite as

$$\int_\Omega c(\theta, t)\,\mathrm{d}A = \int_0^\pi c(\theta, t)\,2\pi\ell^2\sin\theta\,\mathrm{d}\theta = \int_{-1}^1 c(z, t)\,2\pi\ell^2\,\mathrm{d}z \tag{3.59}$$

The boundary conditions (no fluxes and no gradients in concentrations at $\theta = 0$ and $\theta = \pi$ due to symmetry) are the following:

$$\left(\frac{\partial R}{\partial z}\right)_{z=-1} = \left(\frac{\partial R}{\partial\theta}\right)_{\theta=0} = 0, \quad \left(\frac{\partial R}{\partial z}\right)_{z=1} = \left(\frac{\partial R}{\partial\theta}\right)_{\theta=\pi} = 0 \tag{3.60}$$

$$\left(\frac{\partial L}{\partial z}\right)_{z=-1} = \left(\frac{\partial L}{\partial\theta}\right)_{\theta=0} = 0, \quad \left(\frac{\partial L}{\partial z}\right)_{z=1} = \left(\frac{\partial L}{\partial\theta}\right)_{\theta=\pi} = 0 \tag{3.61}$$

$$\left(\frac{\partial C}{\partial z}\right)_{z=-1} = \left(\frac{\partial C}{\partial\theta}\right)_{\theta=0} = 0, \quad \left(\frac{\partial C}{\partial z}\right)_{z=1} = \left(\frac{\partial C}{\partial\theta}\right)_{\theta=\pi} = 0 \tag{3.62}$$

The area of the portion of surface where contact with the substrate has been established, is

$$A_C = A_L = \int_{\pi-\theta_A}^\pi 2\pi\ell^2\sin\theta\,\mathrm{d}\theta = \int_{-\cos(\pi-\theta_A)}^1 2\pi\ell^2\,\mathrm{d}z = 2\pi\ell^2\left(1 + \cos(\pi - \theta_A)\right) =$$
$$= 2\pi\ell^2\left(1 - \cos\theta_A\right) = A_R\,a(t) \tag{3.63}$$

where, for shorthand, we define

$$a(t) = \frac{A_C}{A_R} = \frac{1 - \cos\theta_A}{2}, \qquad a_\infty = a(\infty), \qquad a_0 = a(0). \tag{3.64}$$

3.2.4 Final stationary conditions

At the end of the process we reach a stationary state with uniform concentration of receptors $c_R^\infty = \frac{n_R^\infty}{A_R}$ on the entire spherical surface of area $A_R = 4\pi\ell^2$ and uniform $c_C^\infty = \frac{n_C^\infty}{A_C^\infty}$ of complexes on the substrate, where A_C^∞ is the area of the portion of substrate that eventually gets involved during the process.
Thus, the overall number of free plus bound receptors in contact with the substrate is given by

$$n_{R+\nu C}^\infty|_{substrate} = (c_R^\infty + \nu\,c_C^\infty)\,A_C^\infty = A_C^\infty\,\frac{n_R^\infty}{A_R} + \nu\,n_C^\infty = \frac{A_C^\infty}{A_R}\,A_R\,B\,R_\infty + \nu\,A_C^\infty\,B\,C_\infty \tag{3.65}$$

or, normalized by the initial overall number of receptors, $n_R^0 = A_R\,B\,R_0$,

$$x_\infty = \frac{n_{R+\nu C}^\infty|_{substrate}}{n_R^0} = \frac{A_C^\infty}{A_R}\frac{R_\infty}{R_0} + \nu\,\frac{A_C^\infty}{A_R}\frac{C_\infty}{R_0} = a_\infty\,\frac{R_\infty + \nu\,C_\infty}{R_0} \tag{3.66}$$

40

At the generic time t,

$$x = \frac{n_{R+\nu C}|_{substrate}}{n_R^0} = \frac{1}{n_R^0} \int_{\Omega_L} (c_R + \nu c_C) \, \mathrm{d}A = \frac{1}{A_R R_0} \int_{\Omega} (R + \nu C) \, \alpha \, \mathrm{d}A \qquad (3.67)$$

and, clearly, we have

$$\frac{n_R|_{substrate}}{n_R^0} = \frac{1}{A_R R_0} \int_{\Omega} R\alpha \, \mathrm{d}A, \qquad \frac{n_R^\infty|_{substrate}}{n_R^0} = a_\infty \frac{R_\infty}{R_0}$$

$$\frac{n_C|_{substrate}}{n_R^0} = \frac{1}{A_R R_0} \int_{\Omega} C\alpha \, \mathrm{d}A, \qquad \frac{n_C^\infty|_{substrate}}{n_R^0} = a_\infty \frac{C_\infty}{R_0}$$

Note that at $t = 0$, $R + \nu C = R_0$ as diffusion has had no time to have effects and, therefore,

$$x_0 = a_0 = \frac{1 - \cos \theta_A^0}{2} \qquad (3.68)$$

The final stationary concentrations can be computed directly because in the contact substrate they are uniform and obey the chemical equilibrium condition

$$K_{eq}^c = \frac{c_C^\infty}{(c_R^\infty)^\nu \, c_L^\infty} \quad \text{or} \quad \widetilde{K} = \frac{C_\infty}{(R_\infty)^\nu \, L_\infty} \qquad (3.69)$$

and the overall numbers of receptors and ligands (free plus bound) are invariant, i.e.,

$$c_R^\infty A_R + \nu c_C^\infty A_C^\infty = c_R^0 A_R \qquad (3.70)$$

$$(c_L^\infty + c_C^\infty) A_C^\infty = c_L^0 A_C^\infty \qquad (3.71)$$

Notice that the actual overall number of ligands involved in the process is $c_L^0 A_C^\infty$ where c_L^0 is their initial concentration in the substrate and A_C^∞ is the area of the portion of substrate that eventually gets involved during the process. Rearranging, we have

$$c_R^\infty = c_R^0 - \nu c_C^\infty \frac{A_C^\infty}{A_R} \qquad (3.72)$$

$$c_L^\infty = c_L^0 - c_C^\infty \qquad (3.73)$$

or, in terms of dimensionless concentrations,

$$R_\infty = R_0 - \nu C_\infty \frac{A_C^\infty}{A_R} \qquad (3.74)$$

$$L_\infty = L_0 - C_\infty \qquad (3.75)$$

so that the equilibrium condition becomes

$$\frac{C_\infty}{\left(R_0 - \nu C_\infty \frac{A_C^\infty}{A_R}\right)^\nu (L_0 - C_\infty)} = \widetilde{K} \qquad (3.76)$$

which can be solved for C_∞ for the given initial R_0 and L_0, and the assumed values of $\nu, \widetilde{K}, A_C^\infty, A_R$. In Matlab we solve this equation using the standard function *fsolve*.
Combining, Eqs. (3.66) and (3.74), we obtain

$$x_\infty = a_\infty + \frac{\nu C_\infty}{R_0} a_\infty (1 - a_\infty) \qquad (3.77)$$

and, therefore,

$$\frac{C_\infty}{R_0} = \frac{x_\infty - a_\infty}{\nu \, a_\infty (1 - a_\infty)} \tag{3.78}$$

$$\frac{R_\infty}{R_0} = \frac{1 - x_\infty}{1 - a_\infty} \tag{3.79}$$

$$\frac{L_\infty}{R_0} = \frac{L_0}{R_0} - \frac{x_\infty - a_\infty}{\nu \, a_\infty (1 - a_\infty)} \tag{3.80}$$

$$(c_R^0)^\nu \, K_{\mathrm{eq}}^c = \widetilde{K} \, R_0^\nu = \frac{\frac{x_\infty - a_\infty}{\nu a_\infty (1 - a_\infty)}}{\left(\frac{1 - x_\infty}{1 - a_\infty}\right)^\nu \left[\frac{L_0}{R_0} - \frac{x_\infty - a_\infty}{\nu a_\infty (1 - a_\infty)}\right]} \tag{3.81}$$

These relations are important to extract quantitative information from experimental data.

3.3 Results

Since for our experimental data $\frac{L_0}{R_0} \gg \frac{C_\infty}{R_0}$, Eq. (3.81) can be simplified to

$$(c_R^0)^\nu \, K_{\mathrm{eq}}^c \, \frac{c_L^0}{c_R^0} = \widetilde{K} \, R_0^\nu \, \frac{L_0}{R_0} \approx \frac{x_\infty - a_\infty}{\nu a_\infty (1 - a_\infty)} \left(\frac{1 - a_\infty}{1 - x_\infty}\right)^\nu \tag{3.82}$$

The reaction-diffusion model and comparisons with experimental data just outlined has been implemented in Matlab using the standard function *pdepe* to solve the system of partial differential equations.

Figure 3.4 shows a plot of x versus as a function of dimensionless time $\widetilde{t}$. From the latter, it is interesting to note the change of slope and convexity that occurs at time $\widetilde{\tau}_A$. This is important because, as seen in Chapter 2, the available measurements of fluorescence intensity, from time lapse analysis, can be assumed to be experimental data proportional to $n_{R+\nu C}|_{substrate}$. However, the proportionality constant is unknown from experiment therefore, in Figure 3.4 we plot these data normalized so that the final stationary value corresponds that of x_∞ obtained from the model, i.e., in Figure 3.4 we plot:

$$x^{exp} = \frac{n_{R+\nu C}^{exp}|_{substrate}}{n_{R+\nu C}^{exp,\infty}|_{substrate}} \, x_\infty \tag{3.83}$$

where $x_\infty = 0.73$ from the considerations described on the previous Chapter. The experimental data confirm the expected change of slope and convexity at about $\tau_A^{exp} = 10\,\mathrm{min}$. From this observation and Eq. (3.43) we obtain

$$\widetilde{\tau}_A = \frac{\mathbb{D}_R \, \tau_A^{exp}}{\ell^2} = 0.315 \tag{3.84}$$

where we used $\mathbb{D}_R = 0.198 \, \mu m^2/s$ taken from Chapter 2. Taking the derivative of x from Eq. (3.67) with respect to $\widetilde{t}$ we can evaluate the two contributions to the slope of the curve $x = x(\widetilde{t})$ shown in Figure 3.4. The derivative with respect to $\widetilde{t}$ can be decomposed into a part due to the diffusion and into a mechanical part

$$\frac{\mathrm{d}x}{\mathrm{d}\widetilde{t}} = \left.\frac{\mathrm{d}x}{\mathrm{d}\widetilde{t}}\right|_{diff} + \left.\frac{\mathrm{d}x}{\mathrm{d}\widetilde{t}}\right|_{mech} \tag{3.85}$$

Using the balance equations (3.52) and Eqs. (3.59) and (3.43) we obtain the component due to diffusion into the attached substrate [2]

---

[2] Recall that $(1 - z_A^2) = 1 - \cos^2 \theta_A = \sin^2 \theta_A$.
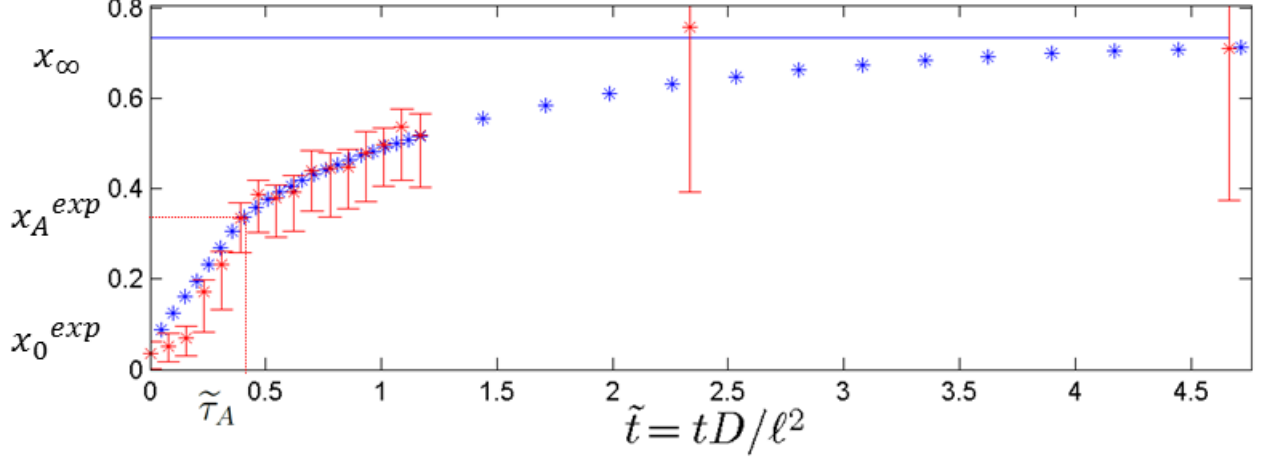
Figure 3.4: VEGFR2 recruitment by substrate-bound gremlin. The red asterisks indicate the experimental data, while the blue asterisks point to the model data from Matlab

$$\frac{\mathrm{d}x}{\mathrm{d}\widetilde{t}}\bigg|_{diff} = \frac{1}{A_R R_0} \int_\Omega \left(\frac{\partial R}{\partial \widetilde{t}} + \nu \frac{\partial C}{\partial \widetilde{t}}\right) \alpha\, \mathrm{d}A = \frac{2\pi \ell^2}{A_R R_0} \int_{-\cos\theta_A(t)}^1 \frac{\partial}{\partial z}\left[(1-z^2)\frac{\partial R}{\partial z}\right]\mathrm{d}z =$$
$$= -\frac{1}{2}(1-z_A^2)\frac{\partial R/R_0}{\partial z}\bigg|_{t,z_A(t)} = -\frac{1}{2}\sin^2\theta_A(t)\frac{\partial R/R_0}{\partial z}\bigg|_{t,z_A(t)} \tag{3.86}$$

where $z_A(t) = \cos\theta_A(t)$ and the component due to the attachment rate is [3]

$$\frac{\mathrm{d}x}{\mathrm{d}\widetilde{t}}\bigg|_{mech} = \frac{1}{A_R R_0}\int_{\Omega_L}(R+\nu C)\left(\frac{\partial\alpha}{\partial\widetilde{t}}\right)\mathrm{d}A =$$
$$= \begin{cases} \frac{1}{2}\sin\theta_A^0\,\frac{\theta_A^\infty - \theta_A^0}{\widetilde{\tau}_A} & \text{for}\quad t = 0 \\ \frac{1}{2}\sin\theta_A(t)\,\frac{\theta_A^\infty-\theta_A^0}{\widetilde{\tau}_A}\,\frac{R+\nu C}{R_0}\bigg|_{t,z_A(t)} & \text{for}\quad t \le \tau_A \\ 0 & \text{for}\quad t > \tau_A \end{cases} \tag{3.87}$$

From the experimental data in Figure 3.4 we can estimate,

$$x_0^{exp} \approx 0.0348 \tag{3.88}$$

$$\frac{\mathrm{d}x^{exp}}{\mathrm{d}t}\bigg|_0 \approx 1.38 \times 10^{-4}\mathrm{s}^{-1} \tag{3.89}$$

and at $\tau_A^{exp} = 10\,\mathrm{min}$,

$$x_A^{exp} \approx 0.335 \tag{3.90}$$

$$\frac{\mathrm{d}x^{exp}}{\mathrm{d}t}\bigg|_0 \approx 1.38 \times 10^{-4}\mathrm{s}^{-1} \tag{3.91}$$

$$\frac{\mathrm{d}x^{exp}}{\mathrm{d}t}\bigg|_{x_A^{exp}}^+ \approx 1.8 \times 10^{-4}\mathrm{s}^{-1} \tag{3.92}$$

---

[3]Recall that $\alpha(\theta,t) = \mathrm{sigm}(\theta, \pi - \theta_A(t))$, therefore, $\partial\alpha/\partial t = -(\partial\theta_A/\partial t)\partial\mathrm{sigm}(\theta,\theta_0)/\partial\theta_0|_{\theta_0=\pi-\theta_A} \approx (\partial\theta_A/\partial t)\delta(\theta-\pi+\theta_A)$ where $(\partial\theta_A/\partial t) = (\theta_A^\infty - \theta_A^0)/\tau_A$ for $t \le t_A$. The delta function picks up in the integral the value of the integrand at $\theta = \pi - \theta_A$.

$$x = \frac{n_{R+\nu C}\big|_{substrate}}{n_R^0}$$
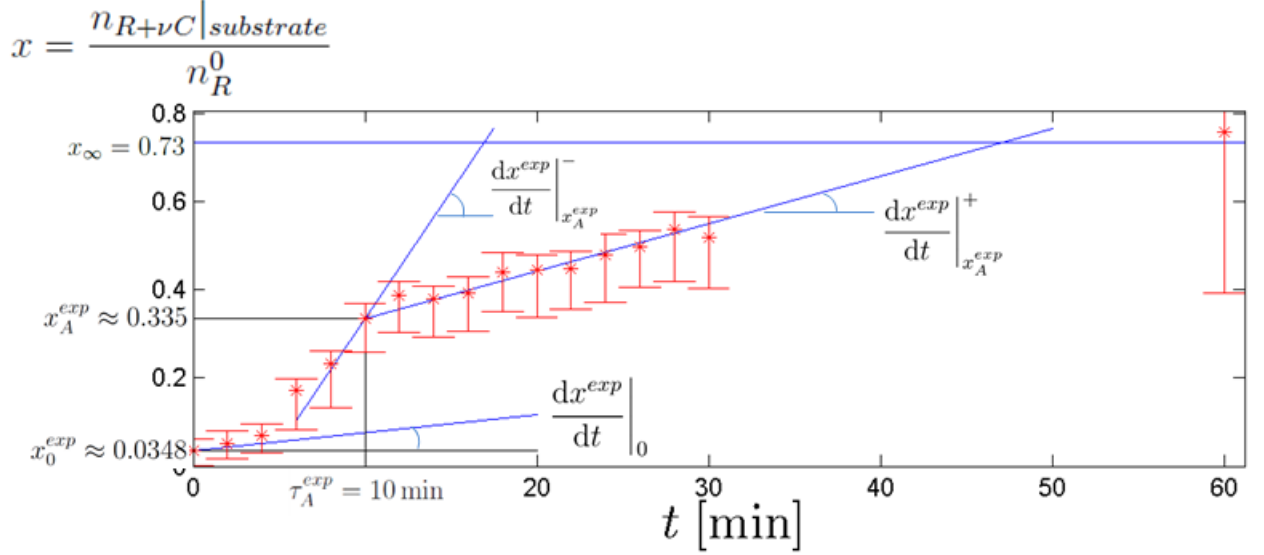
Figure 3.5: The derivatives with respect to time of experimental data.

$$\frac{\mathrm{d}x^{exp}}{\mathrm{d}t}\bigg|_{x_A^{exp}}^{-} \approx 9.6 \times 10^{-4}\mathrm{s}^{-1} \tag{3.93}$$

from which we can infer

$$\frac{\mathrm{d}x}{\mathrm{d}t}\bigg|_{mech,0}^{exp} = 1.38 \times 10^{-4}\mathrm{s}^{-1} \tag{3.94}$$

$$\frac{\mathrm{d}x}{\mathrm{d}t}\bigg|_{diff,\tau_A}^{exp} = 1.8 \times 10^{-4}\mathrm{s}^{-1} \tag{3.95}$$

$$\frac{\mathrm{d}x}{\mathrm{d}t}\bigg|_{mech,\tau_A}^{exp} = 7.8 \times 10^{-4}\mathrm{s}^{-1} \tag{3.96}$$

because at $t = 0$ the distribution is uniform and so the diffusive component is zero; and at $t = \tau_A^+$ the mechanical component drops to zero as the attachment process is assumed to stop.

Combining Eqs. (3.68) and (3.88) we obtain

$$\theta_A^0 = \arccos(1 - 2\,x_0^{exp}) \approx 0.119\,\pi = 21.5° \tag{3.97}$$

Combining Eqs. (3.94) with (3.87) for $t = 0$ yields

$$(\theta_A^\infty - \theta_A^0)\sin\theta_A^0 = 0.1656 \tag{3.98}$$

from which we obtain

$$\theta_A^\infty = 0.263\,\pi = 47.4° \tag{3.99}$$

$$z_A^\infty = \cos\theta_A^\infty = -\cos(\pi - \theta_A^\infty) = 0.677 \tag{3.100}$$

$$a_\infty = 0.1615 \tag{3.101}$$

44
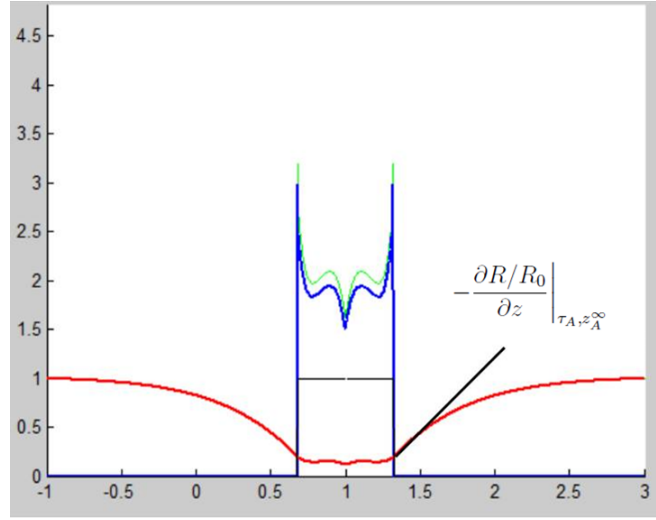
Figure 3.6: Representative frame of the receptors concentration (red line), the contact area between cell and substrate with immobilized-ligands (black line), the complex concentration (blue line), the free receptor plus the complex concentration (green line).

$$(c_R^0)^\nu \, K_{\text{eq}}^c \, \frac{c_L^0}{c_R^0} = \widetilde{K} \, R_0^\nu \, \frac{L_0}{R_0} = \frac{4.3}{\nu}(3.154)^\nu = \begin{cases} 13.6 & \text{for} \quad \nu = 1 \\ 21.4 & \text{for} \quad \nu = 2 \end{cases} \tag{3.102}$$

Using these values and Eq. (3.96) into (3.87) evaluated at $t = \tau_A$ yields

$$\left. \frac{R + \nu\, C}{R_0} \right|_{\tau_A, z_A^\infty} = \frac{2\, \tau_A}{(\theta_A^\infty - \theta_A^0)\sqrt{1 - (z_A^\infty)^2}} \left. \frac{dx}{dt} \right|_{mech, \tau_A} = 2.82 \tag{3.103}$$

Similarly, using Eq. (3.95) into Eq. (3.86) evaluated at $t = \tau_A$, we obtain

$$-\frac{\mathbb{D}_R}{\ell^2} \left. \frac{\partial R/R_0}{\partial z} \right|_{\tau_A, z_A^\infty} = \frac{2}{1 - (z_A^\infty)^2} \left. \frac{dx}{dt} \right|_{diff} = 6.65 \times 10^{-4}\,\text{s}^{-1} \tag{3.104}$$

and, with $\mathbb{D}_R = 0.198 \,\mu m^2/s$, and $\ell = 20 \,\mu m$,

$$-\left. \frac{\partial R/R_0}{\partial z} \right|_{\tau_A, z_A^\infty} = 1.27 \tag{3.105}$$

This 'constraint' is shown in Fig. 3.6.

We now assume the following initial concentrations of receptors on the cell membrane and ligands on the substrate

$$c_R^0 = \frac{7000}{4\,\pi\,\ell^2} = 1.39 \, \frac{\text{molecule}}{\mu m^2} \tag{3.106}$$

$$c_L^0 = 16000 \, \frac{\text{molecule}}{\mu m^2} \tag{3.107}$$

As a result, Eq. (3.102) yields

$$\frac{k^+}{k^-} = K_{\text{eq}}^c = \begin{cases} 8.3 \times 10^{-16} \, \frac{\mu m^2}{\text{molecule}} & \text{for} \quad \nu = 1 \\ 9.62 \times 10^{-4} \, \frac{\mu m^2}{\text{molecule}} & \text{for} \quad \nu = 2 \end{cases} \tag{3.108}$$

45

The only parameter that remains to be identified is k^+, which then inserted in Eq. (3.50) fixes the dimensionless parameter $\widetilde{K}$.

Condition (3.103) is difficult to implement because the value of $R + \nu C$ varies from a small number to a large number precisely at z_A^∞ where it needs to be estimated from the simulation. For this reason we do not use it directly. Rather, we use condition (3.105) with $\frac{\partial R/R_0}{\partial z}$ evaluated just outside of the attachment boundary , i.e., for z just below z_A^∞.

Representative frames of video made from model data are shown in Fig. 3.7. The video is generated with MATLAB, which describe the evolution of the species concentration.
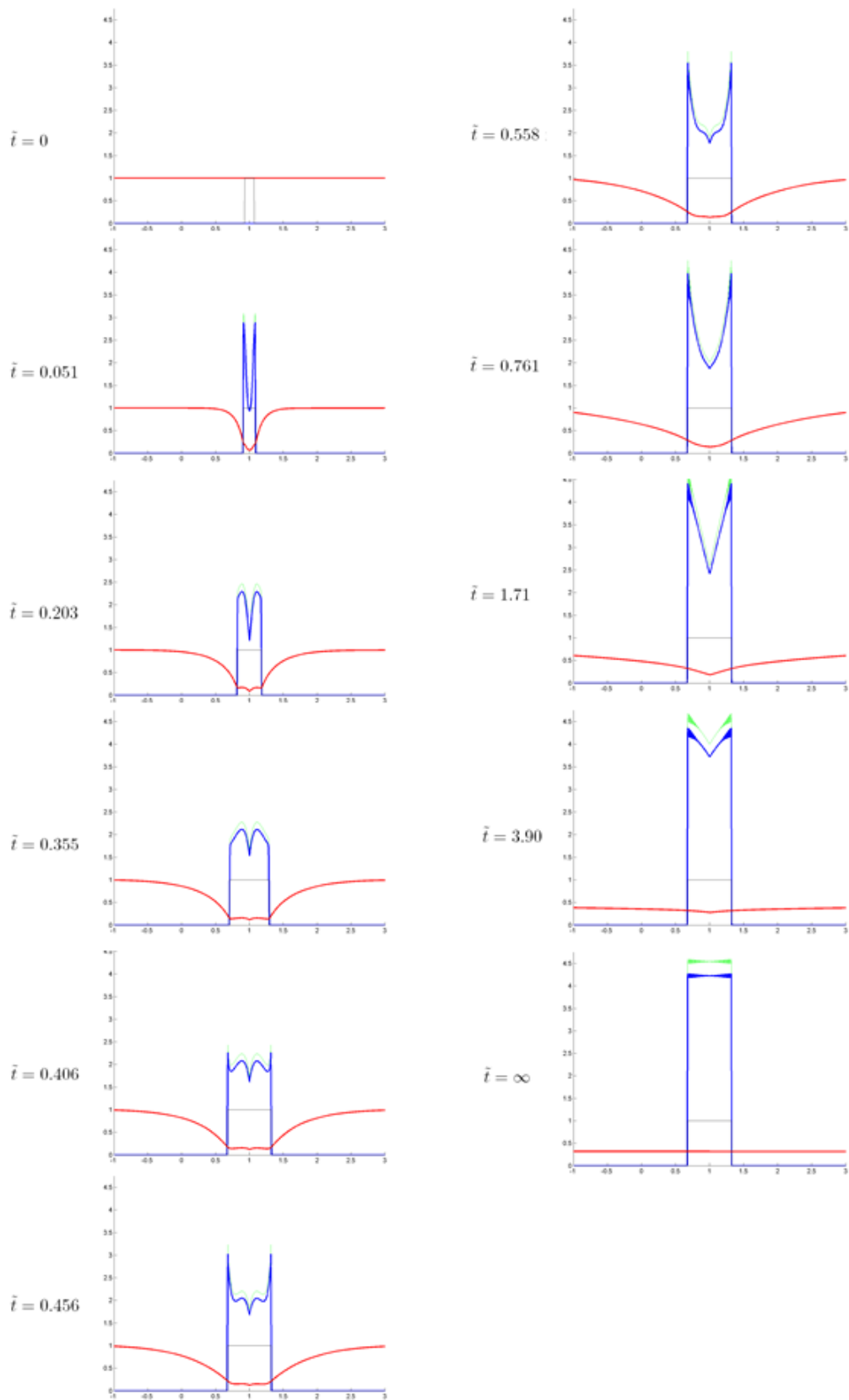
Figure 3.7: Representative frames of the receptors concentration (red line), the contact area between cell and substrate with immobilized-ligands (black line), the complex concentration (blue line), the free receptor plus the complex concentration (green line).

47
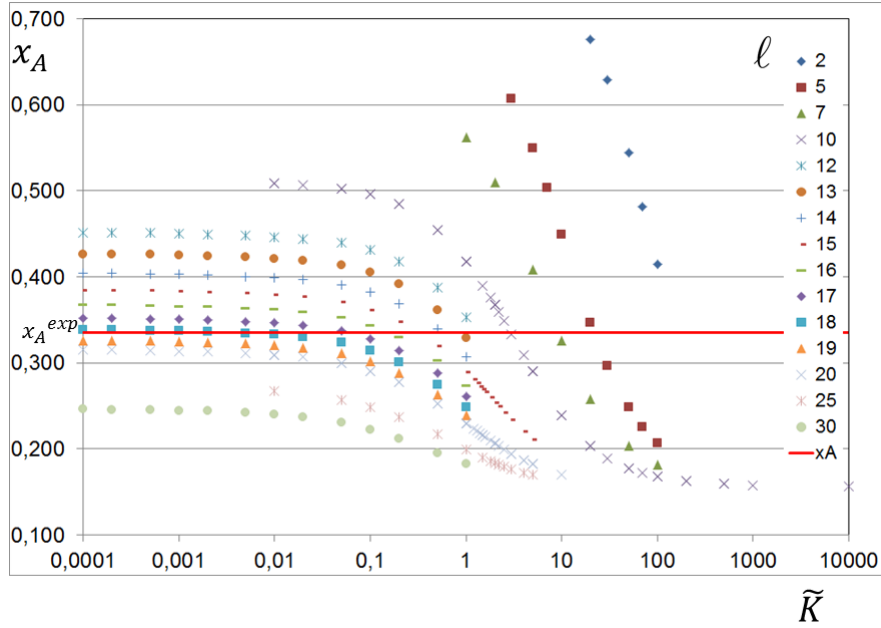
Figure 3.8: The resulting x_A versus the assumed values of $\widetilde{K}$ and ℓ.

To complete at best our objective in this work, we need to extract an estimate of the parameters $\widetilde{K}$ and ℓ. Regarding ℓ we have measured the average volume of the cells in the experimental setup, $V_{cell} \approx 30000\,\mu\text{m}^3$ from which we could infer a spherical radius of about $\ell = 20\,\mu m$. However, the actual cell geometry is rather far from spherical, therefore, we expect some discrepancies and we run a number of simulations by letting $\widetilde{K}$ vary over a wide range and ℓ over a limited range around 20μm. The results about the value of x_A are shown in Figure 3.8, where we plot the resulting x_A versus the assumed values of $\widetilde{K}$ and ℓ. We see that in the limit of $\widetilde{K} \to 0$, the values of x_A for each assumed ℓ 'saturate' to a constant value, indicating that for relatively large values of k^+ the reaction rate is so fast that essentially there is no delay to reach chemical equilibrium. This limit corresponds to an assumption used in the model presented in the next Chapter. Extracting from the data shown in Figure 3.8 the subset that yield values of x_A in a narrow range around the observed value of 0.335 (refers to Eq.(3.90)) we obtain the plot in Figure 3.9 showing the matching values of $\widetilde{K}$ for the various assumed values of the cell radius ℓ.
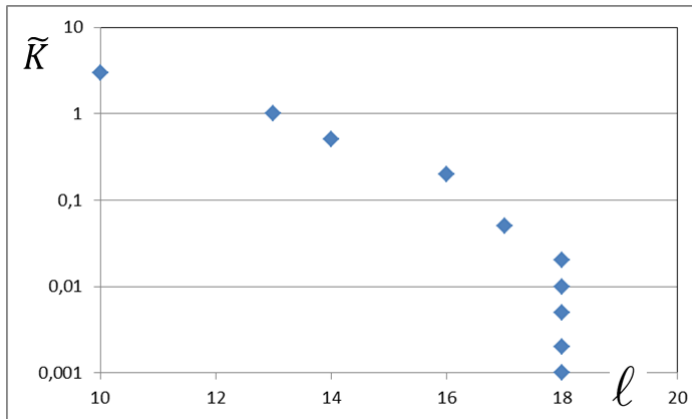
Figure 3.9: The matching values of $\widetilde{K}$ for the various assumed values of the cell radius ℓ.

48

3.4 Conclusion

A preliminary thermodynamical model has been proposed to mimic the VEGFR-2 recruitment and relocalization driven by ligand-immobilized substrate. From the experimental evidence, provided by time lapse analysis, we based our assumptions: at the beginning, we consider an uniform receptors concentration and at the end of the process we reach a stationary state with a uniform complex concentration; in addition we define a contact function α to mimic che cell 'adhesion' on the ligand-enriched substrate. This model takes into account of chemical kinetics and provides a dimensionless parameter $\widetilde{K}$ which depends on receptor diffusivity $\mathbb{D}_R$, cell radius ℓ, forward reaction rate k^+ and equilibrium constant based on the concentrations K_{eq}^c. Dimensionless partial differential equations have been written on spherical coordinates and implemented on a MATLAB code by using a *pdepd* solve. Summarizing, the model predicts:

- the important correlation between the ratio of initial concentration on receptors R_0 and ligand L_0 with the equilibrium constant;

- the overall number of free plus bound receptors normalized by the initial over number of receptors in contact with the substrate in comparison with time lasps measuments;

- the change of slope at about $t = 10\,\mathrm{min}$, which corresponds to the point between the mechanical and the diffusion phases and the final stationary value x;

- the initial and the final contact angles θ_A^0 and θ_A^∞, respectively, during cell attachment phase;

- the evolution of the concentrations of the three species;

- the matching values of $\widetilde{K}$ at the given x_A^{exp} and for the variuos cell radius ℓ.

The analysis in this chapter differs from that in [137], the consecutive model, described in the next chapter, in that the reactions are not assumed at chemical equilibrium and therefore the model requires a reasonable estimate of the forward reaction rate constant k^+. So far we found no experimental data from which to extract such rate constant for the reaction occurring on the cell membrane. However, we think that following the line of analysis in [141] and [94] data from bulk experiments complemented with appropriate surface tension measurements could yield the required surface rate constant.

Chapter 4

A chemo-diffusion-mechanical model

4.1 Introduction

We describe the relocation of VEGFR-2 on the lipid bilayer membrane during the cell adhesion to ligand-enriched extracellular matrix (ECM) by means of a chemo-transport-mechanical model. As previously described, the cell adhesion entails several concurrent phenomena, including cell deformation from an initially shape to a final spread configuration, resulting in an increased interaction between basal cell membrane and ligand enriched-substrate. A mathematical model of the processes described above has been developed [137]. The present model accounts for diffusion of VEGFR-2 along the cellular membrane and for ligands-receptors chemical reactions. The model takes advantage of achieved descriptions of the processes taking place in physically similar systems, as Li-ion batteries [142, 143]. The governing equations for the relocation of VEGFR-2 on the membrane under the below modeling assumptions have been nondimensionlized and multiplied by test functions. The weak form obtained by their integration over the spatial domain can be transformed to a first order Ordinary Differential Equation (ODE) in time if the discretization is performed via separated variables. Therefore, nodal unknowns depend solely on time, while test and shape functions solely on space. Time advancing has been achieved by finite differences, using a backward Euler scheme. Discretization of the unknown fields by means of standard linear shape functions leads to the numerical approximation via the Finite Element Method in each time step. The result of this study is threefold: formulating a mathematical model of VEGFR-2 recruitment in endothelial cell, simulating the dynamics of VEGFR-2 in endothelial cell seeded on ligand-enriched ECM, and finally co-designing experimental and numerical investigations to characterize the dynamic lateral diffusion of VEGFR-2 receptors on the plasma membrane and their interactions with immobilized ligands. The key features of experimental evidence on VEGFR-2 relocation are well captured by a diffusion-reaction model, whereby the evolving geometry of the membrane is extremely simplified. The model is mathematically rigorous and self-consistent, in that it stems from continuity equations (for mass, energy, and entropy), standard chemical kinetics, thermodynamic restrictions, and constitutive specifications [144, 145]. The partial differential equations of the model have been implemented in a computer code, with the ultimate goal to predict conditions for angiogenesis.
The outcomes of this Chapter are shown on the pubblished paper on *Scientific Reports* [137] and on a paper recently accepted on *Mathematical Problems in Engineering* [160].

4.2 Modeling VEGFR2 diffusion driven by its specific ligand

4.2.1 Mass balance equations

A general formulation for the chemo-transport-mechanics problem is here tailored to model the relocation of VEGFR-2 driven by its specific ligand on the lipid bilayer membrane (henceforth denoted with Ω). The interaction between receptors (R) and ligands (L) is described as a chemical reaction, which produces a receptor-ligand complex (C)

$$\text{R} + \text{L} \underset{k^-}{\overset{k^+}{\rightleftharpoons}} \text{C}, \tag{4.1}$$

where k^+ and k^- are the kinetic constants of the forward and backward reaction respectively. The reaction rate $w^{(6.44)}$, measured in $[\frac{mol}{m^3 s}]$, quantifies the net formation of (C) as the difference between the forward and backward reaction rates.

Complex internalization and its return back to the surface are not considered in this model. Therefore, the mass balance equations in the integral form are defined, per each species I, on the membrane Ω and on the curve Γ, shown on Figure 4.1, as follows:

$$\frac{\mathrm{d}}{\mathrm{d}t} \int_\Omega c_I(\vec{x}, t) \, \mathrm{d}S = - \oint_\Gamma \vec{h}_I \cdot \vec{t}_\perp \, \mathrm{d}l + \int_\Omega s_I(\vec{x}, t) \, \mathrm{d}S \tag{4.2}$$

by considering the line integral of Γ, which represents the circulation of the projection of $\vec{h}_I$ around the closed space curve Γ. Let consider the latter line integral: the only contribution is the projection of the flux $\vec{h}_I$ along the vector tangent $\vec{t}_\perp$. The line integral can be written as

$$\oint_\Gamma \vec{h}_I \cdot \vec{t}_\perp \, \mathrm{d}l = \oint_\Gamma \vec{h}_I \cdot (\vec{t}_\shortparallel \times \vec{n}) \, \mathrm{d}l = \oint_\Gamma (\vec{n} \times \vec{h}_I) \cdot \vec{t}_\shortparallel \, \mathrm{d}l = \oint_\Gamma (\vec{n} \times \vec{h}_I) \, \vec{\mathrm{d}l} \tag{4.3}$$

denoting with $\vec{n}$ the cell membrane unit normal, $\vec{t}_\perp$ and $\vec{t}_\shortparallel$ the tangent and parallel vectors, respectively. By using the Stokes' Theorem, the line integral leads to

$$\oint_\Gamma (\vec{n} \times \vec{h}_I) \, \vec{\mathrm{d}l} = \int_\Omega \mathrm{curl} \left[\vec{n} \times \vec{h}_I \right] \cdot \vec{n} \, \mathrm{d}S \tag{4.4}$$

The mass balance equations (4.2) can be rewritten as

$$\frac{\mathrm{d}}{\mathrm{d}t} \int_\Omega c_I(\vec{x}, t) \, \mathrm{d}S = - \int_\Omega \mathrm{curl} \left[\vec{n} \times \vec{h}_I \right] \cdot \vec{n} \, \mathrm{d}S + \int_\Omega s_I(\vec{x}, t) \, \mathrm{d}S \tag{4.5}$$

and finally, its local form, as

$$\frac{\partial c_I}{\partial t} + \mathrm{curl} \left[\vec{n} \times \vec{h}_I \right] \cdot \vec{n} = s_I \qquad \forall \vec{x} \in \Omega \tag{4.6}$$

by denoting with

$$\mathrm{div}_\Omega \left[\vec{h}_I \right] := \mathrm{curl} \left[\vec{n} \times \vec{h}_I \right] \cdot \vec{n} \tag{4.7}$$

Then, we can write the local form of the mass balance equations as follows:

$$\frac{\partial c_R}{\partial t} + \mathrm{div}_\Omega \left[\vec{h}_R \right] + w^{(6.44)} = s_R \,, \tag{4.8a}$$

$$\frac{\partial c_L}{\partial t} + \mathrm{div}_\Omega \left[\vec{h}_L \right] + w^{(6.44)} = s_L \,, \tag{4.8b}$$

$$\frac{\partial c_C}{\partial t} + \mathrm{div}_\Omega \left[\vec{h}_C \right] - w^{(6.44)} = s_C \,. \tag{4.8c}$$

Symbols in Eqs. (4.8) have the following meaning[1]: c_β (with $\beta = R, L, C$) is the molarity (i.e. the number of moles per unit area) of a generic species β; $\vec{h}_\beta$ is the mass flux in terms of molecules, i.e. the number of molecules of species β measured per unit length per unit time, and is a tangent vector field on the membrane;

---

[1]Concentrations c_β are defined in space and time, i.e. $c_\beta = c_\beta(\vec{x}, t)$. The same holds for $\vec{h}_\beta$, $w^{(6.44)}$, and s_β. Functional dependence is specified when necessary only, to favor readability.
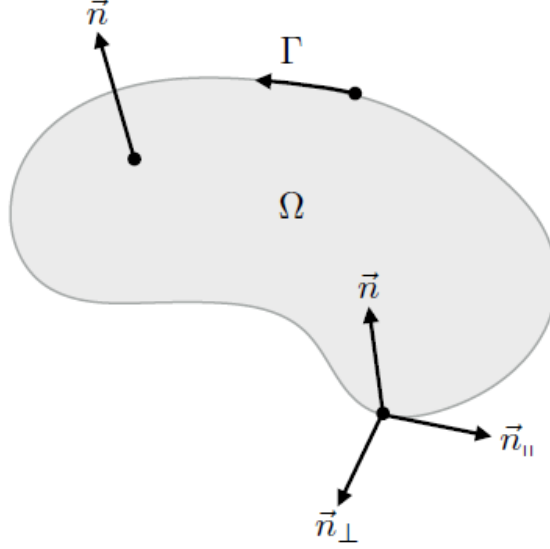
Figure 4.1: Membrane surface domain Ω and the closed curve Γ. The unit vector normal $\vec{n}$ and the tangent and parallel vector $\vec{t}_\perp$ and $\vec{t}_{||}$.

s_β is the rate in number of molecules per unit volume per unit time at which species β is generated by sources, and t is the time.

Ligands, whose degradation is negligible, are immobilized in the substrate as they are in vitro. The complex are assumed to be immobile as well, i.e.

$$\vec{h}_L = \vec{h}_C = \vec{0} \,. \tag{4.9}$$

Since receptors are free to move along the membrane, reaction (6.44) portrays a conversion of mobile to trapped receptors and vice-versa.

Equations (4.8) are defined on the cell membrane. Accordingly, the divergence operator has to be defined on the same surface. Using an important identity, by which

$$\operatorname{curl}\left[\vec{n} \times \vec{h}_R\right] = \vec{n}\operatorname{div}\left[\vec{h}_R\right] - \vec{h}_R\operatorname{div}\left[\vec{n}\right] + \left(\nabla\left[\vec{n}\right]\right)\vec{h}_R - \nabla\left[\vec{h}_R\right]\vec{n} \tag{4.10}$$

The surface divergence becomes

$$\operatorname{div}_\Omega\left[\vec{h}_R\right] = \vec{n}\cdot\operatorname{curl}\left[\vec{n}\times\vec{h}_R\right] = \operatorname{div}\left[\vec{h}_R\right] - \left(\nabla\left[\vec{h}_R\right]\vec{n}\right)\cdot\vec{n}\,. \tag{4.11}$$

Mass balance equations (4.8) shall be accompanied by the balance of force in order to model the mechanical deformation of the cell, whose boundary - the membrane - is the geometrical support of equations (4.8). Modeling the evolution of the Laplace-Beltrami operator that presides formulation concurrently with the large deformation of the cell is a phenomenally ambitious task, which is in progress motivated by the promising outcomes here shown. In the present work, we surrogate the mechanics with some simplifying assumptions.

4.2.2 Surrogated mechanics

During the co-designed experimental test, the cell progressively spreads out on the substrate. Since the latter is enriched with immobilized ligands, the cell surface in contact with the support increases with time and results in a supply of available ligands for the chemical reaction (6.44) to occur. Mechanical models for cell spreading involve very sophisticated descriptions of active and passive behavior of cells [146, 147, 148], leading to simulations of impressive computational burden. In the present work we do not account explicitly for the mechanical evolution of the cell, which keeps its original shape. Rather, we surrogate the effects of its

change in geometry on the chemo-diffusive equations (4.8) by introducing a source term of ligands s_L whose expression is calibrated from experimental evidence. The following expression for s_L in Eq. (4.8b) is taken:

$$s_L(x,t) = \frac{\overline{c_L}}{\overline{t}} \, \mathcal{H}[\,t - \frac{x}{v}\,] \, \mathcal{H}[\,\overline{t} - t + \frac{x}{v}\,] \tag{4.12}$$

The path of reasoning beyond Eq. (4.12) is equivalent to consider the cell as rigid and the substrate much more deformable, so that the latter envelopes the spherical cell, as depicted in Fig. 4.2.
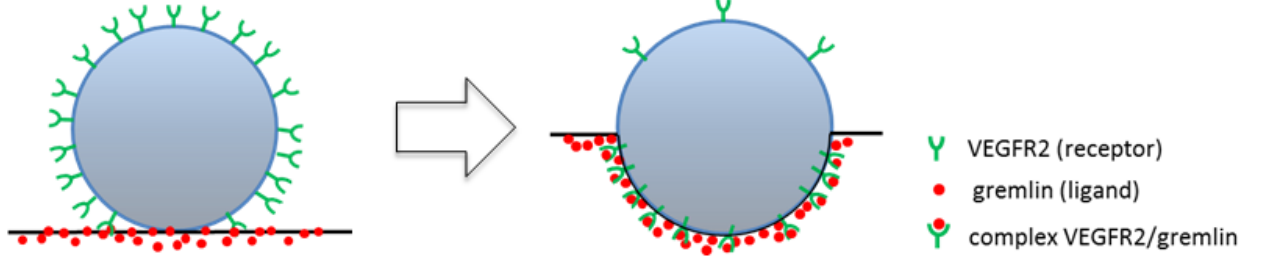
Figure 4.2: Surrogated mechanics: the cell-substrate contact dynamics is simulated by assuming that it is the substrate that gets deformed by the cell membrane, thus inducing a supply of ligands captured by function s_L in eq. (4.12).
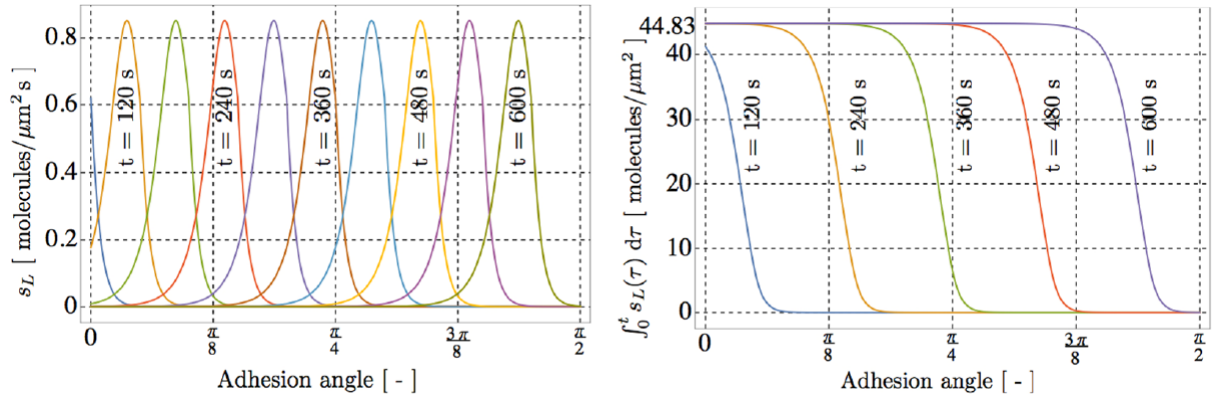
Figure 4.3: Effects of cell deformation mimicked through a supply of ligands s_L expressed by the eq.(4.12) onto the membrane. To the left, spatial evolution of the mass supply s_L and the the right is represented its time-cumulate.

In Eq. (4.12), $\mathcal{H}[-]$ is the Heaviside step function, $\overline{c_L} = 72$ ligands/μm^2 is the concentration of substrate-immobilized ligand available for reaction (6.44), t_f is the time required for the complete mechanical deformation of the cell, $v = \pi\ell/2t_f$ is the velocity of mechanical deformation (assumed to be constant until t_f), ℓ is the cell radius, $\overline{t} \ll t_f$ is a parameter that identifies a finite time required for binding, x is the curvilinear abscissa of our simplified geometry, t the generic time. In view of Eq.(4.12), the supply of ligands at point x on the membrane remains zero until $t < x/v$; then, in the time span between $t = x/v$ and $t = x/v + \overline{t}$, it increases rapidly from zero to $\overline{c_L}$. Figure 4.3 shows the spatial evolution of the mass supply s_L and of the total amount of ligands parametrized in time: at each location, ligands smoothly reach the saturation limit of 44.83 ligands/μm^2.

We assume:

$$s_R = s_C = 0, \tag{4.13}$$

since complex is provided by $w^{(6.44)}$ only, and receptors are not generated.

In view of the above, mass balance equations (4.8) finally become:

$$\frac{\partial c_R}{\partial t} + \text{div}_\Omega \left[\vec{h}_R \right] + w^{(6.44)} = 0 \tag{4.14a}$$

$$\frac{\partial c_L}{\partial t} + w^{(6.44)} - s_L(x, t) = 0 \tag{4.14b}$$

$$\frac{\partial c_C}{\partial t} - w^{(6.44)} = 0 \tag{4.14c}$$

4.2.3 Weak form

The weak formulation of balance equations (4.14) comes out after multiplication by a suitable set of *time independent* test functions - here denoted with a superposed caret - and from an integration upon the membrane, exploiting Green's formula to reduce the order of differentiation. Consider the mass balance (4.14a) as a prototype:

$$\int_\Omega \hat{c}_R \left\{ \frac{\partial c_R}{\partial t} + \text{div}_\Omega \left[\vec{h}_R \right] + w^{(6.44)} \right\} \mathrm{d}S = \tag{4.15}$$

$$= \int_\Omega \hat{c}_R \frac{\partial c_R}{\partial t} \, \mathrm{d}S + \int_\Omega \text{div}_\Omega \left[\hat{c}_R \, \vec{h}_R \right] - \nabla_\Omega \left[\hat{c}_R \right] \cdot \vec{h}_R \, \mathrm{d}S + \int_\Omega \hat{c}_R \, w^{(6.44)} \, \mathrm{d}S$$

$$= \int_\Omega \hat{c}_R \frac{\partial c_R}{\partial t} \, \mathrm{d}S - \int_\Omega \nabla_\Omega \left[\hat{c}_R \right] \cdot \vec{h}_R \, \mathrm{d}S + \int_\Omega \hat{c}_R \, w^{(6.44)} \, \mathrm{d}S = 0 \, .$$

In the former identity, a surface gradient operator arises in view of the integration by parts of the divergence term. Such a surface gradient, on the spherical smooth surface of the membrane, is defined as

$$\nabla_\Omega \left[\hat{c}_R \right] = \nabla \left[\hat{c}_R \right] - (\vec{n} \cdot \nabla \left[\hat{c}_R \right]) \, \vec{n} \tag{4.16}$$

with $\vec{n}$ the cell membrane unit normal. Within weak formulations a contribution is usually defined on the boundary in view of the two-dimensional version of the divergence theorem. This is not the case for the cell membrane Ω since it is a closed surface. The weak form of equations (4.14b, 4.14c) can be easily derived following the same path of reasoning.

In conclusion, the weak form of the balance equations can be written in the time interval $[0, t_f]$ as:

$$\text{Find } y \in \mathcal{V}^{[0, t_f]} \text{ such that} \qquad \frac{\partial}{\partial t} b\left(\hat{y}, y(t)\right) + a(\hat{y}, y(t)) = f(\hat{y}) \qquad \forall \hat{y} \in \mathcal{V} \tag{4.17}$$

where

$$b\left(\hat{y}, y\right) = \left(\int_\Omega \hat{c}_R \, c_R + \hat{c}_L \, c_L + \hat{c}_C \, c_C \right) \mathrm{d}S \, ,$$

$$a\left(\hat{y}, y\right) = -\int_\Omega \nabla_\Omega \left[\hat{c}_R \right] \cdot \vec{h}_R \, \mathrm{d}S + \int_\Omega (\hat{c}_R + \hat{c}_L - \hat{c}_C) \, w^{(6.44)} \, \mathrm{d}S \, ,$$

$$f\left(\hat{y}\right) = \int_\Omega \hat{c}_L \, s_L \, \mathrm{d}S$$

with $y = \{c_R, c_L, c_C\}$ and $\hat{y} = \{\hat{c}_R, \hat{c}_L, \hat{c}_C\}$. Column y collects the time-dependent unknown fields. Column $\hat{y}$ collects the steady-state test functions that correspond to the unknown fields in y.

To computationally solve the (either weak (4.17) or strong (4.14)) problem, constitutive equations must be specified, which is the subject of Section 4.2.4. Ellipticity of the operators, functional and numerical properties of the solution and of its approximation depend on the constitutive assumptions and on the choice of the correct functional spaces $\mathcal{V}^{[0, t_f]}, \mathcal{V}$. However the identification of these spaces falls beyond the scope of the present paper.

4.2.4 Thermodynamics

4.2.4.1 Energy Balance

In view of the assumptions made on the geometrical evolution of the membrane, there is no need to distinguish between material and spatial time derivative. When dealing with composite functions of the form $\phi(a(z), z)$ we will identify the *total* derivative with the roman symbol d and the *partial* derivative with the symbol ∂. It thus holds:

$$\frac{\mathrm{d}}{\mathrm{d}z}\phi(a(z), z) = \frac{\partial \phi}{\partial a}\frac{\mathrm{d}a}{\mathrm{d}z} + \frac{\partial \phi}{\partial z}$$

This notation will be used in the time derivative of internal and Helmholtz free energies, and of entropy.

4.2.4.2 Energy Balance

Denote with Ω the membrane, i.e. the spatial domain of problem. Consider an arbitrary region $\mathcal{P} \subset \Omega$. The first law of thermodynamics represents the balance of the interplay among the internal energy of $\mathcal{P}$, the heat transferred in $\mathcal{P}$ and the power due to mass exchanged on $\mathcal{P}$. The energy balance for the problem at hand reads:

$$\frac{\mathrm{d}\mathcal{U}}{\mathrm{d}t}(\mathcal{P}) = \mathcal{Q}_u(\mathcal{P}) + \mathcal{T}_u(\mathcal{P}) \, , \tag{4.18}$$

where $\mathcal{Q}_u$ is the power due to heat transfer and $\mathcal{T}_u$ is the power due to mass transfer. Denoting with $\partial\mathcal{P}$ the bounding closed curve of $\mathcal{P}$, they read:

$$\mathcal{Q}_u = \int_{\mathcal{P}} s_q \, \mathrm{d}S - \oint_{\partial\mathcal{P}} \vec{q} \cdot \vec{t}_\perp \, \mathrm{d}\Gamma \tag{4.19a}$$

$$\mathcal{T}_u = \int_{\mathcal{P}} \mu_L^u \, s_L \, \mathrm{d}S - \oint_{\partial\mathcal{P}} \mu_R^u \, \vec{h}_R \cdot \vec{t}_\perp \, \mathrm{d}\Gamma \tag{4.19b}$$

The time variation of net internal energy $\mathcal{U}$ thus corresponds to the power expenditure of two external agents: a heat contribution $\mathcal{Q}_u$, where s_q is the heat supplied by external agents and $\vec{q}$ is the heat flux vector; a mass contribution $\mathcal{T}_u$ in which the scalar μ_β^u denotes the change in specific energy provided by a unit supply of *moles* of species $\beta = L, R$.

Since the geometry remains unchanged, one can define specific internal energy u per unit mass or per unit surface, since none of them changes during the process. We choose to define it per unit surface, namely:

$$\mathcal{U}(\mathcal{P}) = \int_{\mathcal{P}} u \, \mathrm{d}S \, . \tag{4.20}$$

Standard application of the surface divergence theorem and of mass balances (4.8) leads from (4.19) to

$$\mathcal{Q}_u = \int_{\mathcal{P}} s_q \, \mathrm{d}S - \int_{\mathcal{P}} \mathrm{div}_\Omega \left[\vec{q} \right] \, \mathrm{d}S \tag{4.21a}$$

$$\mathcal{T}_u = \int_{\mathcal{P}} \mu_L^u \, s_L \, \mathrm{d}S - \int_{\mathcal{P}} \mathrm{div}_\Omega \left[\mu_R^u \, \vec{h}_R \right] \, \mathrm{d}S \tag{4.21b}$$

The first law of thermodynamics is thus stated as follows:

$$\int_{\mathcal{P}} \frac{\mathrm{d}u}{\mathrm{d}t} \, \mathrm{d}S = \int_{\mathcal{P}} s_q \, \mathrm{d}S - \int_{\mathcal{P}} \mathrm{div}_\Omega \left[\vec{q} \right] \, \mathrm{d}S - \int_{\mathcal{P}} \mathrm{div}_\Omega \left[\mu_R^u \, \vec{h}_R \right] \, \mathrm{d}S + \int_{\mathcal{P}} \mu_L^u \, s_L \, \mathrm{d}S \tag{4.22}$$

It must hold for any region $\mathcal{P}$, since the latter is arbitrary. After simple algebra, the local form of the first principle thus reads:

$$
\frac{\mathrm{d}u}{\mathrm{d}t} = s_q - \mathrm{div}_\Omega\,[\,\vec{q}\,] - \mathrm{div}_\Omega\left[\,\mu_R^u\,\vec{h}_R\,\right] + \mu_L^u\,s_L = s_q - \mathrm{div}_\Omega\,[\,\vec{q}\,] - \mu_R^u\,\mathrm{div}_\Omega\left[\,\vec{h}_R\,\right] - \vec{h}_R\cdot\nabla\mu_R^u + \mu_L^u\,s_L =
$$

$$
= s_q - \mathrm{div}_\Omega\,[\,\vec{q}\,] - \mu_R^u\left(-\frac{\partial c_R}{\partial t} - w^{(6.44)}\right) - \vec{h}_R\cdot\nabla_\Omega\,[\,\mu_R^u\,] + \mu_L^u\,s_L =
$$

$$
= s_q - \mathrm{div}_\Omega\,[\,\vec{q}\,] + \mu_R^u\,\frac{\partial c_R}{\partial t} + \mu_R^u\,w^{(6.44)} - \vec{h}_R\cdot\nabla_\Omega\,[\,\mu_R^u\,] + \mu_L^u\,s_L
$$

$$(4.23)$$

It is possibile to sum the mass balance Eq.s $(4.14\mathrm{b}) - (4.14\mathrm{c})$, since are equal to zero:

$$
\frac{\mathrm{d}u}{\mathrm{d}t} = s_q - \mathrm{div}_\Omega\,[\,\vec{q}\,] + \mu_R^u\frac{\partial c_R}{\partial t} + \mu_L^u\frac{\partial c_L}{\partial t} + \mu_C^u\frac{\partial c_C}{\partial t} - \vec{h}_R\cdot\nabla_\Omega\,[\,\mu_R^u\,] + (\mu_R^u + \mu_L^u - \mu_C^u)\,w^{(6.44)}\,. \qquad (4.24)
$$

4.2.4.3 Entropy balance equations

The second law of thermodynamics represents the balance of the interplay among the internal entropy of $\mathcal{P}$ and the entropy transferred in $\mathcal{P}$ due to mass exchange and heat transferred on $\mathcal{P}$. The entropy balance for the problem at hand reads:

$$
\frac{\mathrm{d}S}{\mathrm{d}t}(\mathcal{P}) - \frac{\mathrm{d}S_{irr}}{\mathrm{d}t}(\mathcal{P}) = \mathcal{Q}_\eta(\mathcal{P}) + \mathcal{T}_\eta(\mathcal{P})\,, \qquad (4.25)
$$

where S is the net internal entropy of $\mathcal{P}$, S_{irr} is the entropy produced inside $\mathcal{P}$, Q_η the entropy per unit time due to heat transfer, T_η the entropy per unit time due to mass transfer. The individual contributions read:

$$
Q_\eta = \int_\mathcal{P} \frac{s_q}{T}\,\mathrm{d}S - \oint_{\partial\mathcal{P}} \frac{\vec{q}}{T}\cdot\vec{t}_\perp\,\mathrm{d}\Gamma\,, \qquad (4.26\mathrm{a})
$$

$$
T_\eta = \int_\mathcal{P} \mu_L^\eta\,s_L\,\mathrm{d}S - \oint_{\partial\mathcal{P}} \mu_R^\eta\,\vec{h}_R\cdot\vec{t}_\perp\,\mathrm{d}\Gamma\,. \qquad (4.26\mathrm{b})
$$

The scalar μ_β^η denotes the change in specific entropy provided by a unit supply of moles of species β. Equation (4.25) stems from the non-trivial assumption that mechanics does not contribute directly to the total entropy flow in the entropy balance equation. The second law of thermodynamics states that:

$$
\frac{\mathrm{d}S_{irr}}{\mathrm{d}t} \geq 0. \qquad (4.27)
$$

Analogously to the energy counterpart, we define the specific internal entropy η per unit volume. Standard application of the divergence theorem and of mass balances (4.14) leads to

$$
\int_\mathcal{P} \frac{\mathrm{d}}{\mathrm{d}t}\eta - \frac{s_q}{T} + \mathrm{div}_\Omega\left[\frac{\vec{q}}{T}\right] - \mu_L^\eta\,s_L + \mathrm{div}_\Omega\left[\mu_R^\eta\,\vec{h}_R\right]\,\mathrm{d}S \geq 0 \qquad (4.28)
$$

By multiplying per $T \geq 0$

$$
\int_\mathcal{P} T\frac{\mathrm{d}\eta}{\mathrm{d}t} - s_q + T\,\mathrm{div}_\Omega\left[\frac{\vec{q}}{T}\right] - T\,\mu_L^\eta\,s_L + T\,\mathrm{div}_\Omega\left[\mu_R^\eta\,\vec{h}_R\right]\,\mathrm{d}S \geq 0 \qquad (4.29)
$$

By noting that

$$
T\,\mathrm{div}_\Omega\left[\frac{\vec{q}}{T}\right] = \mathrm{div}_\Omega\,[\,\vec{q}\,] + T\,\vec{q}\cdot\nabla_\Omega\,[\,T\,]\,(-T^{-2}) = \mathrm{div}_\Omega\,[\,\vec{q}\,] - \frac{1}{T}\vec{q}\cdot\nabla_\Omega\,[\,T\,] \qquad (4.30)
$$

and

$$
T\,\mathrm{div}_\Omega\left[\mu_R^\eta\,\vec{h}_R\right] = T\,\mu_R^\eta\,\mathrm{div}_\Omega\left[\vec{h}_R\right] + T\,\vec{h}_R\cdot\nabla_\Omega\,[\,\mu_R^\eta\,] \qquad (4.31)
$$

The entropy imbalance (4.29) becomes

$$\int_{\mathcal{P}} T\frac{\mathrm{d}\eta}{\mathrm{d}t} - s_q + \mathrm{div}_{\Omega}\left[\vec{q}\right] - \frac{1}{T}\vec{q}\cdot\nabla_{\Omega}\left[T\right] + T\mu_R^{\eta}\,\mathrm{div}_{\Omega}\left[\vec{h}_R\right] + T\vec{h}_R\cdot\nabla_{\Omega}\left[\mu_R^{\eta}\right] - T\mu_L^{\eta}\,s_L\,\mathrm{d}S \geq 0 \qquad (4.32)$$

by replacing $-s_q + \mathrm{div}\left[\vec{q}\right]$ by using the energy balance (4.24)

$$\int_{\mathcal{P}} T\frac{\mathrm{d}\eta}{\mathrm{d}t} - \frac{1}{T}\vec{q}\cdot\nabla_{\Omega}\left[T\right] + T\mu_R^{\eta}\,\mathrm{div}_{\Omega}\left[\vec{h}_R\right] + T\vec{h}_R\cdot\nabla_{\Omega}\left[\mu_R^{\eta}\right] - T\mu_L^{\eta}\,s_L\,\mathrm{d}S+$$
$$+\int_{\mathcal{P}} -\frac{\mathrm{d}u}{\mathrm{d}t} + \mu_R^u\frac{\partial c_R}{\partial dt} + \mu_L^u\frac{\partial c_L}{\partial t} + \mu_C^u\frac{\partial c_C}{\partial t} - \vec{h}_R\cdot\nabla_{\Omega}\left[\mu_R^u\right] + (\mu_R^u + \mu_L^u - \mu_C^u)\,w^{(6.44)}\,\mathrm{d}S \geq 0 \qquad (4.33)$$

By exploiting mass balance equations (4.8), the entropy imbalance becomes

$$\int_{\mathcal{P}} T\frac{\mathrm{d}\eta}{\mathrm{d}t} - \frac{\mathrm{d}u}{\mathrm{d}t} - \frac{1}{T}\vec{q}\cdot\nabla_{\Omega}\left[T\right] + T\mu_R^{\eta}\left[-\frac{\partial c_R}{\partial t} - w^{(6.44)}\right] + T\mu_L^{\eta}\left[-\frac{\partial c_L}{\partial t} - w^{(6.44)}\right] + T\mu_C^{\eta}\left[-\frac{\partial c_C}{\partial t} + w^{(6.44)}\right] + T\vec{h}_R\cdot\nabla_{\Omega}\left[$$
$$+\int_{\mathcal{P}} \mu_R^u\frac{\partial c_R}{\partial t} + \mu_L^u\frac{\partial c_L}{\partial t} + \mu_C^u\frac{\partial c_C}{\partial t} - \vec{h}_R\cdot\nabla_{\Omega}\left[\mu_R^u\right] + (\mu_R^u + \mu_L^u - \mu_C^u)\,w^{(6.44)}\,\mathrm{d}S \geq 0$$
$$(4.34)$$

$$\int_{\mathcal{P}} T\frac{\mathrm{d}\eta}{\mathrm{d}t} - \frac{\mathrm{d}u}{\mathrm{d}t} - \frac{1}{T}\vec{q}\cdot\nabla_{\Omega}\left[T\right] + \frac{\partial c_R}{\partial t}\left[\mu_R^u - T\mu_R^{\eta}\right] + \frac{\partial c_L}{\partial t}\left[\mu_L^u - T\mu_L^{\eta}\right] + \frac{\partial c_C}{\partial t}\left[\mu_C^u - T\mu_C^{\eta}\right] + T\vec{h}_R\cdot\nabla_{\Omega}\left[\mu_R^{\eta}\right]+$$
$$+\int_{\mathcal{P}} \mu_R^u\frac{\partial c_R}{\partial t} + \mu_L^u\frac{\partial c_L}{\partial t} + \mu_C^u\frac{\partial c_C}{\partial t} - \vec{h}_R\cdot\nabla_{\Omega}\left[\mu_R^u\right] + (\mu_R^u - T\mu_R^{\eta} + \mu_L^u - T\mu_L^{\eta} - \mu_C^u + T\mu_C^{\eta})\,w^{(6.44)}\,\mathrm{d}S \geq 0$$
$$(4.35)$$

Let denote with the symbol μ_{β} the quantity

$$\mu_{\beta} = \mu_{\beta}^u - T\mu_{\beta}^{\eta} \qquad (4.36)$$

and with the symbol $A^{(6.44)}$ the following

$$A^{(6.44)} = -\mu_R - \mu_L + \mu_C \qquad (4.37)$$

$$\int_{\Omega} T\frac{\mathrm{d}\eta}{\mathrm{d}t} - \frac{\mathrm{d}u}{\mathrm{d}t} - \frac{1}{T}\vec{q}\cdot\nabla_{\Omega}\left[T\right] + \frac{\partial c_R}{\partial t}\left[\mu_R\right] + \frac{\partial c_L}{\partial t}\left[\mu_L\right] + \frac{\partial c_C}{\partial t}\left[\mu_C\right] + T\vec{h}_R\cdot\nabla_{\Omega}\left[\mu_R^{\eta}\right]\,\mathrm{d}V+$$
$$+\int_{\Omega} \mu_R^u\frac{\partial c_R}{\partial t} + \mu_L^u\frac{\partial c_L}{\partial t} + \mu_C^u\frac{\partial c_C}{\partial t} - \vec{h}_R\cdot\nabla_{\Omega}\left[\mu_R^u\right] + (\mu_R + \mu_L - \mu_C)\,w^{(6.44)}\,\mathrm{d}V \geq 0 \qquad (4.38)$$

by noting that:
$$T\vec{h}_R\cdot\nabla_{\Omega}\left[\mu_R^{\eta}\right] = \vec{h}_R\cdot\nabla_{\Omega}\left[T\mu_R^{\eta}\right] - \vec{h}_R\cdot\nabla_{\Omega}\left[T\right]\mu_R^{\eta} \qquad (4.39)$$

one finally writes the entropy balance as:

$$\int_{\mathcal{P}} T\frac{\mathrm{d}\eta}{\mathrm{d}t} - \frac{\mathrm{d}u}{\mathrm{d}t} - \frac{1}{T}\vec{q}\cdot\nabla_{\Omega}\left[T\right] + \mu_R\frac{\partial c_R}{\partial t} + \mu_L\frac{\partial c_L}{\partial t} + \mu_C\frac{\partial c_C}{\partial t} - A^{(6.44)}\,w^{(6.44)} - \vec{h}_R\cdot\nabla_{\Omega}\left[\mu_R\right] - \left(\vec{h}_R\cdot\nabla_{\Omega}\left[T\right]\right)\mu_R^{\eta}\,\mathrm{d}S \geq 0\,. \qquad (4.40)$$

57

4.2.4.4   Helmholz Free Energy

The specific Helmholtz free energy is defined as:

$$\psi = u - T\,\eta \tag{4.41}$$

and is taken as a function of temperature and concentrations, $\psi\,(T, c_R, c_L, c_C)$. It thus holds:

$$T\frac{\mathrm{d}\eta}{\mathrm{d}t} - \frac{\mathrm{d}u}{\mathrm{d}t} = -\frac{\mathrm{d}\psi}{\mathrm{d}t} - \eta\frac{\partial T}{\partial t} = -\frac{\partial\psi}{\partial c_L}\frac{\partial c_L}{\partial t} - \frac{\partial\psi}{\partial c_R}\frac{\partial c_R}{\partial t} - \frac{\partial\psi}{\partial c_C}\frac{\partial c_C}{\partial t} - \left(\eta + \frac{\partial\psi}{\partial T}\right)\frac{\partial T}{\partial t} \tag{4.42}$$

which can be inserted in (4.40) to derive the entropy imbalance in the final form:

$$\int_{\mathcal{P}} \left(-\frac{\partial\psi}{\partial c_R} + \mu_R\right)\frac{\partial c_R}{\partial t} + \left(-\frac{\partial\psi}{\partial c_L} + \mu_L\right)\frac{\partial c_L}{\partial t} + \left(-\frac{\partial\psi}{\partial c_C} + \mu_C\right)\frac{\partial c_C}{\partial t} - \left(\eta + \frac{\partial\psi}{\partial T}\right)\frac{\partial T}{\partial t}\,\mathrm{d}S+$$
$$\int_{\mathcal{P}} -\frac{1}{T}\vec{\underline{q}}\cdot\nabla_\Omega\,[\,T\,] - A^{(6.44)}\,w^{(6.44)} - \vec{h}_R\cdot\nabla_\Omega\,[\,\mu_R\,]\,\mathrm{d}S \geq 0 \tag{4.43}$$

where $\vec{\underline{q}} = \vec{q} + T\,\mu_R^\eta\,\vec{h}_R$.

4.2.4.5   Thermodynamic restrictions

The inequality (4.43) must hold for any region $\mathcal{P}$, since the latter was arbitrarily taken. Therefore, the following local inequality, usually termed after Clausius-Duhem, yields

$$\left(-\frac{\partial\psi}{\partial c_R} + \mu_R\right)\frac{\partial c_R}{\partial t} + \left(-\frac{\partial\psi}{\partial c_L} + \mu_L\right)\frac{\partial c_L}{\partial t} + \left(-\frac{\partial\psi}{\partial c_C} + \mu_C\right)\frac{\partial c_C}{\partial t} - \left(\eta + \frac{\partial\psi}{\partial T}\right)\frac{\partial T}{\partial t}+$$
$$-\frac{1}{T}\vec{\underline{q}}\cdot\nabla_\Omega\,[\,T\,] - Aw^{(6.44)} - \vec{h}_R\cdot\nabla_\Omega\,[\,\mu_R\,] \geq 0 \tag{4.44}$$

This inequality must hold for any value of the time derivative of the temperature and of the concentrations c_R, c_L, and c_C. Since they appear linearly in the inequality, the factors multiplying them must be zero, as otherwise it would be possible to find a value for the time derivatives that violate the inequality. Therefore, the following restrictions apply

$$\mu_R = \frac{\partial\psi}{\partial c_R}, \qquad \mu_L = \frac{\partial\psi}{\partial c_L}, \qquad \mu_C = \frac{\partial\psi}{\partial c_C}, \qquad \eta = -\frac{\partial\psi}{\partial T} \tag{4.45}$$

In view of formula (4.45), the amount μ_β declared in eq. (4.36) acquires the meaning of *chemical potential* and hence the term $A^{(6.44)}$ in eq. (4.37) turns out to be the *affinity of the reaction* (6.44).

Equation (4.45) yields to the so called Clausius-Plank inequality:

$$-\frac{1}{T}\,\vec{\underline{q}}\cdot\nabla_\Omega\,[\,T\,] - A^{(6.44)}\,w^{(6.44)} - \vec{h}_R\cdot\nabla_\Omega\,[\,\mu_R\,] \geq 0 \tag{4.46}$$

that splits under the assumptions of Curie's principle and thermal equilibrium in the following set of inequalities:

$$\vec{h}_R\cdot\nabla_\Omega\,[\,\mu_R\,] \leq 0\,, \tag{4.47a}$$
$$A^{(6.44)}\,w^{(6.44)} \leq 0\,. \tag{4.47b}$$

4.2.5   Constitutive theory

We will assume henceforth that the system is in thermal equilibrium. The Helmholtz free energy density is furthermore additively decomposed into three separate parts:

$$\psi\,(c_R, c_L, c_C) = \psi_R(c_R) + \psi_L(c_L) + \psi_C(c_C) \tag{4.48}$$

The free energy density of mobile guest atoms interacting with a host medium is described by an ideal solution model, which provides the following free energy density for the continuum approximation of mixing of the generic species $\beta = R, L, C$:

$$\psi_\beta(c_\beta) = \mu_\beta^0 \, c_\beta + RT c_\beta^{max} \left[\vartheta_\beta \ln \vartheta_\beta + (1 - \vartheta_\beta) \ln(1 - \vartheta_\beta) \right] \tag{4.49}$$

where $\vartheta_\beta = c_\beta / c_\beta^{max}$ is the ratio between the concentration and the saturation limit for each species. The chemical potential μ_β can be written accordingly to the equation (4.45) as

$$\mu_\beta = \frac{\partial \psi}{\partial c_\beta} = \mu_\beta^0 + RT \left(\ln \vartheta_\beta - \ln\left(1 - \vartheta_\beta\right) \right) \tag{4.50}$$

A strategy to satisfy the thermodynamic restriction (4.47a) is to model the flux of receptors by Fickian-diffusion, that linearly correlates $\vec{h}_R$ to the gradient of its chemical potential μ_R:

$$\vec{h}_R = -\mathbf{M}_R(c_R) \, \nabla_\Omega \left[\mu_R \right] \tag{4.51}$$

by means of a positive definite mobility tensor $\mathbf{M}_R$. The following isotropic non linear specialization for the mobility tensor $\mathbf{M}_R$

$$\mathbf{M}_R(c_R) = \mathsf{m}_R \, c_R^{max} \, \theta_R \, (1 - \theta_R) \, \mathbb{1} \tag{4.52}$$

accounts for saturation. In formula (4.52): $\theta_R = c_R / c_R^{max}$; c_R^{max} is the saturation limit for receptors. The *mobility* $\mathsf{m}_R > 0$ represents the average velocity of receptors when acted upon by a force of 1 N/mol independent of the origin of the force. Definition (4.52) represents the physical requirement that both the pure ($c_R = 0$) and the saturated ($c_R = c_R^{max}$) phases have vanishing mobilities. Neither the mobility m_R nor the saturation concentration c_R^{max} are assumed to change in time. Such a limitation can be removed without altering the conceptual picture if experimental data indicate an influence of temperature, stresses, or concentrations. Noting that

$$\nabla_\Omega \left[\mu_R \right] = RT \frac{1}{c_R^{max}} \frac{1}{\vartheta_R (1 - \vartheta_R)} \, \nabla_\Omega \left[c_R \right]$$

Fick's Law (4.51) specializes as follows

$$\vec{h}_R = -\mathbb{D}_R \, \nabla_\Omega \left[c_R \right] \tag{4.53}$$

where $\mathbb{D}_R = \mathsf{m}_R \, RT$ is the receptor *diffusivity*.

4.2.6 Chemical kinetics

The chemical kinetics of reaction (6.44) is modeled via the law of mass action:

$$w^{(6.44)} = k^+ \frac{\vartheta_L}{(1 - \vartheta_L)} \frac{\vartheta_R}{(1 - \vartheta_R)} - k^- \frac{\vartheta_C}{(1 - \vartheta_C)} \tag{4.54}$$

At chemical equilibrium, as $w^{(6.44)} = 0$ and $A^{(6.44)} = 0$, the concentrations obey the relation

$$\frac{k^+}{k^-} = \frac{\vartheta_C^{eq}}{(1 - \vartheta_C^{eq})} \frac{(1 - \vartheta_R^{eq})}{\vartheta_R^{eq}} \frac{(1 - \vartheta_L^{eq})}{\vartheta_L^{eq}} = \exp\left[-\frac{\mu_C^0 - \mu_L^0 - \mu_R^0}{RT} \right] = K_{eq}^{(6.44)} \tag{4.55}$$

which defines the constant of equilibrium $K_{eq}^{(6.44)}$ of reaction (6.44).

4.2.6.1　Infinitely fast kinetics

Experimental evidences [137] show that: (i) the equilibrium constant is high, thus favoring the formation of ligand-receptor complex and the depletions of receptors and ligands; (ii) the diffusion of receptors on the cell membrane is much slower than interaction kinetics. Accordingly, it can be assumed that the reaction kinetics is infinitely fast, in the sense that the time required to reach chemical equilibrium is orders of magnitudes smaller than the time-scale of other processes. For these reasons we assume that the concentrations of species are ruled by thermodynamic equilibrium at all times, and the concentration of complex c_C is related to the others by the equation $A^{(6.44)} = 0$, i.e. from eqs. (4.37) and (4.50)

$$A^{(6.44)} = \Delta G^0 + R\,T\left(\ln\vartheta_C - \ln\vartheta_R - \ln\vartheta_L - \ln\left(1 - \vartheta_C\right) - \ln\left(1 - \vartheta_L\right) - \ln\left(1 - \vartheta_R\right)\right) = 0 \qquad (4.56)$$

where $\Delta G^0 = \mu_C^0 - \mu_L^0 - \mu_R^0$ is the standard Gibbs free energy. Far from saturation, when $c_\beta \ll c_\beta^{max}$,

$$c_C = \frac{c_R\,c_L}{\alpha} \qquad (4.57)$$

having denoted with α the following constant:

$$\alpha = \frac{c_R^{\max}\,c_L^{\max}}{c_C^{\max}}\,\exp\left(\frac{\Delta G^0}{R\,T}\right). \qquad (4.58)$$

4.2.7　Governing Equations

The conditions (4.57) can be rewritten as

$$c_R\,c_L = \alpha\,c_C \qquad (4.59)$$

with

$$\alpha = \frac{c_R^{\max}\,c_L^{\max}}{c_C^{\max}}\,\exp\left(\frac{\mu_C^0 - \mu_R^0 - \mu_L^0}{R\,T}\right) \qquad (4.60)$$

By deriving (5.3) respect to time, by using the chain rule, we obtain

$$\alpha\frac{\partial\,c_C}{\partial t} = \frac{\partial\,(c_R\,c_L)}{\partial t} = c_L\,\frac{\partial\,c_R}{\partial t} + c_R\,\frac{\partial\,c_L}{\partial t} \qquad (4.61)$$

Then

$$\frac{\partial\,c_C}{\partial t} = \frac{1}{\alpha}\left[c_L\,\frac{\partial\,c_R}{\partial t} + c_R\,\frac{\partial\,c_L}{\partial t}\right] \qquad (4.62)$$

Eq. (4.14c) becomes:

$$\frac{1}{\alpha}\left[c_L\,\frac{\partial\,c_R}{\partial t} + c_R\,\frac{\partial\,c_L}{\partial t}\right] = w^{(1)} \qquad (4.63)$$

substituting (4.14a)

$$\frac{1}{\alpha}\left[c_L\,\frac{\partial\,c_R}{\partial t} + c_R\,\frac{\partial\,c_L}{\partial t}\right] = -\frac{\partial c_R}{\partial t} - \mathrm{div}_\Omega\left[\vec{h}_R\right] \qquad (4.64)$$

$$\left(\frac{c_L}{\alpha} + 1\right)\frac{\partial\,c_R}{\partial t} + \frac{c_R}{\alpha}\frac{\partial\,c_L}{\partial t} + \mathrm{div}_\Omega\left[\vec{h}_R\right] = 0 \qquad (4.65)$$

From Eq.s (4.14a) and (4.14b)

$$\frac{\partial c_R}{\partial t} + \mathrm{div}_\Omega\left[\vec{h}_R\right] = \frac{\partial c_L}{\partial t} - s_L(x,t) \qquad (4.66)$$

$$\frac{\partial c_R}{\partial t} + \mathrm{div}_\Omega\left[\vec{h}_R\right] - \frac{\partial c_L}{\partial t} + s_L(x,t) = 0 \qquad (4.67)$$

60

The governing equations are the following:

$$c_R \, c_L = \alpha \, c_C \tag{4.68a}$$

$$\left(\frac{c_L}{\alpha} + 1\right) \frac{\partial \, c_R}{\partial t} + \frac{c_R}{\alpha} \frac{\partial \, c_L}{\partial t} + \text{div}_\Omega \left[\vec{h}_R \right] = 0 \tag{4.68b}$$

$$\frac{\partial c_R}{\partial t} + \text{div}_\Omega \left[\vec{h}_R \right] - \frac{\partial c_L}{\partial t} + s_L(x,t) = 0 \tag{4.68c}$$

Initial conditions are imposed for the initial concentrations:

$$c_R(t = 0) = c_R^0 \tag{4.69a}$$

$$c_L(t = 0) = c_L^0 \tag{4.69b}$$

$$c_C(t = 0) = 0 \,. \tag{4.69c}$$

4.2.8 Weak form and numerical solution

The weak formulation in space results from multiplying the strong form of governing equations by a suitable set of tests functions and performing an integration upon the domain. Specifically, the weak form Eq. (4.65), defining with $\hat{c}_R$ a test function, reads:

$$\int_\Omega \left(\left(\frac{c_L}{\alpha} + 1 \right) \frac{\partial \, c_R}{\partial t} + \frac{c_R}{\alpha} \frac{\partial \, c_L}{\partial t} + \text{div}_\Omega \left[-\mathbb{D}_R \, \nabla_\Omega \left[c_R \right] \right] \right) \hat{c}_R \, \mathrm{d}S = 0 \tag{4.70}$$

Applying the divergence theorem over Ω, the former equation transforms as follows:

$$\int_\Omega \left(\frac{c_L}{\alpha} + 1 \right) \frac{\partial \, c_R}{\partial t} \hat{c}_R \, \mathrm{d}S + \int_\Omega \frac{c_R}{\alpha} \frac{\partial \, c_L}{\partial t} \hat{c}_R \, \mathrm{d}S + \mathbb{D}_R \int_\Omega \nabla_\Omega \left[c_R \right] \cdot \nabla_\Omega \left[\hat{c}_R \right] \, \mathrm{d}S = 0 \tag{4.71a}$$

The weak form of (4.67), defining with $\hat{c}_L$ a test function, reads after easy algebra:

$$\int_\Omega \hat{c}_L \frac{\partial \, c_R}{\partial t} \, \mathrm{d}S - \int_\Omega \hat{c}_L \frac{\partial \, c_L}{\partial t} \, \mathrm{d}S + \mathbb{D}_R \int_\Omega \nabla_\Omega \left[c_R \right] \cdot \nabla_\Omega \left[\hat{c}_L \right] \, \mathrm{d}S + \int_\Omega \hat{c}_L \, s_L(x,t) \, \mathrm{d}S = 0 \tag{4.71b}$$

The weak form (4.71) can be transformed in a first order Ordinary Differential Equation (ODE) in time if discretization is performed via separated variables, with spatial test $\varphi_i(x)$ and shape functions $\varphi_j(x)$ and nodal unknowns that depend solely on time. The usual Einstein summation convention is taken henceforth for repeated indexes.

$$c_R = \varphi_k^R(x) \, c_{Rk}(t), \qquad \nabla_\Omega \left[c_R \right] = \nabla_\Omega \left[\varphi_k^R(x) \right] \, c_{Rk}$$

$$c_L = \varphi_j^L(x) \, c_{Lj}(t), \qquad \nabla_\Omega \left[c_L \right] = \nabla_\Omega \left[\varphi_j^L(x) \right] \, c_{Lj}$$

$$\hat{c}_R = \varphi_i^R(x), \qquad \nabla_\Omega \left[\hat{c}_R \right] = \nabla_\Omega \left[\varphi_i^R(x) \right]$$

$$\hat{c}_L = \varphi_i^L(x), \qquad \nabla_\Omega \left[\hat{c}_L \right] = \nabla_\Omega \left[\varphi_i^L(x) \right]$$

The non linear ODEs read:

$$\left(\int_\Omega \varphi_i^R(x) \, \varphi_k^R(x) \, \varphi_j^L(x) \, \mathrm{d}S \right) \frac{c_{Lj}(t)}{\alpha} \frac{\partial \, c_{Rk}(t)}{\partial t} + \left(\int_\Omega \varphi_i^R(x) \, \varphi_k^R(x) \, \mathrm{d}S \right) \frac{\partial \, c_{Rk}(t)}{\partial t} +$$

$$+ \left(\int_\Omega \varphi_i^R(x) \varphi_k^R(x) \, \varphi_j^L(x) \, \mathrm{d}S \right) \frac{c_{Rk}(t)}{\alpha} \frac{\partial \, c_{Lj}(t)}{\partial t} + \mathbb{D}_R \left(\int_\Omega \nabla_\Omega \left[\varphi_k^R(x) \right] \cdot \nabla_\Omega \left[\varphi_i^R(x) \right] \, \mathrm{d}S \right) c_{Rk}(t) = 0 \tag{4.72a}$$

$$\left(\int_\Omega \varphi_i^L(x) \, \varphi_k^R(x) \, \mathrm{d}S \right) \frac{\partial \, c_{Rk}(t)}{\partial t} - \left(\int_\Omega \varphi_i^L(x) \, \varphi_j^L(x) \, \mathrm{d}S \right) \frac{\partial \, c_{Lj}(t)}{\partial t} + \int_\Omega \varphi_i^L \, s_L(x,t) \, \mathrm{d}S +$$

$$+ \mathbb{D}_R \left(\int_\Omega \nabla_\Omega \left[\varphi_k^R(x) \right] \cdot \nabla_\Omega \left[\varphi_i^L(x) \right] dS \right) c_{Rk}(t) = 0 \tag{4.72b}$$

For the time discretization of problem (4.72) finite difference schemes are generally used [149], for which the time derivatives of the concentrations are replaced by the finite differences as

$$\frac{\partial c_{Rk}}{\partial t} \simeq \frac{c_{Rk}(t + \Delta t) - c_{Rk}(t)}{\Delta t} , \qquad \frac{\partial c_{Lj}}{\partial t} \simeq \frac{c_{Lj}(t + \Delta t) - c_{Lj}(t)}{\Delta t} . \tag{4.73}$$

We make recourse to the Backward Euler method, that leads to the following non linear problem in $c_{Rk}(t+\Delta t)$ and $c_{Lk}(t + \Delta t)$:

$$\left(\int_\Omega \varphi_i^R(x) \, \varphi_k^R(x) \, \varphi_j^L(x) \, dS \right) \frac{c_{Lj}(t + \Delta t)}{\alpha} \frac{c_{Rk}(t + \Delta t)}{\Delta t} - \left(\int_\Omega \varphi_i^R(x) \, \varphi_k^R(x) \, \varphi_j^L(x) \, dS \right) \frac{c_{Lj}(t + \Delta t)}{\alpha} \frac{c_{Rk}(t)}{\Delta t} +$$

$$+ \left(\int_\Omega \varphi_i^R(x) \, \varphi_k^R(x) \, dS \right) \frac{c_{Rk}(t + \Delta t)}{\Delta t} - \left(\int_\Omega \varphi_i^R(x) \, \varphi_k^R(x) \, dS \right) \frac{c_{Rk}(t)}{\Delta t} +$$

$$+ \left(\int_\Omega \varphi_i^R(x) \varphi_k^R(x) \, \varphi_j^L(x) \, dS \right) \frac{c_{Rk}(t + \Delta t)}{\alpha} \frac{c_{Lj}(t + \Delta t)}{\Delta t} - \left(\int_\Omega \varphi_i^R(x) \varphi_k^R(x) \, \varphi_j^L(x) \, dS \right) \frac{c_{Rk}(t + \Delta t)}{\alpha} \frac{c_{Lj}(t)}{\Delta t} +$$

$$+ \mathbb{D}_R \left(\int_\Omega \nabla_\Omega \left[\varphi_k^R(x) \right] \cdot \nabla_\Omega \left[\varphi_i^R(x) \right] dS \right) c_{Rk}(t + \Delta t) = 0 \tag{4.74a}$$

$$\left(\int_\Omega \varphi_i^L(x) \, \varphi_k^R(x) \, dS \right) \frac{c_{Rk}(t + \Delta t)}{\Delta t} - \left(\int_\Omega \varphi_i^L(x) \, \varphi_k^R(x) \, dS \right) \frac{c_{Rk}(t)}{\Delta t} - \left(\int_\Omega \varphi_i^L(x) \, \varphi_j^L(x) \, dS \right) \frac{c_{Lj}(t + \Delta t)}{\Delta t} +$$

$$+ \left(\int_\Omega \varphi_i^L(x) \, \varphi_j^L(x) \, dS \right) \frac{c_{Lj}(t)}{\Delta t} + \mathbb{D}_R \left(\int_\Omega \nabla_\Omega \left[\varphi_k^R(x) \right] \cdot \nabla_\Omega \left[\varphi_i^L(x) \right] dS \right) c_{Rk}(t + \Delta t) + \int_\Omega \varphi_i^L \, s_L(x,t) \, dS = 0 \tag{4.74b}$$

4.2.9 Dimensionless concentrations

We multiplied each component by a factor $\frac{R\,T}{c_{bulk}}$ to achieve an energy on time, as a power $\left[\frac{J}{s} \right]$. But we have that the dimensionless concentrations c_β^*

$$c_R^* = \frac{c_R}{c_{bulk}}, \qquad c_L^* = \frac{c_L}{c_{bulk}}$$

$$c_R = c_R^* \, c_{bulk}, \qquad c_L = c_L^* \, c_{bulk}$$

$$\hat{c}_R = \hat{c}_R^* \, c_{bulk}, \qquad \hat{c}_L = \hat{c}_L^* \, c_{bulk}$$

Then we have to multiplied for the term $\frac{R\,T}{c_{bulk}} c_{bulk}^2$.

The governing equations of the problem are the following

$$\frac{R\,T}{c_{bulk}} c_{bulk}^2 \left\{ \frac{1}{\alpha} \left(\int_\Omega \varphi_i^R(x) \, \varphi_k^R(x) \, \varphi_j^L(x) \, dS \right) c_{Lj}(t + \Delta t) \frac{c_{Rk}(t + \Delta t)}{\Delta t} + \right.$$

$$- \frac{1}{\alpha} \left(\int_\Omega \varphi_i^R(x) \, \varphi_k^R(x) \, \varphi_j^L(x) \, dS \right) c_{Lj}(t + \Delta t) \frac{c_{Rk}(t)}{\Delta t} + \left(\int_\Omega \varphi_i^R(x) \, \varphi_k^R(x) \, dS \right) \frac{c_{Rk}(t + \Delta t)}{\Delta t} +$$

$$\frac{1}{\alpha} \left(\int_\Omega \varphi_i^R(x) \varphi_k^R(x) \, \varphi_j^L(x) \, dS \right) c_{Rk}(t + \Delta t) \frac{c_{Lj}(t + \Delta t)}{\Delta t} - \frac{1}{\alpha} \left(\int_\Omega \varphi_i^R(x) \varphi_k^R(x) \, \varphi_j^L(x) \, dS \right) c_{Rk}(t + \Delta t) \frac{c_{Lj}(t)}{\Delta t} +$$

$$\left. + \mathbb{D}_R \left(\int_\Omega \nabla_\Omega \left[\varphi_k^R(x) \right] \cdot \nabla_\Omega \left[\varphi_i^R(x) \right] dS \right) c_{Rk}(t + \Delta t) - \left(\int_\Omega \varphi_i^R(x) \, \varphi_k^R(x) \, dS \right) \frac{c_{Rk}(t)}{\Delta t} \right\} = 0 \tag{4.75}$$

$$
\frac{\mathrm{R\,T}}{c_{bulk}}\, c_{bulk}^2 \left\{ \left(\int_\Omega \varphi_i^L(x)\, \varphi_k^R(x)\, \mathrm{d}S \right) \frac{c_{Rk}(t+\Delta t)}{\Delta t} - \left(\int_\Omega \varphi_i^L(x)\, \varphi_k^R(x)\, \mathrm{d}S \right) \frac{c_{Rk}(t)}{\Delta t} \right.
$$

$$
- \left(\int_\Omega \varphi_i^L(x)\, \varphi_j^L(x)\, \mathrm{d}S \right) \frac{c_{Lj}(t+\Delta t)}{\Delta t} + \left(\int_\Omega \varphi_i^L(x)\, \varphi_j^L(x)\, \mathrm{d}S \right) \frac{c_{Lj}(t)}{\Delta t} \tag{4.76}
$$

$$
\left. + \mathbb{D}_R \left(\int_\Omega \nabla_\Omega \left[\, \varphi_k^R(x)\,\right] \cdot \nabla_\Omega \left[\, \varphi_i^L(x)\,\right] \mathrm{d}S \right) c_{Rk}(t+\Delta t) + \int_\Omega \varphi_i^L\, s_L(x,t)\, \mathrm{d}S \right\} = 0\,.
$$

4.2.10 Newton Raphson method

To solve the nonlinear equations $f(x,y)$ we use the Newton Raphson method,

$$
f(x,y) \simeq f(x^{(k)}, y^{(k)}) + D^g \left[f(x^{(k)}, y^{(k)}) \right] = 0 \tag{4.77}
$$

As usual in the Gateaux-derivative D^g sense, the Newton-Raphson scheme at iteration (k) yields

$$
D^g \left[f(x^{(k)}, y^{(k)}) \right] = \left. \frac{\mathrm{d}}{\mathrm{d}\epsilon} \left[f \left(x^{(k)} + \epsilon\, \Delta x^{(k)},\ y^{(k)} + \epsilon\, \Delta y^{(k)} \right) \right] \right|_{\epsilon=0} \tag{4.78}
$$

From now on just for the notation, we neglect the space dependence of the shape functions, then $\varphi_i^I(x) = \varphi_i^I$.

Eq. (4.75) becomes

$$
\frac{\mathrm{R\,T}}{c_{bulk}} c_{bulk}^2 \left\{ \frac{1}{\alpha} \left(\int_\Omega \varphi_i^R\, \varphi_k^R\, \varphi_j^L\, \mathrm{d}S \right) c_{Lj}^{(k)}(t+\Delta t) \frac{c_{Rk}^{(k)}(t+\Delta t)}{\Delta t} - \frac{1}{\alpha} \left(\int_\Omega \varphi_i^R\, \varphi_k^R\, \varphi_j^L\, \mathrm{d}S \right) \frac{c_{Rk}(t)}{\Delta t} c_{Lj}^{(k)}(t+\Delta t) \ + \right.
$$

$$
+ \left(\int_\Omega \varphi_i^R\, \varphi_k^R\, \mathrm{d}S \right) \frac{c_{Rk}^{(k)}(t+\Delta t)}{\Delta t} + \frac{1}{\alpha} \left(\int_\Omega \varphi_i^R \varphi_k^R\, \varphi_j^L\, \mathrm{d}S \right) c_{Rk}^{(k)}(t+\Delta t) \frac{c_{Lj}^{(k)}(t+\Delta t)}{\Delta t} +
$$

$$
- \frac{1}{\alpha} \left(\int_\Omega \varphi_i^R \varphi_k^R\, \varphi_j^L\, \mathrm{d}S \right) \frac{c_{Lj}(t)}{\Delta t} c_{Rk}^{(k)}(t+\Delta t) + \mathbb{D}_R \left(\int_\Omega \nabla_\Omega \left[\, \varphi_k^R(x)\,\right] \cdot \nabla_\Omega \left[\, \varphi_i^R(x)\,\right] \mathrm{d}S \right) c_{Rk}^{(k)}(t+\Delta t) +
$$

$$
\frac{1}{\alpha} \left(\int_\Omega \varphi_i^R\, \varphi_k^R\, \varphi_j^L\, \mathrm{d}S \right) \frac{1}{\Delta t} \left(c_{Rk}^{(k)}(t+\Delta t) \Delta c_{Lj}^{(k)} + c_{Lj}^{(k)}(t+\Delta t) \Delta c_{Rk}^{(k)} \right) - \frac{1}{\alpha} \left(\int_\Omega \varphi_i^R\, \varphi_k^R\, \varphi_j^L\, \mathrm{d}S \right) \frac{c_{Rk}(t)}{\Delta t} \Delta c_{Lj}^{(k)} +
$$

$$
+ \left(\int_\Omega \varphi_i^R\, \varphi_k^R\, \mathrm{d}S \right) \frac{\Delta c_{Rk}^{(k)}}{\Delta t} + \frac{1}{\alpha} \left(\int_\Omega \varphi_i^R \varphi_k^R\, \varphi_j^L\, \mathrm{d}S \right) \frac{1}{\Delta t} \left(c_{Rk}^{(k)}(t+\Delta t) \Delta c_{Lj}^{(k)} + c_{Lj}^{(k)}(t+\Delta t) \Delta c_{Rk}^{(k)} \right) +
$$

$$
\left. - \frac{1}{\alpha} \left(\int_\Omega \varphi_i^R \varphi_k^R\, \varphi_j^L\, \mathrm{d}S \right) \frac{c_{Lj}(t)}{\Delta t} \Delta c_{Rk}^{(k)} + \mathbb{D}_R \left(\int_\Omega \nabla_\Omega \left[\, \varphi_k^R(x)\,\right] \cdot \nabla_\Omega \left[\, \varphi_i^R(x)\,\right] \mathrm{d}S \right) \Delta c_{Ak}^{(k)} - \left(\int_\Omega \varphi_i^R\, \varphi_k^R\, \mathrm{d}S \right) \frac{c_{Rk}(t)}{\Delta t} \right\} = 0
$$

$$
\tag{4.79}
$$

From Eq. (4.76) we obtain

$$
\left\{ \left(\int_\Omega \varphi_i^L\, \varphi_k^R\, \mathrm{d}S \right) \frac{c_{Rk}^{(k)}(t+\Delta t)}{\Delta t} - \left(\int_\Omega \varphi_i^L\, \varphi_j^L\, \mathrm{d}S \right) \frac{c_{Lj}^{(k)}(t+\Delta t)}{\Delta t} + \mathbb{D}_R \left(\int_\Omega \nabla_\Omega \left[\, \varphi_k^R(x)\,\right] \cdot \nabla_\Omega \left[\, \varphi_i^L(x)\,\right] \mathrm{d}S \right) c_{Rk}^{(k)}(t+\Delta t) + \right.
$$

$$
+ \left(\int_\Omega \varphi_i^L\, \varphi_k^R\, \mathrm{d}S \right) \frac{\Delta c_{Rk}^{(k)}}{\Delta t} - \left(\int_\Omega \varphi_i^L\, \varphi_j^L\, \mathrm{d}S \right) \frac{\Delta c_{Lj}^{(k)}}{\Delta t} + \mathbb{D}_R \left(\int_\Omega \nabla_\Omega \left[\, \varphi_k^R(x)\,\right] \cdot \nabla_\Omega \left[\, \varphi_i^L(x)\,\right] \mathrm{d}S \right) \Delta c_{Rk}^{(k)} +
$$

$$
\left. - \left(\int_\Omega \varphi_i^L\, \varphi_k^R\, \mathrm{d}S \right) \frac{c_{Rk}(t)}{\Delta t} + \left(\int_\Omega \varphi_i^L\, \varphi_j^L\, \mathrm{d}S \right) \frac{c_{Lj}(t)}{\Delta t} + \int_\Omega \varphi_i^L\, s_L(x,t)\, \mathrm{d}S \right\} \frac{\mathrm{R\,T}}{c_{bulk}}\, c_{bulk}^2 = 0
$$

$$
\tag{4.80}
$$

4.2.11 Update linearized method (UP)

We propose an alternative method to solve the nonlinear equations so-called update linearized method (UP), that, from Eq. (4.75), leads to

$$
\frac{\mathrm{R}\,\mathrm{T}}{c_{bulk}} c_{bulk}^2 \left\{ \frac{1}{\alpha} \left(\int_\Omega \varphi_i^R \varphi_k^R \varphi_j^L \, \mathrm{d}S \right) c_{Lj}^{(k)}(t+\Delta t) \frac{c_{Rk}^{(k+1)}(t+\Delta t)}{\Delta t} - \frac{1}{\alpha} \left(\int_\Omega \varphi_i^R \varphi_k^R \varphi_j^L \, \mathrm{d}S \right) \frac{c_{Rk}(t)}{\Delta t} c_{Lj}^{(k+1)}(t+\Delta t) + \right.
$$

$$
+ \left(\int_\Omega \varphi_i^R \varphi_k^R \, \mathrm{d}S \right) \frac{c_{Rk}^{(k+1)}(t+\Delta t)}{\Delta t} + \frac{1}{\alpha} \left(\int_\Omega \varphi_i^R \varphi_k^R \varphi_j^L \, \mathrm{d}S \right) c_{Rk}^{(k)}(t+\Delta t) \frac{c_{Lj}^{(k+1)}(t+\Delta t)}{\Delta t} +
$$

$$
- \frac{1}{\alpha} \left(\int_\Omega \varphi_i^R \varphi_k^R \varphi_j^L \, \mathrm{d}S \right) \frac{c_{Lj}(t)}{\Delta t} c_{Rk}^{(k+1)}(t+\Delta t) + \mathrm{D}_R \left(\int_\Omega \nabla_\Omega \left[\varphi_k^R(x) \right] \cdot \nabla_\Omega \left[\varphi_i^R(x) \right] \mathrm{d}S \right) c_{Rk}^{(k+1)}(t+\Delta t) +
$$

$$
- \left(\int_\Omega \varphi_i^R \varphi_k^R \, \mathrm{d}S \right) \frac{c_{Rk}(t)}{\Delta t} \right\} = 0
$$

(4.81)

and from Eq. (4.76), we obtain:

$$
\left\{ \left(\int_\Omega \varphi_i^L \varphi_k^R \, \mathrm{d}S \right) \frac{c_{Rk}^{(k+1)}(t+\Delta t)}{\Delta t} - \left(\int_\Omega \varphi_i^L \varphi_j^L \, \mathrm{d}S \right) \frac{c_{Lj}^{(k+1)}(t+\Delta t)}{\Delta t} + \mathrm{D}_R \left(\int_\Omega \nabla_\Omega \left[\varphi_k^R(x) \right] \cdot \nabla_\Omega \left[\varphi_i^L(x) \right] \mathrm{d}S \right) c_{Rk}^{(k+1)}(t + \right.
$$

$$
- \left(\int_\Omega \varphi_i^L \varphi_k^R \, \mathrm{d}S \right) \frac{c_{Rk}(t)}{\Delta t} + \left(\int_\Omega \varphi_i^L \varphi_j^L \, \mathrm{d}S \right) \frac{c_{Lj}(t)}{\Delta t} + \int_\Omega \varphi_i^L \, s_L(x,t+\Delta t) \, \mathrm{d}S \right\} \frac{\mathrm{R}\,\mathrm{T}}{c_{bulk}} c_{bulk}^2 = 0
$$

(4.82)

4.3 Results

To simulate the interaction between VEGFR-2 and its immobilized ligand, we assume a fixed membrane geometry and account for the effects of cell adhesion with a supply of ligands onto the cell surface at a prescribed rate, s_L. Owing to this modeling simplification, the actual time-evolving geometry of the membrane becomes relatively unimportant and thus, for maximal simplicity, we analyze it as a circumference of radius $\ell = 20\,\mu m$ and assume that the time-dependent concentrations depend on the curvilinear coordinate. The model was implemented in a finite element code as a script in Wolfram Mathematica version 10 and calibrated. The simulations run until the final time $t_F = 7200\,s$ at the constant temperature 310.15 K with a substrate-adsorbed ligand concentration of 44.83 ligands/μm^2.

Parameters for the in silico simulation (see Table 4.1) were defined by in vitro assays. The cell radius ℓ was calculated from the measure of radius of 50 endothelial cells using Zeiss Axiovert 200 M microscope; receptor diffusivity D_R was obtained by FRAP analysis as previously described in Chapter 2. The amount of VEGFR-2 on cell membrane per area was calculated by dividing the number of high affinity binding sites,

Table 4.1: Material parameters used in the simulations and their bibliographic source.

Parameter	Notation	Value	Units	Ref.
cell radius	ℓ	20	μm	[137]
receptor diffusivity	D_R	0.198	$\frac{\mu m^2}{s}$	[137]
initial concentration of R	c_R^0	4.8	$\frac{\text{units}}{\mu m^2}$	[31]
initial concentration of L	c_L^0	0	$\frac{\text{units}}{\mu m^2}$	[31]
equilibrium constant	$K_{\mathrm{eq}}^{(6.44)}$	354059	–	[139]
gremlin saturation	c_L^{max}	16000	$\frac{\text{units}}{\mu m^2}$	[31]
other saturations limit	c_R^{max}	c_C^{max}	$\frac{\text{units}}{\mu m^2}$	[137]

obtained by radiolabeled binding experiments [94] for cell surface area.

As depicted in Fig. 4.4 that represents the overlay of the outcomes of simulation (green line) and in vitro experiments (red dots) [136] normalized to the value of VEGFR-2 at the final time t_F, VEGFR-2 recruitment induced by immobilized ligands shows three phases of complex formation marked by circled roman numbers: an initial plateau (I), a steep branch (II), and finally an evolution with a lower formation rate (III). Our numerical simulations allow connecting these three phases to three distinct mechanisms dominated by different limiting factors. The initial plateau is governed by the cell-ligand contact (I), the second steep phase (that ends at 600 s) is due to a chemo-mechanical evolution, induced by the cell attachment and deformation (II), and the final slow phase reflects the diffusive slow motion of the receptors from the apical to the basal membrane that is in contact with the substrate (III).

The first phase starts when a small portion of membrane gets in contact with the substrate, which provides a sudden supply of ligands that immediately trap the available receptors. This phase is very rapid, because the reaction rate is the controlling factor (in our model assumed infinite), and fully depletes the concentration of free receptors, because the equilibrium constant is very large. The second phase (calibrated in 10 minutes from experiments) is rate-controlled by the mechanical deformation of the cell, which provides additional supply of ligands that afresh immediately react with the available receptors on the newly formed contact area. The mechanical deformation of the cell and the VEGFR-2 recruitment are influenced by the chemical affinity of the VEGFR2-gremlin binding reaction coupled with intracellular cortical actin dynamics. In our co-designed experimental and theoretical study, the cell adhesion is not mediated by integrin engagement, even though integrin involvement cannot be completely ruled out. We observed that in our experimental conditions substrate-immobilized growth factors act as a cell-adhesive stimulus for endothelial cells, which is weaker than the ECM. The cell surface becomes depleted of free receptors very rapidly where the cell adheres to the substrate. When the mechanical deformation terminates and the cell is eventually spread, the diffusion of receptors becomes the rate-controlling mechanism. During this final phase, receptors that diffuse through the boundary of the contact surface are immediately trapped and immobilized by the ligands on the substrate. Therefore, the VEGFR2-gremlin complex tends to accumulate at the boundary of the basal aspect of the cells in close contact with ECM. Such a localization was observed in the ventral plasma membrane (VPM) of endothelial cells adherent on gremlin-enriched surfaces. A higher concentration of receptors at the cell boundary could have relevant biological implications for the cell, which may sense ligand concentration variation and migrate in the direction of stimulus production.

The quantitative correspondence between experimental and numerical outcomes suggests that the number of well-oriented ligands available for the receptor binding is much smaller than the total amount of immobilized ligands. As shown in Fig. 4.4, the simulated evolution in time of the overall amount of bound VEGFR2-ligands complex on the membrane overlaps the experimental outcomes we previously observed [136], validating of the model.
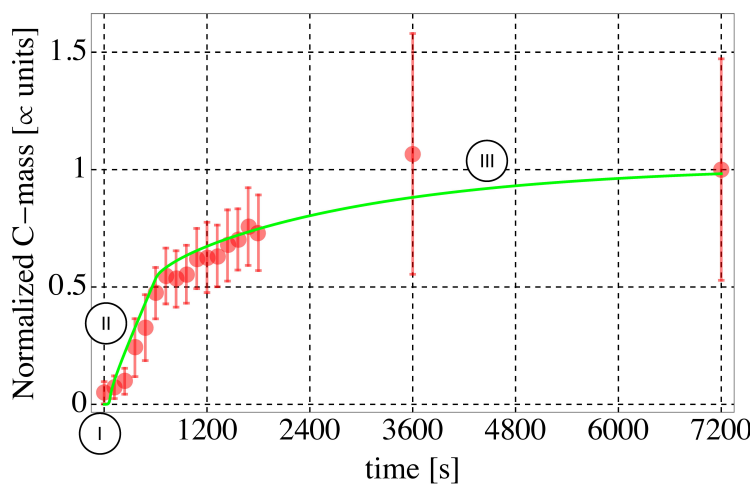
Figure 4.4: Time evolution of the VEGFR2-gremlin complex formation on the EC membrane. Comparison is made between the VEGFR-2 total fluorescence intensity (free and bound) in contact the substrate (red dots) and the numerical simulation data (green lines). To allow comparisons, both sets of data have been normalized to the values reached at the final time $t_F = 7200\,s$.

Numerical simulations predict the evolution of the concentration of free receptors c_R during 2 hours of cell

stimulation. Figure 4.5**A** quantifies c_R at each location along the membrane at different times. Exploiting the axial symmetry of the simulations, each curve on the right side of Figure 4.5**A** depicts the spatial concentration profile every minute. At $t = 0$ the distribution of receptors is uniform at the concentration $c_R = 4.8$ receptors/μm^2. After $60\,s$, the concentration profile is perturbed and decreases at the bottom of the cell due to receptor-ligand complex formation. As time goes by, starting from $120\,s$, an enlarging zone with negligible concentration $c_R \approx 0$ of free receptors is visible at the basal side of the cell (point A), due to the engagement of free receptors by immobilized ligands. At the end of the simulation, at $t_F = 7200\,s$, the concentration of unbound receptors at the apical side amounts at $c_R = 0.5$ receptors/μm^2. The chemo-mechanical transport model allows concluding that the depletion of free receptors is due to three concurrent factors: i) the infinitely fast kinetics of the ligand-receptor interaction; ii) the high equilibrium constant, that favors the formation of ligand-receptor complex; iii) the evidence that diffusion of the receptor on the cell membrane is much slower than interaction kinetics.

The depletion propagates with time, so that at $t_f = 600\,s$, after the cell is completely adhered, the lower portion of the cell membrane is essentially empty of free receptors. Since no further supply s_L is provided afterwards, the process becomes diffusion-dominated, and it slowly evolves towards a final steady state. The thick blue curve plots the distribution of free receptors at the end of the simulation at time t_F. The maximum concentration of free VEGFR-2 at t_F is 0.49 receptors/μm^2 and a steady state has not yet been reached. Numerical simulations predict that after 2 hours of adhesion (at $t_F = 7200\,s$) a zone with high ligand-receptor complex concentration manifests at the boundary of the contact area. Figure 4.5**B** depicts the evolution of complex c_C in space (X axis) and time (different colors) at the basal aspect of ECs. Such distribution profile was confirmed experimentally in EC ventral plasma membranes (VPMs), as shown in Fig. 4.5**C**. VPMs were obtained by an osmotic shock of endothelial cells, that preserves only the basal portion of cell membrane in close contact with ECM, allowing the visualization of the recruited receptors VEGFR-2.
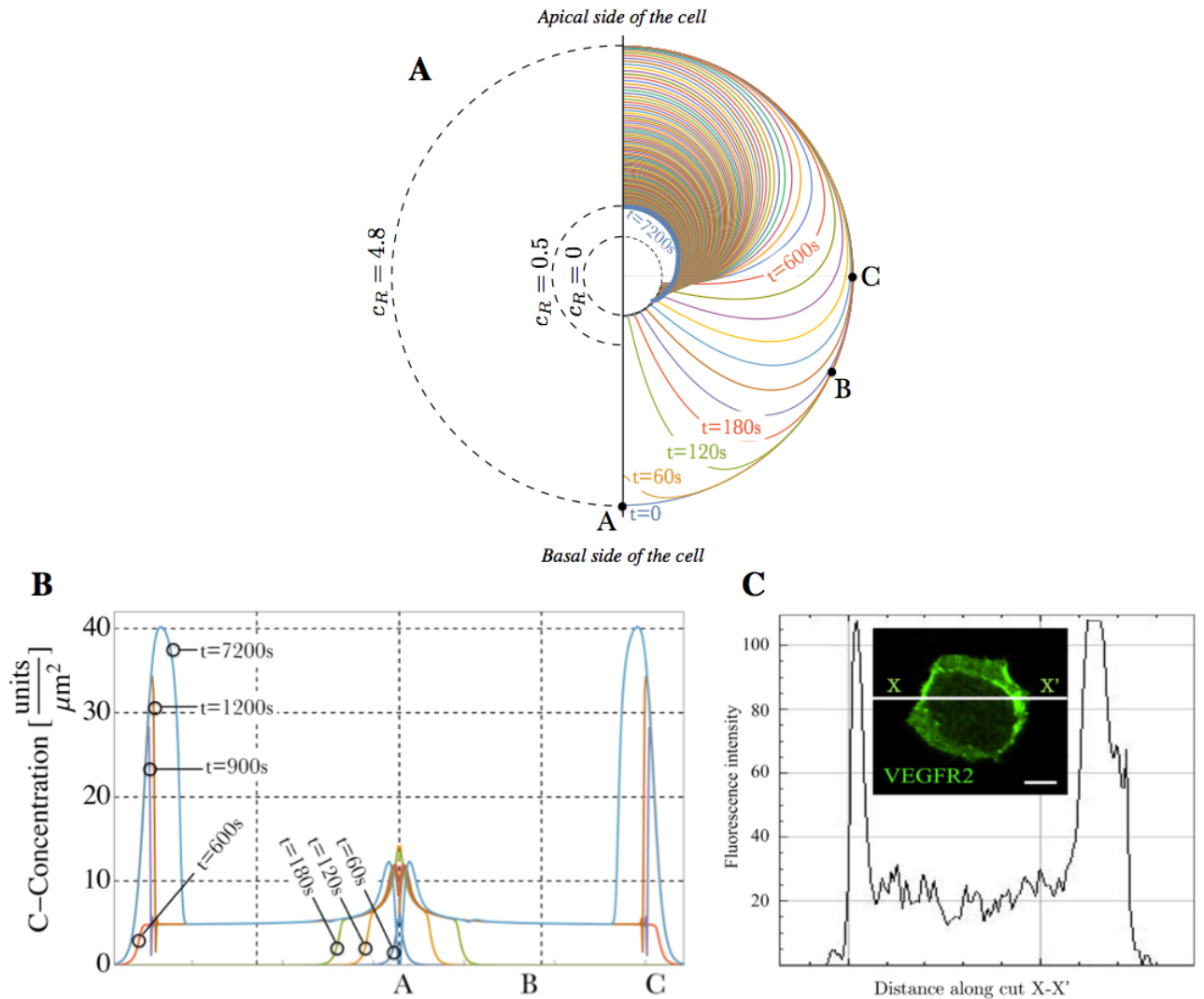
Figure 4.5: The chemo-mechanical transport model describes VEGFR2 relocation dynamics. **(A)** Time evolution of the spatial concentration c_R of free VEGFR-2 along the cell membrane. Each curve plots the distribution of free receptors at different times $t = 60\,n$, with $n = 0, 1, 2, \ldots 120\,s$ from the beginning of the experiment at $t = 0$ to the final time $t_F = 7200\,s$. **(B)** Spatial evolution of the concentration cC of the receptor-ligand complex at various times. The curves report the numerical simulation: points A, B, and C correspond to those in **(A)**. **(C)** ventral plasma membrane staining for VEGFR-2 confirms peaks in the intensity of fluorescence at the boundary of the substrate/membrane contact surface.

4.4 Conclusion

We developed a multi-physics model to describe and predict the effects of ligands on VEGFR-2 relocation during the endothelial cell activation. The interaction between ligands and receptors has been modeled by a chemical reaction that produces a complex. The model accounts for finite reaction kinetics, although simulations have been carried out assuming that the reaction kinetics is infinitely fast. The time-scale of the VEGFR2-ligand binding reaction is in fact assumed to be much faster than the time-scale of the mechanical deformation of the cell and of the diffusion of receptors on cell membrane. The effect of the mechanical

deformation of the cell has been accounted for in the model, by surrogating the explicit description of the cell spreading/deformation with a given increase in time of the surface area available for the chemical reaction by means the function s_L. Under these assumptions, we recovered the experimental evidence that the motion of receptors and their subsequent trapping into immobile VEGFR2-ligands complexes proceed in a sequence of three phases, and we characterized those phases with different rate-controlling factors. The model predicts the amount of well-oriented ligands available for the receptor binding, by noticing that this value is much smaller than the total number of immobilized ligands c_L^{max}.

The key features of our experimental evidence on VEGFR-2 relocation are captured well. In particular, through the numerical simulations carried out in this Chapter, we evaluated:

- the time evolution of the spatial concentration of free receptors VEGFR-2 along the cell membrane;

- the spatial evolution of the ligand-receptor complex concentration at various time, with high concentration manifest at the boundary of the contact area.

Chapter 5

VEGFR-2 and integrin interaction model

5.1   Introduction

Motivated by the biological background summarized in Chapter 1, we are interested in evaluating the interplay between the VEGFR-2/ligand complex and the integrins. The models described in Chapters 3 and 4 do not take into account such complex biophysics mechanisms and the angiogenesis processes cannot be fully understood without a detailed analysis of the mechanics of the cell incorporating the key features of the remodeling of the cytoskeleton. In the present Chapter, the mathematical model described in the previous Chapter will be extended in order to account for the integrins interaction. This section aims at building up the weak form of the balance equations to be used on a computer code eventually enabling a numerical approximation of the partial differential equations of the problem.

5.2   VEGFR-2 and Integrin interaction model

5.2.1   Chemical reactions

In Chapters 3 and 4 a single chemical reaction has been described, which simulates the interaction between VEGFR-2 and its specific ligand (either VEGF or gremlin). By increasing the complexity of the model, we add here two more interactions among:

- low affinity integrin and its specific ECM ligand (either fibrinogen or fibronectin), leading to high affinity integrins cluster responsible of stress fibers and FA formation and

- low affinity integrin and the VEGFR2/VEGF complex, forming another complex type.

By noting that

1. VEGF or gremlin are responsible to the VEGFR-2 recruitment, and fibrinogen is the specific ECM ligand able to bind integrins. They are both immobilized to the ECM, mimicked by the substrate;

2. low affinity integrins are able to diffuse on the cell membrane, as for VEGFR-2;

3. high affinity integrins are trans-membrane proteins that are not able to diffuse on the cell membrane.

We define the species as following

- I_L is the low affinity integrin,

- L^I is the specific ligand for integrin (for example: fibrinogen, fibronectin),

- I_H denotes the high affinity integrin,

- $C^{(1)}$ describes the complex resulted from the interaction between the low affinity integrin I_L and its specific ligand L^I,

- R, is the Vascular Endothelian Growth Factor Receptor 2 (VEGFR-2),

- L^R defines the specific ligand, as VEGF-A$_{121}$, VEGF-A$_{165}$ (canonical ligands) and gremlin (non-canonical ligand),

- $C^{(2)}$ describes the receptor-ligand complex, that is able to trigger the first intra-cellular signal that leads to downstream signaling pathway, altered gene expression, and cell proliferation,

- $C^{(3)}$ identifies the complex produced from low affinity integrin and the complex $C^{(2)}$ of the reaction (5.1b) that drives a long-term VEGFR phosphorilation needed to trigger the first intra-cellular signal.

The chemical reactions reads

$$I_L + L^I = I_H\,L^I = C^{(1)} \tag{5.1a}$$
$$R + L^R = C^{(2)} \tag{5.1b}$$
$$I_L + C^{(2)} = C^{(3)} \tag{5.1c}$$

where (5.1a) is the "focal adhesion" reaction, (5.1b) is the reaction that leads to receptor and ligand binding and the (5.1c) is the interplay between integrin and the VEGFR2/ligand complex.

By assuming that

- ligands L^I and integrins I_H are not able to diffuse on the substrate and on the cell membrane, respectively

- ligands L^R and complex $C^{(2)}$ are not able to diffuse on the substrate and on the cell membrane, respectively

we can now write the mass balance equations.

5.2.2   Mass conservation of species

Denoting with c_I as the concentration of species I, measured in $\left[\frac{\text{number of molecules}}{\mu m^2}\right]$, mass balance equations read,

$$\frac{\partial c_{I_L}}{\partial t} + \text{div}_\Omega\left[\vec{h}_{I_L}\right] = -\text{w}^{(1)} - \text{w}^{(3)} \tag{5.2a}$$

$$\frac{\partial c_{L^I}}{\partial t} = -\text{w}^{(1)} + s_{L^I}(\mathbf{x}, t) \tag{5.2b}$$

$$\frac{\partial c_{C^{(1)}}}{\partial t} = +\text{w}^{(1)} \tag{5.2c}$$

$$\frac{\partial c_R}{\partial t} + \text{div}_\Omega\left[\vec{h}_R\right] = -\text{w}^{(2)} \tag{5.2d}$$

$$\frac{\partial c_{L^R}}{\partial t} = -\text{w}^{(2)} + s_{L^R}(\mathbf{x}, t) \tag{5.2e}$$

$$\frac{\partial c_{C^{(2)}}}{\partial t} = +\text{w}^{(2)} - \text{w}^{(3)} \tag{5.2f}$$

$$\frac{\partial c_{C^{(3)}}}{\partial t} = +\text{w}^{(3)} \tag{5.2g}$$

The gremlin/VEGF L^R mass supply $s_{L^R}(\mathbf{x}, t)$ is defined as in Section "Surrogated mechanics" in Chapter 4, and the fibrinogen L^I mass supply $s_{L^I}(\mathbf{x}, t)$ mimics the contact between the cell membrane and the

substrate. The mass balance equations are written for seven unknown concentrations of the species .

In the assumption of infinitely fast chemical kinectics, as previously described in Chapter 4, for each reaction $A + B \leftrightarrows C$, we can write the reagents as function of the product, by a term α,

$$c_A \, c_B = \alpha \, c_C \tag{5.3}$$

with

$$\alpha = \frac{c_A^{max} \, c_B^{max}}{c_C^{max}} \, \exp\left(\frac{\mu_C^0 - \mu_A^0 - \mu_B^0}{RT} \right) \tag{5.4}$$

Specifically, we can write

$$c_{I_L} \, c_{L^I} = \alpha^{(1)} \, c_{C^{(1)}} \tag{5.5}$$

with

$$\alpha^{(1)} = \frac{c_{I_L}^{max} \, c_{L^I}^{max}}{c_{C^{(1)}}^{max}} \, \exp\left(\frac{\mu_{C^{(1)}}^0 - \mu_{I_L}^0 - \mu_{L^I}^0}{RT} \right) = \frac{c_{I_L}^{max} \, c_{L^I}^{max}}{c_{C^{(1)}}^{max}} \, \exp\left(\frac{\Delta G^{(5.1a)}}{RT} \right) \tag{5.6}$$

$$c_R \, c_{L^R} = \alpha^{(2)} \, c_{C^{(2)}} \tag{5.7}$$

with

$$\alpha^{(2)} = \frac{c_R^{max} \, c_{L^R}^{max}}{c_{C^{(2)}}^{max}} \, \exp\left(\frac{\mu_{C^{(2)}}^0 - \mu_R^0 - \mu_{L^R}^0}{RT} \right) = \frac{c_R^{max} \, c_{L^R}^{max}}{c_{C^{(2)}}^{max}} \, \exp\left(\frac{\Delta G^{(5.1b)}}{RT} \right) \tag{5.8}$$

$$c_{I_L} \, c_{C^{(2)}} = \alpha^{(3)} \, c_{C^{(3)}} \tag{5.9}$$

with

$$\alpha^{(3)} = \frac{c_{I_L}^{max} \, c_{C^{(2)}}^{max}}{c_{C^{(3)}}^{max}} \, \exp\left(\frac{\mu_{C^{(3)}}^0 - \mu_{I_L}^0 - \mu_{C^{(2)}}^0}{RT} \right) = \frac{c_{I_L}^{max} \, c_{C^{(2)}}^{max}}{c_{C^{(3)}}^{max}} \, \exp\left(\frac{\Delta G^{(5.1c)}}{RT} \right) \tag{5.10}$$

$$c_{C^{(1)}} = \frac{1}{\alpha^{(1)}} \, c_{I_L} \, c_{L^I} \tag{5.11a}$$

$$c_{C^{(2)}} = \frac{1}{\alpha^{(2)}} \, c_R \, c_{L^R} \tag{5.11b}$$

$$c_{C^{(3)}} = \frac{1}{\alpha^{(3)}} \, c_{I_L} \, c_{C^{(2)}} \tag{5.11c}$$

The time derivative of Eq.s (5.11) yields:

$$\frac{\partial \, c_{C^{(1)}}}{\partial t} = \frac{1}{\alpha^{(1)}} \left[c_{I_L} \frac{\partial \, c_{L^I}}{\partial t} + c_{L^I} \frac{\partial \, c_{I_L}}{\partial t} \right] \tag{5.12}$$

$$\frac{\partial \, c_{C^{(2)}}}{\partial t} = \frac{1}{\alpha^{(2)}} \left[c_R \frac{\partial \, c_{L^R}}{\partial t} + c_{L^R} \frac{\partial \, c_R}{\partial t} \right] \tag{5.13}$$

$$\frac{\partial \, c_{C^{(3)}}}{\partial t} = \frac{1}{\alpha^{(3)}} \left[c_{I_L} \frac{\partial \, c_{C^{(2)}}}{\partial t} + c_{C^{(2)}} \frac{\partial \, c_{I_L}}{\partial t} \right] \tag{5.14}$$

From the mass balance equations (5.2d) and (5.2e) we obtain the following equation:

$$\frac{\partial c_R}{\partial t} + \text{div}_\Omega \left[\vec{h}_{I_L} \right] = \frac{\partial c_{L^R}}{\partial t} - s_{L^R}(\mathbf{x}, t) \tag{5.15}$$

The mass conservation Eq.s (5.2b) and (5.2c) lead to

$$\frac{\partial c_{C^{(1)}}}{\partial t} = -\frac{\partial c_{L^I}}{\partial t} + s_{L^I}(\mathbf{x}, t) \tag{5.16}$$

by replacing the time derivative (5.12), we obtain after simple algebra

$$\frac{\partial c_{L^I}}{\partial t} \left(\frac{1}{\alpha^{(1)}} c_{I_L} + 1 \right) + \frac{1}{\alpha^{(1)}} c_{L^I} \frac{\partial c_{I_L}}{\partial t} = s_{L^I}(\mathbf{x}, t) \tag{5.17}$$

From Eq. (5.2f), by replacing Eq.s (5.2e) and (5.2g), yields

$$\frac{\partial c_{C^{(2)}}}{\partial t} + \frac{\partial c_{C^{(3)}}}{\partial t} = -\frac{\partial c_{L^R}}{\partial t} + s_{L^R}(\mathbf{x}, t) \tag{5.18}$$

Finally, we replace the time derivatives (5.13) and (5.14) as well as the relation (5.11b), so to write

$$\frac{1}{\alpha^{(2)}} \left[c_R \frac{\partial c_{L^R}}{\partial t} + c_{L^R} \frac{\partial c_R}{\partial t} \right] + \frac{1}{\alpha^{(3)}} \left[c_{I_L} \frac{\partial c_{C^{(2)}}}{\partial t} + c_{C^{(2)}} \frac{\partial c_{I_L}}{\partial t} \right] = -\frac{\partial c_{L^R}}{\partial t} + s_{L^R}(\mathbf{x}, t) \tag{5.19}$$

$$\frac{1}{\alpha^{(2)}} \left[c_R \frac{\partial c_{L^R}}{\partial t} + c_{L^R} \frac{\partial c_R}{\partial t} \right] + \frac{1}{\alpha^{(3)}} \left[c_{I_L} \frac{\partial}{\partial t} \left(\frac{1}{\alpha^{(2)}} c_R c_{L^R} \right) + \frac{1}{\alpha^{(2)}} c_R c_{L^R} \frac{\partial c_{I_L}}{\partial t} \right] = -\frac{\partial c_{L^R}}{\partial t} + s_{L^R}(\mathbf{x}, t) \tag{5.20}$$

From Eq. (5.2a), substituting Eq.s (5.2b) and (5.2g), leads to

$$\frac{\partial c_{C^{(3)}}}{\partial t} = \frac{\partial c_{L^I}}{\partial t} - \frac{\partial c_{I_L}}{\partial t} - \text{div}_\Omega \left[\vec{h}_{I_L} \right] - s_{L^I}(\mathbf{x}, t), \tag{5.21}$$

which, by using the time derivative (5.14) and the relation (5.11b), becomes

$$\frac{1}{\alpha^{(3)}} \left[c_{I_L} \frac{\partial}{\partial t} \left(\frac{1}{\alpha^{(2)}} c_R c_{L^R} \right) + \frac{1}{\alpha^{(2)}} c_R c_{L^R} \frac{\partial c_{I_L}}{\partial t} \right] = \frac{\partial c_{L^I}}{\partial t} - \frac{\partial c_{I_L}}{\partial t} - \text{div}_\Omega \left[\vec{h}_{I_L} \right] - s_{L^I}(\mathbf{x}, t) \tag{5.22}$$

In summary, the governing equations are the following:

$$\frac{\partial c_R}{\partial t} + \text{div}_\Omega \left[\vec{h}_R \right] = \frac{\partial c_{L^R}}{\partial t} - s_{L^R}(\mathbf{x}, t)$$

$$\frac{\partial c_{L^I}}{\partial t} \left(\frac{1}{\alpha^{(1)}} c_{I_L} + 1 \right) + \frac{1}{\alpha^{(1)}} c_{L^I} \frac{\partial c_{I_L}}{\partial t} = s_{L^I}(\mathbf{x}, t)$$

$$\frac{1}{\alpha^{(2)}} \left[c_R \frac{\partial c_{L^R}}{\partial t} + c_{L^R} \frac{\partial c_R}{\partial t} \right] + \frac{1}{\alpha^{(3)}} \left[c_{I_L} \frac{\partial}{\partial t} \left(\frac{1}{\alpha^{(2)}} c_R c_{L^R} \right) + \frac{1}{\alpha^{(2)}} c_R c_{L^R} \frac{\partial c_{I_L}}{\partial t} \right] = -\frac{\partial c_{L^R}}{\partial t} + s_{L^R}(\mathbf{x}, t)$$

$$\frac{1}{\alpha^{(3)}} \left[c_{I_L} \frac{\partial}{\partial t} \left(\frac{1}{\alpha^{(2)}} c_R c_{L^R} \right) + \frac{1}{\alpha^{(2)}} c_R c_{L^R} \frac{\partial c_{I_L}}{\partial t} \right] + \text{div}_\Omega \left[\vec{h}_{I_L} \right] = \frac{\partial c_{L^I}}{\partial t} - \frac{\partial c_{I_L}}{\partial t} - s_{L^I}(\mathbf{x}, t),$$

where c_R, c_{L^R}, c_{I_L}, and c_{L^I} are the unknown concentrations of VEGFR-2 receptor, integrin and their specific ligands, respectively. By using the same procedure shown in Chapter 4, the governing equations have been written in the strong form. The next step is to rewrite these equations in a discretized weak form.

5.2.3 Discretized weak form

Definig the test function $\hat{c}_1$ for Eq. (5.15), standard mathematical passages lead from

$$\int_\Omega \left(\frac{\partial c_R}{\partial t} + \mathrm{div}_\Omega \left[\vec{h}_R \right] - \frac{\partial c_{L^R}}{\partial t} + s_{L^R}(\mathbf{x},t) \right) \hat{c}_1 \, \mathrm{d}S = 0 \tag{5.24}$$

to:

$$\int_\Omega \hat{c}_1 \frac{\partial c_R}{\partial t} \, \mathrm{d}S - \int_\Omega \hat{c}_1 \frac{\partial c_{L^R}}{\partial t} \, \mathrm{d}S + \mathbb{D}_R \int_\Omega \nabla_\Omega \left[c_R \right] \nabla_\Omega \left[\hat{c}_1 \right] \, \mathrm{d}S + \int_\Omega \hat{c}_1 \, s_{L^R} \, \mathrm{d}S = 0 \tag{5.25}$$

Analogously, by denoting with $\hat{c}_2$ test function Eq.(5.17), one has

$$\int_\Omega \frac{\hat{c}_2}{\alpha^{(1)}} \, c_{I_L} \frac{\partial c_{L^I}}{\partial t} \, \mathrm{d}S + \int_\Omega \hat{c}_2 \frac{\partial c_{L^I}}{\partial t} \, \mathrm{d}S + \int_\Omega \frac{\hat{c}_2}{\alpha^{(1)}} \, c_{L^I} \frac{\partial c_{I_L}}{\partial t} \, \mathrm{d}S - \int_\Omega \hat{c}_2 \, s_{L^I}(\mathbf{x},t) \, \mathrm{d}S = 0 \tag{5.26}$$

Finally defining $\hat{c}_3$ as the test funcion for Eq. (5.20)

$$\int_\Omega \frac{\hat{c}_3}{\alpha^{(2)}} \, c_R \frac{\partial c_{L^R}}{\partial t} \, \mathrm{d}S + \int_\Omega \frac{\hat{c}_3}{\alpha^{(2)}} \, c_{L^R} \frac{\partial c_R}{\partial t} \, \mathrm{d}S + \int_\Omega \frac{\hat{c}_3}{\alpha^{(3)} \alpha^{(2)}} \, c_R \, c_{L^R} \frac{\partial c_{I_L}}{\partial t} \, \mathrm{d}S +$$
$$\int_\Omega \frac{\hat{c}_3}{\alpha^{(3)} \alpha^{(2)}} \, c_R \, c_{I_L} \frac{\partial c_{L^R}}{\partial t} \, \mathrm{d}S + \int_\Omega \frac{\hat{c}_3}{\alpha^{(3)} \alpha^{(2)}} \, c_{L^R} \, c_{I_L} \frac{\partial c_R}{\partial t} \, \mathrm{d}S + \int_\Omega \hat{c}_3 \frac{\partial c_{L^R}}{\partial t} \, \mathrm{d}S - \int_\Omega \hat{c}_3 \, s_{L^R}(\mathbf{x},t) \, \mathrm{d}S = 0 \tag{5.27}$$

and indicating with $\hat{c}_4$ the test funcion for Eq. (5.22):

$$\int_\Omega \frac{\hat{c}_4}{\alpha^{(3)} \alpha^{(2)}} c_R \, c_{L^R} \frac{\partial c_{I_L}}{\partial t} \, \mathrm{d}S + \int_\Omega \frac{\hat{c}_4}{\alpha^{(3)} \alpha^{(2)}} c_R \, c_{I_L} \frac{\partial c_{L^R}}{\partial t} \, \mathrm{d}S + \int_\Omega \frac{\hat{c}_4}{\alpha^{(3)} \alpha^{(2)}} c_{I_L} \, c_{L^R} \frac{\partial c_R}{\partial t} \, \mathrm{d}S +$$
$$+ \int_\Omega \hat{c}_4 \frac{\partial c_{I_L}}{\partial t} \, \mathrm{d}S - \int_\Omega \hat{c}_4 \frac{\partial c_{L^I}}{\partial t} \, \mathrm{d}S + \mathbb{D}_{I_L} \int_\Omega \nabla_\Omega \left[c_{I_L} \right] \nabla_\Omega \left[\hat{c}_4 \right] \, \mathrm{d}S + \int_\Omega \hat{c}_4 \, s_{L^I} \, \mathrm{d}S = 0 \tag{5.28}$$

It is convenient to discretize the concentration fields by the finite element method, assuming the following linear conbination as the approximate solutions:

$$c_R = c_R(\mathbf{x},t) = \varphi_k^R(\mathbf{x}) \, c_k^R(t) \tag{5.29a}$$
$$\hat{c}_1 = \varphi_i^R(\mathbf{x}) \tag{5.29b}$$
$$c_{L^R} = c_{L^R}(\mathbf{x},t) = \varphi_h^{L^R}(\mathbf{x}) \, c_h^{L^R}(t) \tag{5.29c}$$
$$\hat{c}_2 = \varphi_i^{L^I}(\mathbf{x}) \tag{5.29d}$$
$$c_{I_L} = c_{I_L}(\mathbf{x},t) = \varphi_j^{I_L}(\mathbf{x}) \, c_j^{I_L}(t) \tag{5.29e}$$
$$\hat{c}_3 = \varphi_i^{L^R}(\mathbf{x}) \tag{5.29f}$$
$$c_{L^I} = c_{L^I}(\mathbf{x},t) = \varphi_m^{L^I}(\mathbf{x}) \, c_m^{L^I}(t) \tag{5.29g}$$
$$\hat{c}_4 = \varphi_i^{I_L}(\mathbf{x}) \tag{5.29h}$$

by assuming that the approximate solution has to be a linear combination of space-dependence functions so-called shape functions $\varphi_i^I(\mathbf{x})$, as shown on the previous Chapter. In Eq.s 5.29 Eistein summation notation holds. From now on we neglect the shape funcions space dependence $\varphi_i^I = \varphi_i^I(\mathbf{x})$ and for now the time-dependence for the concentrations. Then the discrete problem becomes from Eq. (5.25)

73

$$
\left(\int_{\Omega} \varphi_i^R(\mathbf{x})\, \varphi_k^R(\mathbf{x})\, \mathrm{d}S \right) \frac{\partial c_k^R(t)}{\partial t} - \left(\int_{\Omega} \varphi_i^R(\mathbf{x})\, \varphi_h^{L^R}(\mathbf{x})\, \mathrm{d}S \right) \frac{\partial c_h^{L^R}(t)}{\partial t} +
$$
$$
+ \, \mathbb{D}_R \left(\int_{\Omega} \nabla_{\Omega}\left[\varphi_k^R(\mathbf{x})\right] \nabla_{\Omega}\left[\varphi_i^R(\mathbf{x})\right] \mathrm{d}S \right) \mathrm{c}_k^R(t) + \int_{\Omega} \varphi_i^R(\mathbf{x})\, s_{L^R}(\mathbf{x},t)\, \mathrm{d}S = 0
\tag{5.30}
$$

From Eq. (5.26)

$$
\frac{1}{\alpha^{(1)}} \left(\int_{\Omega} \varphi_i^{L^I}(\mathbf{x})\, \varphi_j^{I_L}(\mathbf{x})\, \varphi_m^{L^I}(\mathbf{x})\, \mathrm{d}S \right) c_j^{I_L}(t)\, \frac{\partial c_m^{L^I}(t)}{\partial t} + \left(\int_{\Omega} \varphi_i^{L^I}(\mathbf{x})\, \varphi_m^{L^I}(\mathbf{x})\, \mathrm{d}S \right) \frac{\partial c_m^{L^I}(t)}{\partial t} +
$$
$$
+ \frac{1}{\alpha^{(1)}} \left(\int_{\Omega} \varphi_i^{L^I}(\mathbf{x})\, \varphi_j^{I_L}(\mathbf{x})\, \varphi_m^{L^I}(\mathbf{x})\, \mathrm{d}S \right) c_m^{L^I}(t)\, \frac{\partial c_j^{I_L}(t)}{\partial t} - \int_{\Omega} \varphi_i^{L^I}(\mathbf{x})\, s_{L^I}(\mathbf{x},t)\, \mathrm{d}S = 0
\tag{5.31}
$$

From Eq. (5.27)

$$
\frac{1}{\alpha^{(2)}} \left(\int_{\Omega} \varphi_i^{L^R}\, \varphi_k^R\, \varphi_h^{L^R}\, \mathrm{d}S \right) \frac{\partial c_h^{L^R}}{\partial t} + \frac{1}{\alpha^{(2)}} \left(\int_{\Omega} \varphi_i^{L^R}\, \varphi_k^R\, \varphi_h^{L^R}\, \mathrm{d}S \right) c_h^{L^R}\, \frac{\partial c_k^R}{\partial t} +
$$
$$
\frac{1}{\alpha^{(3)}\,\alpha^{(2)}} \left[\left(\int_{\Omega} \varphi_i^{L^R}\, \varphi_k^R\, \varphi_h^{L^R}\, \varphi_j^{I_L}\, \mathrm{d}S \right) c_k^R\, c_h^{L^R}\, \frac{\partial c_j^{I_L}}{\partial t} + \left(\int_{\Omega} \varphi_i^{L^R}\, \varphi_k^R\, \varphi_h^{L^R}\, \varphi_j^{I_L}\, \mathrm{d}S \right) c_j^{I_L}\, c_k^R\, \frac{\partial c_h^{L^R}}{\partial t} \right]
$$
$$
\frac{1}{\alpha^{(3)}\,\alpha^{(2)}} \left(\int_{\Omega} \varphi_i^{L^R}\, \varphi_k^R\, \varphi_h^{L^R}\, \varphi_j^{I_L}\, \mathrm{d}S \right) c_j^{I_L}\, c_h^{L^R}\, \frac{\partial c_k^R}{\partial t} + \left(\int_{\Omega} \varphi_i^{L^R}\, \varphi_h^{L^R}\, \mathrm{d}S \right) \frac{\partial c_h^{L^R}}{\partial t} - \int_{\Omega} \varphi_i^{L^R}(\mathbf{x})\, s_{L^R}(\mathbf{x},t)\, \mathrm{d}S = 0
\tag{5.32}
$$

From Eq. (5.28)

$$
\frac{\mathrm{R\,T}}{c_{bulk}}\, c_{bulk}^2 \left\{ \frac{1}{\alpha^{(3)}\,\alpha^{(2)}} \left[\left(\int_{\Omega} \varphi_i^{I_L}\, \varphi_k^R\, \varphi_h^{L^R}\, \varphi_j^{I_L}\, \mathrm{d}S \right) c_k^R\, c_h^{L^R}\, \frac{\partial c_j^{I_L}}{\partial t} + \left(\int_{\Omega} \varphi_i^{I_L}\, \varphi_k^R\, \varphi_h^{L^R}\, \varphi_j^{I_L}\, \mathrm{d}S \right) c_k^R\, c_j^{I_L}\, \frac{\partial c_h^{L^R}}{\partial t} \right] \right\} +
$$
$$
+ \frac{\mathrm{R\,T}}{c_{bulk}}\, c_{bulk}^2 \left\{ + \frac{1}{\alpha^{(3)}\,\alpha^{(2)}} \left(\int_{\Omega} \varphi_i^{I_L}\, \varphi_k^R\, \varphi_h^{L^R}\, \varphi_j^{I_L}\, \mathrm{d}S \right) c_j^{I_L}\, c_h^{L^R}\, \frac{\partial c_k^R}{\partial t} + \left(\int_{\Omega} \varphi_i^{I_L}\, \varphi_j^{I_L}\, \mathrm{d}S \right) \frac{\partial c_j^{I_L}}{\partial t} \right\} +
$$
$$
+ \frac{\mathrm{R\,T}}{c_{bulk}}\, c_{bulk}^2 \left\{ - \left(\int_{\Omega} \varphi_i^{I_L}\, \varphi_m^{L^I}\, \mathrm{d}S \right) \frac{\partial c_m^{L^I}}{\partial t} + \mathbb{D}_{I_L} \left(\int_{\Omega} \nabla_{\Omega}\left[\varphi_j^{I_L}\right] \cdot \nabla_{\Omega}\left[\varphi_i^{I_L}\right] \mathrm{d}S \right) c_j^{I_L} + \int_{\Omega} \varphi_i^{I^L}\, s_{L^I}(\mathbf{x},t)\, \mathrm{d}S \right\} = 0
\tag{5.33}
$$

Temporal discretization of problem is achived by finite difference scheme, as the Backward Euler method. The time derivative of the concentrations are discretized such as

$$
\frac{\partial c_k^R}{\partial t} \simeq \frac{c_k^R(t)(t+\Delta t) - c_k^R(t)}{\Delta t} = \frac{c_k^R(t+\Delta t)}{\Delta t} - \frac{c_k^R(t)}{\Delta t}
\tag{5.34}
$$

$$
\frac{\partial c_h^{L^R}(t)}{\partial t} \simeq \frac{c_h^{L^R}(t+\Delta t) - c_h^{L^R}(t)}{\Delta t} = \frac{c_h^{L^R}(t+\Delta t)}{\Delta t} - \frac{c_h^{L^R}(t)}{\Delta t}
\tag{5.35}
$$

$$
\frac{\partial c_j^{I_L}(t)}{\partial t} \simeq \frac{c_j^{I_L}(t+\Delta t) - c_j^{I_L}(t)}{\Delta t} = \frac{c_j^{I_L}(t+\Delta t)}{\Delta t} - \frac{c_j^{I_L}(t)}{\Delta t}
\tag{5.36}
$$

$$
\frac{\partial c_m^{L^I}(t)}{\partial t} \simeq \frac{c_m^{L^I}(t+\Delta t) - c_m^{L^I}(t)}{\Delta t} = \frac{c_m^{L^I}(t+\Delta t)}{\Delta t} - \frac{c_m^{L^I}(t)}{\Delta t}
\tag{5.37}
$$

From Eq. (5.30)

$$
\left(\int_{\Omega} \varphi_i^R \, \varphi_k^R \, \mathrm{d}S \right) \frac{c_k^R(t + \Delta t)}{\Delta t} - \left(\int_{\Omega} \varphi_i^R \, \varphi_h^{L^R}(x) \, \mathrm{d}S \right) \frac{c_h^{L^R}(t + \Delta t)}{\Delta t} +
$$

$$
+ \, \mathbb{D}_R \left(\int_{\Omega} \nabla_{\Omega} \left[\varphi_k^R \right] \cdot \nabla_{\Omega} \left[\varphi_i^R \right] \mathrm{d}S \right) c_k^R(t + \Delta t) =
\tag{5.38}
$$

$$
= \left(\int_{\Omega} \varphi_i^R \, \varphi_k^R \, \mathrm{d}S \right) \frac{c_k^R(t)}{\Delta t} - \left(\int_{\Omega} \varphi_i^R \, \varphi_h^{L^R} \, \mathrm{d}S \right) \frac{c_h^{L^R}(t)}{\Delta t} - \int_{\Omega} \varphi_i^R \, s_L(\mathbf{x}, t) \, \mathrm{d}S
$$

From Eq. (5.31)

$$
\frac{1}{\alpha^{(1)}} \left[\left(\int_{\Omega} \varphi_i^{L^I} \, \varphi_j^{I_L} \, \varphi_m^{L^I} \, \mathrm{d}S \right) c_j^{I_L}(t + \Delta t) \frac{c_m^{L^I}(t + \Delta t)}{\Delta t} - \left(\int_{\Omega} \varphi_i^{L^I} \, \varphi_j^{I_L} \, \varphi_m^{L^I} \, \mathrm{d}S \right) c_j^{I_L}(t + \Delta t) \frac{c_m^{L_I}(t)}{\Delta t} \right] +
$$

$$
+ \left(\int_{\Omega} \varphi_i^{L^I} \, \varphi_m^{L^I} \, \mathrm{d}S \right) \frac{c_m^{L^I}(t + \Delta t)}{\Delta t} + \frac{1}{\alpha^{(1)}} \left(\int_{\Omega} \varphi_i^{L^I} \, \varphi_j^{I_L} \, \varphi_m^{L^I} \, \mathrm{d}S \right) c_m^{L^I}(t + \Delta t) \frac{c_j^{I_L}(t + \Delta t)}{\Delta t} +
$$

$$
- \frac{1}{\alpha^{(1)}} \left(\int_{\Omega} \varphi_i^{L^I} \, \varphi_j^{I_L} \, \varphi_m^{L^I} \, \mathrm{d}S \right) c_m^{L^I}(t + \Delta t) \frac{c_j^{I_L}(t)}{\Delta t} = \left(\int_{\Omega} \varphi_i^{L^I} \, \varphi_m^{L^I} \, \mathrm{d}S \right) \frac{c_m^{L^I}(t)}{\Delta t} + \int_{\Omega} \varphi_i^{L^I} \, s_{L^I}(\mathbf{x}, t) \, \mathrm{d}S
\tag{5.39}
$$

From Eq. (5.32)

$$
\frac{1}{\alpha^{(2)}} \left[\left(\int_{\Omega} \varphi_i^{L^R} \, \varphi_k^R \, \varphi_h^{L^R} \, \mathrm{d}S \right) \frac{c_h^{L^R}(t + \Delta t)}{\Delta t} + \left(\int_{\Omega} \varphi_i^{L^R} \, \varphi_k^R \, \varphi_h^{L^R} \, \mathrm{d}S \right) c_h^{L^R}(t + \Delta t) \frac{c_k^R(t + \Delta t)}{\Delta t} \right] +
$$

$$
- \frac{1}{\alpha^{(2)}} \left(\int_{\Omega} \varphi_i^{L^R} \, \varphi_k^R \, \varphi_h^{L^R} \, \mathrm{d}S \right) c_h^{L^R}(t + \Delta t) \frac{c_k^R(t)}{\Delta t} +
$$

$$
+ \frac{1}{\alpha^{(3)} \, \alpha^{(2)}} \left(\int_{\Omega} \varphi_i^{L^R} \, \varphi_k^R \, \varphi_h^{L^R} \, \varphi_j^{I_L} \, \mathrm{d}S \right) c_k^R(t + \Delta t) \, c_h^{L^R}(t + \Delta t) \frac{c_j^{I_L}(t + \Delta t)}{\Delta t} +
$$

$$
- \frac{1}{\alpha^{(3)} \, \alpha^{(2)}} \left(\int_{\Omega} \varphi_i^{L^R} \, \varphi_k^R \, \varphi_h^{L^R} \, \varphi_j^{I_L} \, \mathrm{d}S \right) c_k^R(t + \Delta t) \, c_h^{L^R}(t + \Delta t) \frac{c_j^{I_L}(t)}{\Delta t} +
$$

$$
+ \frac{1}{\alpha^{(3)} \, \alpha^{(2)}} \left(\int_{\Omega} \varphi_i^{L^R} \, \varphi_k^R \, \varphi_h^{L^R} \, \varphi_j^{I_L} \, \mathrm{d}S \right) c_j^{I_L}(t + \Delta t) \, c_k^R(t + \Delta t) \frac{c_h^{L^R}(t + \Delta t)}{\Delta t} +
$$

$$
- \frac{1}{\alpha^{(3)} \, \alpha^{(2)}} \left(\int_{\Omega} \varphi_i^{L^R} \, \varphi_k^R \, \varphi_h^{L^R} \, \varphi_j^{I_L} \, \mathrm{d}S \right) c_j^{I_L}(t + \Delta t) \, c_k^R(t + \Delta t) \frac{c_h^{L^R}(t)}{\Delta t} +
$$

$$
+ \frac{1}{\alpha^{(3)} \, \alpha^{(2)}} \left(\int_{\Omega} \varphi_i^{L^R} \, \varphi_k^R \, \varphi_h^{L^R} \, \varphi_j^{I_L} \, \mathrm{d}S \right) c_j^{I_L}(t + \Delta t) \, c_h^{L^R}(t + \Delta t) \frac{c_k^R(t + \Delta t)}{\Delta t} +
$$

$$
- \frac{1}{\alpha^{(3)} \, \alpha^{(2)}} \left(\int_{\Omega} \varphi_i^{L^R} \, \varphi_k^R \, \varphi_h^{L^R} \, \varphi_j^{I_L} \, \mathrm{d}S \right) c_j^{I_L}(t + \Delta t) \, c_h^{L^R}(t + \Delta t) \frac{c_k^R(t)}{\Delta t} + \left(\int_{\Omega} \varphi_i^{L^R} \, \varphi_h^{L^R} \, \mathrm{d}S \right) \frac{c_h^{L^R}(t + \Delta t)}{\Delta t} =
$$

$$
\frac{1}{\alpha^{(2)}} \left(\int_{\Omega} \varphi_i^{L^R} \, \varphi_k^R \, \varphi_h^{L^R} \, \mathrm{d}S \right) \frac{c_h^{L^R}(t)}{\Delta t} + \left(\int_{\Omega} \varphi_i^{L^R} \, \varphi_h^{L^R} \, \mathrm{d}S \right) \frac{c_h^{L^R}(t)}{\Delta t} + \int_{\Omega} \varphi_i^{L^R} \, s_{L^R}(\mathbf{x}, t) \, \mathrm{d}S
\tag{5.40}
$$

From Eq. (5.33)

$$\frac{1}{\alpha^{(3)}\,\alpha^{(2)}} \left(\int_\Omega \varphi_i^{I_L}\, \varphi_k^R\, \varphi_h^{L^R}\, \varphi_j^{I_L}\, \mathrm{d}S \right) c_k^R(t+\Delta t)\, c_h^{L^R}(t+\Delta t)\, \frac{c_j^{I_L}(t+\Delta t)}{\Delta t} +$$

$$-\frac{1}{\alpha^{(3)}\,\alpha^{(2)}} \left(\int_\Omega \varphi_i^{I_L}\, \varphi_k^R\, \varphi_h^{L^R}\, \varphi_j^{I_L}\, \mathrm{d}S \right) c_k^R(t+\Delta t)\, c_h^{L^R}(t+\Delta t)\, \frac{c_j^{I_L}(t)}{\Delta t} +$$

$$+\frac{1}{\alpha^{(3)}\,\alpha^{(2)}} \left(\int_\Omega \varphi_i^{I_L}\, \varphi_k^R\, \varphi_h^{L^R}\, \varphi_j^{I_L}\, \mathrm{d}S \right) c_k^R(t+\Delta t)\, c_j^{I_L}(t+\Delta t)\, \frac{c_h^{L^R}(t+\Delta t)}{\Delta t} +$$

$$-\frac{1}{\alpha^{(3)}\,\alpha^{(2)}} \left(\int_\Omega \varphi_i^{I_L}\, \varphi_k^R\, \varphi_h^{L^R}\, \varphi_j^{I_L}\, \mathrm{d}S \right) c_k^R(t+\Delta t)\, c_j^{I_L}(t+\Delta t)\, \frac{c_h^{L^R}(t)}{\Delta t} +$$

$$+\frac{1}{\alpha^{(3)}\,\alpha^{(2)}} \left(\int_\Omega \varphi_i^{I_L}\, \varphi_k^R\, \varphi_h^{L^R}\, \varphi_j^{I_L}\, \mathrm{d}S \right) c_j^{I_L}(t+\Delta t)\, c_h^{L^R}(t+\Delta t)\, \frac{c_k^R(t+\Delta t)}{\Delta t} + \qquad (5.41)$$

$$-\frac{1}{\alpha^{(3)}\,\alpha^{(2)}} \left(\int_\Omega \varphi_i^{I_L}\, \varphi_k^R\, \varphi_h^{L^R}\, \varphi_j^{I_L}\, \mathrm{d}S \right) c_j^{I_L}(t+\Delta t)\, c_h^{L^R}(t+\Delta t)\, \frac{c_k^R(t)}{\Delta t} +$$

$$+\left(\int_\Omega \varphi_i^{I_L}\, \varphi_j^{I_L}\, \mathrm{d}S \right) \frac{c_j^{I_L}(t+\Delta t)}{\Delta t} - \left(\int_\Omega \varphi_i^{I_L}\, \varphi_m^{L^I}\, \mathrm{d}S \right) \frac{c_m^{L^I}(t+\Delta t)}{\Delta t} +$$

$$+\mathbb{D}_{I_L} \left(\int_\Omega \nabla_\Omega \left[\varphi_j^{I_L} \right] \cdot \nabla_\Omega \left[\varphi_i^{I_L} \right] \mathrm{d}S \right) c_j^{I_L}(t+\Delta t) =$$

$$+\left(\int_\Omega \varphi_i^{I_L}\, \varphi_j^{I_L}\, \mathrm{d}S \right) \frac{c_j^{I_L}(t)}{\Delta t} - \left(\int_\Omega \varphi_i^{I_L}\, \varphi_m^{L^I}\, \mathrm{d}S \right) \frac{c_m^{L^I}(t)}{\Delta t} - \int_\Omega \varphi_i^{I_L}\, s_{L^I}(\mathbf{x},t)\, \mathrm{d}S$$

Multiply each component by factor $\frac{\mathrm{R}\,\mathrm{T}}{c_{bulk}}$ to achieve a power $\left[\frac{J}{s} \right]$. Dimensionless concentrations c_β^* are defined as

$$c_\beta^* = \frac{c_\beta}{c_{bulk}} \Rightarrow c_\beta = c_\beta^*\, c_{bulk},$$

The same for the test functions $\hat{c}_\beta^*$,

$$\hat{c}_\beta = \hat{c}_\beta^*\, c_{bulk}.$$

Then we multiply each equation by the term $\frac{\mathrm{R}\,\mathrm{T}}{c_{bulk}}\, c_{bulk}^2 = \mathrm{R}\,\mathrm{T}\, c_{bulk}$.

The Newton Raphson method for Eq. (5.38) reads:

$$\mathrm{R}\,\mathrm{T}\, c_{bulk} \left\{ \left(\int_\Omega \varphi_i^R\, \varphi_k^R\, dV \right) \frac{c_{R_k}^{(k)}(t+\Delta t)}{\Delta t} - \left(\int_\Omega \varphi_i^R\, \varphi_h^{L^R}\, \mathrm{d}S \right) \frac{c_{L_h^R}^{(k)}(t+\Delta t)}{\Delta t} + \right.$$

$$+\mathbb{D}_R \left(\int_\Omega \nabla_\Omega \left[\varphi_k^R(x) \right] \cdot \nabla_\Omega \left[\varphi_i^R \right] \mathrm{d}S \right) c_{R_k}^{(k)}(t+\Delta t) + \left(\int_\Omega \varphi_i^R\, \varphi_k^R\, \mathrm{d}S \right) \frac{\Delta c_{R_k}^{(k)}}{\Delta t} +$$

$$-\left(\int_\Omega \varphi_i^R\, \varphi_h^{L^R}\, \mathrm{d}S \right) \frac{\Delta c_{L_h^R}^{(k)}}{\Delta t} + \mathbb{D}_R \left(\int_\Omega \nabla_\Omega \left[\varphi_k^R(x) \right] \cdot \nabla_\Omega \left[\varphi_i^R \right] \mathrm{d}S \right) \Delta c_{R_k}^{(k)} + \qquad (5.42)$$

$$\left. -\left(\int_\Omega \varphi_i^R\, \varphi_k^R\, \mathrm{d}S \right) \frac{c_k^R(t)}{\Delta t} + \left(\int_\Omega \varphi_i^R\, \varphi_h^{L^R}\, \mathrm{d}S \right) \frac{c_h^{L^R}(t)}{\Delta t} + \int_\Omega \varphi_i^R\, s_{L^R}(\mathbf{x},t)\, \mathrm{d}S \right\} = 0$$

Eq. (5.39) leads to

$$
\begin{aligned}
\mathrm{R\,T}\,c_{bulk}\Bigg\{ &\frac{1}{\alpha^{(1)}}\left[\left(\int_{\Omega}\varphi_i^{L^I}\varphi_j^{I_L}\varphi_m^{L^I}\,\mathrm{d}S\right)c_{I_{L_j}}^{(k)}(t+\Delta t)\frac{c_{L_m^I}^{(k)}(t+\Delta t)}{\Delta t}-\left(\int_{\Omega}\varphi_i^{L^I}\varphi_j^{I_L}\varphi_m^{L^I}\,\mathrm{d}S\right)c_{I_{L_j}}^{(k)}(t+\Delta t)\frac{c_m^{L_I}(t)}{\Delta t}\right]+\\
&+\left(\int_{\Omega}\varphi_i^{L^I}\varphi_m^{L^I}\,\mathrm{d}S\right)\frac{c_{L_m^I}^{(k)}(t+\Delta t)}{\Delta t}+\frac{1}{\alpha^{(1)}}\left(\int_{\Omega}\varphi_i^{L^I}\varphi_j^{I_L}\varphi_m^{L^I}\,\mathrm{d}S\right)c_m^{L^I}(t+\Delta t)\frac{c_{I_{L_j}}^{(k)}(t+\Delta t)}{\Delta t}+\\
&-\frac{1}{\alpha^{(1)}}\left(\int_{\Omega}\varphi_i^{L^I}\varphi_j^{I_L}\varphi_m^{L^I}\,\mathrm{d}S\right)c_{L_m^I}^{(k)}(t+\Delta t)\frac{c_j^{I_L}(t)}{\Delta t}-\left(\int_{\Omega}\varphi_i^{L^I}\varphi_m^{L^I}\,\mathrm{d}S\right)\frac{c_m^{L^I}(t)}{\Delta t}+\\
&\frac{1}{\alpha^{(1)}}\left[\left(\int_{\Omega}\varphi_i^{L^I}\varphi_j^{I_L}\varphi_m^{L^I}\,\mathrm{d}S\right)\frac{1}{\Delta t}\left(c_{I_{L_j}}^{(k)}(t+\Delta t)\Delta c_{L_m^I}^{(k)}+c_{L_m^I}^{(k)}(t+\Delta t)\Delta c_{I_{L_j}}^{(k)}\right)\right]+\\
&+\frac{1}{\alpha^{(1)}}\left[-\left(\int_{\Omega}\varphi_i^{L^I}\varphi_m^{L^I}\,\mathrm{d}S\right)\frac{c_m^{L^I}(t)}{\Delta t}\Delta c_{I_{L_j}}^{(k)}-\left(\int_{\Omega}\varphi_i^{L^I}\varphi_j^{I_L}\varphi_m^{L^I}\,\mathrm{d}S\right)\frac{c_j^{I_L}(t)}{\Delta t}\Delta c_{L_m^I}^{(k)}\right]+\\
&+\frac{1}{\alpha^{(1)}}\left[\left(\int_{\Omega}\varphi_i^{L^I}\varphi_j^{I_L}\varphi_m^{L^I}\,\mathrm{d}S\right)\frac{1}{\Delta t}\left(c_{I_{L_j}}^{(k)}(t+\Delta t)\Delta c_{L_m^I}^{(k)}+c_{L_m^I}^{(k)}(t+\Delta t)\Delta c_{I_{L_j}}^{(k)}\right)\right]+\left(\int_{\Omega}\varphi_i^{L^I}\varphi_m^{L^I}\,\mathrm{d}S\right)\frac{\Delta c_{L_m^I}^{(k)}}{\Delta t}\Bigg\}=0
\end{aligned}
$$

(5.43)

From Eq. (5.40) we obtain the following lengthy expression

$$
\begin{aligned}
\mathrm{R\,T}\,c_{bulk} \Bigg\{ & \frac{1}{\alpha^{(2)}} \left[\left(\int_\Omega \varphi_i^{L^R} \varphi_k^{R} \varphi_h^{L^R}\, dV \right) \frac{c_{L_h^R}^{(k)}(t+\Delta t)}{\Delta t} + \left(\int_\Omega \varphi_i^{L^R} \varphi_k^{R} \varphi_h^{L^R}\, dS \right) c_{L_h^R}^{(k)}(t+\Delta t)\,\frac{c_{R_k}^{(k)}(t+\Delta t)}{\Delta t} \right] + \\
& - \frac{1}{\alpha^{(2)}} \left(\int_\Omega \varphi_i^{L^R} \varphi_k^{R} \varphi_h^{L^R}\, dS \right) \frac{c_k^{R}(t)}{\Delta t}\, c_{L_h^R}^{(k)}(t+\Delta t) + \left(\int_\Omega \varphi_i^{L^R} \varphi_h^{L^R}\, dS \right) \frac{c_{L_h^R}^{(k)}(t+\Delta t)}{\Delta t} + \\
& + \frac{1}{\alpha^{(3)}\,\alpha^{(2)}} \left(\int_\Omega \varphi_i^{L^R} \varphi_k^{R} \varphi_h^{L^R} \varphi_j^{I_L}\, dS \right) c_{R_k}^{(k)}(t+\Delta t)\, c_{L_h^R}^{(k)}(t+\Delta t)\,\frac{c_{I_{L_j}}^{(k)}(t+\Delta t)}{\Delta t} + \\
& - \frac{1}{\alpha^{(3)}\,\alpha^{(2)}} \left(\int_\Omega \varphi_i^{L^R} \varphi_k^{R} \varphi_h^{L^R} \varphi_j^{I_L}\, dS \right) \frac{c_j^{I_L}(t)}{\Delta t}\, c_{R_k}^{(k)}(t+\Delta t)\, c_{L_h^R}^{(k)}(t+\Delta t) + \\
& + \frac{1}{\alpha^{(3)}\,\alpha^{(2)}} \left(\int_\Omega \varphi_i^{L^R} \varphi_k^{R} \varphi_h^{L^R} \varphi_j^{I_L}\, dS \right) c_{I_{L_j}}^{(k)}(t+\Delta t)\, c_{R_k}^{(k)}(t+\Delta t)\,\frac{c_{L_h^R}^{(k)}(t+\Delta t)}{\Delta t} + \\
& - \frac{1}{\alpha^{(3)}\,\alpha^{(2)}} \left(\int_\Omega \varphi_i^{L^R} \varphi_k^{R} \varphi_h^{L^R} \varphi_j^{I_L}\, dS \right) \frac{c_h^{L^R}(t)}{\Delta t}\, c_{I_{L_j}}^{(k)}(t+\Delta t)\, c_{R_k}^{(k)}(t+\Delta t) + \\
& + \frac{1}{\alpha^{(3)}\,\alpha^{(2)}} \left(\int_\Omega \varphi_i^{L^R} \varphi_k^{R} \varphi_h^{L^R} \varphi_j^{I_L}\, dS \right) c_{I_{L_j}}^{(k)}(t+\Delta t)\, c_{L_h^R}^{(k)}(t+\Delta t)\,\frac{c_{R_k}^{(k)}(t+\Delta t)}{\Delta t} + \\
& - \frac{1}{\alpha^{(3)}\,\alpha^{(2)}} \left(\int_\Omega \varphi_i^{L^R} \varphi_k^{R} \varphi_h^{L^R} \varphi_j^{I_L}\, dS \right) \frac{c_k^{R}(t)}{\Delta t}\, c_{I_{L_j}}^{(k)}(t+\Delta t)\, c_{L_h^R}^{(k)}(t+\Delta t) + \\
& - \frac{1}{\alpha^{(2)}} \left(\int_\Omega \varphi_i^{L^R} \varphi_k^{R} \varphi_h^{L^R}\, dS \right) \frac{c_h^{L^R}(t)}{\Delta t} - \left(\int_\Omega \varphi_i^{L^R} \varphi_h^{L^R}\, dS \right) \frac{c_h^{L^R}(t)}{\Delta t} - \int_\Omega \varphi_i^{L^R} s_{L^R}(\mathbf{x},t)\, dS + \\
& + \frac{1}{\alpha^{(2)}} \left[\left(\int_\Omega \varphi_i^{L^R} \varphi_k^{R} \varphi_h^{L^R}\, dS \right) \frac{\Delta c_{L_k^R}^{(k)}}{\Delta t} + \left(\int_\Omega \varphi_i^{L^R} \varphi_k^{R} \varphi_h^{L^R}\, dS \right) \frac{1}{\Delta t} \left(c_{L_h^R}^{(k)}(t+\Delta t)\Delta c_{R_k}^{(k)} + c_{R_k}^{(k)}(t+\Delta t)\Delta c_{L_h^R}^{(k)} \right) \right] + \\
& - \frac{1}{\alpha^{(2)}} \left(\int_\Omega \varphi_i^{L^R} \varphi_k^{R} \varphi_h^{L^R}\, dS \right) \frac{c_k^{R}(t)}{\Delta t}\,\Delta c_{L_h^R}^{(k)} + \left(\int_\Omega \varphi_i^{L^R} \varphi_h^{L^R}\, dS \right) \frac{\Delta c_{L_h^R}^{(k)}}{\Delta t} + \\
& + \frac{3}{\alpha^{(3)}\,\alpha^{(2)}} \left[\left(\int_\Omega \varphi_i^{L^R} \varphi_k^{R} \varphi_h^{L^R} \varphi_j^{I_L}\, dS \right) \frac{1}{\Delta t} \left(c_{R_k}^{(k)}(t+\Delta t)\, c_{L_h^R}^{(k)}(t+\Delta t)\,\Delta c_{I_{L_j}}^{(k)} + \right. \right. \\
& \left. c_{I_{L_j}}^{(k)}(t+\Delta t)\, c_{L_h^R}^{(k)}(t+\Delta t)\,\Delta c_{R_k}^{(k)} + c_{R_k}^{(k)}(t+\Delta t)\, c_{I_{L_j}}^{(k)}(t+\Delta t)\,\Delta c_{L_h^R}^{(k)} \right) \bigg] + \\
& - \frac{1}{\alpha^{(3)}\,\alpha^{(2)}} \left(\int_\Omega \varphi_i^{L^R} \varphi_k^{R} \varphi_h^{L^R} \varphi_j^{I_L}\, dS \right) \frac{c_h^{L^R}(t)}{\Delta t} \left(c_{R_k}^{(k)}(t+\Delta t)\Delta c_{I_j^L}^{(k)} + c_{I_j^L}^{(k)}(t+\Delta t)\Delta c_{R_k}^{(k)} \right) + \\
& - \frac{1}{\alpha^{(3)}\,\alpha^{(2)}} \left(\int_\Omega \varphi_i^{L^R} \varphi_k^{R} \varphi_h^{L^R} \varphi_j^{I_L}\, dS \right) \frac{c_k^{R}(t)}{\Delta t} \left(c_{L_h^R}^{(k)}(t+\Delta t)\Delta c_{I_j^L}^{(k)} + c_{I_j^L}^{(k)}(t+\Delta t)\Delta c_{L_h^R}^{(k)} \right) \Bigg\}
\end{aligned}
$$

(5.44)

and the Eq. (5.41) yields

$$
\begin{aligned}
\mathrm{R\,T}\,c_{bulk} \Bigg\{ & \frac{1}{\alpha^{(3)}\,\alpha^{(2)}} \left(\int_\Omega \varphi_i^{I_L}\,\varphi_k^R\,\varphi_h^{L^R}\,\varphi_j^{I_L}\,\mathrm{d}S \right) c_{R_k}^{(k)}(t+\Delta t)\,c_{L_h^R}^{(k)}(t+\Delta t)\,\frac{c_{I_{L_j}}^{(k)}(t+\Delta t)}{\Delta t} + \\
& - \frac{1}{\alpha^{(3)}\,\alpha^{(2)}} \left(\int_\Omega \varphi_i^{I_L}\,\varphi_k^R\,\varphi_h^{L^R}\,\varphi_j^{I_L}\,\mathrm{d}S \right) \frac{c_j^{I_L}(t)}{\Delta t}\,c_{R_k}^{(k)}(t+\Delta t)\,c_{L_h^R}^{(k)}(t+\Delta t) + \\
& + \frac{1}{\alpha^{(3)}\,\alpha^{(2)}} \left(\int_\Omega \varphi_i^{I_L}\,\varphi_k^R\,\varphi_h^{L^R}\,\varphi_j^{I_L}\,\mathrm{d}S \right) c_{R_k}^{(k)}(t+\Delta t)\,c_{I_{L_j}}^{(k)}(t+\Delta t)\,\frac{c_{L_h^R}^{(k)}(t+\Delta t)}{\Delta t} + \\
& - \frac{1}{\alpha^{(3)}\,\alpha^{(2)}} \left(\int_\Omega \varphi_i^{I_L}\,\varphi_k^R\,\varphi_h^{L^R}\,\varphi_j^{I_L}\,\mathrm{d}S \right) \frac{c_h^{L^R}(t)}{\Delta t}\,c_{R_k}^{(k)}(t+\Delta t)\,c_{I_{L_j}}^{(k)}(t+\Delta t) + \\
& + \frac{1}{\alpha^{(3)}\,\alpha^{(2)}} \left(\int_\Omega \varphi_i^{I_L}\,\varphi_k^R\,\varphi_h^{L^R}\,\varphi_j^{I_L}\,\mathrm{d}S \right) c_{I_{L_j}}^{(k)}(t+\Delta t)\,c_{L_h^R}^{(k)}(t+\Delta t)\,\frac{c_{R_k}^{(k)}(t+\Delta t)}{\Delta t} + \\
& - \frac{1}{\alpha^{(3)}\,\alpha^{(2)}} \left(\int_\Omega \varphi_i^{I_L}\,\varphi_k^R\,\varphi_h^{L^R}\,\varphi_j^{I_L}\,\mathrm{d}S \right) \frac{c_k^R(t)}{\Delta t}\,c_{I_{L_j}}^{(k)}(t+\Delta t)\,c_{L_h^R}^{(k)}(t+\Delta t) + \\
& + \left(\int_\Omega \varphi_i^{I_L}\,\varphi_j^{I_L}\,\mathrm{d}S \right) \frac{c_{I_{L_j}}^{(k)}(t+\Delta t)}{\Delta t} - \left(\int_\Omega \varphi_i^{I_L}\,\varphi_m^{L^I}\,\mathrm{d}S \right) \frac{c_{L_m^I}^{(k)}(t+\Delta t)}{\Delta t} + \\
& + \mathbb{D}_{I_L} \left(\int_\Omega \nabla_\Omega \left[\varphi_j^{I_L} \right] \cdot \nabla_\Omega \left[\varphi_i^{I_L} \right]\,\mathrm{d}S \right) c_{I_{L_j}}^{(k)}(t+\Delta t) + \\
& - \left(\int_\Omega \varphi_i^{I_L}\,\varphi_j^{I_L}\,\mathrm{d}S \right) \frac{c_j^{I_L}(t)}{\Delta t} + \left(\int_\Omega \varphi_i^{I_L}\,\varphi_m^{L^I}\,\mathrm{d}S \right) \frac{c_m^{L^I}(t)}{\Delta t} + \\
& + \frac{3}{\alpha^{(3)}\,\alpha^{(2)}} \left(\int_\Omega \varphi_i^{I_L}\,\varphi_k^R\,\varphi_h^{L^R}\,\varphi_j^{I_L}\,\mathrm{d}S \right) \frac{1}{\Delta t} \left(c_{R_k}^{(k)}(t+\Delta t)\,c_{L_h^R}^{(k)}(t+\Delta t)\,\Delta c_{I_{L_j}}^{(k)} + \right. \\
& c_{I_{L_j}}^{(k)}(t+\Delta t)\,c_{L_h^R}^{(k)}(t+\Delta t)\,\Delta c_{R_k}^{(k)} + c_{R_k}^{(k)}(t+\Delta t)\,c_{I_{L_j}}^{(k)}(t+\Delta t)\,\Delta c_{L_h^R}^{(k)} \Big) + \\
& - \frac{1}{\alpha^{(3)}\,\alpha^{(2)}} \left(\int_\Omega \varphi_i^{I_L}\,\varphi_k^R\,\varphi_h^{L^R}\,\varphi_j^{I_L}\,\mathrm{d}S \right) \frac{c_j^{I_L}(t)}{\Delta t} \left(c_{L_h^R}^{(k)}(t+\Delta t)\Delta c_{R_k}^{(k)} + c_{R_k}^{(k)}(t+\Delta t)\Delta c_{L_h^R}^{(k)} \right) + \\
& - \frac{1}{\alpha^{(3)}\,\alpha^{(2)}} \left(\int_\Omega \varphi_i^{I_L}\,\varphi_k^R\,\varphi_h^{L^R}\,\varphi_j^{I_L}\,\mathrm{d}S \right) \frac{c_h^{L^R}(t)}{\Delta t} \left(c_{R_k}^{(k)}(t+\Delta t)\Delta c_{I_j^L}^{(k)} + c_{I_j^L}^{(k)}(t+\Delta t)\Delta c_{R_k}^{(k)} \right) + \\
& + \frac{1}{\alpha^{(3)}\,\alpha^{(2)}} \left(\int_\Omega \varphi_i^{I_L}\,\varphi_k^R\,\varphi_h^{L^R}\,\varphi_j^{I_L}\,\mathrm{d}S \right) c_{I_{L_j}}^{(k)}(t+\Delta t)\,c_{L_h^R}^{(k)}(t+\Delta t)\,\frac{c_{R_k}^{(k)}(t+\Delta t)}{\Delta t} + \\
& - \frac{1}{\alpha^{(3)}\,\alpha^{(2)}} \left(\int_\Omega \varphi_i^{I_L}\,\varphi_k^R\,\varphi_h^{L^R}\,\varphi_j^{I_L}\,\mathrm{d}S \right) \frac{c_k^R(t)}{\Delta t} \left(c_{L_h^R}^{(k)}(t+\Delta t)\Delta c_{I_j^L}^{(k)} + c_{I_j^L}^{(k)}(t+\Delta t)\Delta c_{L_h^R}^{(k)} \right) + \\
& + \left(\int_\Omega \varphi_i^{I_L}\,\varphi_j^{I_L}\,\mathrm{d}S \right) \frac{\Delta c_{I_{L_j}}^{(k)}}{\Delta t} - \left(\int_\Omega \varphi_i^{I_L}\,\varphi_m^{L^I}\,\mathrm{d}S \right) \frac{\Delta c_{L_m^I}^{(k)}}{\Delta t} \Bigg\} = 0
\end{aligned}
\tag{5.45}
$$

79

5.3   Conclusion

The numerical implementation of the governing equations has not been fully developed yet, but several activities have been achieved:

1. The weak form of the balance equations of the three reactions has been written, which considers:

   - the interaction between low affinity integrin (unbent configuration) and its specific ligand (e.g. fibrinogen) that leads to a high affinity integrin ("bent" configuration) triggering stress fibers formation and focal adhesion,

   - the interaction between VEGFR-2 and VEGF which forms the complex VEGFR2/VEGF,

   - the reaction between the low affinity integrins and the VEGFR2/VEGF complex which triggers a long-term VEGFR-2 activation.

2. The weak form, with these three reactions, has been discretized in space, with Finite Element Method, and in time, with Backward Euler scheme. To solve the nonlinear part, Newton-Raphson method has been designed.

This model may provide new insights about the important interplay among different transmembrane proteins and may be applied to other interactions among receptors and co-receptors, such as Neuropilin-1 and VEGFR-2 [150]. Much work still needs to be done: we are working on the determination of the parameters necessary for the computational implementation, such as the integrins diffusivity $\mathbb{D}_I$, the initial concentration of low affinity integrin $c_{I_L}^0$ and its ligand $c_{L^I}^0$, their saturation values $c_{I_L}^{\max}$ and $c_{I_L}^{\max}$, the equilibrium constants of reactions (5.1a) and (5.1c), shown on the following table:

Parameter	$Notation$	value	unit
cell radius	ℓ	20	μm
receptor diffusivity	$\mathbb{D}_R$	0.198	$\frac{\mu m^2}{s}$
integrin diffusivity	$\mathbb{D}_I$	?	$\frac{\mu m^2}{s}$
temperature	T	37	C
gas constant	R	8.31	$\frac{J}{mol}$
initial concentration of receptor R	c_R^0	3.46	$\frac{molecule}{\mu m^2}$
initial concentration of gremlin/VEGF	c^0	$16 \cdot 10^3$	$\frac{molecule}{\mu m^2}$
initial concentration of low affinity integrin	$c_{I_L}^0$	?	$\frac{molecule}{\mu m^2}$
initial concentration of fibrinogen	$c_{L^I}^0$	?	$\frac{molecule}{\mu m^2}$
standard Gibbs free Energy	$\Delta G^{(5.1b)}$	-32949	$\frac{J}{mol}$
standard Gibbs free Energy (or Equilibrium constant)	$\Delta G^{(5.1a)}$	?	$\frac{J}{mol}$
standard Gibbs free Energy (or Equilibrium constant)	$\Delta G^{(5.1c)}$	?	$\frac{J}{mol}$
gremlin saturation	$c_{L^R}^{max}$	$16 \cdot 10^3$	$\frac{molecule}{\mu m^2}$
fibrinogen saturation	$c_{L^I}^{max}$	?	$\frac{molecule}{\mu m^2}$
integrin saturation	$c_{I_L}^{max}$	?	$\frac{molecule}{\mu m^2}$

Chapter 6

Receptor-ligand model in large deformations

6.1 Introduction

Modeling the relocation of VEGFR-2 on the lipid bilayer membrane in living cells involves the description of coupled processes such as transport of mass and mechanical deformation. This coupled problem has been solved in a simplified manner in Chapter 4, through a surrogated mechanical spreading of the cell. Such an approach does not consider the mechanical governing equations at all, instead their effect are modeled by introducing a fictitious source therm in the mass balance laws on the cell membrane.

In this chapter the description of such multi-physics phenomena on living cells is tackled with a rigorous methodology in the framework of continuum mechanics. The description of these processes is rather challenging. On one hand, the mechanical behavior of living cells exhibits large deformations that has to be modeled through a non-linear solid mechanics theory. On the other, the chemo-transport processes of interest take place on the cell membrane, leading to an additional degree of complexity.

The chapter is organized as follows: we first introduce the essential concepts of a finite deformation formulation of the problem, starting from well-known definitions and conservation laws, i.e. balance laws for diffusing species and balance of linear and angular momentum. In particular, in Section 6.3.2 the mass balance equations are specialized for advecting surfaces, in order to deal with transport of proteins on deformable cells. Models describing the mechanical response of living cells are finally reviewed in Section 6.5 along with some preliminary numerical examples.

6.2 Finite strain theory

Configuration and motions of continuum Bodies. The finite deformation theory [151] is based on the following assumptions that strains and rotations are arbitrarily large, then the infinitesimal strain theory is not accepted. If deformations are large, the deformed and undeformed configurations of the continuum body $\mathcal{B}$ are meaningfully distinct. The configuration is a region occupied by $\mathcal{B}$, embedded in three-dimensional Euclidean space, which is determined exclusively at any istant of time. Each point of $\mathcal{B}$ can be identified by the position vector (or referential position) $\vec{X}$ relative to the fixed origin O of the Cartesian orthogonal reference system, to the reference configuration. The characterization of any quantity with respect to the material coordinates $\vec{X}$ is called material or Lagrangian description, by observing what happens to the body as it moves. The displacement vector $\vec{u}(\vec{X},t)$ describes the motion of each point in the solid deforming under external actions. The displacent field, which contains all the displacement vectors, describes the configuration changes of the body $\mathcal{B}$. The Lagrangian description of the displacement vector is

$$\vec{u}(\vec{X},t) = u_i\,\vec{e}_i \tag{6.1}$$

where $\vec{e}_i$ are the orthonormal basis vectors of the spatial coordinate system.

The displacement field, expressed in terms of the material coordinates, is

$$\vec{u}(\vec{X}, t) = \vec{x}(\vec{X}, t) - \vec{X} \tag{6.2}$$

where $\vec{x}$ are the spatial coordinates or current position in the Eulerian description, in which it is studied what happens at the point of the body $\mathcal{B}$ as time changes.
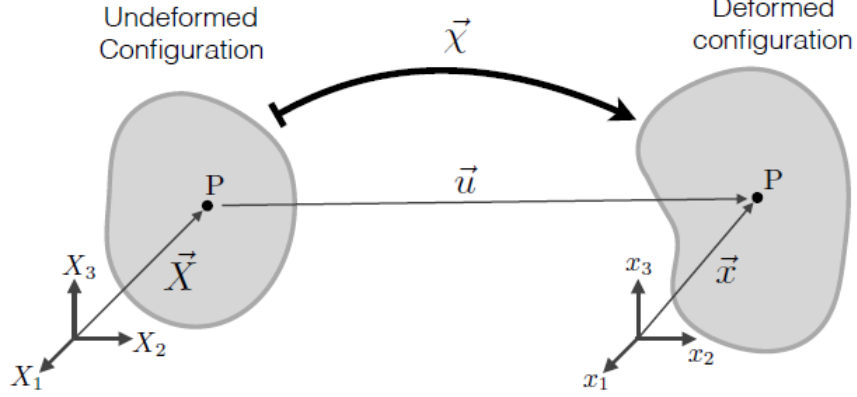
Figure 6.1: Configuration and motion of a continuum body.

Deformation Gradient. The partial derivative of the displacement vector with respect to the material coordinates yields the material displacement gradient tensor $\mathrm{Grad}\,[\,\vec{u}\,]$, as

$$\mathrm{Grad}\,[\,\vec{u}\,] = \mathrm{Grad}\,[\,\vec{x}\,] - \mathbb{1} = \mathbf{F} - \mathbb{1} \tag{6.3}$$

where $\mathbf{F}$ is the deformation gradient tensor and $\mathbb{1}$ is the identity tensor. $\mathbf{F}(\vec{X}, t)$ represents the gradient of the mapping function $\vec{\chi}(\vec{X}, t)$ which describes the motion of the body $\mathcal{B}$, i.e. $\vec{x} = \vec{\chi}(\vec{X}, t)$. The material deformation gradient tensor characterizes the local deformation at a material point with position vector $\vec{X}$, by transforming a material line element arising from that point from the reference configuration to the current or deformed configuration, assuming continuity in the mapping function $\vec{\chi}(\vec{X}, t)$. Thus we have,

$$\mathrm{d}\vec{x} = \frac{\partial \vec{x}}{\partial \vec{X}}\,\mathrm{d}\vec{X} = \mathrm{Grad}\left[\vec{\chi}(\vec{X}, t)\right] = \mathbf{F}(\vec{X}, t)\,\mathrm{d}\vec{X} \tag{6.4}$$

$\mathbf{F}$ plays a central role in nonlinear solid mechanics and is a primary measure of finite deformations kinematics, because it is the fundamental kinematic tensor that characterizes changes of material elements during motion; $\mathbf{F}$ it is related to both the reference and current configurations and is said to be a two-point tensor. Note that a unit vector $\vec{N}$ in the reference frame is not necessary mapped, through formula (6.4), to a vector of unit length.

We now consider two material points P and Q (respectively p and q in the deformed configuration) given by the position vector $\vec{X}$ and the distance between them is given by the vector $\mathrm{d}\vec{X}$ (and $\mathrm{d}\vec{x}$ in the deformed configuration). We can define the relative displacement vector $\mathrm{d}\vec{u}$ from

$$\vec{x} + \mathrm{d}\vec{x} = \vec{X} + \mathrm{d}\vec{X} + \vec{u}(\vec{X} + \mathrm{d}\vec{X}) \tag{6.5}$$

then

$$\mathrm{d}\vec{x} = \vec{X} - \vec{x} + \mathrm{d}\vec{X} + \vec{u}(\vec{X} + \mathrm{d}\vec{X}) = -\vec{u}(\vec{X}) + \mathrm{d}\vec{X} + \vec{u}\,(\vec{X} + \mathrm{d}\vec{X}) = \mathrm{d}\vec{X} + \mathrm{d}\vec{u} \tag{6.6}$$

The time derivative of the deformation gradient is

$$\frac{\partial \mathbf{F}}{\partial t} = \frac{\partial}{\partial t}\left[\frac{\partial \vec{x}(\vec{X}, t)}{\partial \vec{X}}\right] = \frac{\partial}{\partial \vec{X}}\left[\frac{\partial \vec{x}(\vec{X}, t)}{\partial t}\right] = \frac{\partial}{\partial \vec{X}}\left[\vec{V}(\vec{X}, t)\right] \tag{6.7}$$
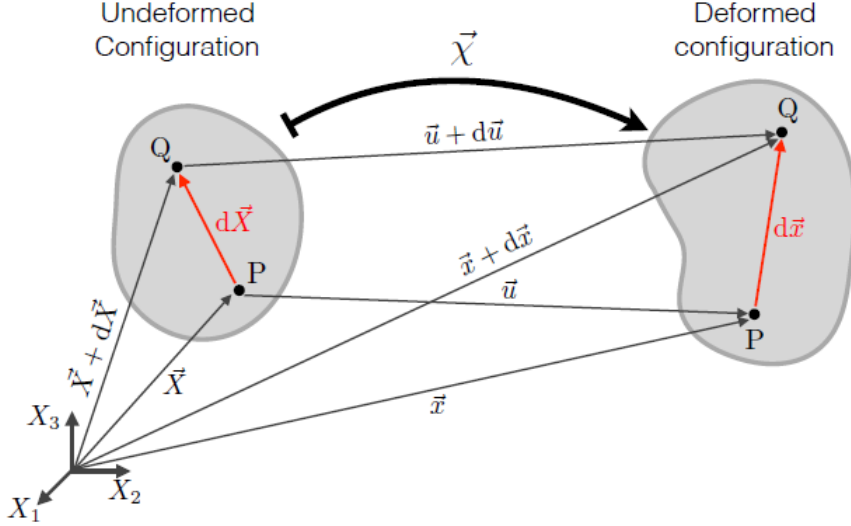
Figure 6.2: Displacement and position vectors of a typical particle.

where $\vec{V}$ is the material velocity, the velocity vector as a function of the material coordinates.

We define the Jacobian determinant, known as volume ratio, which performs the change in volume between the reference and the current configuration at time t, as

$$J(\vec{X}, t) = \frac{\mathrm{d}v}{\mathrm{d}v_R} \tag{6.8}$$

in which J is the determinant of the deformation gradient $J(\vec{X}, t) = \det \mathbf{F}(\vec{X}, t)$ and $\mathrm{d}v$ and $\mathrm{d}v_R$ denote infinitesimal volume elements defined in the current and reference configuration, respectively. The infinitesimal volume element $\mathrm{d}v$ can be written as the product

$$\mathrm{d}v = \mathrm{d}\vec{a} \cdot \mathrm{d}\vec{x} = J \, \mathrm{d}\vec{a}_R \cdot \mathrm{d}\vec{X} \tag{6.9}$$

with $\mathrm{d}\vec{a} = \mathrm{d}a \, \vec{n}$ and $\mathrm{d}\vec{a}_R = \mathrm{d}a_R \, \vec{n}_R$ indicating vector elements of infinitesimal areas in the current and reference configurations pointing to the outward normal to the infinitesimal surface, i.e. $\vec{n}$ and $\vec{n}_R$. By using the linear tranformation (6.4) and the identity

$$\vec{v} \cdot \mathbf{A}^T \, \vec{u} = \vec{u} \cdot \mathbf{A} \, \vec{v} = \mathbf{A} \, \vec{v} \cdot \vec{u} \tag{6.10}$$

equation (6.9) can be rewritten as

$$(\mathbf{F}^T \, \mathrm{d}\vec{a} - J \, \mathrm{d}\vec{a}_R) \cdot \mathrm{d}\vec{X} = 0 \qquad \text{for all } \mathrm{d}\vec{X}. \tag{6.11}$$

Since $\mathbf{F}$ is invertible we find the so-called Nanson's formula

$$\mathrm{d}\vec{a} = J \, \mathbf{F}^{-T} \, \mathrm{d}\vec{a}_R \tag{6.12}$$

which defines the mapping of infinitesimal area vectors. From equation (6.12) we can also find a relationship between deformed and undeformed infinitesimal area, i.e.

$$j(\vec{X}, t) = \frac{\mathrm{d}a}{\mathrm{d}a_R} \tag{6.13}$$

with $j = J |\mathbf{F}^{-T} \, \vec{n}_R|$.

Strain Tensors. We now introduce the changes of materials elements during motion in the form of second-order strain tensors, both in reference and current frames. The right Cauchy-Green deformation tensor is defined as

$$C = F^T F \tag{6.14}$$

From definition (6.14), C is fully lagrangian, symmetric, and positive definite tensor. The inverse of C identifies the so called Piola deformation tensor

$$B = C^{-1} = (F^T F)^{-1} = F^{-1} F^{-T} \tag{6.15}$$

As a further strain measure, let introduce the Green-Lagrange strain tensor E as,

$$E = \frac{1}{2} \left(F^T F - I \right) = \frac{1}{2} \left(C - I \right) \tag{6.16}$$

Then, in order to relate strains measures to quantities which are associated with the current configuration, we can define the left Cauchy-Green tensor b which is defined by $b = F F^T$, which is an important strain measure in spatial coordinates.

Reynolds' Transport Theorem. Suppose we have a spatial scalar field $f(\vec{x}, t)$ describing some physical quantity per unit volume (for example mass density or species concentration) and we want to compute the material derivative of its integral over a volume advecting with the body, namely

$$\frac{d}{dt} \int_{\mathcal{P}_t} f(\vec{x}, t) \, dv \tag{6.17}$$

It can be proven that the time rate of change of the integral (6.17) result in two contributions: the local time rate of change of the spatial scalar field f, and the rate of transport of $f\vec{v}$ across the boundary surface $\partial \mathcal{P}_t$ ($\vec{v}$ is the velocity of advection), i.e.

$$\frac{d}{dt} \int_{\mathcal{P}_t} f \, dv = \int_{\mathcal{P}_t} \frac{\partial f}{\partial t} \, dv + \int_{\partial \mathcal{P}_t} f\vec{v} \cdot \vec{n} \, da \tag{6.18}$$

Similarly, we can evaluate the material derivative of the surface integral of a spatial scalar field $g(\vec{x}, t)$ describing some physical quantity per unit of surface (i.e surface mass density or surface molar concentration), i.e.

$$\frac{d}{dt} \int_{\mathcal{S}_t} g(\vec{x}, t) \, da \tag{6.19}$$

Also in this case, since the surface $\mathcal{S}_t$ advects with velocity $\vec{v}$, we need to consider additional terms besides the local time change of the spatial scalar field g (see [145] for the details)

$$\frac{d}{dt} \int_{\mathcal{S}_t} g \, da = \int_{\mathcal{S}_t} \frac{\partial g}{\partial t} \, da + \int_{\mathcal{S}_t} \text{div} \left[g\vec{v} \right] \, da - \int_{\mathcal{S}_t} g \, \frac{\vec{n} \cdot d\vec{n}}{|\vec{n}|^2} \, da \tag{6.20}$$

In equation (6.20), $d = (l + l^T)/2$ refers to the rate of deformation tensor ($l = \nabla \left[\vec{v} \right]$ is the velocity gradient).

6.3 General form of balance equations

6.3.1 Mass balance on a volume that advects

When species diffuse in large deformations setting, one has to account for two velocities: the velocity of advection, and the velocity of the species. If we assume that there is no mass flux, density may change because volumes either shrink or enlarge with velocity $\vec{v}$. For the sake of generality, we consider a continuum body with a set of particles occupying an arbitrary region $\mathcal{P}_t$ with boundary surface $\partial \mathcal{P}_t$. The content of diffusive species α in the body is characterized by its molar concentration $C_\alpha(\vec{x}, t)$, i.e. moles per unit current volume. We assume that the time variation of of species content is due to flux across the boundary surface $\partial \mathcal{P}_t$ and species generation inside the volume $\mathcal{P}_t$. The integral form of species conservation in the spatial frame thus reads

$$\frac{\mathrm{d}}{\mathrm{dt}} \int_{\mathcal{P}_t} C_\alpha \, \mathrm{d}v = - \int_{\partial \mathcal{P}_t} \vec{h}_\alpha \cdot \vec{n} \, \mathrm{d}a + \int_{\mathcal{P}_t} S_\alpha \, \mathrm{d}v \tag{6.21}$$

where $\vec{h}_\alpha = C_\alpha \, \vec{v}_\alpha$ is the flux vector of species α ($\vec{v}_\alpha$ its the velocity of species α); S_α the generated mass of species α, i.e. moles per unit current volume and unit time. Owing to equation (6.18) and divergence theorem, the left hand side of equation (6.21) can be rewritten as

$$\frac{\mathrm{d}}{\mathrm{dt}} \int_{\mathcal{P}_t} C_\alpha \, \mathrm{d}v = \int_{\mathcal{P}_t} \frac{\partial C_\alpha}{\partial t} + \mathrm{div} \left[C_\alpha \vec{v} \right] \mathrm{d}v \tag{6.22}$$

that allows us to obtain the local form of conservation of species in the current configuration

$$\frac{\partial C_\alpha}{\partial t} + \mathrm{div} \left[C_\alpha \vec{v} + \vec{h}_\alpha \right] = S_\alpha \tag{6.23}$$

As customary, the referential forms of the conservation of diffusing species can be easily recovered by substituting formulae (6.8) - (6.12) in equation (6.21), obtaining

$$\frac{\mathrm{d}}{\mathrm{dt}} \int_{\mathcal{P}} C_{\alpha R} \, \mathrm{d}v_R = - \int_{\partial \mathcal{P}} \vec{h}_{\alpha R} \cdot \vec{n}_R \, \mathrm{d}a_R + \int_{\mathcal{P}} S_{\alpha R} \, \mathrm{d}v_R \tag{6.24}$$

and

$$\frac{\partial C_{\alpha R}}{\partial t} + \mathrm{Div} \left[\vec{h}_{\alpha R} \right] = S_{\alpha R} \tag{6.25}$$

Note that the referential molar concentration $C_{\alpha R}$, referential flux $\vec{h}_{\alpha R}$, and referential species supply $S_{\alpha R}$ have been introduced in (6.24) - (6.25) as

$$C_{\alpha R} = J \, C_\alpha \qquad \vec{h}_{\alpha R} = J \, \mathbf{F}^{-1} \, \vec{h}_\alpha \qquad S_{\alpha R} = J \, S_\alpha \tag{6.26}$$

6.3.2 Mass balance on a surface that advects

We now discuss the conservation of diffusing species on a surface that advects with velocity $\vec{v} \, (\vec{x}, t)$. For the sake of generality we consider an open surface $\mathcal{S}_t$ bounded by a closed line $\mathcal{C}_t$ (see Fig. 6.3). Similarly to the the approach followed in Section 6.3.1, the surface content of a diffusive species α is characterized by its surface molar concentration $c_\alpha(\vec{x}, t)$, i.e. moles per unit current surface. We assume that the time variation of specis content is due to normal flux across the boundary $\mathcal{C}_t$, as well as species generation on the surface $\mathcal{S}_t$. The integral form of species in the current configuration thus reads

$$\frac{\mathrm{d}}{\mathrm{dt}} \int_{\mathcal{S}t} c_\alpha \, \mathrm{d}a = - \int_{\mathcal{C}t} \vec{h}_\alpha \cdot \vec{t}_\perp \, \mathrm{d}\ell + \int_{\mathcal{S}t} s_\alpha \, \mathrm{d}s \tag{6.27}$$

where $\vec{h}_\alpha$ is the flux vector of species α (as it was defined in Section 6.3.1); s_α is the generated concentration of species α, i.e. moles per unit current surface and unit time. Owing to equation (6.20), the left hand side of equation (6.27) can be rewritten as

$$\frac{\mathrm{d}}{\mathrm{dt}} \int_{\mathcal{S}_t} c_\alpha \, \mathrm{d}a = \int_{\mathcal{S}_t} \frac{\partial c_\alpha}{\partial t} \, \mathrm{d}a + \int_{\mathcal{S}_t} \mathrm{div} \left[c_\alpha \vec{v} \right] \mathrm{d}a - \int_{\mathcal{S}_t} c_\alpha \frac{\vec{n} \cdot \mathbf{d}\vec{n}}{|\vec{n}|^2} \, \mathrm{d}a \tag{6.28}$$

As shown in Chapter 4, the line integral in equation (6.27) yields

$$\int_{\partial \mathcal{C}t} \vec{h}_\alpha \cdot \vec{t}_\perp \, \mathrm{d}\ell = \int_{\mathcal{S}_t} \mathrm{div}_\Omega \left[\vec{h}_\alpha \right] \mathrm{d}a \tag{6.29}$$

where div_Ω refers to the projected divergence operator, namely

$$\mathrm{div}_\Omega \left[\vec{h}_\alpha \right] = \mathrm{div} \left[\vec{h}_\alpha \right] - \left(\mathrm{grad} \left[c_\alpha \right] \vec{n} \right) \cdot \vec{n} \tag{6.30}$$
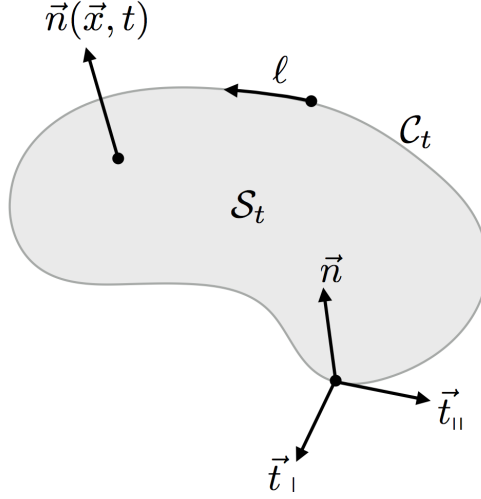
Figure 6.3: Schematic representation of an advecting surface.

In addition we have that

$$\operatorname{div}\left[c_\alpha \vec{v}\right] = \operatorname{div}_\Omega\left[c_\alpha \vec{v}\right] + \operatorname{grad}\left[c_\alpha \vec{v}\right]\frac{\vec{n}}{|\vec{n}|}\cdot\frac{\vec{n}}{|\vec{n}|} = \operatorname{div}_\Omega\left[c_\alpha \vec{v}\right] + c_\alpha\frac{\vec{n}\cdot\mathbf{l}\vec{n}}{|\vec{n}|^2} \tag{6.31}$$

Therefore, by substituting equations (6.28) - (6.29) - (6.31) into formula (6.27), we obtain

$$\int_{\mathcal{S}_t}\frac{\partial c_\alpha}{\partial t}\,\mathrm{d}a + \int_{\mathcal{S}_t}\operatorname{div}_\Omega\left[c_\alpha \vec{v}\right]\,\mathrm{d}a + \int_{\mathcal{S}_t}\operatorname{div}_\Omega\left[\vec{h}_\alpha\right]\,\mathrm{d}a + \int_{\mathcal{S}_t}c_\alpha\frac{\vec{n}\cdot\mathbf{l}\vec{n}}{|\vec{n}|^2}\,\mathrm{d}a - \int_{\mathcal{S}_t}c_\alpha\frac{\vec{n}\cdot\mathbf{d}\vec{n}}{|\vec{n}|^2}\,\mathrm{d}a = \int_{\mathcal{S}t}s_\alpha\,\mathrm{d}s \tag{6.32}$$

that allows us to derive the local form of conservation of diffusing species in the current configuration as

$$\frac{\partial c_\alpha}{\partial t} + \operatorname{div}_\Omega\left[c_\alpha \vec{v} + \vec{h}_\alpha\right] = s_\alpha \tag{6.33}$$

Note that the we have exploited the fact that

$$c_\alpha\frac{\vec{n}\cdot\mathbf{l}\vec{n}}{|\vec{n}|^2} - c_\alpha\frac{\vec{n}\cdot\mathbf{d}\vec{n}}{|\vec{n}|^2} = c_\alpha\frac{\vec{n}\cdot\mathbf{w}\vec{n}}{|\vec{n}|^2} = 0 \tag{6.34}$$

since the so called spin tensor $\mathbf{w} = (\mathbf{l} - \mathbf{l})/2$ is skew-symmetric by definition.

Following the same path of reasoning of Section 6.3.1, the referential forms of the conservation of diffusing species can be easily recovered by substituting formulae (6.4) - (6.13) into equation (6.27), obtaining

$$\frac{\partial c_{\alpha R}}{\partial t} + \operatorname{Div}_\Omega\left[h_{\alpha R}\right] = s_{\alpha R} \tag{6.35}$$

where the reference form of the projected divergence operator yields

$$\operatorname{Div}_\Omega\left[\vec{h}_{\alpha R}\right] = \operatorname{Div}\left[\vec{h}_{\alpha R}\right] - \left(\operatorname{Grad}\left[c_{\alpha R}\right]\vec{n}_R\right)\cdot\vec{n}_R \tag{6.36}$$

Note that the referential surface concentration $c_{\alpha R}$, referential flux $\vec{h}_{\alpha R}$, and referential species supply $s_{\alpha R}$ have been introduced in (6.35) as

$$c_{\alpha R} = j\,c_\alpha \qquad \vec{h}_{\alpha R} = j\,\mathbf{F}^{-1}\,\vec{h}_\alpha \qquad s_{\alpha R} = j\,s_\alpha \tag{6.37}$$

6.3.3 Balance of Linear and Angular Momentum

The quasi-static forms of balance of linear and angular momentum are briefly summarized in their spatial and referential form. The local form of the spatial formulation is

$$\text{div}\,[\,\sigma\,] + \vec{b} = \vec{0} \qquad \sigma = \sigma^T \tag{6.38}$$

where the (symmetric) Cauchy stress tensor σ and the body forces for unit current volume $\vec{b}$ account respectively for contact and action-at-a-distance forces (e.g. due to gravity). The referential form are instead

$$\text{div}\,[\,\mathbf{P}\,] + \vec{b}_R = \vec{0}, \qquad \mathbf{P}\mathbf{F}^T = \mathbf{F}\mathbf{P}^T, \tag{6.39}$$

where the (non-symmetric) First-Piola-Kirchoff stress tensor $\mathbf{P}$ and the body forces per unit reference volume $\vec{b}_R$ are defined as follow

$$\mathbf{P} = J\,\sigma\,\mathbf{F}^{-T} \qquad \vec{b}_R = J\,\vec{b} \tag{6.40}$$

An alternative stress tensor is the second Piola-Kirchhoff stress tensor $\mathbf{S}$, which represents a very useful stress measure in computational mechanics and in the formulation of constitutive equations. It is defined as

$$\mathbf{S} = \mathbf{F}^{-1}\,\tau\,\mathbf{F}^{-T} \tag{6.41}$$

where $\boldsymbol{\tau} = J\,\boldsymbol{\sigma}$ is the so-called Kirchhoff stress tensor (which differs from the Cauchy stress tensor by the volume ratio J). Therefore we have that

$$\mathbf{S} = \mathbf{F}^{-1}\,\mathbf{P} = \mathbf{S}^T \tag{6.42}$$

which allows us to find a fundamental relationship between the First Piola-Kirchhoff stress tensor $\mathbf{P}$ and the Second Piola-Kirchhoff stress tensor $\mathbf{S}$

$$\mathbf{P} = \mathbf{F}\,\mathbf{S} \tag{6.43}$$

6.4 Modeling the receptors-ligands binding on advecting surfaces

6.4.1 Spatial formulation

As carried out in Chapter 4, the interaction between receptors (R) and ligands (L) is described as a chemical reaction, which produces a receptor-ligand complex (C),

$$\mathrm{R} + \mathrm{L} \underset{k^-}{\overset{k^+}{\rightleftarrows}} \mathrm{C}, \tag{6.44}$$

Ligands, whose degradation is negligible, and complex are assumed to be immobile. Since receptors are free to move along the membrane, reaction (6.44) portrays a conversion of mobile to trapped receptors and vice-versa. Its rate is denoted with $w^{(6.44)}$. Therefore, the spatial form of mass balance equations for the three species involved in reaction (6.44) are

$$\frac{\partial c_R}{\partial t} + \text{div}_\Omega\left[\,c_R\,\vec{v} + \vec{h}_R\,\right] + w^{(6.44)} = 0 \tag{6.45a}$$

$$\frac{\partial c_L}{\partial t} + \text{div}_\Omega\left[\,c_L\,\vec{v}\,\right] + w^{(6.44)} = 0 \tag{6.45b}$$

$$\frac{\partial c_C}{\partial t} + \text{div}_\Omega\left[\,c_C\,\vec{v}\,\right] - w^{(6.44)} = 0 \tag{6.45c}$$

It is worth noting that here, differently from the governing equations derived in Chapter 4, the mechanics of cell impacts on balance equations (6.45) through the advecting contribution $\text{div}_\Omega\left[\,c_\alpha\,\vec{v}\,\right]$ as derived in Section 6.3.1.

Following the same path of reasoning of Chapter 4, the kinetics of reaction (6.44) is modeled by means of mass action law, thus

$$w^{(6.44)} = k^+ \frac{\vartheta_L}{(1 - \vartheta_L)} \frac{\vartheta_R}{(1 - \vartheta_R)} - k^- \frac{\vartheta_C}{(1 - \vartheta_C)} \tag{6.46}$$

where k^+ and k^- are the forward and backward kinetic constants respectively. Symbol ϑ_α in equation (6.46) denotes the molar fraction of species α, i.e.

$$\vartheta_\alpha = \frac{c_\alpha}{c_\alpha^{max}} \tag{6.47}$$

with c_α^{max} denoting the saturation limit of species α. Since ϑ_α are non-dimensional, the forward and backward constants entail the dimensionality of $w^{(6.44)}$, i.e. the units of k^+ and k^- are

$$\left[k^+ \right] = \left[k^- \right] = \left[\frac{\text{molecule}}{\text{area}} \frac{1}{\text{time}} \right] \tag{6.48}$$

6.4.2   Referential formulation

The referential form of balance equations can be written as follow

$$\frac{\partial c_{RR}}{\partial t} + \text{Div}_\Omega \left[\vec{h}_{RR} \right] + w_R^{(6.44)} = 0 \tag{6.49a}$$

$$\frac{\partial c_{LR}}{\partial t} + w_R^{(6.44)} = 0 \tag{6.49b}$$

$$\frac{\partial c_{CR}}{\partial t} - w_R^{(6.44)} = 0 \tag{6.49c}$$

with

$$c_{RR} = J\,c_R \qquad c_{LR} = J\,c_L \qquad c_{CR} = J\,c_C \qquad \vec{h}_{RR} = J\,\mathbf{F}^{-1}\vec{h}_R \qquad w_R^{(6.44)} = J\,w^{(6.44)} \tag{6.50}$$

as derived in Section 6.3.2. The term ϑ_α in formula is (6.46) is dimensionless and as such it should remain unchanged with the configuration. In order for this to happen, c_α^{max} must change in the reference configuration, not being a constant anymore in time. This makes sense since at each point $\vec{X}$, the maximum amount that can be stored depends upon the area at time t rather than at initial time t_0. One thus defines

$$c_{\alpha R}^{max} = j\,c_\alpha^{max} \tag{6.51}$$

accordingly

$$\vartheta_\alpha(\vec{x}, t) = \frac{c_\alpha(\vec{x}, t)}{c_\alpha^{max}} = \frac{c_{\alpha R}(\vec{X}, t)}{j(\vec{X}, t)c_\alpha^{max}} = \frac{c_{\alpha R}}{c_{\alpha R}^{max}} = \vartheta_\alpha(\vec{X}, t) \tag{6.52}$$

Owing to formulae (6.50), (6.52), and (6.46), the rate of chemical reaction (6.44) holds

$$w_R^{(6.44)} = j \left[k^+ \frac{\vartheta_L}{(1 - \vartheta_L)} \frac{\vartheta_R}{(1 - \vartheta_R)} - k^- \frac{\vartheta_C}{(1 - \vartheta_C)} \right] \tag{6.53}$$

This expression suggests that the forward and backward costants are such in the current configuration but thay change with time in the reference configuration according to

$$k_R^+ = j\,k^+ \qquad k_R^- = j\,k^- \tag{6.54}$$

therefore equation (6.53) yields

$$w_R^{(6.44)} = k_R^+ \frac{\vartheta_L}{(1 - \vartheta_L)} \frac{\vartheta_R}{(1 - \vartheta_R)} - k_R^- \frac{\vartheta_C}{(1 - \vartheta_C)} \tag{6.55}$$

The mass balance equations (6.49) become

$$\frac{\partial c_{RR}}{\partial t} + \text{Div}_\Omega \left[\vec{h}_{RR} \right] = - \left[k^+ \frac{\vartheta_L}{(1-\vartheta_L)} \frac{\vartheta_R}{(1-\vartheta_R)} - k^- \frac{\vartheta_C}{(1-\vartheta_C)} \right] J |\mathbf{F}^{-T} \vec{n}_R| \tag{6.56a}$$

$$\frac{\partial c_{LR}}{\partial t} = - \left[k^+ \frac{\vartheta_L}{(1-\vartheta_L)} \frac{\vartheta_R}{(1-\vartheta_R)} - k^- \frac{\vartheta_C}{(1-\vartheta_C)} \right] J |\mathbf{F}^{-T} \vec{n}_R| \tag{6.56b}$$

$$\frac{\partial c_{CR}}{\partial t} = \left[k^+ \frac{\vartheta_L}{(1-\vartheta_L)} \frac{\vartheta_R}{(1-\vartheta_R)} - k^- \frac{\vartheta_C}{(1-\vartheta_C)} \right] J |\mathbf{F}^{-T} \vec{n}_R| \tag{6.56c}$$

with

$$\vec{h}_{RR}(\vec{x}, t) = -\mathbb{D}_R \nabla_{\Omega_R} [c_{RR}] \tag{6.57}$$

and

$$\nabla_{\Omega_R} [c_{RR}] = \nabla c_{RR} - (\nabla c_{RR} \cdot \vec{n}_R) \, \vec{n}_R. \tag{6.58}$$

6.5 Modeling the mechanical response of living cells

The fundamental equations described on the privious Sections are essential to characterize kinematics, stresses and balance principles, and hold for any continuum body for all times. However, they do not recognize the body's material and they are not sufficient to establish the material response. For this aim, we must introduce additional equations in the form of appropriate constitutive laws, which are provide equations that approximate the observed physical behaviour of the material. The objective of constitutive theories is to develop mathematical models for representing the real behavior of matter. We represent a non-linear constitutive theory suitable to describe hyperelastic materials, in particular compressible, and a recent theory proposed by [146] to describe the cell contractility.

6.5.1 A simple, Neo-Hookean model

A Neo-Hookean is a hyperelastic material model [151], constitutively described as

$$\Psi^{NH}(\mathbf{C}) = \frac{\mu}{2} \left(\text{tr}\,(\mathbf{C}) - 3 \right) \,, \tag{6.59}$$

whence the second Piola stress tensor can be derived as usual

$$\mathbf{S} = 2 \frac{\partial \Psi^{NH}(\mathbf{C})}{\partial \mathbf{C}} \,. \tag{6.60}$$

For compressible materials, the regularized version of the Neo-Hookean model stems from the splitting

$$\Psi^{NH}(\mathbf{C}) = \Psi^{NH}_{\text{vol}}(J) + \Psi^{NH}_{\text{iso}}(\bar{\mathbf{C}}) \,, \tag{6.61}$$

where $\Psi_{\text{vol}}(J)$ describes the volumetric elastic response and $\Psi_{\text{iso}}(\bar{\mathbf{C}})$ the isochoric elastic response. They both are given scalar-valued function of J and $\bar{\mathbf{C}}$, whereby the latter is the modified right Cauchy-Green tensor $\mathbf{C} = J^{2/3} \bar{\mathbf{C}}$. We introduce a strain-energy function for compressible hyperelastic material in terms of [152]

$$\Psi^{NH}_{\text{vol}}(J) = \frac{K}{2} \left(J - 1 \right) \ln(J) \tag{6.62a}$$

$$\Psi^{NH}_{\text{iso}}(\bar{\mathbf{C}}) = \frac{\mu}{2} \left(\text{tr}\,(\bar{\mathbf{C}}) - 3 \right) \tag{6.62b}$$

where μ and K are the NeoHookean shear and bulk moduli. A class of nonlinear, viscoelastic constitutive models has been proposed in [153] in terms of a set of internal variables $\mathbf{Q}_i(t)$:

$$\mathbf{S} = 2 \, \frac{\partial \, \Psi^{NH}(\mathbf{C})}{\partial \, \mathbf{C}} - J^{-2/3} \, \mathrm{dev} \left[\sum_i \mathbf{Q}_i(t) \right] \tag{6.63}$$

where the deviatoric operator is defined as usual as

$$\mathrm{dev} \left[\, \mathbf{Q}_i(t) \, \right] = \mathbf{Q}_i(t) - 1/3 \, (\mathbf{Q}_i(t) : \mathbf{C}) \, \mathbf{C}^{-1} \, . \tag{6.64}$$

Different classes of viscoelastic models are based upon specific selections for $\mathbf{Q}_i(t)$. We followed the approach of [153], Chapter 10. Standard yet lengthy algebra, not reported here, leads to a straightforward integration algorithm. The interested reader can refer to [153], Chapter 10.

Simulations with the HPC open source finite element library deal.II (http://www.dealii.org) have been performed using the formulation above. We investigated the large mechanical deformations that occur in an endothelial cell once it spreads from a spherical initial configuration onto a flat surface. This evolution indeed takes place in the experimental tests described in Chapter 2. To this aim, we used the spherical configuration as reference, and followed the evolution of the shape imposing a contact scheme on a flat surface, which is the tangent plane to the sphere at its bottom. Contact algorithm entail the solution of variational inequalities, since the admissible numerical approximation belongs to a convex set of admissible displacements. To solve our problem we slightly modified a scheme proposed in [154] and already implemented in the tutorial section of deal.II. Material parameters for the simulations are taken from [155]. The nucleus parameters have been takes as $145,985.4 fN/\mu m^2$ for the shear modulus and $512,820.5 fN/\mu m^2$ for the bulk modulus. The parameters for the cytosol have been reduced, since the cells considered in [155] were not endothelial and a much higher deformation have been evidenced for the latter. We thus picked $36.49635 fN/\mu m^2$ for the shear modulus and $128.205 fN/\mu m^2$ for the bulk modulus. Further analysis are required to calibrate these last parameters. Following the experimental evidences described in Chapter 2, we selected a relaxation time of half minute, and $\gamma_1 = 0.9$ (namely, 90% of the stiffness is in the dashpot spring and only 10% in the intrinsic stiffness). The cell radius ℓ amounts at 20.0 microns, whereby the nucleus radius is 3.5 microns in the reference configuration.

The cell was loaded with rising load from time zero to the gravity weight in about a second. The cell spread out in view of its viscous behavior, and the steady state configuration are printed in Figures 6.4 and 6.5. They show the plots of cell density, vertical displacement, and deformation. The white frame in the background is the reference, initial configuration. The appearance of the nucleus is self-evident, in view of its largest stiffness. For the sake of time, neither specific remeshing algorithms nor the mass balance equations (6.56) have been implemented.

6.5.2 One-dimensional model for cell contractility. Stress generated by stress fibers bundles

A general model for cell contractility [146], that relies on experimental studies [156], based on continuum scale, explains why force vectors into living cells, acting on a compliant substrate, are occuring where no stress fibers are visible. The model includes the formation and dissociation of stress fibers and the generation of tension within the cell. In addition, the simulations data show the decrease of the forces generated by the cell with increasing subtrate stiffness and include the cell shape and boundary conditions effects on structural anisotropy [146]. Stress fibres (SFs) formation in a living cell is triggered by an activation signal as an external cue, by the release of Ca^{2+} from the endoplasmic reticulum. The influx of Ca^{2+} activates gelsolin, a protein that regulates actin filaments depolarization (i.e. formation of tiny fragments). The large numbers of free ends generated in this manner are rapidly elongated by the monomeric actin group, forming many long filaments, some cross-linked with some bundled by $\alpha-$actinin. Phosphorylation triggered by Ca^{2+} causes myosin II to preferentially assume its extended state. This promotes the assembly of myosin II into bipolar filaments that enter into the $\alpha-$actinin-bound actin filament bundles, resulting in the formation of SFs. These fibres generate tension by cross-bridge cycling between the actin and the myosin filaments.
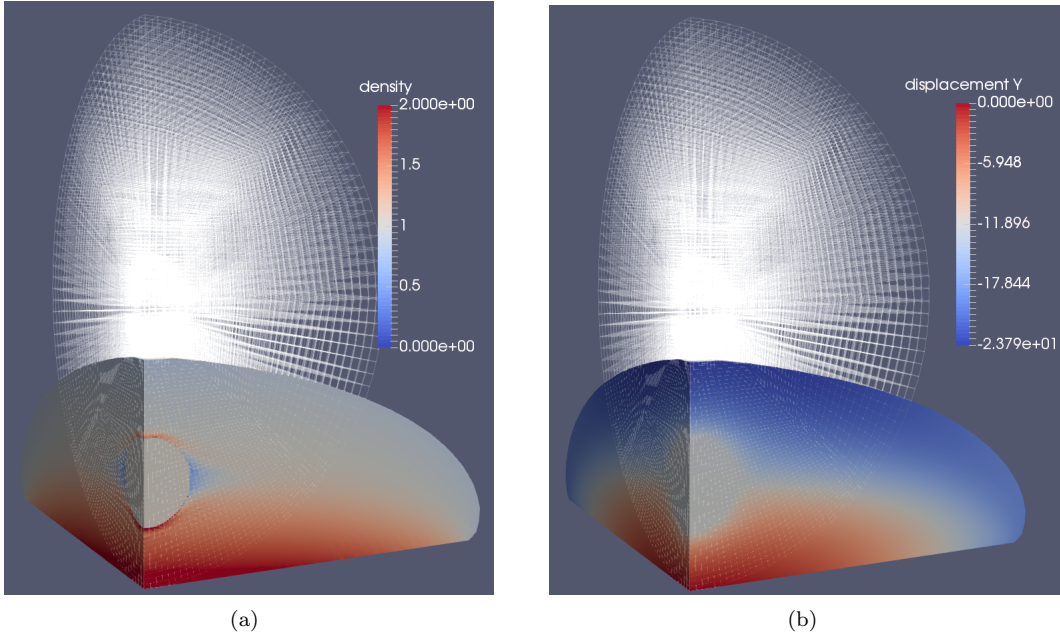
Figure 6.4: Evolution of the shape imposing a contact scheme on a flat surface. (a) density, (b) vertical displacement. The nucleus clearly emerges. The white frame in the background is the reference, initial configuration.
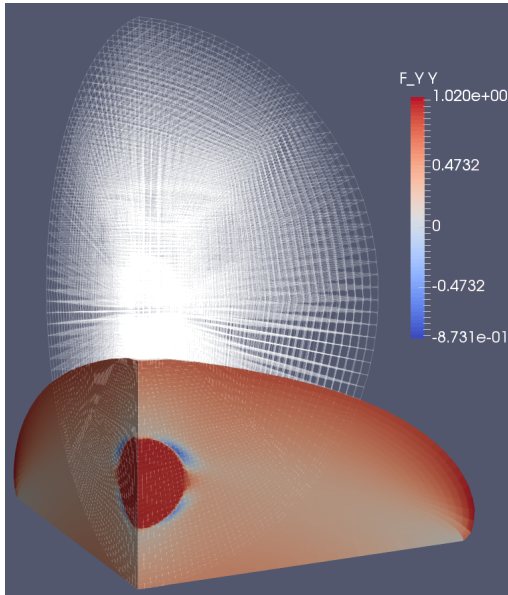
Figure 6.5: Evolution of the shape imposing a contact scheme on a flat surface: cell deformation measured by F_{yy}. The nucleus clearly emerges. The white frame in the background is the reference, initial configuration.

When the tension decreases, the actin filaments are no longer held in place by the bipolar myosin filaments and the SFs disassemble [157]. A rapid transmission of the extracellular signal triggers the polymerization of the actin filaments and the phosphorylation of the myosin. The signal level may be thought of as the concentration of Ca^{2+}, designated C $(0 < C < 1)$ is assumed given by [146, 157]

$$C = \exp\left(-\frac{t_i}{\theta}\right) \tag{6.65}$$

where t_i is the decay constant of the signal and θ is the time measured from the instant of the most recent signal.

The transduction of the signal results in: (i) the polymerization of the actin filaments and the bundling of these filaments by α−actinin and (ii) the phosphorylation of myosin II, which promotes the assembly of the myosin into bipolar filaments. The interaction between the myosin II heads and the actin filaments forms contractile bundles. We characterize the activation level of the SF bundles by a dimensionless parameter, η $(0 \leq \eta \leq 1)$, defined as the ratio of the concentration of the polymerized actin and phosphorylated myosin in the bundle to the maximum concentrations permitted by the biochemistry [146]. The formation and the dissociation of the SFs, as parameterized through η, are represented by a first-order kinetic scheme,

$$\frac{\mathrm{d}\eta}{\mathrm{d}t} = \left([1-\eta]\,\frac{C\,\overline{k}_f}{\theta} \right) - \left[\left(1 - \frac{T}{T_0} \right) \eta\,\frac{\overline{k}_b}{\theta} \right] \tag{6.66}$$

where T is the tension in the SF and $T_0(\eta)$ the corresponding isometric tension for a given η and $T_0 = \eta\,T_{\max}$. The dimensionless constants $\overline{k}_f$ and $\overline{k}_b$ govern the rate of formation (forward) and dissociation (backward) of the SFs, respectively. A tension versus velocity relation to describe the muscle mechanics has been written by A.V. Hill [158],

$$(T + a)(v + b) = (T_0 + a)\,b \tag{6.67}$$

where T is the force, v is the shortening velocity, the isometric tension T_0 defines the force against which the muscle neither shortens nor lengthens and the speed $v_{max} = b\,T_0/a$ is the shortening velocity against no load. Eq. (6.67) underlines the contractile behavior of SFs in non-muscle cell is similar to the Hill model [159] and the tension in the SFs is generated by the cross-bridge cycling between the actin and the myosin filaments. This force generation mechanism is similar (but not identical) to that in muscle cells.

$$v' = \frac{v}{v_{max}} = \frac{(1 - \frac{T}{T_0})}{(1 + \frac{T}{T_0}\frac{1}{k})} \tag{6.68}$$

where $k = a/T_0 = b/v_{max}$, usually assumed within the range $0.15 < k < 0.25$ [159]. Eq. (6.68) is plotted in Figure 6.6 for $k = 0.25$.
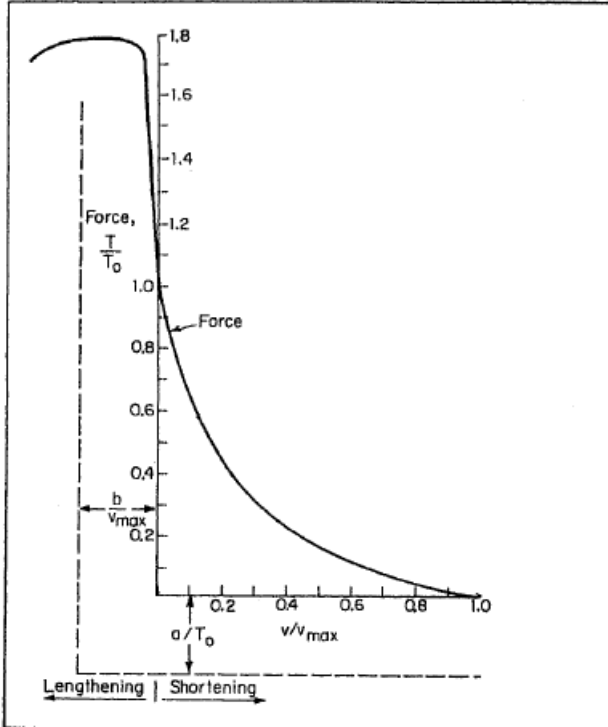
Figure 6.6: Hill's force-velocity curve. The shortening part of the curve was calculated from Eq.(6.68) with $k = 0.25$. Modified from [159]

The influence of tension on the extension/shortening rate of the fibres is described by a Hill-like relation [157], shown in Figure 6.7, described by,

$$\frac{T}{T_0} = \begin{cases} 0 & \frac{v}{v_0} < -\frac{\eta}{\overline{k}_v} \\ 1 + \frac{\overline{k}_v}{\eta}\frac{v}{v_0} & -\frac{\eta}{\overline{k}_v} \le \frac{v}{v_0} \le 0 \\ 1 & \frac{v}{v_0} > 0 \end{cases} \tag{6.69}$$

Here, v is the rate of change in the length of SF (positive for lengthening and negative for shortening). The dimensionless constant, $\overline{k}_v$, is the fractional reduction in tension when the shortening rate increases by the reference value, v_0.
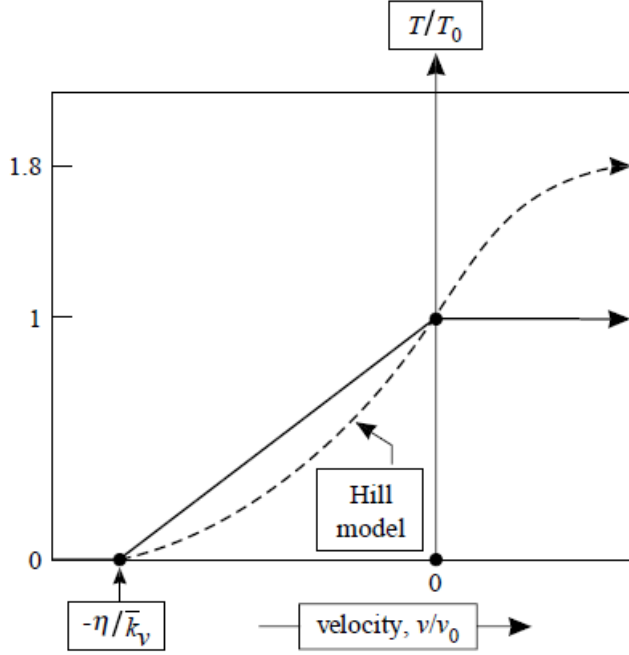
Figure 6.7: Hill tension-velocity relation for muscle cells. The approximation of the Eq.(6.69) is shown From [157] by the continuous line, while the dashed line represents the Eq. (6.68).

Eq.s (6.66) and (6.69) are generalized to the SF intensive quantities σ and fiber strain rate $\dot{\varepsilon}$ as the following equations:

$$\frac{d\eta}{dt} = [1 - \eta]\, C\frac{\overline{k}_f}{\theta} - \left[\left(1 - \frac{\sigma_f}{\sigma_0}\right)\eta\,\frac{\overline{k}_b}{\theta}\right] \tag{6.70}$$

$$\frac{\sigma_f}{\sigma_0} = \begin{cases} 0 & \frac{\dot{\varepsilon}}{\dot{\varepsilon}_0} < -\frac{\eta}{\overline{k}_v} \\ 1 + \frac{\overline{k}_v}{\eta}\frac{\dot{\varepsilon}}{\dot{\varepsilon}_0} & -\frac{\eta}{\overline{k}_v} \le \frac{\dot{\varepsilon}}{\dot{\varepsilon}_0} \le 0 \\ 1 & \frac{\dot{\varepsilon}}{\dot{\varepsilon}_0} > 0 \end{cases} \tag{6.71}$$

where σ_f is the stress in the SF bundle, σ_0 is the isometric tension, and $\overline{k}_v$ is the reduction in stress upon increasing the shortening strain rate, $\dot{\varepsilon}$ by a reference strain rate $\dot{\varepsilon}_0$. Remembering that $\sigma_0 = \eta\,\sigma_{\max}$ we obtain

$$\frac{d\eta}{dt} = [1 - \eta]\,\frac{C\,\overline{k}_f}{\theta} - \left[\left(\eta - \frac{\sigma_f}{\sigma_{\max}}\right)\frac{\overline{k}_b}{\theta}\right] \tag{6.72}$$

$$\sigma_f = \begin{cases} 0 & \dot{u} < -\frac{\eta\,v_0}{\overline{k}_v} \\ \eta\,\sigma_{\max}\left(1 + \frac{\overline{k}_v}{\eta}\frac{\dot{u}}{v_0}\right) & -\frac{\eta\,v_0}{\overline{k}_v} \le \dot{u} \le 0 \\ \eta\,\sigma_{\max} & \dot{u} > 0 \end{cases} \tag{6.73}$$

6.5.3   Result: one-dimensional model

We consider a simple rheological model with a single SF (red line shown in Fig.6.8) and an elastic spring, with elastic constant k_s, connected in parallel. They undergo an assigned displacement $\overline{u}(t)$, on the right side and are totally constrained on the left side as boundary conditions.
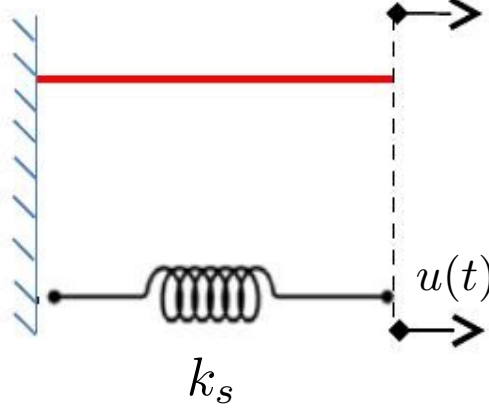
Figure 6.8: Contractility model: SFs, represented by the red line, and a spring in parallel.

We decided to consider this model in according with the model for the contractility of the cytoskeleton proposed by Deshpande at al. [157] and Ronan et al. [148] that define the total stress as a combination of two contributions: (i) the active SF contractility and (ii) the passive elastic stress provided mainly by the cytoskeleton filaments attached to the nuclear and plasma membranes, which means the passive material surrounding the SFs.

The resulting total stress will be

$$\sigma_{\text{tot}} = \sigma_f + \sigma_s \tag{6.74}$$

where σ_f is the stress on SFs, that is governed by the Eq. (6.73) and σ_s is the well-known spring stress,

$$\sigma_s = k_s \, \overline{u}(t) \tag{6.75}$$

6.5.3.1   Dimensionless equations

It is convenient to rewrite all the parameters in dimensionless form. For time t, displacement u, velocity $\dot{u}$, stresses σ and k_s we choose

$$\overline{t} = \frac{t}{\theta} \Rightarrow C = \exp\left(-\overline{t}\right) \tag{6.76}$$

$$\overline{u} = \frac{u}{\theta \, v_0}, \qquad \overline{\dot{u}} = \frac{\dot{u}}{v_0} \tag{6.77}$$

$$\overline{\sigma}_f = \frac{\sigma_f}{\sigma_{\max}}, \qquad \overline{\sigma}_s = \frac{\sigma_s}{\sigma_{\max}} \tag{6.78}$$

$$\overline{k}_s = \frac{k_s \, \theta \, v_0}{\sigma_{\max}} \tag{6.79}$$

using the chain rule we can write

$$\frac{\partial \eta}{\partial \overline{t}} = \frac{\partial \eta}{\partial t} \frac{\partial t}{\partial \overline{t}} = \frac{\partial \eta}{\partial t} \frac{\partial \theta \, \overline{t}}{\partial \overline{t}} = \frac{\partial \eta}{\partial t} \theta \tag{6.80}$$

94

Eq.s (6.72) and (6.73) transform into the dimensionless governing equations,

$$\overline{\sigma}_f = \begin{cases} 0 & \dot{u} < -\frac{\eta}{\overline{k}_v} \\ \eta \left(1 + \frac{\overline{k}_v}{\eta} \overline{\dot{u}}\right) & -\frac{\eta}{\overline{k}_v} \leq \dot{u} \leq 0 \\ \eta & \dot{u} > 0 \end{cases} \tag{6.81}$$

$$\frac{\partial \eta}{\partial \overline{t}} = \left[(1 - \eta) \exp(-\overline{t}) \overline{k}_f\right] - \left[(\eta - \overline{\sigma}_f(\eta)) \ \overline{k}_b\right] \tag{6.82}$$

6.5.3.2   Numerical solution: backward Euler and Newton-Raphson methods

For the time discretization of the problem we use the finite difference method (the backward Euler method). The backward Euler scheme is stable with no restriction on Δt. Then the discrete problem becomes

$$\frac{\Delta \eta}{\Delta \overline{t}} = \left[(1 - \eta_{n+1}) \exp(-\overline{t}) \overline{k}_f\right] - \left[(\eta_{n+1} - \overline{\sigma}_f(\eta)|_{n+1}) \ \overline{k}_b\right] \tag{6.83}$$

where

$$\Delta \eta = \eta_{n+1} - \eta_n \tag{6.84}$$

$$R(\eta_{n+1}) = \frac{\Delta \eta}{\Delta \overline{t}} - \left[(1 - \eta_{n+1}) \exp(-\overline{t}) \overline{k}_f\right] - \left[(\eta_{n+1} + \overline{\sigma}_f(\eta)|_{n+1}) \ \overline{k}_b\right] \tag{6.85}$$

Ones solve the non linear equation $R(\eta_{n+1}) = 0$ in order to find η_{n+1} for each t_{n+1} by means of the Newton-Raphson method,

$$R^{(k+1)} \simeq R^{(k)}|_{n+1} + \left.\frac{\mathrm{d}R}{\mathrm{d}\eta}\right|_{\eta_{n+1}^{(k)}} \delta\eta_{n+1}^{(k)} = 0 \tag{6.86}$$

hence,

$$\delta\eta_{n+1}^{(k)} = -\frac{R^{(k)}|_{n+1}}{\left.\frac{\mathrm{d}R}{\mathrm{d}\eta}\right|_{\eta_{n+1}^{(k)}}} \tag{6.87}$$

The residual is

$$R^{(k)}|_{n+1} = \frac{\eta_{n+1}^{(k)} - \eta_n}{\Delta t} - \left[\left(1 - \eta_{n+1}^{(k)}\right) \exp(-\overline{t}_{n+1}) \overline{k}_f\right] + \left[\left(\eta_{n+1}^{(k)} - \overline{\sigma}_f(\eta_{n+1}^{(k)})\right) \ \overline{k}_b\right] \tag{6.88}$$

and its derivative,

$$\left.\frac{\mathrm{d}R}{\mathrm{d}\eta}\right|_{\eta_{n+1}^{(k)}} = \frac{1}{\Delta t} + \exp(-\overline{t}_{n+1}) \overline{k}_f + \overline{k}_b + \left.\frac{\partial \overline{\sigma}_f \eta_{n+1}^{(k)}}{\partial \eta}\right|_{\eta_{n+1}^{(k)}} \overline{k}_b \tag{6.89}$$

where

$$\overline{\sigma}_f(\eta_{n+1}^{(k)}) = \begin{cases} 0 & \overline{\dot{u}} < -\frac{\eta_{n+1}^{(k)}}{\overline{k}_v} \\ \eta_{n+1}^{(k)} \left(1 + \frac{\overline{k}_v}{\eta_{n+1}^{(k)}} \overline{\dot{u}}\right) & -\frac{\eta_{n+1}^{(k)}}{\overline{k}_v} \leq \overline{\dot{u}} \leq 0 \\ \eta_{n+1}^{(k)} & \overline{\dot{u}} > 0 \end{cases} \tag{6.90}$$
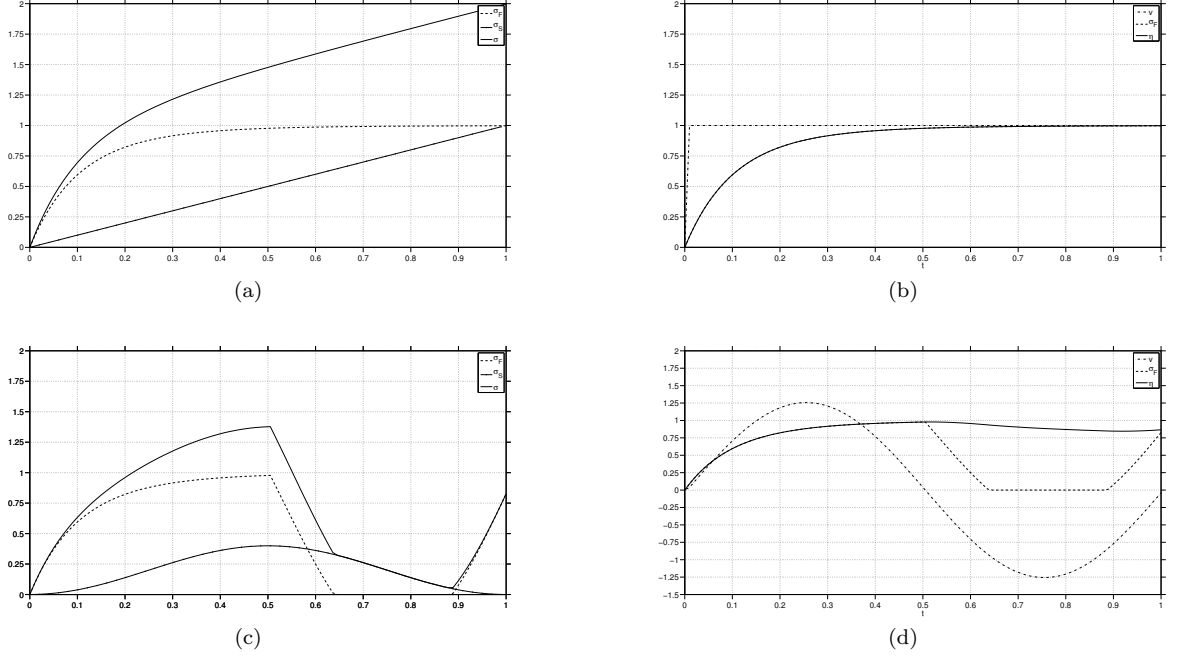
Figure 6.9: Case (1) (a) -(b) Linear function of u respect to time t: stress fibers stress σ_f, spring σ_s and total tension σ_{tot}, velocity v, parameter η and stress fibers tension σ_f. Case (2) (c) -(d): stress fibers σ_f, spring σ_s and total tension σ_{tot} velocity v, parameter η and stress fibers tension σ_f.

$$\left.\frac{\partial \overline{\sigma}_f}{\partial \eta}\right|_{\eta_{n+1}^{(k)}} = \begin{cases} 0 & \overline{\dot{u}} < -\frac{\eta_{n+1}^{(k)}}{\overline{k}_v} \\ 1 & -\frac{\eta_{n+1}^{(k)}}{\overline{k}_v} \leq \overline{\dot{u}} \leq 0 \\ 1 & \overline{\dot{u}} > 0 \end{cases} \tag{6.91}$$

Results. Two different cases are plotted, choosing two displacements: case 1) a linear time-dependent displacement has been taken $u_1(t) = t$; case 2) a cosinusoidal time-dependent function has been considered $u_2(t) = -0.2\cos(2\pi t)$. Fig. 6.9($a$) shows the stress evolution with respect to time, for the case 1). The spring tension increases linearly with Eq. (6.75); since we considered merely the velocity $\dot{u} \geq 0$ the evolution of σ_f follows Eq. (6.81). The plot in Fig. 6.9(b) shows the evolution in time of the velocity, the parameter η and σ_f. Fig. 6.9(c) and 6.9(d) are the evolution for the case 2).

The time evolution of η follows Eq. (6.72) and is due to two contributions: (i) the first square bracket means that the rate of the formation of the SF, which decreases with increasing fibre activation η and is proportional to the strength of the decaying signal (ii) the second square bracket identifies the rate of dissociation, which is proportional to the concentration of the polymerized actin and phosphorylated myosin II; the dissociation rate is zero when the fibres are held at their isometric tension σ_0, but increases linearly at lower tension.

Fig. 6.9(c) shows that the stress increases until $\overline{t} = 0.5$ as long as the displacement is positive, so σ_f follows the Eq. (6.81). After $\overline{t} = 0.5$, σ_f decreases until vanishing.

6.6   Conclusion

The modeling of coupled chemo-mechanical processes on living cells has been discussed in this chapter. Differently from the approach adopted in Chapter 4, the mechanical deformation of the cell has been described rigorously in the framework of finite strain kinematics. In this way the transport of receptors on the cell membrane is coupled with the mechanics through an advective contribution due to cell spreading. In order to provide an exhaustive description, the conservation laws (i.e. conservation of diffusing species and balance of linear of angular momentum) are first derived in abstract setting and then specialized to the problem at hand. Subsequently, after having formulated the constitutive laws, the governing equations have been written in both spatial and reference frames. The solution of the resulting coupled problem of transport, binding reaction, and mechanics has been addressed numerically through the finite element method. Althoug the numerical implementation has not been fully developed yet, some remarkable outcomes have been achived. Among these, the spreading of a single cell on a rigid substratum has been simulated accounting for the conctact-problem between cell and substrate. Future developments will be focus on coupling the receptor-ligand binding surface equations with the simulated mechanical response of the cell.

Chapter 7

Conclusions

The present PhD thesis concerned the coupling between cellular mechanics and VEGFR2/VEGF interactions.

Motivations. The motivations for a mechano-biological model of endothelial cells and either pro- or anti-angiogenic factors have been described in Chapter 1. It has been clarified there why and how angiogenesis plays a basic role in formation of new blood vessels and that therapeutic angiogenesis is considered a major strategy for revascularizing ischemic tissue. Among several possible examples, it has been pointed out that recovery of the vascular network after injuries prevents wound expansion and ulcer formation. Furthermore, diseases such as limb, cardiac, coronary artery ischemias arise from reduced vascular perfusion. For this sake, therapeutic angiogenesis is of prime importance for tissue engineering and regenerative medicine. Clinical applications are still limited, mostly because of the lack of strategies capable to provide adequate amount of oxygen and nutrients through blood vessels. Strategies to overcome this issue, such as the delivery of growth factors (VEGF, BMP) that stimulate the recruitment of endothelial cells, are subject of abundant research. In fact, the modulation of angiogenesis processes - such as the activation of vascular endothelial growth factor receptors by ligands - can enhance these strategies. Angiogenesis plays a fundamental role in tumor growth and cancer proliferation, too. Tumor development is sustained by angiogenesis, which is required to provide the nutriments for cancer proliferation. Tumor angiogenesis is modulated by the interaction between specific pairs of membrane receptors expressed by endothelial cells and extracellular ligands produced by the tumor cell. The understanding of tumor angiogenesis leaded to the development of anti-angiogenic therapies, but these therapies have not matched the expectations, yet.

Interdisciplinary nature of this work. Angiogenesis phenomena are still largely unknown. In vitro and in vivo information from experiments are difficult to analyze, tailor, replicate. Disciplines as mathematics, thermodynamics, and computational modeling can enable to fully understand how and why biological processes work. Interdisciplinary is the keyword to success: recently, several ongoing collaborations between contiguous scientific areas, such as biology and engineering, allowed achieving novel and impactful biological insights in angiogenesis. Mathematical and computational approaches, if applied correctly, can boost the discovery of general principles. Experimentalists and modelers shall work together, because predictive capability of mathematical models will increase with the level of communication with experimentalists.

This thesis is the result of a first collaboration among the Mechanical and Industrial Engineering, Structural Engineering, and Molecular and Translational Medicine Departments at the University of Brescia. As such, this research is the outcome of the interplay among several disciplines, as biology, thermodynamics, solid mechanics, and numerical methods. The main goal was to describe the VEGFR-2 recruitment and re-localization on endothelial cell membrane driven by ligands. We started from the simplest mathematical description of the membrane phenomena by a chemo-diffusion preliminary model, which has been successfully published in [137, 160]. Afterwards the model has been enriched, by adding complexity: we coupled integrins and the cell mechanics in large deformations, with the ultimate aim of reproducing the real condition for receptor relocation driven by growth factors. Summarizing, we investigated VEGFR-2 re-localization modeling by means of

- a preliminary thermodynamical and chemo-diffusion framework accounting for chemical kinetics on a spherical geometry, presented in Chapter 3,

- a chemo-diffusion model through a discretized weak form with a simplified mechanics to describe the cell-substrate contact on a surface, proposed in Chapter 4;

- interaction between VEGFR-2/ligand complex coupled with low affinity integrins through a mathematical formulation taking into account the interplay with the latter co-receptors, presented in Chapter 5;

- the VEGFR-2 relocalization by considering cell spreading, contractility and the cell-substrate contact accounting for large deformations, described in Chapter 6.

Computational simulations have been performed in Chapters 3 and 4 by comparison with experimental evidence and co-designed tests have been carried out to validate our results. Experimental data necessary to run the simulations, such as the receptor diffusivity and the species concentrations, are depicted in Chapter 2.

Co-designed experiments. Time-laspse experiments have been performed to analyze VEGFR-2 recruitment on the EC membrane. Both immobilized Gremlin and immobilized VEGF-A induce the re-localization of VEGFR-2 to the plasma membrane at the basal aspect of ECs, thus leading to a localized and directional receptor activation. The major outcome are that VEGFR-2 has a lateral mobility of about $D_R = 0.198 \, \mu m^2 \, s^{-1}$, as measured by means of FRAP experiments, and that free and ECM-immobilized ligands induce VEGFR-2 rearrangement on EC plasma membrane. After ligand interaction, VEGFR-2 dimerizes and transduces an intracellular signaling via its relocation on the cell membrane and the recruitment of intracellular proteins. All these data, collected in our work [137], highlight that non-activated receptors are mainly free to move on the cell membrane, thus suggesting that VEGFR-2 phosphorylation, its dimerization, and its interaction with membrane co-receptors or intracellular signaler may reduce its motility.

Modeling. A simple thermodynamical framework has been proposed in Chapter 3 to mimic the VEGFR-2 recruitment and re-localization driven by ligands that are immobilized upon a substrate. From the experimental evidence, provided by time lapse analysis, we based two main assumptions: at the beginning, we consider an uniform receptors concentration and at the end of the process we reach a stationary state with a uniform complex concentration; in addition we define a contact function α to mimic che cell 'adhesion' on the ligand-enriched substrate. This model takes into account of chemical kinetics and provides a dimensionless parameter $\widetilde{K}$ which depends on receptor diffusivity D_R, cell radius ℓ, forward reaction rate k^+ and equilibrium constant based on the concentrations K_{eq}^c. Dimensionless partial differential equations have been written on spherical coordinates and implemented on a MATLAB code by using a *pdepd* solve. Summarizing, the model predicts:

- the important correlation between the ratio of initial concentration on receptors R_0 and ligand L_0 with the equilibrium constant;

- the overall number of free plus bound receptors normalized by the initial over number of receptors in contact with the substrate in comparison with time lasps measuments;

- the change of slope at about $t = 10 \, \text{min}$, which corresponds to the point between the mechanical and the diffusion phases and the final stationary value x;

- the initial and the final contact angles θ_A^0 and θ_A^∞, respectively, during cell attachment phase;

- the evolution of the concentrations of the three species;

- the matching values of $\widetilde{K}$ at the given x_A^{exp} and for the variuos cell radius ℓ.

The model in Chapter 3 differs from that in the following Chapter and published in [137], in that the reactions are not assumed at chemical equilibrium and therefore the model requires a reasonable estimate of the forward reaction rate constant k^+. So far we found no experimental data from which to extract such rate constant for the reaction occurring on the cell membrane. However, we believe that following the line of analysis in [141] and [94] data from bulk experiments complemented with appropriate surface tension measurements could yield the required surface rate constant.

We developed in Chapter 4 a multi-physics model to describe and predict the effects of ligands on VEGFR-2 relocation during the endothelial cell activation. The interaction between ligands and receptors has been modeled by a chemical reaction that produces a complex. The model accounts for finite reaction kinetics, although simulations have been carried out assuming that the reaction kinetics is infinitely fast. The time-scale of the VEGFR2-ligand binding reaction is in fact assumed to be much faster than the time-scale of the mechanical deformation of the cell and of the diffusion of receptors on cell membrane. The effect of the mechanical deformation of the cell has been accounted for in the model, by surrogating the explicit description of the cell spreading/deformation with a given increase in time of the surface area available for the chemical reaction by means the function s_L. Under these assumptions, we recovered the experimental evidence that the motion of receptors and their subsequent trapping into immobile VEGFR2-ligands complexes proceed in a sequence of three phases, and we characterized those phases with different rate-controlling factors. The model predicts the amount of well-oriented ligands available for the receptor binding, by noticing that this value is much smaller than the total number of immobilized ligands c_L^{max}.

The key features of our experimental evidence on VEGFR-2 relocation are captured well. In particular, through the numerical simulations carried out in this Chapter, we evaluated:

- the time evolution of the spatial concentration of free receptors VEGFR-2 along the cell membrane;

- the spatial evolution of the ligand-receptor complex concentration at various time, with high concentration manifest at the boundary of the contact area.

The outcomes of this Chapter are shown on the pubblished paper on *Scientific Reports*, [137], and on a paper recently accepted on *Mathematical Problems in Engineering* [160].

Such a model was further developed in Chapter 5, by including transmembrane proteins as the integrins that are responsible of focal adhesion. The numerical implementation of the governing equations has not been fully developed yet, but several goals have been achieved:

1. The weak form of the balance equations of three reactions has been written, which considers:

   - the interaction between low affinity integrin ("unbent" configuration) and its specific ligand (e.g. fibrinogen) that leads to a high affinity integrin ("bent" configuration) triggering stress fibers formation and focal adhesion,

   - the interaction between VEGFR-2 and VEGF which forms the complex VEGFR-2/VEGF,

   - the reaction between the low affinity integrins and the VEGFR-2/VEGF complex which triggers a long-term VEGFR-2 activation.

2. The weak form, with these three reactions, has been discretized in space, with Finite Element Method, and in time, with Backward Euler scheme. To solve the nonlinear part, Newton-Raphson method has been designed.

This model may provide new insights about the important interplay among different transmembrane proteins and may be applied to other interactions among receptors and co-receptors, such as Neuropilin-1 and VEGFR-2 [150].

The modeling of coupled chemo-mechanical processes on living cells has been discussed in Chapter 6. Differently from the approach adopted before, the mechanical deformation of the cell has been described rigorously in the framework of finite strain kinematics. In this way the transport of receptors on the cell membrane is coupled with the mechanics through an advective contribution due to cell spreading.

In order to provide an exhaustive description, the conservation laws (i.e. conservation of diffusing species and balance of linear of angular momentum) are first derived in abstract setting and then specialized to the problem at hand. Subsequently, after having formulated the constitutive laws, the governing equations have been written in both spatial and reference frames.

The solution of the resulting coupled problem of transport, binding reaction, and mechanics has been addressed numerically through the finite element method. Although the numerical implementation has not been fully developed in the time-frame of this thesis, some remarkable outcomes have been achieved. Among these, the spreading of a single cell on a rigid substratum has been simulated accounting for the conctact-problem between cell and substrate.

Future developments will focus on coupling the receptor-ligand binding surface equations with the simulated mechanical response of the cell [148, 161].

Bibliography

[1] Forough R., *New Frontiers in Angiogenesis*, Springer, 2006

[2] Patan S., *Vasculogenesis and angiogenesis as mechanisms of vascular network formation, growth and remodeling*, J Neurooncol. 50:1-15, 2000

[3] Alberts B., Johnson A., Lewis J., Morgan D., Raff M., Roberts K., Walter P., *Molecular Biology of The Cell*, Garland Science, 2015

[4] Yancopoulos G. D., Davis S., Gale N. W.,Rudge J. S. , Wiegand S. J. and Holash J., *Vascular-specific growth factors and blood vessel formation*, Nature. 407(6801):242-8, 2000

[5] Risau W., *Mechanisms of angiogenesis*, Nature. 386(6626):671-4, 1997

[6] Karkkainen M. J., Mkinen T. and Alitalo K., *Lymphatic endothelium: a new frontier of metastasis research*, Nat Cell Biol. 4(1):E2-5, 2002

[7] Dijke P., Arthur H. M., *Extracellular control of TGFβ signalling in vascular development and disease*, Nat Rev Mol Cell Biol. 8(11):857-69. 2007

[8] Lamalice L., Le Boeuf F., Huot J., *Endothelial Cell Migration During Angiogenesis*, Circ Res. 100(6):782-94, 2007

[9] Caille N., Thoumine O., Tardy Y., Meister. J., *Contribution of the nucleus to the mechanical properties of endothelial cells*, J Biomech. 35(2):177-87, 2002

[10] Kuznetsova T. G., Starodubtseva M.N., Yegorenkov N. I., Chizhik S. A., Zhdanov R. I., *Atomic force microscopy probing of cell elasticity*, Micron. 38:824-833, 2007

[11] Sato H., Kataoka N., Kajiya F., Katano M., Takigawa T., Masuda T., *Kinetic study on the elastic change of vascular endothelial cells on collagen matrices by atomic force microscopy*, Colloids Surf B Biointerfaces. 34(2):141-6, 2004

[12] Costa K. D., Sim A. J., Yin F. C-P., *Non-Hertzian Approach to Analyzing Mechanical Properties of Endothelial Cells Probed by Atomic Force Microscopy*, J Biomech Eng. 128(2):176-84, 2006

[13] Mathur A.B., Truskey G.A., Reichert W.M., *Atomic force and total internal reflection fluorescence microscopy for the study of force transmission in endothelial cells*, Biophys J. 78(4): 1725-1735, 2000

[14] Carmeliet P. , *Angiogenesis in life, disease and medicine*, Nature. 438(7070):932-6, 2005

[15] Selvaprithviraj V. Sankar D., Sivashanmugam A., Srinivasan S., Jayakumar R. *Pro-angiogenic molecules for therapeutic angiogenesis*, Curr Med Chem. 24(31):3413-3432, 2017

[16] Bhise, N.S., Shmueli R.B., Sunshine J.C., Tzeng S.Y., Green J.J., *Drug delivery strategies for therapeutic angiogenesis and antiangiogenesis*, Expert Opin Drug Deliv. 8(4):485-504, 2011

[17] Bergers G., Benjamin L.E., *Tumorgenesis and the angiogenic switch*, Nat Rev Cancer. 3(6):401-10, 2003

[18] Carmeliet P., Jain R.K., *Angiogenesis in cancer and other diseases*, Nature. 407(6801):249-57, 2000

[19] Dongsheng H,, Huanrong Lan., Fanlong L., Shibing W., Xiaoyi C., Ketao J., and Xiaozhou M., *Anti-angiogenesis or pro-angiogenesis for cancer treatment: focus on drug distribution*, Int J Clin Exp Med. 8(6):8369-8376, 2015

[20] Fischer C., Jonckx B., Mazzone M., Zacchigna S., Loges S., Pattarini L., Chorianopoulos E., Liesen-borghs L., Koch M., De Mol M., Autiero M., Wyns S., Plaisance S., Moons L., van Rooijen N., Giacca M., Stassen J.M., Dewerchin M., Collen D., Carmeliet P., *Anti-PlGF inhibits growth of VEGF(R)-inhibitor resistant tumors without affecting healthy vessels*, Cell. 131(3):463-475, 2007

[21] Moss A. *The angiopoietin:Tie 2 interaction: a potential target for future therapies in human vascular disease*, Cytokine Growth Factor Rev. 24(6):579-592, 2013

[22] Dufraine J., Funahashi Y., Kitajewski J., *Notch signaling regulates tumor angiogenesis by diverse mechanisms*, Oncogene. 27(38):5132-5137, 2008

[23] Hellberg C., Ostman A., Heldin C.H., *PDGF and vessel maturation*, Recent Results Cancer Res. 180:103-114, 2010

[24] Legg J.A., Herbert J.M., Clissold P., Bicknell R., *Slits and Roundabouts in cancer, tumour angiogenesis and endothelial cell migration*, Angiogenesis. 11(1):13-21, 2008

[25] Haddad R., Lipson K.E., Webb C.P., *Hepatocyte growth factor expression in human cancer and therapy with specific inhibitors*, Anticancer Res. 21(6B):4243-4252, 2001

[26] Ben-Baruch A. *The multifaceted roles of chemokines in malignancy*, Cancer Metastasis Rev. 25(3):357-71, 2006

[27] Jagielska J., Kapopara P.R., Salguero G., Scherr M., Schutt H., Grote K., Schieffer B., Bavendiek U., *Interleukin-1 assembles a proangiogenic signaling module consisting of caveolin-1, tumor necrosis factor receptor-associated factor 6, p38-mitogen-activated protein kinase (MAPK), and MAPK-activated protein kinase 2 in endothelial cells*, Arterioscler Thromb Vasc Biol. 32(5):1280-1288, 2012

[28] Nilsson M.B., Langley R.R., Fidler I.J., *Interleukin-6, secreted by human varian carcinoma cells, is a potent proangiogenic cytokine*, Cancer Res. 65(23):10794-800, 2005

[29] Basile J.R., Afkhami T., Gutkind J.S., *Semaphorin 4D/plexin-B1 induces endothelial cell migration through the activation of PYK2, Src, and the phosphatidylinositol 3-kinase-Akt pathway*, Mol Cell Biol. 25(16):6889-6898, 2005

[30] Basile J.R., Barac A., Zhu T., Guan K.L., Gutkind J.S., *Class IV semaphorins promote angiogenesis by stimulating Rho-initiated pathways through plexin-B*, Cancer Res. 64(15):5212-5224, 2004

[31] Stabile H., Mitola S., Moroni E., Belleri M., Nicoli S., Coltrini D., Peri F., Pessi A., Orsatti L., Talamo F., Castronovo V., Waltregny D., Cotelli F., Ribatti D., Presta M., *Bone morphogenic protein antagonist Drm/Gremlin is a novel proangiogenic factor*, Blood. 109(5):1834-40, 2007

[32] Brogi E., Wu T., Namiki A., Isner J.M., *Indirect angiogenic cytokines upregulate VEGF and bFGF gene expression in vascular smooth muscle cells, whereas hypoxia upregulates VEGF expression only*, Circulation. 90(2):649-652, 1994

[33] Frater-Schroder M., Risau W., Hallmann R., Gautschi P., Bohlen P., *Tumor necrosis factor type alpha, a potent inhibitor of endothelial cell growth in vitro, is angiogenic in vivo*, Proc Natl Acad Sci USA. 84(15):5277-5281, 1987

[34] Presta M., Moscatelli D., Joseph-Silverstein J., Rifkin D.B., *Purification from a human hepatoma cell line of a basic fibroblast growth factor-like molecule that stimulates capillary endothelial cell plasminogen activator production, DNA synthesis, and migration*, Mol Cell Biol. 6(11):4060-4066, 1986

[35] Vrancken K., Vervaeke P., Balzarini J., Liekens S., *Viruses as key regulators of angiogenesis*, Rev Med Virol. 21(3):181-200, 2011

[36] Rusnati M., Presta M., *HIV-1 Tat protein and endothelium: from protein/cell interaction to AIDS-associated pathologies*, Angiogenesis. 5(3):141-151, 2002

[37] Caccuri F., Giagulli C., Bugatti A., Benetti A., Alessandri G., Ribatti D., Marsico S., Apostoli P., Slevin M.A., Rusnati M., Guzman C.A., Fiorentini S., Caruso A. *HIV1 matrix protein p17 promotes angiogenesis via chemokine receptors CXCR1 and CXCR2*, Proc Natl Acad Sci USA. 109(36):1458014585, 2012

[38] Vene R., Benelli R., Noonan D.M., Albini A., *HIV-Tat dependent chemotaxis and invasion, key aspects of tat mediated pathogenesis.* Clin Exp Metastasis. 18(7):533-538, 2000

[39] Rusnati M., Tulipano G., Urbinati C., Tanghetti E., Giuliani R., Giacca M., Ciomei M., Corallini A., Presta M., *The basic domain in HIV-1 Tat protein as a target for polysulfonatedheparin-mimicking extracellular Tat antagonists*, J Biol Chem. 273(26):16027-16037, 1998:

[40] Indraccolo S. *Interferon-alpha as angiogenesis inhibitor: learning from tumor models*, Autoimmunity. 43(3):244-247, 2010

[41] Silvestre J.S., Mallat Z., Duriez M., Tamarat R., Bureau M.F., Scherman D., Duverger N., Branellec D., Tedgui A., Levy B.I., *Antiangiogenic effect of interleukin-10 in ischemia-induced angiogenesis in mice hindlimb*, Circ Res. 87(6):448-452, 2000

[42] Imagawa Y., Satake K., Kato Y., Tahara H., Tsukuda M., *Antitumor and antiangiogenic effects of interleukin 12 gene therapy in murine head and neck carcinoma model*, Auris Nasus Larynx. 31(3):239-245, 2004

[43] Shen J., Choy D.F., Yoshida T., Iwase T., Hafiz G., Xie B., Hackett S.F., Arron J.R., Campochiaro P.A., *Interleukin-18 has antipermeablity and antiangiogenic activities in the eye: reciprocal suppression with VEGF*, J Cell Physiol. 229(8):974-983, 2014

[44] Sakurai A., Doci C.L., Gutkind J.S., *Semaphorin signaling in angiogenesis, lymphangiogenesis and cancer.* Cell Res. 22(1):23-32, 2012

[45] Wang Z., Huang H., *Platelet factor-4 (CXCL4/PF-4): an angiostatic chemokine for cancertherapy*, Cancer Lett. 331(2):147-153, 2013

[46] Lawler P.R., Lawler J., *Molecular basis for the regulation of angiogenesis by thrombospondin-1 and -2.* Cold Spring Harb Perspect Med. 2(5), 2012

[47] Rodriguez-Manzaneque J.C., Lane T.F., Ortega M.A., Hynes R.O., Lawler J., Iruela-Arispe M.L., *Thrombospondin-1 suppresses spontaneous tumor growth and inhibits activation of matrix metalloproteinase-9 and mobilization of vascular endothelial growth factor*, Proc Natl Acad Sci USA. 98(22):12485-12490, 2001

[48] Greenaway J., Lawler J., Moorehead R., Bornstein P., Lamarre J., Petrik J., *Thrombospondin-1 inhibits VEGF levelsin the ovary directly by binding and internalization via the low density lipoprotein receptor-related protein-1 (LRP-1)*, J Cell Physiol. 210(3):807-818, 2007

[49] Gupta K., Gupta P., Wild R., Ramakrishnan S., Hebbel R.P., *Binding and displacement of vascular endothelial growth factor (VEGF) by thrombospondin: effect on human microvascular endothelial cell proliferation and angiogenesis*, Angiogenesis. 3(2):147-158, 1999

[50] Hynes R.O., *Cell-matrix adhesion in vascular development*, J Thromb Haemost. 5 Suppl 1(32-40), 2007

[51] Kalluri R., *Basement membranes: structure, assembly and role in tumour angiogenesis*, Nat Rev Cancer. 3(6):422-433, 2003

[52] Kostourou V., Papalazarou V., *Non-collagenous ECM proteins in blood vessel morphogenesis and cancer*, Biochim Biophys Acta. 1840(8):2403-2413, 2014

[53] Daley W.P., Peters S.B., Larsen M., *Extracellular matrix dynamics in development and regenerative medicine*, J Cell Sci. 121(Pt3):255-264, 2008

[54] Hynes R.O., *The extracellular matrix: not just pretty fibrils*, Science. 326(5957):1216-1219, 2009

[55] Ferrara N., *Binding to the extracellular matrix and proteolytic processing: two key mechanisms regulating vascular endothelial growth factor action*, Mol Biol Cell. 21(5):687-690, 2010

[56] Tanghetti E., Ria R., Dell'Era P., Urbinati C., Rusnati M., Ennas M.G., Presta M., *Biological activity of substrate-bound basic fibroblast growth factor (FGF2): recruitment of FGF receptor-1 in endothelial cell adhesion contacts*, Oncogene. 21(24):3889-3897, 2002

[57] Chen T.T., Luque A., Lee S., Anderson S.M., Segura T., Iruela-Arispe M.L., *Anchorage of VEGF to the extracellular matrix conveys differential signaling responses to endothelial cells*, J Cell Biol. 188(4):595-609, 2010

[58] Fuster M.M., Wang L., *Endothelial heparan sulfate in angiogenesis*, Prog Mol Biol Transl Sci. 93:179-212, 2010

[59] Jimenez B., Volpert O.V., Crawford S.E., Febbraio M., Silverstein R.L., Bouck N., *Signals leading to apoptosis-dependent inhibition of neovascularization by thrombospondin-1*, Nat Med. 6(1):41-48, 2000

[60] Egeblad M., Werb Z., *New functions for the matrix metalloproteinases in cancer progression*, Nat Rev Cancer. 2(3):161-174, 2002

[61] Schwartz M.A., *Integrins and extracellular matrix in mechanotransduction*, Cold Spring Harb Perspect Biol. 2(12), 2010

[62] Sarrazin S., Lamanna W.C., Esko J.D., *Heparan sulfate proteoglycans.* Cold Spring Harb Perspect Biol. 3(7), 2011

[63] Turnbull J., Powell A., Guimond S., *Heparan sulfate: decoding a dynamic multifunctional cell regulator*, Trends Cell Biol. 11(2):75-82, 2001

[64] Xu D., Fuster M.M., Lawrence R., Esko J.D., *Heparan sulfate regulates VEGF165- and VEGF121-mediated vascular hyperpermeability*, J Biol Chem. 286(1):737-745, 2011

[65] Chiodelli P., Mitola S., Ravelli C., Oreste P., Rusnati M., Presta M., *Heparan sulfate proteoglycans mediate the angiogenic activity of the vascular endothelial growth factor receptor-2 agonist Gremlin*, Arterioscler Thromb Vasc Biol. 31(12):e116-127, 2011

[66] Wolfenson H., Lavelin I., Geiger B., *Dynamic regulation of the structureand functions of integrin adhesions*, Dev Cell. 24(5):447-458, 2013

[67] ffrench-Constant C., Colognato H. *Integrins: versatile integrators of extracellular signals.* Trends Cell Biol. 14(12):678-686, 2004

[68] Serini G., Napione L., Arese M., Bussolino F., *Besides adhesion: new perspectives of integrin functions in angiogenesis*, Cardiovasc Res. 78(2):213-222, 2008

[69] Brooks P.C., Clark R.A., Cheresh D.A., *Requirement of vascular integrin alpha v beta 3 for angiogenesis*, Science. 264(5158):569-571, 1994

[70] Alghisi G.C., Ruegg C., *Vascular integrins in tumor angiogenesis:mediators and therapeutic targets*, Endothelium. 13(2):113-135, 2006

[71] Ruegg C, Alghisi GC. *Vascular integrins: therapeutic and imaging targets of tumor angiogenesis*, Recent Results Cancer Res. 180:83-101, 2010

[72] Brian P. Eliceiri, *Integrin and Growth Factor Receptor Crosstalk*, Circ Res. 89(12):1104-10, 2001

[73] Plow E.F., Meller J., Byzova T.V., *Integrin function in vascular biology: a view from 2013*, Curr Opin Hematol. 21(3):241-247, 2014

[74] Soldi R., Mitola S., Strasly M., Defilippi P., Tarone G. and Bussolino F., *Role of $\alpha_v\beta_3$ integrin in the activation of vascular endothelial growth factor receptor-2*, EMBO J. 18(4):882-892, 1999

[75] Mahabeleshwar G.H, Feng W., Phillips D.R., Byzova T.V., *Integrin signaling is critical for pathological angiogenesis*, J Exp Med. 203(11):2495-2507, 2006

[76] Bianchi-Smiraglia A., Paesante S., Bakin A.V., *Integrin beta5 contributes to the tumorigenic potential of breast cancer cells through the Src-FAK and MEK-ERK signaling pathways*, Oncogene. 32(25):3049-3058, 2013

[77] Pallaghy P.K., Nielsen K.J., Craik D.J., Norton R.S., *A common structural motif incorporating a cystine knot and a triple-stranded beta-sheet in toxic and inhibitory polypeptides*, Protein Sci. 3(10):1833-1839, 1994

[78] Daly N.L., Craik D.J., *Bioactive cystine knot proteins*, Curr Opin Chem Biol. 15(3):362-368, 2011

[79] Ribatti D., *The contribution of Harold F. Dvorak to the study of tumor angiogenesis and stroma generation mechanisms*, Endothelium. 14(3):131-5, 2007

[80] Ferrara N. and Davis-Smyth T., *The biology of vascular endothelial growth factor*, Endocr Rev. 18(1):4-25, 1997

[81] Kerbel R. S., *Tumor angiogenesis: past, present and the near future*, Carcinogenesis. 21(3):505-15, 2000

[82] Holmes K., Roberts O., Thomas A. M., Cross M. J., *Vascular endothelial growth factor receptor-2: Structure, function, intracellular signalling and therapeutic inhibition,*Send to Cell Signal. 19(10):2003-12, 2007

[83] Nishida N., Yano H., Nishida T., Kamura T., and Kojiro M., *Angiogenesis in cancer*, Vasc Health Risk Manag. 2(3):213-219, 2006

[84] Bates. D. O., *Vascular endothelial growth factors and vascular permeability*, Cardiovasc Res. 87(2):262-271, 2010

[85] Nagy J. A., Benjamin L., Zeng H., Dvorak A. M., Dvorak H. F., *Vascular permeability, vascular hyperpermeability and angiogenesis*, Angiogenesis. 11(2):109-19, 2008

[86] Sirois M. G., Edelman E. R., *VEGF effect on vascular permeability is mediated by synthesis of platelet-activating factor*, Send to Am J Physiol. 272(6 Pt 2):H2746-56, 1997

[87] Bussolino F., Serini G., Mitola S., Bazzoni G., Dejana E., *Dynamic modules and heterogeneity of function: a lesson from tyrosine kinase receptors in endothelial cells*, EMBO Rep. 2(9): 763-767, 2001

[88] Alitalo K., *The lymphatic vasculature in disease*, Nat Med. 17(11):1371-80, 2011

[89] David L., Feige J.J., Bailly S., *Emerging role of bone morphogenetic proteins in angiogenesis*, Cytokine Growth Factor Rev. 20(3):203-212, 2009

[90] Bragdon B., Moseychuk O.,Saldanha S., King D., Julian J., Nohe A., *Bone Morphogenetic Proteins: A critical review*, Cell Signal. 23(4):609-20, 2011

[91] Rider C.C., Mulloy B. *Bone morphogenetic protein and growth differentiation factor cytokine families and their protein antagonists*, Biochem J. 429(1):1-12, 2010:

[92] Mitola S., Ravelli C., Moroni E., Salvi V., Leali D., Ballmer-Hofer K., Zammataro L., Presta M., *Gremlin is a novel agonist of the major proangiogenic receptor VEGFR2*, Blood. 116(18):3677-80, 2010

[93] Hahnefeld C., Drewianka S., andHerberg F. W., *Determination of Kinetic Data Using Surface Plasmon Resonance Biosensors, from Methods in Molecular Medicine*, Methods in molecular medicine. 94:299-320, 2004

[94] Maiolo D., Mitola S., Leali D., Oliviero G., Ravelli C., Bugatti A., Depero L.E., Presta M., Bergese P., *Role of Nanomechanics in Canonical and Noncanonical Pro-angiogenic Ligand/VEGF Receptor-2 Activation*, J. Am. Chem. Soc., 134(35):14573-14579, 2012

[95] Karlsson R., Fäilt A., *Experimental design for kinetic analysis of protein-protein interactions with surface plasmon resonance biosensors*, Journal of Immunological Methods. 200:121-133, 1997

[96] Gavutis M., Jaks E., Lamken P., and Piehler J., *Determination of the Two-Dimensional Interaction Rate Constants of a Cytokine Receptor Complex*, Biophys J. 90:3345-3355, 2006

[97] Avraamides C.J., Garmy-Susini B. and. Varner J. A, *Integrins in angiogenesis and lymphangiogenesis*, Nat Rev Cancer. 8:604-17, 2008

[98] Hynes R. O., *Integrins: Bidirectional, Allosteric Signaling Machines*, Cell. 110(6):673-87, 2002

[99] Valdembri D. and Serini G., *Regulation of adhesion site dynamics by integrin traffic*, Curr Opin Cell Biol. 24(5):582-91, 2012

[100] Parsons J. T., Horwitz A. R. and Schwartz M. A., *Cell adhesion: integrating cytoskeletal dynamics and cellular tension*, Nat Rev Mol Cell Biol. 11(9): 633-643, 2010

[101] Tojkander S., Gateva G. and Lappalainen P., *Actin stress fibers - assembly, dynamics and biological roles*, J Cell Sci. 125(Pt 8):1855-64, 2012

[102] Cooper G.M., *The Cell: A Molecular Approach*, Sunderland (MA), Sinauer Associates, 2000.

[103] D. A. Fletcher and R. Dyche Mullins, *Cell mechanics and the cytoskeleton*, Nature. 463(7280):485-492, 2010

[104] Hotulainen P. and Lappalainen P., *Stress fibers are generated by two distinct actin assembly mechanisms in motile cells*, J Cell Biol. 173(3):383-394, 2006

[105] Pellegrin S. and Mellor H., *Actin stress fibres*, J Cell Sci. 120(Pt 20):3491-3499, 2007

[106] Ravelli C., Mitola S., Corsini M., Presta M., *Involvement of $\alpha_v\beta_3$ integrin in Gremlin-induced angiogenesis*, Angiogenesis. 16(1):235-43, 2013

[107] Borges E., Jan Y., Ruoslahti E., *Platelet-derived growth factor receptor beta and Vascular Endothelial Growth Factor Receptor 2 Bind to the beta 3 Integrin through Its Extracellular Domain*,J Biol Chem. 275(51):39867-73, 2000

[108] Somanath P.R., Malinin N.L., Byzova T.V., *Cooperation between integrin $\alpha_v\beta_3$ and VEGFR2 in angiogenesis*, Angiogenesis. 12(2):177-185, 2009

[109] Bell G.I., *Models for the Specific Adhesion of Cells to Cells*, Science. 200(4342):618-27, 1978

[110] Myers A.C., Kovach J.S., Vuk-Pavlovic S., *Binding, internalization, and intracellular processing of protein ligands. Derivation of rate constants by computer modeling.* J Biol Chem. 262(14):6494-9, 1987

[111] DiMilla P.A., Barbee K., Lauffenburger D.A., *Mathematical model for the effects of adhesion and mechanics on cell migration speed*, Biophys J. 60(1):15-37, 1991

[112] Gilson M.K., Given J.A., Head M.S., *A new class of models for computing receptor-ligand binding affinities* Chem Biol. 4(2):87-92, 1997

[113] Leitner D.M., Brown F.L., Wilson K.R., *Regulation of protein mobility in cell membranes: a dynamic corral model*, Biophys J. 78(1):125-35, 2000

[114] Mac Gabhann F., Popel A.S., *Model of competitive binding of vascular endothelial growth factor and placental growth factor to VEGF receptors on endothelial cells.* Am J Physiol Heart Circ Physiol. 286(1):H153-64, 2004.

[115] Mac Gabhann F., Yang M.T., Popel A.S., *Monte Carlo simulations of VEGF binding to cell surface receptors in vitro.* Biochim Biophys Acta. 1746(2):95-107, 2005

[116] Stefanini M., Wu F.T.H., Mac Gabhann F. and Popel A. S., *A compartment model of VEGF distribution in blood, healthy and diseased tissues*, BMC Syst Biol. 2:77, 2008

[117] Khn-Luque A., de Back W., Yamaguchi Y., Yoshimura K., Herrero M.A., Miura T., *Dynamics of VEGF matrix-retention in vascular network patterning*, Phys. Biol. 10(6):066007, 2013

[118] Gao H., Shi W., Freund L.B., *Mechanics of receptor-mediated endocytosis* Proc Natl Acad Sci U S A. 102(27):9469-74, 2005

[119] Golestaneh A.F., Nadler B., *Modeling of cell adhesion and deformation mediated by receptor-ligand interactions*, Biomech Model Mechanobiol. 15(2):371-87, 2016

[120] Boal D., *Mechanics of the cell*, Cambridge University, Cambridge, 2002

[121] Deshpande V.S., McMeeking R.M., Evans A.G., *A bio-chemo-mechanical model for cell contractility*, Proc Natl Acad Sci U S A. 103(38):14015-20, 2006

[122] Deshpande V.S., Mrksich M., McMeeking R.M., EvansA.G., *A bio-mechanical model for coupling cell contractility with focal adhesion formation.* J Mech Phys Solids. 56(4):1484-1510, 2008

[123] Ronan W., Deshpande V. S., McMeeking R. M., McGarry J. P., *Cellular contractility and substrate elasticity: a numerical investigation of the actin cytoskeleton and cell adhesion*, Biomech Model Mechanobiol. 13:417-435, 2014

[124] Nicolson G.L., *The Fluid-Mosaic Model of Membrane Structure: Still relevant to understanding the structure, function and dynamics of biological membranes after more than 40 years*, Biochim Biophys Acta. 1838(6):1451-66, 2014

[125] Pike L. J., *Growth factor receptors, lipid rafts and caveolae: An evolving story*, Biochim Biophys Acta. 1746(3):260-73, 2005

[126] Wang R., Bi J., Ampah K.K., Ba X., Liu W., Zeng X., *Lipid rafts control human melanoma cell migration by regulating focal adhesion disassembly*, Biochim Biophys Acta. 1833(12):3195-3205, 2013

[127] Pike L. J., *Lipid rafts: bringing order to chaos*, J Lipid Res. 44(4):655-67, 2003

[128] Guzman A., Zelman-Femiak M., Boergermann J.H., Paschkowsky S., Kreuzaler P.A., Fratzl P., Harms G.S., Knaus P., *SMAD versus non-SMAD signaling is determined by lateral mobility of bone morphogenetic protein (BMP) receptors*, J Biol Chem. 287(47):39492-504, 2012

[129] Metzler R., Jeonc J.H., Cherstvy A.G., Non-Brownian diffusion in lipid membranes: Experiments and simulations, Biochim Biophys Acta. 1858(10):2451-2467, 2016

[130] Lippincott-Schwartz J., Snapp E., Kenworthy A., *Studying protein dynamics in living cells*, Nat Rev Mol Cell Biol. 2(6):444-56, 2001

[131] Sprague B. L. and McNally J. G., *FRAP analysis of binding: proper and fitting*, Trends Cell Biol. 15(2):84-91, 2005

[132] Lippincott-Schwartz J.and Patterson G. H., *Development and use of fluorescent protein markers in living cells*, Science. 300(5616):87-91. 2003

[133] Dunn G. A. and Jones G. E., *Cell motility under the microscope: Vorsprung durch Technik,* Nat Rev Mol Cell Biol. 5(8):667-72, 2004

[134] Goehring N., Chowdhury D., Hyman A., and Grill S. W., *FRAP analysis of membrane-associated proteins: lateral diffusion and membrane-cytoplasmic exchange,* Biophys J. 99(8):2443-52, 2010

[135] StahelinR. V., *Surface plasmon resonance: a useful technique for cell biologists to characterize biomolecular interactions.* Mol Biol Cell. 24(7): 883-886, 2013

[136] Ravelli C., Grillo E.., Corsini M., Coltrini D., Presta M., Mitola S., *β_3 Integrin Promotes Long-Lasting Activation and Polarization of Vascular Endothelial Growth Factor Receptor 2 by Immobilized Ligand.* Arterioscler Thromb Vasc Biol. 35(10):2161-71, 2015

[137] Damioli, V., Salvadori, A., Beretta, G.P., Ravelli, C., Mitola S., *Multi-physics interactions drive VEGFR2 relocation on endothelial cells,* Sci Rep. 7(1):16700, 2017

[138] Dulbecco R., Vogt M. *Plaque formation and isolation of pure lines with poliomyelitis viruses.* J Exp Med. 99(2):167-82, 1954

[139] Brozzo M.S., Bjelic S., Kisko K., Schleier T., Leppanen V.M., Alitalo K., Winkler F.K., Ballmer-Hofer K., *Thermodynamic and structural description of allosterically regulated VEGFR-2 dimerization,* Blood. 119(7):1781-8, 2012

[140] Gyftopoulos E.P., Beretta G.P., *Thermodynamics: Foundations and Applications,* Dover Publications, Mineola, NY, 2005

[141] Federici, S., Oliviero, G., Maiolo, D., Depero, L. E., Colombo, I., Bergese, P., *On the thermodynamics of biomolecule surface transformations,* J Colloid Interface Sci. 375(1):1-11, 2012

[142] Salvadori, A., Grazioli, D., Geers M.G.D., Danilov D., Notten P.H.L., *A multiscale-compatible approach in modeling ionic transport in the electrolyte of (Lithium ion) batteries,* J. of Power Sources, 293:92-911, 2015

[143] Salvadori A., Grazioli D., Magri M., Geers M.G.D., Danilov D., Notten P.H.L., *On the role of saturation in modeling ionic transport in the electrolyte of (Lithium ion) batteries,* J of Power Sources, 294:696-710, 2015

[144] Gurtin M., Fried E., Anand L., *The Mechanics and Thermodynamics of Continua.* Cambridge University Press, 2010

[145] Paolucci S., *Continuum Mechanics and Thermodynamics of Matter.* Cambridge University Press, 2016

[146] Deshpande V.S., McMeeking R.M., Evans A.G., *A bio-chemo-mechanical model for cell contractility,* Proc Natl Acad Sci U S A. 103(38):14015-20, 2006

[147] Deshpande V.S., Mrksich M., McMeeking R.M., EvansA.G., *A bio-mechanical model for coupling cell contractility with focal adhesion formation.* J Mech Phys Solids. 56(4):1484-1510, 2008

[148] Ronan W., Deshpande V. S., McMeeking R. M., McGarry J. P., *Cellular contractility and sub-strate elasticity: a numerical investigation of the actin cytoskeleton and cell adhesion,* Biomech Model Mechanobiol. 13:417-435, 2014

[149] Quarteroni A. and Valli. A., *Numerical approximation of partial differential equations.* Springer Verlag, Berlin, 1997.

[150] Gelfand M.V., Hagan N., Tata A., Oh W.J., Lacoste B., Kang K.T., Kopycinska J., Bischoff J., Wang J.H., Gu C., *Neuropilin-1 functions as a VEGFR2 co-receptor to guide developmental angiogenesis independent of ligand binding,* Elife. 3:e03720, 2014

[151] Holzapfel G. A., *Nonlinear Solid Mechanics. A continuum approach for engineering,* 2006

[152] Doll S. and Schweizerhof K., *On the Development of Volumetric Strain Energy Functions*, J. Appl. Mech. 67(1):17-21, 1999

[153] Simo J.C. and Hughes T.J.R., *Computational inelasticity*, Springer-Verlag, 1998

[154] Frohne J., Heister T., Bangerth W.; *Efficient numerical methods for the large-scale, parallel solution of elastoplastic contact problems.* International Journal for Numerical Methods in Engineering, 2015

[155] McGarry J.G., Prendergast P.J., *A three-dimensional finite element model of an adherent eukaryotic cell*, Eur Cell Mater. 7:27-33, 2004

[156] Tan J.L., Tien J., Pirone D.M., Gray D.S., Bhadriraju K., Chen C.S., *Cells lying on a bed of microneedles: An approach to isolate mechanical force*, Proc Natl Acad Sci U S A. 100(4):1484-9, 2003

[157] Deshpande V.S., McMeeking R.M. and Evans A.G., *A model for the contractility of the cytoskeleton including the effects of stress-fibre formation and dissociation*, Proc. R. Soc. A, 463:787-815, 2007

[158] Hill A. V., *The heat of shortening and the dynamic constants of muscle*, Proc. R. Soc. Lond. B 126: 136-195, 1938

[159] McMahon T., *Muscles, Reflexes, and Locomotion.* Princeton University Press, 1984

[160] Salvadori A., Damioli V., Ravelli C., Mitola S., *Modeling and simulation of VEGF receptors recruitment in angiogenesis*, Math Probl Eng. Accepted on 6 May 2018

[161] Deseri L., Zurlo G., *The stretching elasticity of biomembranes determines their line tension and bending rigidity*, Biomech. Model. Mechanobiol., 12(6):1233-, 2013